Geometric and numerical methods in optimal control and applications to the swimming problem at low Reynolds number and to low thrust orbital transfer

Jérémy Rouot

▶ **To cite this version:**

Jérémy Rouot. Geometric and numerical methods in optimal control and applications to the swimming problem at low Reynolds number and to low thrust orbital transfer. Other. Université Côte d'Azur, 2016. English. NNT : 2016AZUR4103 . tel-01472370v2

HAL Id: tel-01472370
https://inria.hal.science/tel-01472370v2

Submitted on 22 Feb 2017

HAL is a multi-disciplinary open access archive for the deposit and dissemination of scientific research documents, whether they are published or not. The documents may come from teaching and research institutions in France or abroad, or from public or private research centers.

L'archive ouverte pluridisciplinaire **HAL**, est destinée au dépôt et à la diffusion de documents scientifiques de niveau recherche, publiés ou non, émanant des établissements d'enseignement et de recherche français ou étrangers, des laboratoires publics ou privés.

École doctorale SFA
en Sciences Fondamentales et Appliquées
Unité de Recherche : UFR Sciences

Thèse de Doctorat

Présentée en vue de l'obtention du
grade de docteur en Mathématiques Appliquées
de
l'UNIVERSITE COTE D'AZUR

par

Jérémy ROUOT

Méthodes géométriques et numériques en contrôle optimal et applications au transfert orbital à poussée faible et à la nage à faible nombre de Reynolds.

Dirigée par Bernard BONNARD et Jean-Baptiste POMET

Soutenue le 21 novembre 2016
Devant le jury composé de :

Ugo Boscain	DR, CNRS, École Polytechnique	Rapporteur
Emmanuel Trélat	PR, Univ. Paris VI	Rapporteur
Bernard Bonnard	PR, Univ. Bourgogne	Directeur
Jean-Baptiste Pomet	DR, INRIA Sophia Antipolis	Directeur
François Alouges	PR, École Polytechnique	Examinateur
Piernicola Bettiol	PR, Univ. Bretagne Occidentale	Examinateur
Richard Epenoy	Ingénieur CNES Toulouse	Examinateur
Marius Tucsnak	PR, Univ. Bordeaux	Examinateur

Ce travail a été financé partiellement par le Conseil Régional Provence Alpes Côte d'Azur (PACA) et par le Centre national d'études spatiales (CNES).

Le fou a chanté 17 fois
Puis il est mort de désespoir
Dans un champ de labiales carnivores
Tous les tombeaux se sont ouverts
Pour voir passer le mort vainqueur
L'alcool s'est figé sur ton verre
Ta cigarette tombe sur ton coeur
Et tu cherches une vérité par-delà l'espace
Ouais, tu cherches une vérité par-delà l'espace

Le Chant du fou, Hubert-Félix Thiéfaine

Résumé

Notre travail est composé de deux parties utilisant les méthodes du contrôle optimal géométrique et numériques, appliquées respectivement à l'étude de la nage optimale à faible nombre de Reynolds et au transfert orbital d'un satellite dans le cadre de la poussée faible en tenant de perturbations conservatives et minimisant le temps de transfert.
Si les deux études concernent des problèmes physiques très distincts, dans les deux cas le contrôle optimal géométrique est crucial pour notre analyse et utilise des outils communs : principe du maximum, conditions d'optimalité du second ordre, utilisation de méthodes numériques adaptées directes et indirectes et implémentées dans les logiciels `Bocop` et `HamPath`.
D'une façon plus subtile, l'unité repose sur notre méthodologie. Dans le cas du nageur, en supposant par exemple que le déplacement du nageur minimise l'énergie mécanique des forces de trainée, le problème de contrôle optimal devient un problème de géométrie sous-Riemanienne et une des contributions de cette théorie est d'approcher la dynamique optimale par un modèle simplifié fournit par l'approximation nilpotente. Dans le cas du nageur de Purcell, le modèle est plus complexe et cette approximation est cruciale pour calculer les nages optimales à partir de continuations numériques initialisées à l'aide du modèle nilpotent. Dans le cas du transfert orbital, le problème peut se traduire par le problème optimal où « l'énergie » est minimisée ou bien le temps minimal. La dynamique optimale est là encore trop complexe pour être analysée directement, soit analytiquement, soit avec des méthodes numériques. Dans le cadre de la poussée faible, on peut utiliser une approximation fournie par des techniques de moyennisation. L'étude analytique du moyenné se révèle intéressante et permet d'initialiser la continuation des méthodes numériques.

La première partie de ce travail est consacrée au modèle de nage optimale sous l'hypothèse de faible nombre de Reynolds et il s'applique aux micronageurs. Notre étude concerne deux modèles bien spécifiques. Le premier est un modèle de nageur symétrique qui modélise la nage d'une variété de plancton, les copépodes et qui a été introduit récemment par D. Takagi dans un contexte de biologie marine [119]. Ce type de nageur consiste à coller deux coquilles Saint-Jacques et est un des modèles le plus simple contrôlable envisageable. Le second modèle est le modèle historique de E.M. Purcell [109]. En se limitant à des modèles de nageurs formés de tiges minces, on obtient une famille de nageurs facilement réalisables et donc propres à valider nos calculs de contrôle sur des prototypes simples, ce qui est en cours de réalisation en collaboration avec D. Takagi et M. Chyba à l'université d'Hawaii.

S'il existe de nombreuses études sur des modèles de nage pour les micronageurs, **notre contribution se situe entièrement dans le contexte du contrôle optimal**. En effet, c'est le cadre naturel propre à étudier les nages optimales avec une variété de coûts : temps minimal, minimisation de l'énergie, etc... Ici on se limitera

au second critère en considérant l'énergie mécanique dissipée, cette étude étant d'ailleurs équivalente au temps minimal en paramétrant les nages sur un niveau d'énergie fixé. Le contrôle optimal moderne permet de traiter efficacement tous ces problèmes. Les outils classiques sont le principe du maximum de Pontriaguine qui permet de sélectionner les nages optimales extrémales solutions d'une famille d'Hamiltoniens. Les conditions du second ordre sont bien adaptées pour compléter les conditions nécessaires via le concept de point conjugué et les conditions suffisantes via un concept de point focal, toutes deux tenant compte de la spécificité du problème de nage optimale où **le contrôle optimal est périodique**. Aussi le contexte sous-Riemannien est aussi riche pour notre étude, notamment avec la notion d'approximation nilpotente utilisée pour le calcul des brassées optimales de petites amplitudes. Enfin le contrôle optimal a connu le développement de logiciels propres à finaliser notre étude à l'aide de calculs numériques, spécifiquement, on utilisera les méthodes numériques directes et indirectes en contrôle optimal, implémentées dans les logiciels `Bocop` et `HamPath` .

La philosophie de notre approche est bien illustrée par le modèle dit de Heisenberg en géométrie sous-Riemannienne, introduit par Brockett [43] et qui curieusement fournit le modèle de nage le plus simple. Ce problème peut s'interpréter comme le problème classique de Didon en calcul des variations : maximiser la surface limitée par une courbe fermée de longueur fixée et dont les solutions sont des cercles. Ce problème peut se résoudre avec des arguments géométriques en interprétant l'aire comme l'intégrale d'une 1-forme du plan et le contrôle est utilisé pour modifier la courbure. Le point de vue de Brockett est de calculer la solution optimale à partir de l'analyse du flot Hamiltonien extrémal complet, et sans se limiter, *a priori*, aux courbes fermées. Dans ce contexte, le problème se réduit à analyser les trajectoires de ce flot, en utilisant l'intégrabilité et cela conduit à calculer le front d'onde et la boule sous-Riemanienne où on se limite aux solutions optimales. La notion d'optimalité est liée au calcul des points conjugués, une première étape pour en déduire les points cut.

On se propose de développer ce programme pour le cas de nos deux nageurs : le modèle symétrique en dimension 3 et le modèle non symétrique en dimension 5. Notre programme dans le cadre sous-Riemannien est de déterminer les nages optimales qui forment donc, à déplacement fixé, des points de la sphère sous-Riemanienne. In fine, elles fourniront des solutions au problème de minimiser l'efficacité dite géométrique, rapport entre le déplacement et la longueur ou l'efficacité physique, rapport entre l'énergie mécanique et l'énergie fournie pour produire le même déplacement en bloquant la configuration initiale de nage.

Dans le cas des copépodes, l'étude géométrique, complétée par des calculs numériques, fournie une solution complète au problème. En utilisant le principe du maximum on distingue deux types de nage : des triangles correspondant au bord du domaine et formant des extrémales anormales et des nages lisses correspondant aux extrémales normales. Ces dernières forment des courbes lisses soit simples soit avec des points multiples. Le calcul de point conjugué permet de ne conserver que les courbes simples comme candidates à l'optimalité. Les triangles anormaux sont

éliminés en calculant l'efficacité géométrique. Les simulations numériques combinant `Bocop` et `HamPath` conduisent à calculer sur chaque niveau d'énergie une seule courbe simple, certains formant une solution optimale à déplacement fixé et le concept d'efficacité géométrique permet de calculer la nage optimale en un sens la plus efficace.

Le modèle de Purcell est plus complexe car les variables de position sont au nombre de trois : le centre de gravité du corps et son orientation par rapport à une direction de référence. Ici, contrairement au cas des copépodes, le calcul de l'approximation nilpotente est crucial pour déterminer les brassées optimales de petite amplitude. Elles sont formées de courbes simples et de lemniscates de Bernoulli, paramétrées par des fonctions elliptiques. De nouveau le calcul de points conjugués permet de ne conserver que les courbes simples comme candidates à l'optimalité. Les techniques de continuation numériques conduisent à calculer des brassées de plus grande amplitude pour le système réel. Elles sont complétées par une étude géométrique pour étudier les symétries du problème et de conclure sur l'optimalité en utilisant les conditions suffisantes (pour un minimum dit faible).

La seconde partie concerne le transfert orbital à faible poussée en temps minimal en tenant compte de perturbations conservatives. Ici on se limite à l'effet lunaire et le terme en J_2 du potentiel terrestre, qui est la perturbation la plus importante pour les missions courantes. La dynamique contrôlée non moyennée du problème de transfert orbital est obtenue comme une perturbation d'un système intégrable et ce type de système a été étudié par V.I. Arnold. Le modèle considéré est celui du problème à deux corps composé du satellite et de la Terre et perturbé par des forces conservatives correspondant à la perturbation lunaire et/ou à la perturbation résultante des termes de plus haut degré dans le potentiel gravitationnel terrestre. La dynamique obtenue met en jeu des variables x à variation temporelle lente, décrivant la géométrie de l'orbite du satellite et/ou de la Lune, et des variables angulaires φ à variation temporelle rapide, décrivant la position du satellite et/ou de la Lune sur son orbite. Le problème étudié est de considérer les variables lentes x fixées à l'instant initial et final, tandis que la phase φ est libre à ces deux instants.

Dans le cadre de la poussée faible, on peut utiliser les techniques de moyennisation où la dynamique moyennée est celle de la dynamique optimale calculée avec le principe du maximum. L'approche est d'utiliser les techniques de moyennisation, décrites pour un problème de Cauchy, sur le problème aux deux bouts donné par le principe du maximum. On normalise cette dynamique de sorte que le système est écrit en terme de variables (x, p) (p étant l'état adjoint) à variation temporelle lente devant celle de la variable angulaire φ.

Cela conduit à une moyennation simple à une seule fréquence dans le cas non perturbé et à double fréquence si la perturbation lunaire est prise en compte. Nos résultats sont partiels et concernent essentiellement des conditions de convergence entre le moyenné et le non moyenné mais dont l'originalité est de tenir compte des conditions limites aux deux bouts. Le travail est complété par des simulations numériques pour la moyennisation simple et la moyennisation double.

Introduction

Our work is composed of two parts using geometric and numeric optimal control methods, applied respectively to the study of the optimal swimming at low Reynolds numbers and to time minimal orbital transfer problem with periodic conservative perturbations.

If these two studies deal with different physical problems, in both cases, geometric optimal control is crucial for our analysis, especially using the following tools: maximum principle, second order optimality conditions and complemented by numerical methods adapted to the optimal control problem (direct and indirect) which are implemented in the `Bocop` and `HamPath` software.

Our methodology splits the two parts. For the swimming problem, assuming that the displacement of the swimmer minimizes the mechanical energy of the drag forces, the optimal control problem becomes a sub-Riemannian problem and one contribution of this theory is to approximate the optimal dynamic by a simplified one via the nilpotent approximation. For the Purcell swimmer, the model is more intricate and this approximation is crucial to compute optimal strokes from numerical continuation methods initialized from the nilpotent model. For the orbital transfer problem, "the energy" or the final time may be minimized. Again, the optimal dynamic is too complicated to be straightly analyzed, either by analytical methods or by numerical methods. In the framework of low thrust orbital transfer, averaging techniques are used to approximate the optimal dynamic. The analytic study of the averaged dynamic turns out to be interesting and is used to initialize the numerical methods.

For the swimming at low Reynolds numbers, our study involves two swimmer's models. The first model is a symmetric swimmer and it is related to the swimming of a variety of plankton, the copepods. He was introduced by D. Takagi in the framework of marine biology [119]. This model consists in gluing two scallops and is one of the simplest controllable swimmer interesting to study. The second model is the historical model of E.M. Purcell [109]. Both swimmers are modeled by thin rigid links which allow experimental studies to build micro-devices and to validate our computations. This is an ongoing joint work with D. Takagi and M. Chyba from university of Hawaii.

If there exists many works to study these models of swimmers, **our contribution get involved in the framework of optimal control**. Indeed, this is the natural approach to analyze optimal strokes with various cost: minimal final time, energy minimization, etc... We focus here in the latter criterion considering the dissipated mechanical energy, this approach being equivalent to a time minimal problem by reparameterizing strokes on a fixed energy level. The modern techniques in optimal control are adapted to treat these kind of problems efficiently. Classical tools are maximum principle which select extremal strokes, solutions of a family of

Hamiltonian differential equations. Second order optimality conditions are useful to complete necessary conditions via the notion of conjugate point and sufficient condition via the notion of focal point, both taking into account the particularity of the optimal swimming where the **optimal control is periodic**. Also, we use many tools of sub-Riemannian geometry, especially the concept of nilpotent approximation used to compute optimal strokes with small amplitude. Finally, due to the recent development of numerical methods for optimal control problems, we complete our analyze using the software `Bocop` and `HamPath` .

Our approach is motivated by the Heisenberg's model in sub-Riemannian geometry, introduced by Brockett [43] and which provides a simple swimming model. It can be interpreted as the classical problem of Dido in calculus of variations : maximize the area enclosed by a closed curve with fixed length, whose solutions are circles. This problem can be solved using geometric argument where the area is given by integrating a 1-form of the plane. According to Brockett's approach, the optimal solution is computed from the analysis of the complete optimal flow, without restraining it to the closed trajectories. In this context, the problem consists in analyzing trajectories arising from this flow using the integrability properties. It leads to compute the wave front and the sub-Riemannian ball where only optimal solutions are considered. The concept of optimality is related to the computation of conjugate point, a first step to deduce cut points.

This program is developed for the two swimmers: the symmetric model in dimension 3 and the non symmetric one in dimension 5. The purpose is to determine optimal strokes where the displacement of the swimmer is fixed and which are points of the sub-Riemannian ball. In fine, they provide solutions of the problem where we minimize the geometric efficiency, defined as the ratio between the displacement and the length of the stroke or the physical efficiency, defined as the ratio between the mechanical energy and the energy needed to produce the same displacement blocking the initial shape of the swimmer.

The geometric study, completed by numerical computations, lead to a complete solution of the problem. Using the maximum principle, we distinguish two types of stroke: triangles corresponding to the boundary of the domain and standing for abnormal extremals and smooth strokes corresponding to normal extremals. The latter are either simple closed planar curves or curves with multiple points. Conjugate points computation leads to consider only simple curves as candidates for optimality. Abnormal triangles are discarded computing the geometric efficiency. Numerical simulations, combining `Bocop` and `HamPath` , amount to compute a simple curve on each energy level, optimal solution where the displacement is fixed and the concept of geometric efficiency select, among those curves, curves with a better efficiency.

Purcell's model is more sophisticated. Three variables describe the position of the swimmer: the gravity center of the body and its orientation with respect to a reference direction. Contrary to the Copepod's case, computation of the nilpotent approximation is crucial to determine optimal strokes with small amplitude. They correspond to simple curves and Bernoulli's lemniscate, parameterized by elliptic

functions. Again, necessary second order optimality conditions given by conjugate points lead to consider only simple curves as candidates for optimality. Numerical continuation techniques are performed to compute strokes with bigger amplitude for the true system.They are completed by a geometric study of the symmetries of the model and we use sufficient second order optimality conditions to conclude about their optimality (in the weak sense).

The second part concern the time minimal orbital transfer with low thrust taking into account conservative periodic perturbations such as lunar perturbation and the gravitational potential of the Earth ($J2$ effect) which are the most important perturbations for typical orbital transfer. The non averaged dynamic of the optimal control problem is obtained by a perturbation of an integrable system studied by V.I. Arnold. The model is the two-body problem composed by the satellite and the Earth which is perturbed by a conservative force written as the disturbing potential of the Moon and/or the disturbing potential of the Earth where higher order terms are considered (J_2-effect). The resulting dynamic is given in terms of variables (x, φ) where x has a slow time evolution and it describes the geometry of the orbit of the satellite and the Moon, while φ is an angular variable with fast time evolution and it corresponds to the position of the satellite and the Moon on their orbits. We consider the problem where the initial and final value of x are fixed while those of φ are free.

Due to the periodicity of the system, we use averaging techniques. The averaged dynamic is obtained by averaging the dynamic given by the maximum principle. The approach is to use averaging techniques, described for a Cauchy problem, on the boundary value problem given by the maximum principle. We reduce the dynamic such that the system is written in terms of the variables (x, p) (p being the adjoint vector) which have a slow time evolution compared to the time evolution of the angular variable φ.

It leads to averaging with respect to one frequency in the non perturbed case and double averaging if the lunar perturbation is taken into account. Our results are partial and are related to convergence theorems between the averaged system and the non averaged system in the case of boundary value problems. These theoretical results are completed by numerical simulations for the single and double averaging.

Remerciements

Mes premiers remerciements vont à mes deux directeurs de thèse Bernard Bonnard et Jean-baptiste Pomet. Merci Bernard, bien plus qu'un directeur de thèse, il m'a été une source d'inspiration scientifique et aussi humaine. J'ai beaucoup bénéficié de son expérience, et sa vision pragmatique sur des problèmes physiques m'ont ouvert l'esprit pour continuer dans la voie de la recherche. Qu'il reçoive toute ma gratitude et mes amitiés. Durant chaque semaine passée à Sophia, j'ai apprécié le travail avec Jean-Baptiste, sa rigueur scientifique m'a beaucoup apportée. Merci pour sa générosité et pour m'avoir guidé tout au long de cette thèse. Des remerciements tout aussi sincères à Piernicola Bettiol et Jean-Baptiste Caillau. Quel plaisir d'échanger avec de telles personnes tant sur le plan scientifique que relationnel. Votre aide a grandement contribué à ce travail, je vous suis redevable. De plus, je salue le suivi sérieux et le partage d'informations pour un cours, un séminaire, une conférence... de Jean-Baptiste Caillau tout au long de cette thèse.

Je voudrais remercier Ugo Boscain, Directeur de Recherche au CNRS et Emmanuel Trélat, Professeur à l'Université Paris VI d'avoir accepté d'être les rapporteurs de ma thèse ainsi que François Alouges, Professeur à l'École Polytechnique, Piernicola Bettiol, Professeur à l'Université de Bretagne Occidentale, Richard Epenoy, Ingénieur au CNES de Toulouse et Marius Tucsnak, Professeur à l'Université de Bordeaux de faire partie de mon jury. C'est un grand honneur pour moi.

Les conseils de Thierry Dargent et Richard Epenoy, notamment sur les résulats numériques de la partie spatiale ont été d'une aide précieuse, j'en suis reconnaissant. Par le biais de Bernard qui a pu le rencontrer, je remercie Daisuke Takagi pour nous avoir présenté le modèle de ces curieux copépodes. La collaboration qui y est née, avec Monique Chyba et Zhu Rong, fut une expérience très positive, je regrette ne pas avoir pu participer à l'élaboration pratique de ce premier prototype...

Merci à tous les membres de l'équipe McTAO, avec une pensée particulière à Christel pour avoir éradiquer tout souci administratif et qui avait le dynamisme pour le bien de l'équipe. À Olivier Cots, maintenant à l'ENSEEIHT, pour le développement du logiciel `HamPath` . Au sein de l'IMB, j'aimerais remercier Abdelaziz et sa bonne humeur généreuse, Francis pour nos discussions outre maths et Caroline pour... Caroline. Je salue la bonne ambiance et l'intérêt porté à notre séminaire hebdomadaire des étudiants, ces rencontres avec des doctorants d'autres horizons ont été très enrichissantes. Les fredaines, menées sagement par la camaraderie des doctorants, laisseront d'excellents souvenirs, merci à vous tous (avec un message publicitaire pour notre bière légèrement maltée, « la Fond d'tonneau »).

Une pensée particulière aux affreux haut marnais... que nos apéros-sportifs puissent perdurer. À ma famille qui s'est agrandit, je vous embrasse... qu'il était bon de revenir parmi vous, sur notre petite colline où il fait bon d'y vivre. Enfin, merci Céleste.

Contents

I Swimming at low Reynolds number **1**

1 Swimming problem formulation **3**
1.1 Bibliographical Note . . . 3
1.2 The Copepod swimmer . . . 3
1.2.1 Model . . . 3
1.2.2 Classification of periodic planar curves . . . 5
1.3 The Three-link Purcell swimmer . . . 5
1.4 The swimming problem as an optimal control problem . . . 10

2 Necessary and sufficient optimality conditions **13**
2.1 Pontryagin Maximum Principle . . . 13
2.1.1 Application to the swimming problems. . . . 14
2.2 Second order conditions . . . 15
2.2.1 Necessary conditions . . . 15
2.2.2 Sufficient conditions . . . 17

3 Concepts of sub-Riemannian geometry **21**

4 Numerical methods for optimal control **27**
4.1 General methods in optimal control . . . 27
4.2 Direct method in the `Bocop` software . . . 28
4.3 Indirect method in the `HamPath` software . . . 28
4.3.1 The simple shooting . . . 28
4.4 Homotopic method in optimal control . . . 30
4.4.1 Discrete homotopy . . . 31
4.4.2 Differential homotopy . . . 31
4.4.3 Application to the Purcell swimmer . . . 31

5 The Purcell Three-link swimmer **33**
5.1 Description of the contributions of the article: The Purcell Three-link swimmer: some geometric and numerical aspects related to periodic optimal controls. . . . 34
5.2 The Purcell Three-link swimmer: some geometric and numerical aspects related to periodic optimal controls . . . 35
5.3 Introduction . . . 35
5.4 First and second order optimality conditions . . . 37
5.5 The Purcell Three-link swimmer . . . 39
5.5.1 Mathematical Model . . . 39
5.6 Local analysis for the three-link Purcell swimmer . . . 41
5.6.1 Computations of the nilpotent approximation . . . 41

5.6.2 Integration of extremal trajectories . . . 43
5.7 Numerical results . . . 49
5.7.1 Nilpotent approximation . . . 50
5.7.2 True mechanical system . . . 52
5.7.3 The Purcell swimmer in a round swimming pool . . . 55
5.8 Conclusions and future work . . . 56

6 Optimal strokes at low Reynolds number for the Copepod and the Purcell swimmers 59
6.1 Description of the article: Optimal strokes at low Reynolds number for the Copepod and the Purcell swimmers . . . 60
6.2 Optimal strokes at low Reynolds number: a geometric and numeric study using the Copepod and Purcell swimmers. . . . 62
6.3 Introduction . . . 62
6.4 Generalities . . . 64
6.4.1 The mathematical model . . . 64
6.4.2 Elements of sub-Riemannian geometry . . . 66
6.4.3 `Bocop` and `HamPath` software . . . 69
6.5 The Copepod swimmer . . . 70
6.5.1 Abnormal curves in the copepod swimmer . . . 71
6.5.2 The normal case . . . 73
6.6 The Three-Link Purcell swimmer . . . 81
6.6.1 Symmetry properties . . . 81
6.6.2 Nilpotent approximation . . . 82
6.6.3 Numerical results . . . 89
6.6.4 Sufficient second order conditions for the Purcell strokes . . . 94
6.7 Conclusion . . . 97

II Averaging for the orbital transfer problem with low thrust 99

7 Preliminairies 101
7.1 Controlled two-body (Newtonian) problem . . . 101
7.2 Two body problem . . . 102
7.3 Lagrange and Gauss equations . . . 103
7.3.1 The Lagrange equations . . . 104
7.3.2 The Gauss equations . . . 105
7.4 Gravitational perturbations . . . 106
7.4.1 Gravitational potential of the Moon . . . 106
7.4.2 Gravitational potential of the Earth . . . 110
7.4.3 Problem formulation of the minimal time control problem . . . 111
7.5 Averaging principle in perturbation theory . . . 112

8 Averaging and Pontryagin maximum principle **117**
8.1 Non averaged extremal system 117
8.2 Averaging extremals 119
8.2.1 Preparation for averaging 119
8.2.2 Averaged dynamic for a single frequency 121
8.2.3 Pulsation depending upon the fast angular variable 123
8.2.4 Case of several frequencies 125
8.3 Convergence theorems for the boundary value problems 127
8.3.1 The non averaged and averaged boundary value problem . . . 127
8.3.2 Convergence theorems 128

9 Numerical results **133**
9.1 Description of the simulated problems 133
9.1.1 Initialization of the non averaged shooting algorithm 134
9.1.2 Commented numerical results 134
9.2 Numerical conjecture 138
9.2.1 Simple averaging 138
9.2.2 Double averaging 141

Bibliography **145**

Conclusion **153**

Part I

Swimming at low Reynolds number

Chapter 1

Swimming problem formulation

Contents

1.1 Bibliographical Note . . . 3
1.2 The Copepod swimmer . . . 3
1.2.1 Model . . . 3
1.2.2 Classification of periodic planar curves . . . 5
1.3 The Three-link Purcell swimmer . . . 5
1.4 The swimming problem as an optimal control problem . . . 10

1.1 Bibliographical Note

There exists a large amount of references related to the problem of microswimmers and we indicate only a few of them.

The model can be derived in all generality from [74] but in the case of N-slender rigid links, [104] provided a neat model which is suitable to computations. From the physical point of view, seminal references are [86, 92, 109]. In relation with recent studies, we must cite the two Ph.D. theses [66, 93] and related references of F. Alouges and M. Tucsnak co-workers. In relation with geometric optimal control, preliminary references are [53, 95].

1.2 The Copepod swimmer

1.2.1 Model

In [119], D. Takagi introduces the so-called Copepod swimmer model, roughly composed by N scallops to obtain a swimmer composed by N symmetric rigid links. We are interested in periodic deformation of the shape variables, called a stroke, which produces a displacement along the axis (Ox). For a Copepod with N symmetric rigid links of length l, the velocity of the displacement is given by

$$\dot{x} = \frac{\sum_{i=1}^{N} l^2\, \dot{\theta}_i \sin(\theta_i)}{n + \sum_{i=1}^{N} \sin^2(\theta_i)} \tag{1.1}$$

where $\theta = (\theta_i)_{i=1\dots N}$ is the shape variable and x the position of the center, see Fig.1.1.

Remark 1.1. *We recover the result of Purcell for a scallop swimmer. For such swimmer, the velocity is given by*

$$\dot{x} = \frac{\dot{l}\,\theta \sin(\theta)}{1 - \cos^2(\theta)} \tag{1.2}$$

By integration over a period T of the shape variable, we get $x(T) - x(0) = 0$ (a scallop cannot swim).

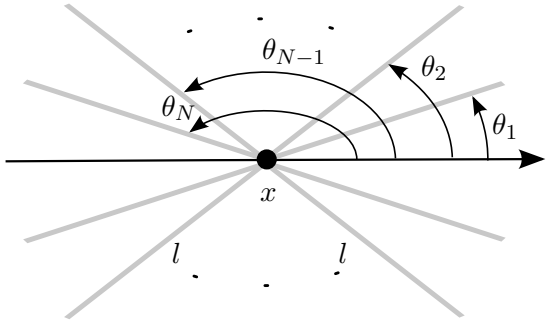

Figure 1.1: Sketch of the N-link symmetric Copepod swimmer.

Symmetric two-link swimmer. Limiting to the symmetric two-link swimmer, the dynamic of $\theta_i,\ i = 1, 2$ is given by $\dot{\theta}_i = u_i,\ i = 1, 2$ where $u_i,\ i = 1, 2$ are the controls parameterizing the solutions. To avoid collisions between arms, we have the state constraint $0 \leq \theta_1, \theta_2 \leq \pi$, forming a triangle in the $(\theta_1, \theta_2)-$ space.
To define an optimal control problem, we introduce a cost that the swimmer should minimize. Usually, the swimmer moves differently depending upon its activities: following other copepods, hunting, being hunted... An interesting problem is to consider that it minimizes the work of drag forces. It amounts to define the mechanical energy as $q^\intercal M q$ where $q = (x, \theta_1, \theta_2)$ and M is the symmetric positive-definite matrix

$$M = \begin{pmatrix} 2 - 1/2(\cos^2(\theta_1) + \cos^2(\theta_2)) & -1/2\sin(\theta_1) & -1/2\sin(\theta_2) \\ -1/2\sin(\theta_1) & 1/3 & 0 \\ -1/2\sin(\theta_2) & 0 & 1/3 \end{pmatrix}$$

that is to minimize the quadratic cost

$$\int_0^T \left(a_{11}(q)u_1^2 + 2a_{12}(q)u_1u_2 + a_{22}(q)u_2^2\right) \mathrm{d}t \tag{1.3}$$

where

$$\begin{aligned} a_{11} &= \frac{1}{3} - \frac{\sin^2\theta_1}{2(2+\sin^2\theta_1+\sin^2\theta_2)}, \\ a_{12} &= -\frac{\sin\theta_1\sin\theta_2}{2(2+\sin^2\theta_1+\sin^2\theta_2)}, \\ a_{22} &= \frac{1}{3} - \frac{\sin^2\theta_2}{2(2+\sin^2\theta_1+\sin^2\theta_2)} \end{aligned} \tag{1.4}$$

and T is the fixed period of the shape deformation. It can be fixed to any value since we are dealing with a sub-Riemannian problem.

1.2.2 Classification of periodic planar curves

Our work is related to the classification of closed planar curves up to diffeomorphisms described for instance in [13] and [23]. Basic invariants of the classification are

- number of doubles points,
- the rotation's index K equals to the number of full rotations of the tangent vector that is

$$K := \frac{1}{T}\int_0^T \frac{\dot\theta_1\ddot\theta_2 - \dot\theta_2\ddot\theta_1}{(\dot\theta_1^2+\dot\theta_2^2)}\mathrm{d}t.$$

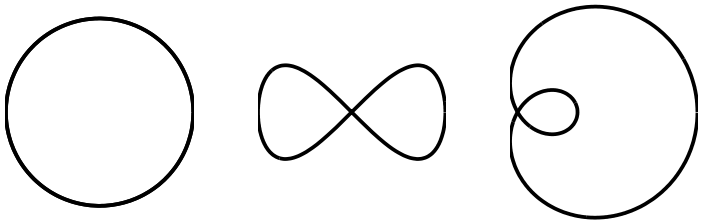

Figure 1.2: The simple loop, the lemniscate of Bernoulli and the limaçon with inner loop.

Our study is related mainly to the curves described in Fig.1.2 in relation with the model of strokes.

1.3 The Three-link Purcell swimmer

In his historical paper [109], E.M. Purcell gives a more complicated model with 2 degree of motions and composed by 3 rigid links. The state variables is of dimension 5, θ_1, θ_2 being the shape variables, x, y being the position variables and α being the orientation variable (see Fig.1.3).

The configuration of the swimmer is described by two angles $\theta = (\theta_1, \theta_2)$ with three position variables $q = (x, y, \alpha)$ representing respectively the position and the

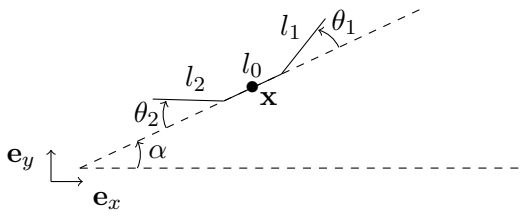

Figure 1.3: Model of the Tree-Link Purcell swimmer.

orientation of the body. The system can be written as

$$\dot{q} = D(\alpha)G(\theta)\dot{\theta},$$
$$\dot{\theta} = H(\theta)\tau,$$

where $D(\alpha)$ is the rotation matrix

$$D(\Phi) = \begin{pmatrix} \cos(\alpha) & -\sin(\alpha) & 0 \\ \sin(\alpha) & \cos(\alpha) & 0 \\ 0 & 0 & 1 \end{pmatrix}.$$

The matrix G is given by $G_{ij} = g_{ij}/\Delta G$, $i = 1 \dots 3$, $j = 1, 2$ (see [104]) where

- $\Delta G = l_1 l_2 (l_0{}^3 + 4 l_1{}^3 + 4 l_2{}^3) \cos(2\theta_1 + 2\theta_2) - 3 l_0{}^3 l_1 l_2 \cos(2\theta_1 - 2\theta_2) - 12 l_0{}^2 l_1 l_2 \cos(2\theta_1 - \theta_2) + 12 l_0 l_1{}^2 l_2 (l_0 + 2l_1) \cos(\theta_1 + 2\theta_2) + 12 l_0 l_1 l_2 (2 l_2{}^2 + l_0) \cos(2\theta_1 + \theta_2) - 12 l_0{}^2 l_1{}^2 l_2 \cos(\theta_1 - 2\theta_2) - 24 l_0 l_1{}^2 l_2 \cos(\theta_1 - \theta_2) + 72 l_2 l_1{}^2 (2/3 l_2{}^2 + l_0 + 2/3 l_1) \cos(\theta_1 + \theta_2) + 8 l_1 l_0 (l_0{}^3 + 9/2 l_0{}^2 l_2 + l_1{}^3 - 2 l_2{}^3 + 6 l_0 l_2)(\cos(\theta 1))^2 + 48 l_1{}^2 l_0 (l_0{}^2 + (l_1 + 3l_2) l_0 + 3/2 l_1 l_2 + 2 l_2) \cos(\theta_1) + 8 l_2 l_0 (l_0{}^3 + 9/2 l_0{}^2 l_1 + 6 l_0 l_1{}^2 - 2 l_1{}^3 + l_2{}^3)(\cos(\theta_2))^2 + 48 l_1{}^2 (l_0{}^2 + (l_2{}^2 + 3l_1) l_0 + 3/2 l_1 l_2{}^2 + 2 l_1{}^2) l_0 \cos(\theta_2) + 8 l_0{}^5 + (32 l_1 + 32 l_2) l_0{}^4 + (32 l_1{}^2 + 90 l_1 l_2 + 32 l_2) l_0{}^3 + (32 l_1{}^3 + 48 l_1{}^2 l_2 + 32 l_2{}^3 + 48 l_1 l_2) l_0{}^2 + (32 l_1{}^4 + 80 l_1{}^3 l_2 + 80 l_1 l_2{}^3 + 32 l_2{}^4) l_0 + 8 l_1{}^5 + 36 l_1{}^4 l_2 + 32 l_1{}^2 l_2{}^3 + 36 l_1 l_2{}^4 + 8 l_2{}^5 + 32 l_1{}^3 l_2,$

- $g_{11} = 8 l_1{}^2 (1/4 l_0 l_1{}^2 l_2 \sin(2\theta_1 + 2\theta_2) + 9/2 (1/3 l_2{}^2 + l_0 + 2/3 l_1) l_0 l_2 \sin(\theta_1 - \theta_2) + 1/4 l_2 (-2 l_2{}^3 + l_0{}^2 (l_0 + 3l_1)) \sin(\theta_1 + 2\theta_2) + 3/4 l_0{}^2 l_2 (l_1 + l_0) \sin(\theta_1 - 2\theta_2) + 1/2 l_1{}^2 l_2 \sin(2\theta_1 + \theta_2) + 3/2 l_0 l_2 (-l_2{}^2 + l_0 + 2l_1) \sin(\theta_1 + \theta_2) + 1/2 (l_0 + 3/2 l_2) l_1{}^2 l_0 \sin(2\theta_1) - l_1 (l_0 + 3/4 l_1) l_0 l_2 \sin(2\theta_2) + (3/2 l_2{}^4 + (4l_0 + 2l_1) l_2{}^3 + 3 l_0{}^2 (3/2 l_1 + l_0) l_2 + l_0{}^3 (l_0 + 2l_1)) \sin(\theta_1) - 4 (1/2 l_2{}^2 + l_0 + 3/8 l_1) l_1 l_2 \sin(\theta_2)),$

- $g_{21} = -4 (9/2 l_2 l_0 (2/3 l_2{}^2 + l_0 + 4/3 l_1) \cos(\theta_1 - \theta_2) + 3/4 l_0{}^2 l_2 (l_0 + 2l_1) \cos(\theta_1 - 2\theta_2) + (1/4 l_0{}^3 l_2 + l_2{}^4) \cos(\theta_1 + 2\theta_2) + l_1{}^2 l_2 \cos(2\theta_1 + \theta_2) + 9/2 (4/3 l_2{}^2 + l_0 + 2/3 l_1) l_2 l_0 \cos(\theta_1 + \theta_2) + 1/2 l_0 l_1{}^2 (l_0 + 3l_2) \cos(2\theta_1) + l_0 l_1 l_2 (3/2 l_1 + l_0) \cos(2\theta_2) + (3 l_2{}^4 + (4l_0 + 4l_1) l_2{}^3 + 6 (3/4 l_1 + l_0 + 1) l_0{}^2 l_2 + l_0{}^3 (l_0 + l_1)) \cos(\theta_1) - 3/2 (-8/3 (l_2{}^2 + l_0 + 3/4 l_1) l_2 \cos(\theta_2) + ((-2l_0 - 8/3) l_2 + l_1 (l_0 + 2/3 l_1)) l_0) l_1) l_1{}^2,$

- $g_{31} = -24 (1/6 l_1{}^2 l_2 \cos(2\theta_1 + 2\theta_2) + 1/4 l_0 l_2 (l_0 + 2l_1) \cos(\theta_1 + 2\theta_2) - 1/4 l_0{}^2 l_2 \cos(\theta_1 - 2\theta_2) - 1/2 l_0 l_2 \cos(\theta_1 - \theta_2) + 3/2 (2/3 l_2{}^2 + l_0 + 2/3 l_1) l_2 \cos(\theta_1 +$

$\theta_2) + 1/3 l_0 {l_1}^2 (\cos(\theta_1))^2 + ({l_0}^2 + (l_1 + 3l_2)l_0 + (3/2l_1 + 2)l_2)l_0 \cos(\theta_1) + 4/3(-1/2 l_0 l_2 (\cos(\theta_2))^2 + {l_0}^2 + (l_1 + 5/2 l_2)l_0 + (\frac{9l_1}{8} + 1)l_2 + 1/4 {l_1}^2) l_1 {l_1}^2$.

Seeing g_{11}, g_{21}, g_{31} as a function of $(\theta_1, \theta_2, l_1, l_2)$, we have

- $g_{12} = -g_{11}(\theta_2, \theta_1, l_2, l_1)$,
- $g_{22} = g_{21}(\theta_2, \theta_1, l_2, l_1)$,
- $g_{32} = -g_{31}(\theta_2, \theta_1, l_2, l_1)$.

By denoting $u = \dot{\theta} = (\dot{\theta}_1, \dot{\theta}_2) = (u_1, \quad u_2)^\intercal$, the mechanical power is

$$\tau u = u^\intercal H^{-1} u$$

and the energy minimization problem becomes

$$\int_0^T (u^\intercal W u) \mathrm{d}t, \text{ where } W := H^{-1}. \tag{1.5}$$

Again, from [104], we have the following expressions: $W_{ij} = w_{ij}/\Delta W, \ i, j = 1, 2$ where

- $\Delta W = 3 l_1 l_2 ({l_0}^3 + 4{l_1}^3 + 4{l_2}^3) \cos(2\theta_1 + 2\theta_2) - 9{l_0}^3 l_1 l_2 \cos(2\theta_1 - 2\theta_2) - 36{l_0}^2 l_1 l_2 \cos(2\theta_1 - \theta_2) + 36 l_0 {l_1}^2 l_2 (2l_1 + l_0) \cos(\theta_1 + 2\theta_2) + 36 l_0 l_1 l_2 (2{l_2}^2 + l_0) \cos(2\theta_1 + \theta_2) - 36{l_0}^2 {l_1}^2 l_2 \cos(\theta_1 - 2\theta_2) - 72 l_0 {l_1}^2 l_2 \cos(\theta_1 - \theta_2) + 12({l_0}^3 + 9/2 l_2 {l_0}^2 + {l_1}^3 - 2{l_2}^3 + 6 l_0 l_2) l_1 l_0 \cos(2\theta_1) + 12({l_0}^3 + 9/2 {l_0}^2 l_1 + 6 l_0 {l_1}^2 - 2{l_1}^3 + {l_2}^3) l_2 l_0 \cos(2\theta_2) + 216(2/3 {l_2}^2 + l_0 + 2/3 l_1) {l_1}^2 l_2 \cos(\theta_1 + \theta_2) + 144 {l_1}^2 ({l_0}^2 + (l_1 + 3l_2)l_0 + 3/2 l_1 l_2 + 2l_2) l_0 \cos(\theta_1) + 144({l_0}^2 + ({l_2}^2 + 3l_1)l_0 + 3/2 l_1 {l_2}^2 + 2{l_1}^2) l_2 l_0 \cos(\theta_2) + 24{l_0}^5 + (108 l_1 + 108 l_2){l_0}^4 + (96{l_1}^2 + 378 l_1 l_2 + 96 l_2){l_0}^3 + (96{l_1}^3 + 216{l_1}^2 l_2 + 96{l_2}^3 + 216 l_1 l_2){l_0}^2 + (108{l_1}^4 + 216{l_1}^3 l_2 + 216 l_1 {l_2}^3 + 108{l_2}^4) l_0 + 24{l_1}^5 + 108{l_1}^4 l_2 + 96{l_1}^2 {l_2}^3 + 108 l_1 {l_2}^4 + 24{l_2}^5 + 96{l_1}^3 l_2$,
- $w_{11} = 3(-1/3 l_1 l_2 ({l_0}^3 + 4{l_2}^3) \cos(2\theta_1 + 2\theta_2) + {l_0}^3 l_1 l_2 \cos(2\theta_1 - 2\theta_2) + 4{l_0}^2 l_1 {l_2}^2 \cos(2\theta_1 - \theta_2) - 4 l_0 l_1 {l_2}^2 (l_0 + 2l_2) \cos(2\theta_1 + \theta_2) - 4/3 l_0 ({l_0}^3 + 9/2 l_2 {l_0}^2 + 6{l_2}^2 l_0 - 2{l_2}^3) l_1 \cos(2\theta_1) + 8/3 l_2 l_0 ({l_0}^3 + 9/4 {l_0}^2 l_1 + 3/2 l_0 {l_1}^2 + {l_2}^3) \cos(2\theta_2) + 32{l_2}^2 l_0 ({l_0}^2 + (3/2 l_1 + l_2)l_0 + 1/2(l_1 + 3/2 l_2) l_1) \cos(\theta_2) + 16/3 {l_0}^5 + (12 l_1 + 24 l_2){l_0}^4 + (16/3 {l_1}^2 + \frac{64{l_2}^2}{3} + 42 l_1 l_2){l_0}^3 + (\frac{64{l_2}^3}{3} + 24 l_1 {l_2}^2 + 12{l_1}^2 l_2) {l_0}^2 + 24{l_2}^3 (l_1 + l_2) l_0 + 12 l_1 {l_2}^4 + 16/3 {l_1}^2 {l_2}^3 + 16/3 {l_2}^5) {l_1}^3 c_t$,
- $w_{12} = 8{l_2}^2 (3/4 {l_0}^2 {l_1}^2 \cos(2\theta_1 - \theta_2) - 1/2 {l_1}^2 {l_2}^2 \cos(2\theta_1 + 2\theta_2) + 3({l_0}^2 + (3/2 l_1 + 3/2 l_2) l_0 + 3/2 l_1 l_2) {l_0}^2 \cos(\theta_1 - \theta_2) - 3/4 l_0 {l_2}^2 (2l_1 + l_0) \cos(\theta_1 + 2\theta_2) - 3/4 l_0 {l_1}^2 (l_0 + 2l_2) \cos(2\theta_1 + \theta_2) + 3/4 {l_0}^2 {l_2}^2 \cos(\theta_1 - 2\theta_2) - 3/2 {l_0}^2 ((l_1 + l_2)l_0 + 3 l_1 l_2) \cos(\theta_1 + \theta_2) + l_0 {l_1}^2 l_2 \cos(2\theta_1) + l_0 l_1 {l_2}^2 \cos(2\theta_2) + 6 l_2 l_0 ({l_0}^2 + (l_1 + 3/2 l_2) l_0 + 3/4 l_2 (l_1 + 2/3 l_2)) \cos(\theta_1) + 6(l_0 ({l_0}^2 + (3/2 l_1 + l_2) l_0 + 1/2(l_1 + 3/2 l_2) l_1) \cos(\theta_2) + 4/3 l_2 ({l_0}^2 + (\frac{9l_1}{8} + \frac{9l_2}{8}) l_0 + 1/4 {l_1}^2 + \frac{9 l_1 l_2}{16} + 1/4 {l_2}^2)) l_1 {l_1}^2 c_t$,
- $w_{21} = w_{12}$.

Seeing w_{11} as a function of $(\theta_1, \theta_2, l_1, l_2)$, we have

- $w_{22} = w_{11}(\theta_2, \theta_1, l_2, l_1)$.

In our work, we set $l_0 = 2$, $l_1 = l_2 = 1$, $c_t = 1$, ($c_n = 2, c_t = 2$) and the expressions of the controlled vector fields are simpler. Indeed, writing the dynamics as (see [24])

$$\dot{q} = u_1 F_1(q) + u_2 F_2(q) \text{ where } q = (\theta_1, \theta_2, x, y, \alpha), \tag{1.6}$$

we have the following expressions

$$F_1 = \begin{pmatrix} 1 & 0 & f_{13} & f_{14} & f_{15} \end{pmatrix}^\intercal, F_2 = \begin{pmatrix} 0 & 1 & f_{23} & f_{24} & f_{25} \end{pmatrix}^\intercal \tag{1.7}$$

where
$\delta = 336\cos(\theta_1-\theta_2) + 84\cos(2\theta_1) - 24\cos(\theta_1+2\theta_2) - 48\cos(\theta_1+\theta_2) + 816\cos(\theta_2) + 72\cos(-2\theta_2+\theta_1) + 816\cos(\theta_1) - 6\cos(2\theta_1+2\theta_2) + 18\cos(-2\theta_2+2\theta_1) + 84\cos(2\theta_2) - 24\cos(2\theta_1+\theta_2) + 72\cos(-\theta_2+2\theta_1) + 1692$
in

- $f_{13} = 1/\delta\big(4\sin(\alpha-2\theta_2) - \sin(\alpha+2\theta 2-\theta_1) + 18\sin(\alpha-\theta_1-\theta_2) + 3\sin(\alpha-\theta_1-2\theta_2) + 2\sin(\alpha-2\theta_1+2\theta_2) - 9\sin(\alpha+\theta_1-2\theta_2) - 21\sin(\alpha+\theta_1+2\theta_2) - 126\sin(\alpha+\theta_1+\theta_2) - 30\sin(\alpha-\theta_1+\theta_2) - 2\sin(\alpha+2\theta_1-2\theta_2) + 2\sin(\alpha-2\theta_1) - 78\sin(\alpha+\theta_1-\theta_2) + 16\sin(\alpha-\theta_2) - 104\sin(\alpha+\theta_2) - 8\sin(\alpha+2\theta_1-\theta_2) - 24\sin(\alpha+2\theta_2) - 18\sin(\alpha+2\theta_1) - 36\sin(\alpha) - 262\sin(\alpha+\theta_1) + 26\sin(\alpha-\theta_1)\big)$,

- $f_{14} = 1/\delta\big(18\cos(\alpha+2\theta_1) + 24\cos(\alpha+2\theta_2) + 30\cos(\alpha-\theta_1+\theta_2) - 3\cos(\alpha-\theta_1-2\theta_2) + 126\cos(\alpha+\theta_1+\theta_2) + 78\cos(\alpha+\theta_1-\theta_2) - 18\cos(\alpha-\theta_1-\theta_2) + 21\cos(\alpha+\theta_1+2\theta_2) + 9\cos(\alpha+\theta_1-2\theta_2) - 26\cos(\alpha-\theta_1) + 104\cos(\alpha+\theta_2) - 16\cos(\alpha-\theta 2) + 8\cos(\alpha+2\theta_1-\theta_2) - 4\cos(\alpha-2\theta_2) + 36\cos(\alpha) + 262\cos(\alpha+\theta_1) + \cos(\alpha+2\theta_2-\theta_1) - 2\cos(\alpha-2\theta_1) - 2\cos(\alpha-2\theta_1+2\theta_2) + 2\cos(\alpha+2\theta_1-2\theta_2)\big)$,

- $f_{15} = 1/\delta\big(-216 - 4\cos(2\theta_1) + 6\cos(\theta_1+2\theta_2) + 12\cos(\theta_1+\theta_2) - 204\cos(\theta_1) - 18\cos(-2\theta_2+\theta_1) - 84\cos(\theta_1-\theta_2) - 4\cos(-2\theta_2+2\theta_1) + 8\cos(2\theta_2)\big)$,

- $f_{23} = 1/\delta\big(-2\sin(\alpha+2\theta_1-2\theta_2) + 21\sin(\alpha+\theta_2+2\theta_1) + 9\sin(\alpha+\theta_2-2\theta_1) + 2\sin(\alpha-2\theta_1+2\theta_2) + 30\sin(\alpha+\theta_1-\theta_2) + 8\sin(\alpha+2\theta_2-\theta_1) - 2\sin(\alpha-2\theta_2) - 3\sin(\alpha-\theta_2-2\theta_1) - 18\sin(\alpha-\theta_1-\theta_2) + 126\sin(\alpha+\theta_1+\theta 2) + 78\sin(\alpha-\theta_1+\theta_2) + \sin(\alpha+2\theta_1-\theta_2) + 262\sin(\alpha+\theta_2) + 104\sin(\alpha+\theta_1) - 4\sin(\alpha-2\theta_1) - 16\sin(\alpha-\theta_1) - 26\sin(\alpha-\theta_2) + 24\sin(\alpha+2\theta_1) + 18\sin(\alpha+2\theta_2) + 36\sin(\alpha)\big)$,

- $f_{24} = 1/\delta\big(4\cos(\alpha-2\theta_1) - 24\cos(\alpha+2\theta_1) + 2\cos(\alpha-2\theta_2) - 18\cos(\alpha+2\theta_2) + 26\cos(\alpha-\theta_2) + 16\cos(\alpha-\theta_1) - \cos(\alpha+2\theta_1-\theta_2) - 8\cos(\alpha+2\theta_2-\theta_1) - 36\cos(\alpha) + 2\cos(\alpha+2\theta_1-2\theta_2) - 30\cos(\alpha+\theta_1-\theta_2) - 21\cos(\alpha+\theta_2+2\theta_1) - 126\cos(\alpha+\theta_1+\theta_2) -$

$78\cos(\alpha-\theta_1+\theta_2) + 3\cos(\alpha-\theta_2-2\theta_1) - 9\cos(\alpha+\theta_2-2\theta_1) + 18\cos(\alpha-\theta_1-\theta_2) - 2\cos(\alpha-2\theta_1+2\theta_2) - 104\cos(\alpha+\theta_1) - 262\cos(\alpha+\theta_2)\big)$,

. $f_{25} = 1/\delta\big(-216+8\cos(2\theta_1)+12\cos(\theta_1+\theta 2)+6\cos(2\theta_1+\theta_2) - 18\cos(2\theta_1-\theta_2) - 204\cos(\theta_2) - 4\cos(-2\theta_2+2\theta_1) - 84\cos(\theta_1-\theta 2) - 4\cos(2\theta_2)\big)$.

Also, with the same normalization ($l_0=2$, $l_1=l_2=1$, $c_t=1$) the cost function (1.5) is written as

$$\int_0^T (b_{11}u_1^2 + 2\,b_{12}u_1u_2 + b_{22}u_2^2)\mathrm{d}t \tag{1.8}$$

where

$\kappa = -12\cos(2\theta_1+2\theta_2) - 222\cos(2\theta_1) - 3258 - 1116\cos(\theta_2) - 222\cos(2\theta_2) + 18\cos(-2\theta_2+2\theta_1) - 72\cos(2\theta_1+\theta_2) + 36\cos(2\theta_1-\theta_2) - 1116\cos(\theta_1) + 36\cos(\theta_1-\theta_2) + 36\cos(-2\theta_2+\theta_1) - 72\cos(\theta_1+2\theta_2) - 180\cos(\theta_1+\theta_2)$
in

- $b_{11} = 1/\kappa\big(3\cos(2\theta_1+2\theta_2) - 6\cos(-2\theta_2+2\theta_1) - 12\cos(2\theta_1-\theta_2) + 24\cos(2\theta_1+\theta_2) + 72\cos(2\theta_1) - 84\cos(2\theta_2) - 492\cos(\theta_2) - 1233\big)$,

- $b_{12} = 1/\kappa\big(\cos(2\theta_1+2\theta_2) - 246\cos(\theta_1) - 246\cos(\theta_2) + 12\cos(2\theta_1+\theta_2) - 6\cos(2\theta_1-\theta_2) + 12\cos(\theta_1+2\theta_2) + 84\cos(\theta_1+\theta_2) - 276\cos(\theta_1-\theta_2) - 6\cos(-2\theta_2+\theta_1) - 4\cos(2\theta_2) - 4\cos(2\theta_1) - 153\big)$,

- $b_{22} = 1/\kappa\big(3\cos(2\theta_1+2\theta_2) - 492\cos(\theta_1) - 6\cos(-2\theta_2+2\theta_1) + 24\cos(\theta_1+2\theta_2) - 12\cos(-2\theta_2+\theta 1) + 72\cos(2\theta_2) - 84\cos(2\theta_1) - 1233\big)$.

A geometric stroke In Fig.1.4 we give an example of stroke for the Purcell swimmer that produces a displacement which was given in the historical paper of Purcell [109].

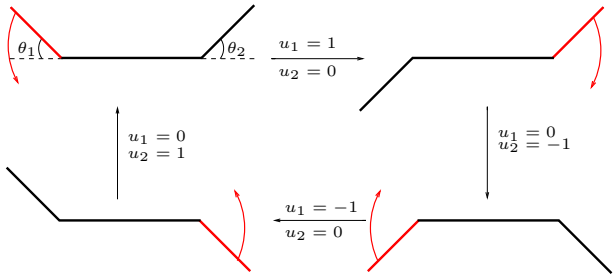

Figure 1.4: Purcell stroke.

The Copepod swimmer and the Purcell swimmer can be expressed as

$$\dot{q} = u_1F_1(q) + u_2F_2(q)$$

where q is the state variable of dimension n and F_1, F_2 are the controlled vector fields given in the previous section.

Using Lie brackets computations, we recall the following proposition

Proposition 1.2. *Both the Copepod swimmer and the Purcell swimmer can swim.*

Proof. The displacement associated with the following periodic control sequence

$$\begin{aligned} &u_1 = 1, \quad u_2 = 0, \quad t \in [0, \varepsilon[, \text{ where } \varepsilon > 0 \text{ is fixed} \\ &u_1 = 0, \quad u_2 = 1, \quad t \in [\varepsilon, 2\varepsilon[, \\ &u_1 = -1, \quad u_2 = 0, \quad t \in [2\varepsilon, 3\varepsilon[, \\ &u_1 = 0, \quad u_2 = -1, \quad t \in [3\varepsilon, 4\varepsilon] \end{aligned}$$

is given by

$$\beta(t) = (\exp tF_2 \ \exp -tF_1 \ \exp -tF_2 \ \exp tF_1)\,(q(0)), \quad t \in [0, 4\varepsilon]$$

and using Baker-Campbell-Hausdorff formula one has

$$\beta(t) = \exp(t^2[F_1, F_2] + o(t^2))(q(0)), \quad t \in [0, 4\varepsilon]$$

which gives for small stroke t a displacement of

$$\beta(t) \sim q(0) + t^2[F_1, F_2](q(0)), \quad t \in [0, 4\varepsilon]$$

Since the components of $[F_1, F_2](q(0))$ along the position variables for the Copepod swimmer and the Purcell swimmer are non-zero, the displacement $\beta(4\varepsilon) - q(0)$ is non-zero. Compare with [19]. □

1.4 The swimming problem as an optimal control problem

To compute strokes, we shall use optimal control theory. Many costs can be considered but we shall concentrate of minimizing the mechanical energy dissipated by the direct forces. It can be also reframed as a time minimal control problem fixing the energy level. Hence, these two swimming problems fall into the framework of sub-Riemannian geometry.

From this point of view, the optimal control problem amounts to fix the displacement of the swimmer and minimizing the energy. By introducing a geometric efficiency representing the ratio between the displacement and the energy, this corresponds to a simplification of the concept of efficiency used in the literature [92], this leads to an additional problem in the framework of sub-Riemannian geometry.

Mathematical formulation:

$$
\text{(OCP)}\qquad
\begin{array}{l}
\min\ g(\bar{q}(0),\bar{q}(T)) \\
\text{subject to bounded measurable functions } u:[0,T]\to\mathbb{R}^m \\
\qquad\qquad \text{and arcs } \bar{q}\in W^{1,1}([0,T];\mathbb{R}^n) \text{ satisfying} \\
\dot{\bar{q}}(t)=f(\bar{q}(t),u(t)) \quad \text{a.e. } t\in[0,T]\,, \\
u(t)\ \in\ U\subset\mathbb{R}^m \quad \text{a.e. } t\in[0,T]\,, \\
(\bar{q}(0),\bar{q}(T))\in C\ ,
\end{array}
$$

in which $T>0$ is fixed, $g(.,.), f(.,.)$ are continuously differentiable, C is a closed set of $\mathbb{R}^{2n}$ and $u(.)$ is a measurable mapping.

More precisely, we study the following optimization problems with the following boundary conditions given by C.

1. For the Copepod swimmer, we consider the following settings

(SPC)
- $\bar{q}=(q,q^0)=(x,\theta_1,\theta_2,q^0)$,
- $u=(u_1,u_2)\in U\subset\mathbb{R}^2$,
- $f(\bar{q},u)=(u_1\,F_1(q)+u_2\,F_2(q),J(q,u))$ where F_1,F_2 are deduced from the dynamics given by (1.1) and $J(q,u)$ is the integrand of the mechanical cost given by (1.3),
- $g(\bar{q}(0),\bar{q}(T))=q^0(T)$,
- $C=\Big\{\ \big(\bar{q}(0),\bar{q}(T)\big)\ \Big|\ \theta_i(0)=\theta_i(T),\quad i=1,2,$
  $x(0)=0, x(T)=x_T$ (fixed),
  $q^0(0)=0\ \Big\}$.

2. For the Purcell swimmer, we consider

(SPP)
- $\bar{q}=(q,q^0)=(\theta_1,\theta_2,x,y,\alpha,q^0)$,
- $u=(u_1,u_2)\in U$ where U is an open subset of $\mathbb{R}^2$,
- $f(\bar{q},u)=(u_1\,F_1(q)+u_2\,F_2(q),J(q,u))$ where F_1,F_2 are defined in (1.7) and $J(q,u)$ is the integrand of the mechanical cost (1.8),
- $g(\bar{q}(0),\bar{q}(T))=q^0(T)$,
- $C=\Big\{\ \big(\bar{q}(0),\bar{q}(T)\big)\ \Big|\ \theta_i(0)=\theta_i(T),\quad i=1,2,$
  $x(0)=0,\ y(0)=0,$
  $x(T)^2+y(T)^2=R^2$ (fixed),
  $\alpha(0)=0,\alpha(T)=\alpha_T$ (fixed),
  $q^0(0)=0\ \Big\}$.

Geometric efficiency: In this case, the cost stands for the ratio between the displacement of the swimmer and the length of the stroke. In particular, for the Copepod swimmer, it leads us to study the same swimming problem as (SPC), but with $g(\bar{q}(0),\bar{q}(T))=-\frac{x(T)}{\sqrt{2Tq^0(T)}}$ and $x(T)$ as a free variable. This concept is a

simplification of the physical concept of efficiency found in the literature [53] but is a natural concept in the framework of sub-Riemannian geometry. Also, the physical concept can be treated similarly using the same tools of optimal control developed in this work.

Chapter 2

Necessary and sufficient optimality conditions

In this chapter, we recall necessary optimality conditions of first and second order adapted to the swimming problems seen in chapter 1. We give transversality conditions related to periodic boundary conditions and to the endpoint cost to minimize. For our problems, standard sufficient second order conditions fail and we present refined sufficient conditions adapted to our swimmer. Many references deal with these problems, we refer the reader to [122], [126], [34].

Contents

2.1 Pontryagin Maximum Principle 13
2.1.1 Application to the swimming problems. 14
2.2 Second order conditions 15
2.2.1 Necessary conditions 15
2.2.2 Sufficient conditions 17

2.1 Pontryagin Maximum Principle

The following theorem is the Pontryagin Maximum Principle without constraints on the state and with mixed boundary conditions on the state (see [122]).

Let us consider the optimal control problem (OCP) presented in chapter 1 where we use the same notations.

Theorem 2.1. *If $u \in U$, associated with the trajectory $\bar{q}(.)$, is optimal on $[0,T]$, then there exists an application $\bar{p}(.) : [0,T] \to \mathbb{R}^n$ absolutely continuous called adjoint vector, and $\lambda \geq 0$, such that $(\bar{p}(.), \lambda)$ is non trivial and for almost every $t \in [0,T]$,*

$$\dot{\bar{q}} = \frac{\partial H}{\partial \bar{p}}(\bar{q}, \bar{p}, u) \qquad \dot{\bar{p}} = -\frac{\partial H}{\partial \bar{q}}(\bar{q}, \bar{p}, u) \tag{2.1}$$

where $H(\bar{q}, \bar{p}, u) = \bar{p} \cdot f(\bar{q}, u)$ is the pseudo-Hamiltonian of the system, and the generalized Weierstrass condition holds almost everywhere on $[0,T]$

$$H(\bar{q}, \bar{p}, u) = \max_{v \in U} H(\bar{q}, \bar{p}, v). \tag{2.2}$$

Moreover, $\max_{v\in U} H(\bar{q},\bar{p},v)$ *is constant on* $[0,T]$ *and the following transversality conditions hold,*

$$(\bar{p}(0),-\bar{p}(T)) \in \lambda\nabla_{\bar{q}(0),\bar{q}(T)} g(\bar{q}(0),\bar{q}(T)) + N_C(\bar{q}(0),\bar{q}(T)) \tag{2.3}$$

where N_C *is the limiting normal cone of the endpoints constraint set* C *defined below.*

Definition 2.2. *For a closed set* $C \subset \mathbb{R}^k$ *and a point* $x \in C$*, the limiting normal cone of the set* C *at a point* x *is defined by*

$$N_C(x) := \left\{\eta \in \mathbb{R}^k : \exists x_i \in C, x_i \to x, \text{ and } \eta_i \to \eta \mid \eta_i \in N_C^P(x_i) \text{ for all } i\right\}$$

where $N_C^P(y) := \left\{\eta \in \mathbb{R}^k : \exists M \geq 0 \mid \eta\cdot(x-y) \leq M|x-y|^2 \text{ for all } y \in C\right\}$.
In the case where C *is a smooth manifold,* $N_C(x)$ *reduces to the set of outward normals at* x*.*

2.1.1 Application to the swimming problems.

We apply these first necessary optimality conditions to the swimming problems (SPC) and (SPP) presented in chapter 1.

- For the Copepod swimmer, we denote by $\bar{p} = (p_1, p_2, p_3, p^0)$ the adjoint vector. The transversality conditions related to the problem (SPC) are

$$p_i(0) = p_i(T) \text{ for } i = 2,3 \qquad p^0(T) = -\lambda,\ \lambda \geq 0.$$

- For the Purcell swimmer, we denote by $\bar{p} = (p_1, p_2, p_3, p_4, p_5, p^0)$ the adjoint vector. The transversality conditions related to the problem (SPP) are

$$p_i(0) = p_i(T) \text{ for } i = 1,2 \qquad p^0(T) = -\lambda,\ \lambda \geq 0.$$

Remark 2.3. *For the geometric efficiency* $g(\bar{q}(0),\bar{q}(T)) = -\frac{x(T)}{\sqrt{2Tq^0(T)}}$ *(with* $x(T)$ *free) presented at the end of Chapter 1, the transversality conditions for the Copepod swimmer are*

$$\begin{aligned} &p_i(0) = p_i(T) \text{ for } i = 2,3 \\ &p_1(T) = \frac{\lambda}{\sqrt{2T}}\frac{1}{q^0(T)} \qquad\qquad p^0(T) = -\frac{\lambda}{2\sqrt{2T}}\frac{x(T)}{q^0(T)^{3/2}},\ \lambda \geq 0. \end{aligned}$$

We can normalize $p^0(T) = -1/2$, $p_1(T) = q^0(T)/x(T)$ *with* $\lambda = \sqrt{2T}\frac{q^0(T)^{3/2}}{x(T)} \geq 0$.

Note that the swimming problems (SPC) and (SPP) are augmented systems where the mechanical cost of the swimmer is represented by the q^0 variable. Since H doesn't depend upon q^0, then $p^0(.)$ is a nonpositive constant that we usually set

to $-1/2$. These two problems fall under the framework of sub-Riemannian geometry that are written classically as

$$\begin{aligned} &\min \leftarrow \int_0^T (a(q)\,u_1^2 + 2b(q)\,u_1u_2 + c(q)\,u_2^2)\,\mathrm{d}s \\ &\dot{q} = u_1\,F_1(q) + u_2\,F_2(q) \\ &q(0) \in M_0, \quad q(T) \in M_1. \end{aligned} \tag{2.4}$$

where a, b, c are smooth functions and M_i, $i = 0, 1$ are smooth submanifolds of $\mathbb{R}^n$.

Definition 2.4. *An extremal is a quadruplet $(q(.), p(.), u, \lambda)$ such that $\bar{q} = (q, q^0)$, $\bar{p} = (p, p^0)$ is solution of (2.1) and (2.2). If $p^0 = 0$, it is called abnormal extremal, and if $p^0 < 0$, it is called normal extremal. If moreover the transversality conditions (2.3) are satisfied, the extremal is said a BC-extremal.*
Projection of normal (resp. abnormal) extremal onto the q-space is called normal (resp. abnormal) geodesic. A normal geodesic is called strict if it is not the projection of an abnormal extremal.

Since there are no constraints on the control, the Weierstrass condition (2.2) becomes $\frac{\partial H}{\partial u}(q, p, u) = 0$. Besides, H is continuously differentiable, we can compute locally u as a function of q and p. Substituting into the pseudo Hamiltonian, we get the true Hamiltonian $H(q, p)$ also denoted by H.

Definition 2.5. *We define $z := (q, p)$. The Hamiltonian system (2.1) can be written*

$$\dot{z} = \overrightarrow{H}(z) \tag{2.5}$$

where $\overrightarrow{H}(z) = \left(\frac{\partial H}{\partial p}(z), -\frac{\partial H}{\partial q}(z)\right)$ is called the Hamiltonian vector field.

2.2 Second order conditions

2.2.1 Necessary conditions

Definition 2.6. *Let $\overrightarrow{H}$ be a smooth Hamiltonian vector field, and let $z = (q, p)$ an extremal of $\overrightarrow{H}$ defined on $[0, T]$. The variational equation is defined by*

$$\dot{\delta z} = \mathrm{d}\overrightarrow{H}(z)\,\delta z \tag{2.6}$$

is called the Jacobi equation. A Jacobi field $J = (\delta q, \delta p)$ is a non trivial solution of the Jacobi equation. It is said vertical at time t if $\delta q(t) = 0$. A time t_c is a conjugate time if there exists a vertical Jacobi field at times 0 and t_c. If so, $q(t_c)$ is said conjugate to $q(0)$.

The following theorem gives a nice characterization of conjugate points. We used the following test to compute conjugate points for normal strokes.

Proposition 2.7. *We denote $\delta z_i = (\delta q_i, \delta p_i)$, $i = 1...n$, n-independent solutions of (2.6) vertical at time $t = 0$. Then at time t_c we have the following rank condition*

$$rank\ \{\, \delta q_1(t_c), ..., \delta q_n(t_c) \,\} < n. \tag{2.7}$$

Since the extremals doesn't depend on their parameterization, fixing the period T is equivalent to fix the level of energy H. Also the dimension of the control set U is less than the dimension of the state space $X \subset \mathbb{R}^n$, therefore p belongs to a cylinder $\mathcal{C}$.

Definition 2.8. *Let (q_0, p_0) be an initial condition and $(q(., q_0, p_0), p(., q_0, p_0))$ the extremal solution associated with the flow of $\overrightarrow{H}$. The exponential map based at q_0 is defined by*

$$\exp_{q_0} : \mathbb{R} \times \mathcal{C} \longrightarrow \mathbb{R}^n, \quad (t, p_0) \mapsto q(t, q_0, p_0).$$

Remark 2.9. *Let $q_0 \in \mathbb{R}^n$. We say that q is conjugate to q_0 along $\gamma(t) = \exp_{q_0}(t, p_0)$ if $q = \gamma(t_c)$ and (t_c, p_0) is a critical point of the exponential map $\exp_{q_0}$.*

Remark 2.10. *The exponential mapping is useful to parameterize normal extremals by their initial adjoint vectors. Namely for the Copepod swimmer, the normal true Hamiltonian is of the form ($p^0 = -1/2$)*

$$H(q, p) = \frac{1}{2}\left(a_{11}(q)v_1^2 + 2a_{12}(q)v_1v_2 + a_{22}(q)v_2^2\right)$$

where a_{ij}, for $i, j = 1, 2$ are given by (1.3), $H_i(q, p) = p \cdot F_i(q)$, for $i = 1, 2$ are the Hamiltonian lifts of the vector fields F_1, F_2 deduced from (1.1) and v_1, v_2 are the optimal controls given by

$$v_1 = \frac{a_{22}H_1 - b_{12}H_2}{a_{11}b_{22} - a_{12}^2}, \qquad v_2 = \frac{a_{11}H_2 - b_{12}H_1}{a_{11}b_{22} - a_{12}^2}.$$

Fixing $H = 1/2$, the domain of the exp *mapping is $\mathbb{R} \times \mathcal{C}$ where $\mathcal{C} = \{\, p_0 \mid H(q_0, p_0) = 1/2 \,\}$. Depending of value of p_0, we observe sectors related to different kind of strokes corresponding to the classification of periodic planar curves (see Fig.2.1).*

We briefly recall a necessary local optimality conditions related to the conjugate points [126, 34, 42] .

Theorem 2.11. *Let $q : [0, T] \longrightarrow \mathbb{R}^n$ be a strict normal stroke. If $q(.)$ has at least one conjugate point on $]0, T[$, then q is not a local minimizer in the L^∞-topology for controls and considering the problem with fixed extremities.*

Finally, we emphasize that the normal flow contains all the information to analyze the optimality of the normal extremals. Given an extremal, it corresponds a SR-problem with fixed extremities. The transversality conditions are used to select extremals with respect to the cost g and the exponential mapping gives necessary conditions of optimality related to conjugate points.

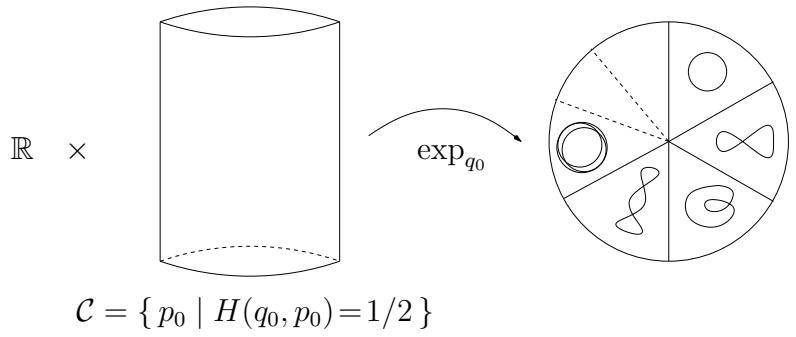

Figure 2.1: Exponential mapping and different sectors of strokes depending on value of p_0 for the Copepod swimmer.

2.2.2 Sufficient conditions

We summarize here a second order 'alternative test' which gives sufficient conditions for non-unique minimizers [62]. We consider the optimal control problems with end-point constraints of the form

$$\left\{\begin{array}{l} \text{Minimize } J(q(.),u(.)) = \int_0^T L(q(t),u(t))\mathrm{d}t \\ \text{subject to} \\ \dot{q}(t) \;=\; F(q(t),u(t)) \quad \text{a.e. } t \in [0,T]\,, \\ u(t) \;\in\; U \quad \text{a.e. } t \in [0,T]\,, \\ c(q(0),q(T)) = 0\,, \end{array}\right. \tag{2.8}$$

in which $F(.,.) : \mathbb{R}^n \times \mathbb{R}^m \to \mathbb{R}^n$ and $L(.,.) : \mathbb{R}^n \times \mathbb{R}^m \to \mathbb{R}$ are given functions of class $\mathcal{C}^2$ with continuous second derivatives w.r.t. (q,u) variables, $c(.,.) : \mathbb{R}^n \times \mathbb{R}^n \to \mathbb{R}^\ell$ is a given function of class $\mathcal{C}^2$ with continuous second derivatives w.r.t. (q_0, q_T) variables, and $U \subset \mathbb{R}^m$ is a given set. We say that $((\bar{q}(.),\bar{u}(.))$ is a (local) *weak* minimizer if there exists $\delta > 0$ such that

$$J((\bar{q}(.),\bar{u}(.)) \leq J((q(.),u(.)))$$

for any trajectory/control couple $(q(.),u(.))$ which is admissible for the control system of (2.8) such that $\|\bar{q}(.) - q(.)\|_{L^\infty} \leq \delta$ and $\|\bar{u}(.) - u(.)\|_{L^\infty} \leq \delta$. Take a reference weak normal extremal $(\bar{q}(.),\bar{u}(.),p(.),\nu)$ which means that the vector-valued function $p(.) \in W^{1,1}([0,T];\mathbb{R}^n)$, the vector $\nu \in \mathbb{R}^\ell$ together with the trajectory/control couple $(\bar{q}(.),\bar{u}(.))$ satisfy the following conditions

(i) $-\dot{p}(t) \;=\; p^T(t)\,\frac{\partial F}{\partial q}(\bar{q}(t),\bar{u}(t)) \;-\; \frac{1}{2}\frac{\partial L}{\partial q}(\bar{q}(t),\bar{u}(t))$ a.e.

(ii) $p(t)\cdot F(\bar{q}(t),\bar{u}(t)) - \frac{1}{2}L(\bar{q}(t),\bar{u}(t)) = \max\limits_{u\in U}\{\, p(t)\cdot F(\bar{q}(t),u) - \frac{1}{2}L(\bar{q}(t),u)\,\}$ a.e.

(iii) $[-p^T(0),\; p^T(T)] = \nu^T D_{q_0,q_T} c(\bar{q}(0),\bar{q}(T))$.

We say that $(\bar{q}(.), \bar{u}(.), p(.), \nu)$ is continuously embedded in a family of weak normal extremals

$$\{(q^\alpha(.), u^\alpha(.), p^\alpha(.), \nu^\alpha) \mid \alpha \in \mathcal{A}\}$$

where $\mathcal{A}$ is an open ball centered at the origin in some Euclidean space, such that $(\bar{q}(.), \bar{u}(.), p(.), \nu) = (q^0(.), u^0(.), p^0(.), \nu^0)$, and the following properties are satisfied:

(C1): for each $\alpha \in \mathcal{A}$, $(q^\alpha(.), u^\alpha(.), p^\alpha(.), \nu^\alpha)$, is a weak normal extremal such that:

$$J((q^\alpha(.), u^\alpha(.))) = J((\bar{q}(.), \bar{u}(.))) \quad \text{and} \quad c(q^\alpha(0), q^\alpha(T)) = c(\bar{q}(0), \bar{q}(T)) = 0,$$

(C2): the map $\alpha \to (q^\alpha(.), u^\alpha(.), p^\alpha(.), \nu^\alpha) \ : \ \mathcal{A} \to L^\infty \times L^\infty \times L^\infty \times \mathbb{R}^\ell$ is strongly continuous,

(C3): the map $\alpha \to (q^\alpha(0), q^\alpha(T)) \ : \ \mathcal{A} \to \mathbb{R}^n \times \mathbb{R}^n$, is of class $\mathcal{C}^1$,

(C4): the following $(d+k) \times 2n$ matrix has full row rank:

$$\begin{pmatrix} \Gamma^T \\ D_{q_0,q_T} c((\bar{q}(0), \bar{q}(T))) \end{pmatrix}$$

where

$$\Gamma := \left[\begin{array}{c} D_\alpha q^\alpha(0) \\ D_\alpha q^\alpha(T) \end{array} \right]\Big|_{\alpha=0} .$$

Consider the Riccati system:

$$\left\{ \begin{array}{l} \dot{P} + PA + A^T P + Q - (B^T P + D^T)^T R^{-1}(B^T P + D^T) = 0 \\ P^T(.) \ = \ P(.) \ , \end{array} \right. \tag{2.9}$$

where

$$A(t) := \frac{\partial F}{\partial q}(\bar{q}(t), \bar{u}(t)), \quad B(t) := \frac{\partial F}{\partial u}(\bar{q}(t), \bar{u}(t))$$

and

$$\begin{pmatrix} Q(t) & D(t) \\ D^T(t) & R(t) \end{pmatrix} := \begin{pmatrix} \frac{\partial^2 \mathcal{H}}{\partial q^2}(\bar{q}(t), p(t), \bar{u}(t)) & \frac{\partial^2 \mathcal{H}}{\partial q u}(\bar{q}(t), p(t), \bar{u}(t)) \\ \frac{\partial^2 \mathcal{H}}{\partial q u}^T(\bar{q}(t), p(t), \bar{u}(t)) & \frac{\partial^2 \mathcal{H}}{\partial u^2}(\bar{q}(t), p(t), \bar{u}(t)) \end{pmatrix} .$$

Consider the transition matrix associated with the linearized Hamiltonian system

$$\left\{ \begin{array}{l} \frac{\mathrm{d}}{\mathrm{d}t}\Phi(t,s) = Z\Phi(t,s) \\ \Phi(s,s) = \mathrm{Id} \ , \end{array} \right. \tag{2.10}$$

where

$$Z := \left[\begin{array}{cc} A - BR^{-1}D^T & -BR^{-1}B^T \\ -Q + DR^{-1}D^T & -AR^{-1}B^T \end{array} \right]$$

Set

$$\Phi(0,T) =: \left[\begin{array}{cc} \phi_{11} & \phi_{12} \\ \phi_{21} & \phi_{22} \end{array} \right]$$

and

$$W := \left[\begin{array}{cc} \phi_{22}\phi_{12}^{-1} & \phi_{21} - \phi_{22}\phi_{12}^{-1}\phi_{11} \\ -\phi_{12} & \phi_{12}^{-1}\phi_{11} \end{array} \right] . \tag{2.11}$$

We shall also assume

(H1): the functions F, L, c are of class $\mathcal{C}^2$ with continuous second derivatives w.r.t. all variables,

(H2): there exists $\rho > 0$ such that $R(t) > \rho \mathrm{I}$, for all $t \in [0,T]$,

(H3): $(A(.), B(.))$ is controllable on $[0,T]$,

(H4): $\bar{u}(.)$ is essentially bounded.

Theorem 2.12 (Standard conditions, [62]). *Take a weak normal extremal for $(q(.), u(.))$. Assume hypotheses (H1)-(H4) are satisfied. Suppose that*

(i): the Riccati equation ((2.9)) has a symmetric solution on $[0,T]$,

(ii): there exists $\gamma > 0$ such that

$$\left[\xi_0^T \ \xi_1^T\right] W \left[\begin{array}{c} \xi_0 \\ \xi_1 \end{array}\right] > \gamma \left| \left[\begin{array}{c} \xi_0 \\ \xi_1 \end{array}\right] \right|^2 ,$$

for all vectors $\xi_0, \xi_1 \in \mathbb{R}^n \setminus \{0\}$ satisfying $D_{q_0} c((\bar{q}(0), \bar{q}(T)))\xi_0 + D_{q_T} c((\bar{q}(0), \bar{q}(T)))\xi_1 = 0$.
Then $(\bar{q}(.), \bar{u}(.))$ is a weak locally unique minimizer.

The sufficient second order conditions of the previous theorem are well-known and we stress here that such conditions provide that the weak local minimizer is actually unique.

Theorem 2.13 (Refined conditions, [62]). *Assume that hypotheses (H1)-(H4) are satisfied. Suppose that a weak normal extremal $(\bar{q}(.), \bar{u}(.), p(.), \nu)$ can be continuously embedded in a family of weak normal extremals, and that*

(i): the Riccati equation ((2.9)) has a symmetric solution on $[0,T]$,

(ii): there exists $\gamma > 0$ such that

$$\left[\xi_0^T \ \xi_1^T\right] W \left[\begin{array}{c} \xi_0 \\ \xi_1 \end{array}\right] > \gamma \left| \left[\begin{array}{c} \xi_0 \\ \xi_1 \end{array}\right] \right|^2 ,$$

for all vectors $\xi_0, \xi_1 \in \mathbb{R}^n \setminus \{0\}$ satisfying

$$D_{q_0} c((\bar{q}(0), \bar{q}(T)))\xi_0 + D_{q_T} c((\bar{q}(0), \bar{q}(T)))\xi_1 = 0 \qquad \text{and} \qquad \Gamma^T \left[\begin{array}{c} \xi_0 \\ \xi_1 \end{array}\right] = 0 \ .$$

Then $(\bar{q}(.), \bar{u}(.))$ is a weak local minimizer.

Chapter 3

Concepts of sub-Riemannian geometry

In this chapter, a quick introduction to sub-Riemannian (SR) geometry is presented which is the proper geometry framework for the swimming problem at low Reynolds number.

Sub-Riemannian manifold

Definition 3.1. *A sub-Riemannian manifold is a triple (M, D, g) where M is a smooth connected manifold, D is a smooth distribution of rank m on M and g is a Riemannian metric on M.*

An *horizontal curve* is an absolutely continuous curve $t \to x(t)$, $t \in I$ such that $\dot{x}(t) \in D(x(t))$. The length of a curve γ is $l(\gamma) = \int_I g(\gamma(t))^{1/2} \mathrm{d}t$ and its *energy* is given by $E(\gamma) = \frac{1}{2}\int_0^T g(\dot{\gamma}(t))\mathrm{d}t$ where one can choose $T = 1$.

Controllability Let $D_1 = D$, $D_k = D_1 + [D_1, D_{k-1}]$. We assume that there exists for each $x \in M$ an integer $r(x)$, called the *degree of nonholonomy*, such that $D_{r(x)} = T_x M$. Moreover at a point $x \in M$, the distribution D is characterized by the *growth vector* $(n_1, n_2, ..., n_r)$ where $n_k = \dim D_k(x)$.

Distance According to Chow's theorem, for each pair $(x, y) \in M$, there exists an horizontal curve $\gamma : [0, 1] \mapsto M$ such that $\gamma(0) = x,\ \gamma(1) = y$. We denote by d the *sub-Riemannian distance*:

$$d(x, y) = \inf\{l(\gamma);\ \gamma \text{ is an horizontal curve joining } x \text{ to } y\}.$$

Geodesics equations According to Maupertuis principle the length minimization problem is equivalent to the energy minimization problem. Additionally if we parametrize the curves by arc-length, then the length minimization problem is equivalent to the time minimization problem.

To compute the geodesics equations it is convenient to minimize the energy $E(x)$. We proceed as follows. We choose a local orthonormal frame $\{F_1, ..., F_m\}$ of D and we consider the minimization problem

$$\frac{\mathrm{d}x}{\mathrm{d}t}(t) = \sum_{i=1}^{m} u_i(t) F_i(x(t)), \qquad \min_{u(.)} \frac{1}{2}\int_0^1 \left(\sum_i u_i^2(t)\right) \mathrm{d}t$$

According to the weak maximum principle (control domain $U = \mathbb{R}^m$) we introduce the pseudo-Hamiltonian:

$$H(x,p,u) = \sum_{i=1}^{m} u_i H_i(x,p) + p^0 \sum_{i=1}^{m} u_i^2$$

where $H_i = \langle p, F_i(x)\rangle$ is the Hamiltonian lift of F_i. By homogeneity p^0 can be normalized to 0 or $-\frac{1}{2}$.

Normal case: $p^0 = -1/2$ According to the maximum principle the condition $\frac{\partial H}{\partial u} = 0$ leads to $u_i = H_i$. Plugging this last expression for u_i into H leads to the true Hamiltonian in the normal case

$$H_n(z) = \frac{1}{2}\sum_{i=1}^{m} H_i^2(z)$$

where $z = (x,p)$. A normal extremal is a solution and its projection on the state space is called a normal geodesic.

Abnormal case: $p^0 = 0$ In this case the maximum principle leads to the conditions: $H_i = 0,\ i = 1,...,m$, thus defining implicitly the abnormal curves related to the structure of the distribution. Solutions are abnormal extremals and their projections on the state space are abnormal geodesics.

Next we introduce the basic definitions related to the analysis of the geodesics equations, and generalizing the Riemannian concepts.

Definition 3.2. *Parameterizing the normal geodesics solutions of $\vec{H}_n(z)$ and fixing $x \in M$, the exponential map is:* $\exp_x : (p,t) \to \Pi(\exp t\vec{H}_n(z))$ *where $z = (x,p)$ and Π is the projection $(x,p) \to x$.*

Definition 3.3. *Let us fix $x \in M$. The set of points at a SR-distance less or equal to r from x form the ball of radius r centered at x and the sphere $S(x,r)$ is formed by the set of points at a distance r from x.*

Evaluation of the SR-ball The computation of the SR-ball, even with small radius is a very complicated task. One of the most important result in SR-geometry is an approximation result about balls of small radius, in relation with the structure of the distribution.

Definition 3.4. *Let $x \in M$ and let f be a germ of a smooth function at x. The multiplicity of f at x is the number $\mu(f)$ defined by:*

- $\mu(f) = \min\{n;$ *there exist* $X_1,...,X_n \in D(x)$ *such that:* $(L_{X_1} \circ .... \circ L_{X_n} f)(x) \neq 0\}$,
- *if* $f(x) \neq 0$, $\mu(f) = 0$ *and* $\mu(0) = +\infty$.

Definition 3.5. *Let f be a germ of a smooth function at x, f is called privileged at x if $\mu(f) = \min\{k;\ df_x(D^k(x)) \neq 0\}$. A coordinate system $\{x_1, ..., x_n\} : U \to \mathbb{R}$ defined on an open subset V of x is called privileged if all the coordinates functions x_i, $1 \leq i \leq n$ are privileged at x.*

Nilpotent Approximation Having fixed a privileged coordinate system at $x = (x_1, ..., x_n)$, where the weight of x_i is $\mu(x_i)$. Each smooth vector field V at x has a formal expansion $V \sim \sum_{j \geq -1} V^j$, where each $V^j = \sum_{i=1}^n P_i^j(x_1, ..., x_n)\frac{\partial}{\partial x_i}$ is homogeneous of degree j for the weights associated with the coordinate system, and the weight of $\frac{\partial}{\partial x_i}$ is $-\mu(x_i)$. $P_i^j(x_1, ..., x_n)$ is a homogenous polynomial of degree j.

Proposition 3.6. *Let $\{F_1, ..., F_m\}$ be the orthonormal subframe of the distribution D and set $\hat{F}_i = F_i^{-1}$, $i = 1, ..., m$ in the formal expansion. Then the family $\hat{F}_i$ is a first order approximation of $\{F_1, ..., F_m\}$ at x as they generate a nilpotent Lie algebra with similar growth vector. Moreover for small x it gives the following estimate of the SR-norm $|x| = d(0, x) \asymp |x_1|^{1/w_1} + ...|x_n|^{1/w_n}$.*

See [21], [84] and [78] for the details of the construction of privileged coordinates. Note also that [96] contain also the relation of the integrability issues, important for the practical implementation.

Conjugate and cut loci in SR-geometry The standard concepts of conjugate and cut point from Riemannian geometry can be generalized in optimal control and thus in SR-geometry. Consider the SR-problem

$$\dot{x} = \sum_{i=1}^m u_i F_i(x), \quad \min_{u(.)} \int_0^T \left(\sum_{i=1}^m u_i^2 \right)^{1/2} \mathrm{d}t.$$

Definition 3.7. *Let $x(.)$ be a reference (normal or abnormal) geodesic on $[0, T]$. The time t_c is called the cut time if the reference geodesic is no more optimal for $t > t_c$ and $x(t_c)$ is called the cut point. Taking all geodesics starting from $x_0 = x(0)$, their cut points will form the cut locus $C_{cut}(x_0)$. The time t_{1c} is called the first conjugate time if the reference geodesic is no more optimal for $t > t_{1c}$ for the C^1-topology on the set of curves, the point $x(t_{1c})$ is called the first conjugate point. Calculated over all geodesics, the set of first conjugate points will form the (first) conjugate locus $C(x_0)$.*

An important step is to relate the computation of the geometric conjugate locus (using a test based on Jacobi fields) to the computation of the conjugate locus associated to optimality. It can be done under suitable assumptions in both normal and abnormal case [33] but for simplicity we shall restrict to the normal case.

Conjugate locus computation Using Maupertuis principle, the SR-problem is equivalent to the (parametrized) energy minimization problem

$$\min_{u(.)} \int_0^T \left(\sum_{i=1}^m u_i^2 \right) \mathrm{d}t$$

where T is fixed, and one can choose $T = 1$.

Let $H_i(z) = \langle p, F_i(x)\rangle$ and let $H_n = \frac{1}{2}\sum_{i=1}^m H_i^2$ be the Hamiltonian in the normal case. Take a reference normal geodesic $x(t), t \in [0,1]$ and let $z(t) = (x(t), p(t))$ be a symplectic lift solution of $\overrightarrow{H}_n$. Moreover assume that $x(t)$ is strict, which means that it is not a projection of an abnormal curve. Then the following proposition holds.

Proposition 3.8. *The first conjugate time t_{1c} along $x(t)$ corresponds to the first geometric conjugate point and can be computed numerically using the rank test (2.7).*

Integrable case If the geodesic flow is Liouville integrable, then the Jacobi equation is integrable and the conjugate points can be computed using the parametrization of the geodesic curve. This result is a consequence of the following standard lemma from differential geometry.

Lemma 3.9. *Let $J(t) = (\delta x(t), \delta p(t))$ be a Jacobi curve along $z(t) = (x(t), p(t))$, $t \in [0,1]$ and vertical at time $t = 0$, i.e. $\delta x(0) = 0$. Let $\alpha(\varepsilon)$ be any curve in $T^*_{x_0}M$ defined by $p(0) + \varepsilon\delta p(0) + o(\varepsilon)$. Then*

$$J(t) = \frac{\mathrm{d}}{\mathrm{d}\varepsilon}_{|\varepsilon=0} \exp tH_n(x(0), \alpha(\varepsilon)).$$

Nilpotent models in relation with the swimming problem The models in dimension 3 are related to the classification of stable 2-dimensional distribution, see [128] and will be used for the copepod swimmer. See also [43] for the analysis of the Heisenberg case. For the Purcell swimmer (in dimension 5) we use [111].

Contact case A point $x_0 \in \mathbb{R}^3$ is a *contact point* of the distribution $D = \mathrm{span}\{F_1, F_2\}$ if $[F_1, F_2](x_0) \notin D(x_0)$ and the growth vector is $(2, 3)$.
A normal form at $x_0 \sim 0$ is given by

$$x = (x_1, x_2, x_3), \quad D = \ker\alpha, \quad \alpha = x_2\mathrm{d}x_1 + \mathrm{d}x_3.$$

Observe that

- $\mathrm{d}\alpha = \mathrm{d}x_2 \wedge \mathrm{d}x_1$: Darboux form,
- $\frac{\partial}{\partial x_3}$: Lie bracket $[F_1, F_2]$ and characteristic direction of $\mathrm{d}\alpha$.

This form is equivalent to the so-called *Dido representation*

$$D = \ker\alpha', \quad \alpha' = \mathrm{d}x_3 + (x_1\mathrm{d}x_2 - x_2\mathrm{d}x_1)$$

with

$$D = \mathrm{Span}\{F_1, F_2\}, \quad F_1 = \frac{\partial}{\partial x_1} + x_2\frac{\partial}{\partial x_3}, \quad F_2 = \frac{\partial}{\partial x_2} - x_1\frac{\partial}{\partial x_3}.$$

If we set $F_3 = \frac{\partial}{\partial z}$, we get $[F_1, F_2] = 2\,F_3$ and the corresponding so-called *Heisenberg SR-case*

$$\dot{x} = \sum_{i=1}^{2} u_i F_i, \quad \min \to \int_0^T (u_1^2 + u_2^2)\mathrm{d}t$$

and it corresponds to minimize the euclidean length of the projection of $t \to x(t)$ on the (x_1, x_2)-plane.

Starting from 0, we observe that

$$x_3 = \int_0^T (\dot{x_1} x_2 - \dot{x_2} x_1)\mathrm{d}t$$

is proportional to the area swept by the curve $t \to (x_1(t), x_2(t))$. The SR-problem is dual to the Dido problem: among the closed curves in the plane with fixed length find those for which the enclosed area is maximal [43]. Solutions are well known and are circles.

They can be easily obtained using simple computations. The geodesic equations in the (x, H) coordinates where $H = (H_1, H_2, H_3),\ H_i = p \cdot F_i,\ i = 1, 2, 3$

$$\begin{aligned} \dot{x}_1 = H_1, \quad \dot{x}_2 = H_2, \quad \dot{x}_3 = H_1 x_2 - H_2 x_1, \\ \dot{H}_1 = 2H_2 H_3, \quad \dot{H}_2 = -2H_1 H_3, \quad \dot{H}_3 = 0. \end{aligned}$$

Setting: $H_3 = \lambda/2$, we get the equation of a linear pendulum: $\ddot{H}_1 + \lambda^2 H_1 = 0$. The integration is direct observing

$$\ddot{x}_3 - \frac{\lambda}{2}\frac{\mathrm{d}}{\mathrm{d}t}(x_1^2 + x_2^2) = 0$$

and we get the well known parametrization when $\lambda \neq 0$, which can be assumed positive

$$\begin{aligned} x_1(t) &= \frac{A}{\lambda}\left(\sin(\lambda t + \varphi) - \sin(\varphi)\right) \\ x_2(t) &= \frac{A}{\lambda}\left(\cos(\lambda t + \varphi) - \cos(\varphi)\right) \\ x_3(t) &= \frac{A^2}{\lambda} t - \frac{A^2}{\lambda^2}\sin(\lambda t) \end{aligned}$$

with $A = \sqrt{H_1^2 + H_2^2}$ and φ is the angle of the vector $(\dot{x}_1, -\dot{x}_2)$.
If $\lambda = 0$, we have straight-lines.

Conjugate points The computations of first conjugate points is straightforward using this parameterization.

Only geodesics whose projections are circles have first conjugate point given by $t_c = 2\pi/\lambda$ and corresponds to the first intersection of the geodesic with the axis Ox_3.

Geometrically it is due to the symmetry of revolution along this axis, a one-parameter family of geodesics starting from 0 intersects at such point. This point is also a cut point and a geodesic is optimal up to this point (included).

Note that the Heisenberg case will lead to a geometric interest of the SR-model in the swimming problem: the circles projections correspond to the concept of *stroke*. But while this model can provide some insights on optimal swimming, it is too primitive because:

1. The geodesic flow is integrable due to the symmetries and every (x_1, x_2) motion is periodic,

2. The model is quasi-homogeneous and x_1, x_2 are not weight 1 and x_2 of weight 2 and invariant in the Heisenberg group.

Martinet case: A point x_0 is a *Martinet point* if at x_0, $[F_1, F_2] \in \mathrm{Span}\{F_1, F_2\}$ and at least one Lie bracket $[[F_1, F_2], F_1]$ or $[[F_1, F_2], F_2]$ does not belong to D . Hence the growth vector is $(2, 2, 3)$. Then there exist local coordinates near x_0 identified to 0 such that

$$D = \ker \omega, \quad \omega = \mathrm{d}x_3 - \frac{x_2^2}{2}\mathrm{d}x_1$$

where

$$F_1 = \frac{\partial}{\partial x_1} + \frac{x_2^2}{2}\frac{\partial}{\partial x_3}, \quad F_2 = \frac{\partial}{\partial x_2}, \quad F_3 = [F_1, F_2] = x_2\frac{\partial}{\partial x_3}$$

The surface $\Sigma : \det(F_1, F_2, [F_1, F_2]) = 0$ is identified to $x_2 = 0$ and is called the *Martinet surface*. It is foliated by abnormal curves, integral curves of $\frac{\partial}{\partial x_1}$. In particular through 0 it corresponds to the curve $t \to (t, 0, 0)$.

Those two cases are nilpotent Lie algebras associate two nilpotent approximations of the SR-metric in the copepod swimmer and are respectively the Heisenberg case and the Martinet flat case. Also it can be easily checked that this second case leads to integrable geodesic flow using elliptic functions.

Cartan flat case: The *Cartan flat case* corresponds to the nilpotent distribution in dimension 5, with growth vector $(2, 3, 5)$, all Lie brackets of length more than 4 being zero. A normal form is

$$\begin{aligned} F_1(x) &= \frac{\partial}{\partial x_1}, \\ F_2(x) &= \frac{\partial}{\partial x_2} + x_1\frac{\partial}{\partial x_3} + x_3\frac{\partial}{\partial x_4} + x_1^2\frac{\partial}{\partial x_5}. \end{aligned}$$

Chapter 4

Numerical methods for optimal control

The purpose of this chapter is to present numerical methods that we used to compute numerically local optimal solutions of the swimming problems. We give overviews of direct methods used with the `Bocop` software and indirect methods used with the `HamPath` software. We emphasize the indirect approach describing the simple shooting method and the computations of conjugate points, crucial for our analysis.

Contents

4.1 General methods in optimal control 27
4.2 Direct method in the `Bocop` software 28
4.3 Indirect method in the `HamPath` software 28
4.3.1 The simple shooting 28
4.4 Homotopic method in optimal control 30
4.4.1 Discrete homotopy 31
4.4.2 Differential homotopy 31
4.4.3 Application to the Purcell swimmer 31

4.1 General methods in optimal control

First we can classify numerical methods in optimal control into two families, global methods and local methods.

We don't use global methods in this thesis. For the sake of curiosity, we mention two software: `BocopHJB` [27] and `GloptiPoly` [76].

Among local methods, we distinguish mainly two kind of families: direct methods and indirect methods. For direct methods, a basic discretization in time and space (state and/or control space) is performed and we don't need to know, *a priori*, the structure of the control. For indirect methods, we do need to know the structure of the control. In particular, by geometry analysis, such structure is given by first order optimality conditions. Depending on this structure, simple shooting method or multiple shooting method are used. Simple shooting methods aim to solve boundary

value problems to compute BC-extremals when the true Hamiltonian is smooth with respect to time. A first situation is to use multiple shooting method to improve the numerical accuracy by fixing a grid where the initial point at each time of the grid are unknown for the multiple shooting. When the control set is closed and the control saturates the constraint, it is necessary to use a multiple shooting method.

4.2 Direct method in the `Bocop` software

The direct approach transforms the infinite dimensional optimal control problem (OCP) of chapter 1 into a finite dimensional optimization problem (NLP). This transformation consists in discretizing in time applied to the state and the control variables, as well as the dynamics equation.
Usually these methods are less precise than indirect methods. However they appear most robust with respect to the initialization and they are easier to use.

	(OCP)	(NLP)
	$t \in [0,T]$	$t_i \in \{t_1 = 0, \dots, t_N = T\}$
	$\bar{q} \in \mathbb{R}^n, u \in \mathbb{R}^m$	$\bar{q}_i, u_i \in \{\bar{q}_1, \dots, \bar{q}_N, u_1, \dots, u_{N-1}\}$
Criterion:	$\min\ g(\bar{q}(0), \bar{q}(T))$	$\min\ g(\bar{q}_0, \bar{q}_N)$
Dynamics:	$\dot{\bar{q}} = f(\bar{q}, u)$	Numerical scheme:
		(ex Euler) $\bar{q}_{i+1} = f(\bar{q}_i, u_i)$
Path Constraints:	$m_1 \leq h_1(\bar{q}) \leq M_1$	$m_1 \leq h_1(\bar{q}_i) \leq M_1$
Admissible controls:	$m_2 \leq h_2(u) \leq M_2$	$m_2 \leq h_2(u) \leq M_2$
Boundary conditions:	$c(\bar{q}(0), \bar{q}(T))$	$c(\bar{q}_0, \bar{q}_N)$

Various numerical schemes of different orders are proposed to integrate the numerical integration and the (NLP) optimization problem is solved by `IPOPT` solver [124] with `MUMPS` [12].

The `Bocop` software provides the adjoint state p corresponding to the Lagrange multipliers for the dynamics constraints in the (NLP) problem. Our approach consists in using the robustness of the direct method with respect to the initialization to obtain an initial guess to initialize the indirect method implemented in the `HamPath` software and presented below.

4.3 Indirect method in the `HamPath` software

We recall the indirect method used to solve the swimming problem based on the `HamPath` code, see [55]. We will focus on the simple shooting, discrete continuation and computation of the solutions of the variational equations, needed to check second order conditions of local optimality.

4.3.1 The simple shooting

The Pontryagin maximum principle gives a first order necessary condition and asserts that every optimal trajectory is the projection from an extremal. If you are able to compute the control with the Weierstrass condition (2.2), then the extremal

system is composed by a differential system of the form $\dot{z} = F(z)$ where $z = (\bar{q}, p)$ (see (2.5)), and initial and final boundary conditions on $\bar{q}(.)$, and transversality conditions (2.3), can be written of the form $B(z(0), z(T)) = 0$. Finally the extremal system is a boundary value problem

$$\dot{z} = \mathrm{d}\overrightarrow{H}(z), \qquad B(z(0), z(T)) = 0 \tag{4.1}$$

This system is well-posed since $B(z(0), z(T)) = 0$ is composed by $2n = \dim z$ independent equations.

Definition 4.1. *The shooting function is defined by*

$$S(z_0) := R(z_0, z(T, z_0))$$

where $z(T, z_0)$ denotes the solution of the Cauchy problem $\dot{z} = F(z)$, $z(0) = z_0$.

The system (4.1) is then equivalent to

$$S(z_0) = 0$$

which is solved numerically by a Newton method implemented in the `HamPath` software by the routine `hybrj` (from minpack library [100]). The hybrj code implements the Powell hybrid algorithm [108] based upon Newton-Raphson method combined with Levenberg-Marquardt algorithm. The Jacobian of S have to be given to `hybrj` and have to be invertible to get convergence.

Although Newton type methods provide good precision for computing zeros, its main drawbacks are

- Indirect method compute open loop controls.
- The domain of convergence is small so we should have an idea of the seeking solution. This can be done by using `Bocop` software to have a good guess z_0. An other approach to obtain the convergence of the indirect method is to use homotopy method (or continuation method) presented in the section below.
- To check the optimality of the solution, one of the objectives of geometric control is to derive higher-order optimality conditions in order to restrict more the set of candidate optimal trajectories. `HamPath` provide computations of conjugate points by the rank test presented in 2.7.

Application to the Copepod swimming problem. Using the same notation as the (SPP) problem, the shooting function takes the form

$$
\begin{aligned}
&S : \mathbb{R}^{2n} \longrightarrow \mathbb{R}^{2n} \\
&z_0 = (x_0, \theta_{10}, \theta_{20}, q_0^0, p_{10}, p_{20}, p_{30}, p_0^0) \mapsto S(z_0) \quad = \begin{pmatrix} x_0 \\ \theta_{10} - \theta_1(T, z_0) \\ \theta_{20} - \theta_2(T, z_0) \\ q_0^0 \\ p_{20} - p_2(T, z_0) \\ p_{30} - p_3(T, z_0) \\ x(T, z_0) - x_T \\ p_0^0 + \lambda \end{pmatrix}
\end{aligned}
$$

where $\lambda \geq 0$ is fixed, $k(T, z_0) = \Pi_k \left(\exp(T\overrightarrow{H}) z_0 \right)$ and $\Pi_k : \mathbb{R}^{2n} \to \mathbb{R}$, $z \mapsto k$ for $k = \theta_1, \theta_2, p_2, p_3, x$.

4.4 Homotopic method in optimal control

As the proceeding section outlined, shooting methods, based on Newton type algorithm, are sensitive to the initial point. This difficulty can be overcome by using an homotopic method.

The idea is to solve a difficult problem step by step from a known solution of a derived problem obtained by parameter deformation. This derived problem is associated with an application H, called homotopy, which relates the both problems and have good properties.

Definition 4.2. *Let $f_0, f_1 : \mathbb{R}^n \to \mathbb{R}^n$ two applications. An homotopy is an application $\mathcal{H}$ connecting f_0, f_1 in the following way:*

$$
\begin{aligned}
&\mathcal{H} : \bar{V} \times [0, 1] \to \mathbb{R}^n \\
&(z, \mu) \mapsto \mathcal{H}(z, \mu)
\end{aligned}
$$

where V is an open subset of $\mathbb{R}^n$ and $\mathcal{H}$ is continuous such that

$$\mathcal{H}(., 0) = f_0 \text{ and } \mathcal{H}(., 1) = f_1.$$

The homotopic parameter μ may apply on the objective function, the final time, boundary values of the constraints... The choice of function $\mathcal{H}$ is in general heuristic and is guided by the simpler problem to solve but also by the curve between the two problems that we want sufficiently smooth and convergent.

For the shooting method, we get a one parameter family of non linear equations

$$S_\mu(p) = 0, \quad \mu \in [0, 1].$$

Assume a known zero p_0 of the shooting function $S_0(.)$ and following a zero curve $c_\mu(.) \in S_\mu^{-1}(0)$ until we reach $\mu = 1$. Then we obtain a zero of $S_1(.)$.

Under some regularity assumptions on S_μ, the implicit function theorem gives the existence, at least locally, of the zero curve. The fact that this zero curve intersects the homotopy level $\mu = 1$ is difficult in the general case. It can be controlled by setting some boundary conditions or deriving sufficient conditions to ensure the existence of this branch until $\lambda = 1$, see [4] for more detailed. Numerical methods implemented in the `HamPath` software are described in [55].

4.4.1 Discrete homotopy

A first idea is to choose a discretization $0 = \mu_0 < \mu_1 < \ldots < \mu_N = 1$ of $[0, 1]$. Suppose that the equation $S_{\mu_0}(p) = 0$ is solved, then the solution can be used to initialize the Newton type algorithm to solve the equation $S_{\mu_1}(p) = 0$ and step by step, we can get a solution of $S_{\mu_N}(p) = 0$.
However, since there may exists several zero curves, or a bifurcation points along the zero curve, this method has its limit and we rely on differential homotopy described below.

4.4.2 Differential homotopy

One may see the zero curve as a differential curve. This requires regularity properties on S_μ such as C^2-differentiability and maximum rank of the Jacobian on the zero curve which is related to the non existence of a conjugate point. A closer method consists in parameterizing the zero curve by arc length, $s \to c(p(s), \mu(s))$ which lead to solve

$$\frac{\mathrm{d}}{\mathrm{d}s} c(p(s), \mu(s)) = 0,\ p(0) = p_0,\ \mu(0) = 0$$

where p_0 is the know solution of the equation $S_0(p) = 0$ and $\dot{\mu}(s)^2 + \dot{p}(s)^2 = 1$.

4.4.3 Application to the Purcell swimmer

The nilpotent approximation for the Purcell swimmer is the Cartan flat case. Let $z_1(.)$ a normal extremal obtained from the nilpotent approximation, therefore associated with the simplified cost $\int_0^T u_1^2 + u_2^2 \mathrm{d}t$. If the amplitude of $\gamma_1(.)$ is relatively small, a simple shooting method is used to compute a stroke $\gamma_2(.)$ with the same amplitude and the same displacement but with the original dynamics of the Purcell swimmer given in 1.7. Then, we perform two discrete homotopy methods

- homotopy on $x(T)^2 + y(T)^2$ to increase the amplitude of the stroke $\gamma_2(.)$. We obtain a stroke $\gamma_3(.)$ for the Purcell swimmer but with the simplified cost $\int_0^T u_1^2 + u_2^2 \mathrm{d}t$.
- convex homotopy on the cost to obtain from $\gamma_3(.)$ a stroke with respect to the mechanical cost. More precisely, we consider the following Hamiltonian:

$$\begin{aligned} H(q, p; \mu) :=& \frac{1-\mu}{2}(H_1(q,p)^2 + H_2(q,p)^2) \\ &+ \frac{\mu}{2}\left(b_{11}(q)v_1(q,p)^2 + b_{12}(q)v_1(q,p)v_2(q,p) + b_{22}(q)v_2(q,p)^2\right) \end{aligned}$$

where H_1, H_2 are the Hamiltonian lifts of the vector fields F_1, F_2 deduced from (1.1) and v_1, v_2 are the optimal controls given by maximization condition for the mechanical cost:

$$v_1 = \frac{b_{22}H_1 - b_{12}H_2}{b_{11}b_{22} - b_{12}^2}, \qquad v_2 = \frac{b_{11}H_2 - b_{12}H_1}{b_{11}b_{22} - b_{12}^2}.$$

Remark 4.3. *The differential homotopy provided by* `HamPath` *failed due to the presence of several zero curves. That's why we used the discrete homotopy which provided us different families of strokes (see chapter 6).*

Chapter 5

The Purcell Three-link swimmer: some geometric and numerical aspects related to periodic optimal controls

Contents

5.1 Description of the contributions of the article: The Purcell Three-link swimmer: some geometric and numerical aspects related to periodic optimal controls. 34

5.2 The Purcell Three-link swimmer: some geometric and numerical aspects related to periodic optimal controls 35

5.3 Introduction 35

5.4 First and second order optimality conditions 37

5.5 The Purcell Three-link swimmer 39

5.5.1 Mathematical Model 39

5.6 Local analysis for the three-link Purcell swimmer 41

5.6.1 Computations of the nilpotent approximation 41

5.6.2 Integration of extremal trajectories 43

5.7 Numerical results 49

5.7.1 Nilpotent approximation 50

5.7.2 True mechanical system 52

5.7.3 The Purcell swimmer in a round swimming pool 55

5.8 Conclusions and future work 56

5.1 Description of the contributions of the article: The Purcell Three-link swimmer: some geometric and numerical aspects related to periodic optimal controls.

In this article, we make a self contained presentation of the three-link Purcell swimmer and the optimal control techniques suitable to analyze the problem.

The standard modelization is recalled in full details to construct the dynamics and the cost to minimize, associated with the mechanical energy (1.7).

The first contribution is to compute a nilpotent approximation which is the so-called Cartan flat model. The construction being explicit to relate the physical variables and the canonical variables in the approximation. The second step is to integrate the extremal equations in the normal and abnormal case. In the normal case, they can be integrated using the elliptic integrals of the first and second kind. Such computations is a first step to determine for the nilpotent model the strokes and further computations given in Chapter 6 prove that they correspond to simple curves, diffeomorphic to circles, and eight curves (Bernoulli's lemniscates). In the abnormal case, they are given by polynomials functions.

To check the optimality, we use conjugate points computations and the normal case, only simple curves remain candidates as minimizers. In the abnormal case, similar computations allow to check optimality for length large enough.

Finally, a first sequence of numeric computations allows to compute more general strokes for the true model using the `Bocop` and `HamPath` software.

As a conclusion, we simplify the analysis of the problem using geometric remark which will be develop in the second article.

5.2 The Purcell Three-link swimmer: some geometric and numerical aspects related to periodic optimal controls

Authors: P. Bettiol[1], B. Bonnard[2], L. Giraldi[3], P. Martinon[4], J. Rouot[5].

The maximum principle combined with numerical methods is a powerful tool to compute solutions for optimal control problems. This approach turns out to be extremely useful in applications, including solving problems which require establishing periodic trajectories for Hamiltonian systems, optimizing the production of photobioreactors over a one-day period, finding the best periodic controls for locomotion models (e.g. walking, flying and swimming). In this article we investigate some geometric and numerical aspects related to optimal control problems for the so-called Purcell Three-link swimmer [109], in which the cost to minimize represents the energy consumed by the swimmer. More precisely, employing the maximum principle and shooting methods we derive optimal trajectories and controls, which have particular periodic features. Moreover, invoking a linearization procedure of the control system along a reference extremal, we estimate the conjugate points, which play a crucial role for the second order optimality conditions. We also show how, making use of techniques imported by the sub-Riemannian geometry, the nilpotent approximation of the system provides a model which is integrable, obtaining explicit expressions in terms of elliptic functions. This approximation allows to compute optimal periodic controls for small deformations of the body, allowing the swimmer to move minimizing its energy. Numerical simulations are presented using HAMPATH and BOCOP codes.

5.3 Introduction

The study of periodic trajectories for Hamiltonian system represents a longstanding problem in dynamical systems and has attracted the interest of many researches, in particular for the N-body problem. The well-known Lyapunov-Poincaré theorem (cf. [38]) establishes, under suitable assumptions, the existence of a one-parameter

[1]Laboratoire de Mathématiques, Unité CNRS UMR 6205, Université de Bretagne Occidentale, 6, Avenue Victor Le Gorgeu, 29200 Brest, piernicola.bettiol@univ-brest.fr

[2]Inria Sophia Antipolis et Institut de Mathématiques de Bourgogne, 9 avenue Savary, 21078 Dijon, bernard.bonnard@u-bourgogne.fr

[3]Inria Sophia Antipolis, 2004 route des lucioles, F-06902 Sophia Antipolis, laetitia.giraldi@inria.fr

[4]Inria Saclay et CMAP Ecole Polytechnique, Route de Saclay, 91128 Palaiseau pierre.martinon@inria.fr

[5]Inria Sophia Antipolis, 2004 route des lucioles, F-06902 Sophia Antipolis, jeremy.rouot@inria.fr

family of periodic trajectories emanating from a given equilibrium point. The proof is based on the continuation method and leads to obtain periodic trajectories with small amplitudes. A different method to compute periodic trajectories was introduced by Poincaré investigating the N-body problem: this is the so-called direct method. The latter technique consists in finding a particular periodic trajectory which minimizes the action $S(x(t)) = \int_{t_0}^{t_1} L(t, x(t), \dot{x}(t))\mathrm{d}t$ (here L is a given Lagrangian and $[t_0, t_1]$ is the time interval of reference), and which is a limit of a minimizing sequence (cf. [38]). The problem can be recast in the framework of optimal control theory, interpreting the derivative of $t \to x(t)$ as a control function $u(.)$. These two methods justify the use of a variational approach to compute periodic trajectories in optimal control, and, more precisely, a family of periodic trajectories depending on parameters such as the periods. The first-order necessary conditions for optimality, expressed in terms of the Euler-Lagrange equation in the context of the Calculus of Variations, are provided in optimal control by the maximum principle, which, due to the periodic structure of the problem, might detect a (parameterized) family of extremals. In these circumstances second-order analysis turns out to be an important tool in detecting the minimizers for the reference problem. Since the non-uniqueness of periodic minimizers does not allow in general to invoke standard second-order sufficient conditions, the necessity of refined second-order conditions was discussed in a series of articles (see for instance [116],[126],[62]), yielding important results which were tested in some 'academic' examples.

In control engineering, the importance of the study of periodic optimal controls is illustrated by the following problem areas: the optimization of the production of photobioreactors over a one-day prescribed time period (see for instance [71]), and, more recently, the search of periodic optimal controls in locomotion problems (e.g. walking, flying, swimming), where the state variable x decomposes into two variables (x', x'') where x' corresponds to the displacement variable and x'' stands for the shape variable (the latter must often satisfy periodic requirements in locomotion modeling). In the swimming problem, a swimmer displacement is produced by the deformation of the body interacting with the fluid and a periodic 'strategy of deformation' is called a *stroke*. In the case of micro-organisms evolving in a fluid, inertia is negligible with respect to the viscous effects, and the locomotion at this scale can be presented as a sub-Riemannian (SR) problem in which the cost functional to minimize represents the power expanded by the swimmer. A simplified mathematical model of swimmer is the Three linked spheres introduced by [101]. It turns out that the SR-geometry associated with this simplified model corresponds to the Heisenberg group case. This problem is equivalent to the Dido problem and the optimal solutions can be easily computed (cf. [34]). In the latter case, the optimal stroke are ellipses and they allow the swimmer to move along a desired direction [10]. An earlier pioneering model of micro-swimmer was introduced in the fifties in [121]; this was subsequently investigated using analytical tools coming from control theory in a recent paper [6].

In this article, we focus on the so-called Purcell Three-link swimmer [109]. By using the resistive force theory (see [70]), it was shown that the dynamics of the

swimmer can be expressed explicitly in terms of an ordinary differential equation in which the speed of deformation can be interpreted as a control function (see for instance [67, 68]). As a result, one obtains a drift-less control system which is linear with respect to the control variables, such as $\dot{x} = u_1 F_1(x) + u_2 F_2(x)$. Since the detailed expression of functions F_i's is quite involved, deriving the minimizers in an explicit form is not an easy task. In the present article we employ the expressions of the vector fields F_i's provided by previous work (cf. [6, 67, 68]) and, applying both geometric and numerical methods, we investigate the minimizers of our reference optimal control problem (modeling the Purcell swimmer) having some periodicity requirements.

The paper is organized as follows. Sections 2 is a short introduction to some tools and concepts imported from optimal control theory. These are subsequently employed for the study of some optimal control problems related to the mathematical model of the Purcell Three-link swimmer, which is described in Section 3. In Section 4, applying a classical SR-geometry approach, we provide an approximation associated with strokes of small amplitudes. This is the so-called *nilpotent approximation* and we show that it corresponds to the Cartan flat case [51],[111]. It turns out that the associated extremal curves are integrable in the class of elliptic functions. We provide detailed expressions of the extremals to make easier for the reader how to relate the period of the strokes to Jacobi complete integrals. Subsequently, Section 5 is devoted to the numerical analysis of the reference problem. More precisely, we estimate conjugate points for both normal and abnormal extremals, in relation with second order conditions. (In this context an open interesting question concerns the concept of focal point in relation with periodic optimal trajectories). Conjugate points are computed numerically using the HAMPATH code. They are completed by numerical computations using BOCOP code to evaluate strokes with general amplitudes using the system without any approximation and its energy function.

5.4 First and second order optimality conditions

First order necessary conditions for optimality (e.g. the Pontryagin maximum principle) and second order conditions play a crucial role in the selection and the characterization of solutions (minimizers) for problems in optimal control. Very general versions of first and second order optimality conditions are now available. Here, we restrict attention to optimal control problems with end-point constraints of the form

$$\left\{\begin{array}{l} \text{Minimize } \int_0^T L(x(t),u(t))dt \\ \text{subject to} \\ \dot{x}(t) \;=\; f(x(t),u(t)) \quad \text{a.e. } t\in[0,T]\,, \\ u(t) \;\in\; U \quad \text{a.e. } t\in[0,T]\,, \\ c(x(0),x(T))=0\,, \end{array}\right. \tag{5.1}$$

in which $f(.,.) : \mathbb{R}^n \times \mathbb{R}^m \to \mathbb{R}^n$ and $L(.,.) : \mathbb{R}^n \times \mathbb{R}^m \to \mathbb{R}$ are given functions of class $\mathcal{C}^2$, $c(.,.) : \mathbb{R}^n \times \mathbb{R}^n \to \mathbb{R}^\ell$ is a given function of class $\mathcal{C}^2$, and $U \subset \mathbb{R}^m$ is a given set.

Take an optimal trajectory/control couple $(\bar{x}(.), \bar{u}(.))$ for (5.1). The Pontryagin maximum principle (see e.g. [107]) asserts (under appropriate hypotheses) that there exist a vector-valued function $p(.) \in W^{1,1}([0,T]; \mathbb{R}^n)$, a vector $\nu \in \mathbb{R}^\ell$ and a constant $\lambda \geq 0$ such that

(i) $(p(.), \lambda) \neq (0,0)$ (The Nontriviality Condition),

(ii) $-\dot{p}(t) = p^T(t) \frac{\partial f}{\partial x}(\bar{x}(t), \bar{u}(t)) - \lambda \frac{\partial L}{\partial x}(\bar{x}(t), \bar{u}(t))$ a.e.
(The Adjoint System),

(iii) $\langle p(t), f(\bar{x}(t), \bar{u}(t)) \rangle - \lambda L(\bar{x}(t), \bar{u}(t)) = \max_{u \in U} \{ \langle p(t), f(\bar{x}(t), u) \rangle - \lambda L(\bar{x}(t), u) \}$ a.e.
(The Weierstrass or 'Maximization of the Hamiltonian' Condition),

(iv) $[-p^T(0),\ p^T(T)] = \nu^T D_{x_0, x_T} c(\bar{x}(0), \bar{x}(T))$. (The Transversality Condition).

Take a trajectory/control couple $(x(.), u(.))$ satisfying the control system of (5.1). If all the conditions (i)-(iv) of the Pontryagin maximum principle are satisfied for some absolutely continuous function $p(.)$, vector $\nu \in \mathbb{R}^\ell$, and $\lambda \geq 0$, then we call $(x(.), p(.))$ an *extremal*.
We shall consider the necessary conditions above both in the 'normal' and 'abnormal' form. 'Normal' means that the maximum principle is valid with the Lagrange multiplier λ (associated with the objective function) different from zero (in this case it is not restrictive to take $\lambda = 1/2$, by standard normalization). Whereas 'abnormal' means that the maximum principle applies with $\lambda = 0$.
The pseudo Hamiltonian (also referred to as 'unmaximized' Hamiltonian) $\mathcal{H} : \mathbb{R}^n \times \mathbb{R}^n \times \mathbb{R}^m \to \mathbb{R}^m$ is the function

$$\mathcal{H}(x, p, u) := \langle p, f(x, u) \rangle - \lambda L(x, u) .$$

If $\bar{u}(t)$ belongs to the interior of U (this holds true whenever we take $U = \mathbb{R}^m$), condition (iii) above can be re-written in the form:

(iii)′ $\frac{\partial \mathcal{H}}{\partial u}(\bar{x}(t), p(t), \bar{u}(t)) = 0$.

Consider the particular case of (5.1) in which we impose partial periodic end-point constraints:

$$x'(0) = x'_0 , \quad x'(T) = x'_T , \quad x''(0) = x''(T) ,$$

in which $x = (x', x'') \in \mathbb{R}^k \times \mathbb{R}^{n-k}$ for some fixed integer $0 \leq k < n$, and $x'_0, x'_T \in \mathbb{R}^k$ are given points. Then, $x''(.)$ represents the periodic component of the state trajectory $x(.)$. Notice that the transversality condition (iv) involves only the component $p''(.)$ of the adjoint arc $p(.)$ (which is associated with the 'periodic component' of a state arc $\bar{x}(.)$, that is $\bar{x}''(.)$),

$$p''(0) = p''(T) .$$

Second order sufficient conditions for (local) optimality have been extensively investigated to derive optimal solutions with the property to be (locally) unique. This cannot be the case of pure periodic (i.e. when $k = 0$ in problem (5.1) above) optimal control problems, in which given any periodic trajectory/control pair, any time translation produces a new periodic trajectory/control pair with the same cost. Therefore there is a growing interest in studying second order conditions in a framework which comprises periodic optimal control problems, and testing them in examples coming from applications (cf. [116], [126] and [62]).
The optimal control problem (5.1) above can be regarded as a sub-Riemannian problem whenever f and L have a particular structure:

$$f(x,u) = \sum_{i=1}^{m} u_i F_i(x) \qquad L(x,u) = \sum_{i=1}^{m} u_i^2 \ ,$$

where $\{F_i : \mathbb{R}^n \to \mathbb{R}^n \mid i = 1, \dots, m\}$ is a family smooth *vector fields* which is bracket generating. (In the representation above, for simplicity, we are also assuming that the vector fields F_i's are orthonormal).
In this case the integral cost $\int_0^T \sum_{i=1}^m u_i^2(t)dt$ represents the energy of a reference trajectory/control couple $(x(.), u(.))$ at a (given) final time T.
The concept of conjugate time (and conjugate point) plays a crucial role in optimality conditions, and can be characterized in terms of the degeneracy of the exponential mapping or, equivalently, of the quadratic form associated with the second variation of the endpoint mapping. A further important feature in the analysis of minimizers is represented by the notion of *cut locus*. We say that a point $\hat{x}$ is in the cut locus of a reference (left-end) point x_0 if we can find two minimizers joining x_0 and $\hat{x}$. It is well known that in Riemannian geometry every extremal is normal and $x(.)$ is not a minimizer if and only if there exist a cut or a conjugate point along $x(.)$ referred to the left end-point $x(0)$ (see for more details [38]).

5.5 The Purcell Three-link swimmer

5.5.1 Mathematical Model

Purcell's 3-link swimmer. The 3-link swimmer is modeled by the position of the center of the second stick $\mathbf{x} = (x, y)$, the angle θ between the x-axis and the second stick (the orientation of the swimmer). The shape of the swimmer defined by the two relative angles α_1 and α_2 (see Fig 5.1). We also denote respectively by L and L_2 the length of the two external arms and central link. In what follows, x' (resp. x'') corresponds to (x, y) (resp. to $(\theta, \alpha_1, \alpha_2)$).
Dynamics via Resistive Force Theory. We approximate the non local hydrodynamic forces exerted by the fluid on the swimmer with local drag forces depending linearly on the velocity. For each $i \in \{1, 2, 3\}$, we denote by $\mathbf{e}_i^{\parallel}$ and $\mathbf{e}_i^{\perp}$ the unit vectors parallel and perpendicular to the i-th link, and we also introduce $\mathbf{v}_i(s)$ the

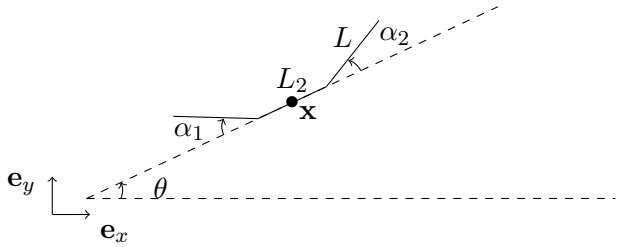

Figure 5.1: Purcell's 3-link swimmer.

velocity of the point at distance s from the extremity of the i-th link, that is

$$\mathbf{v}_1(s) = \dot{\mathbf{x}} - \frac{L_2}{2}\dot{\theta}\mathbf{e}_2^{\perp} - s(\dot{\theta} - \dot{\alpha}_1)\mathbf{e}_1^{\perp}, \quad s \in [0, L],$$
$$\mathbf{v}_2(s) = \dot{\mathbf{x}} - (s - \frac{L_2}{2})\dot{\theta}\mathbf{e}_2^{\perp}, \quad s \in [0, L_2],$$
$$\mathbf{v}_3(s) = \dot{\mathbf{x}} + \frac{L_2}{2}\dot{\theta}\mathbf{e}_2^{\perp} + s(\dot{\theta} - \dot{\alpha}_2)\mathbf{e}_3^{\perp}, \quad s \in [0, L].$$

The force $\mathbf{f}_i$ acting on the i-th segment is taken as

$$\mathbf{f}_i(s) := -\xi \left(\mathbf{v}_i(s) \cdot \mathbf{e}_i^{\parallel}\right) \mathbf{e}_i^{\parallel} - \eta \left(\mathbf{v}_i(s) \cdot \mathbf{e}_i^{\perp}\right) \mathbf{e}_i^{\perp},$$

where ξ and η are respectively the drag coefficients in the directions of $\mathbf{e}_i^{\parallel}$ and $\mathbf{e}_i^{\perp}$. Neglecting inertia forces, Newton laws are written as

$$\begin{cases} \mathbf{F} = 0\,, \\ \mathbf{e}_z \cdot \mathbf{T}_{\mathbf{x}} = 0\,, \end{cases}$$

where $\mathbf{F}$ is the total force exerted on the swimmer by the fluid and $\mathbf{e}_z = \mathbf{e}_x \wedge \mathbf{e}_y$,

$$\mathbf{F} = \int_0^L \mathbf{f}_1(s)\, ds + \int_0^{L_2} \mathbf{f}_2(s)\, ds + \int_0^L \mathbf{f}_3(s)\, ds\,,$$

and $\mathbf{T}_{\mathbf{x}}$ is the corresponding total torque computed with respect to the central point $\mathbf{x}$,

$$\mathbf{T}_{\mathbf{x}} = \int_0^L (\mathbf{x}_1(s) - \mathbf{x}_1) \times \mathbf{f}_1(s)\, ds + \int_0^{L_2} (\mathbf{x}_2(s) - \mathbf{x}_1) \times \mathbf{f}_2(s)\, ds + \int_0^L (\mathbf{x}_3(s) - \mathbf{x}_1) \times \mathbf{f}_3(s)\, ds\,,$$

where $x_i = (x_i, y_i)$, for $i = 1, 2, 3$, corresponds to the left-end point of the i-th link, and $x_i(s) = x_i + se_i$.
Since the $\mathbf{f}_i(s)$ are linear in $\dot{\mathbf{x}}$, $\dot{\theta}$, $\dot{\alpha}_1$, $\dot{\alpha}_2$, the system (5.5.1) can be rewritten as

$$\mathbf{A}(z) \cdot \begin{pmatrix} \dot{\mathbf{x}} \\ \dot{\theta} \end{pmatrix} - \mathbf{B}(z) \cdot \begin{pmatrix} \dot{\alpha}_1 \\ \dot{\alpha}_2 \end{pmatrix} = 0,$$

where $z(t) := (\alpha_1, \alpha_2, x, y, \theta)(t)^T$. The matrix $\mathbf{A}(z)$ is known as the "Grand Resistance Matrix" and is invertible (see [6]). Then the dynamics of the swimmer is finally expressed as an ODE system

$$\dot{z}(t) = f(z, \dot{\alpha}_1, \dot{\alpha}_2) = \dot{\alpha}_1(t)\, F_1(z(t)) + \dot{\alpha}_2(t)\, F_2(z(t))\,,$$

where $\begin{pmatrix} F_1(z) & F_2(z) \end{pmatrix} := \begin{pmatrix} \mathbb{I}_2 \\ \mathbf{A}^{-1}(z)\mathbf{B}(z) \end{pmatrix}$ with $\mathbb{I}_2$ the 2×2 identity matrix. The detailed expression for the F_i is quite complicated and takes several pages (see e.g. [6, 67, 68]).

At the end, the dynamics of the swimmer is governed by an ordinary differential equation linear with respect to the speed of deformation, $\dot{\alpha}_i$, $i = 1, 2$. By considering the latter as a control function, $u_i := \dot{\alpha}_i$, $i = 1, 2$, we then obtain a linear control problem without drift.

By definition, the power expanded during a time interval $[0, T]$ by the swimmer is given by (see [10] for more details)

$$\int_0^T \left(\int_0^L \mathbf{f}_1 \cdot \mathbf{v}_1 + \int_0^{L_2} \mathbf{f}_2 \cdot \mathbf{v}_2 + \int_0^L \mathbf{f}_3 \cdot \mathbf{v}_3 \right). \tag{5.2}$$

Notice that the power is then a quadratic function with respect to the speed of deformation of the body.

5.6 Local analysis for the three-link Purcell swimmer

The sub-Riemannian structure of the Purcell swimmer model allows to consider a motion of first-order approximation which takes into account the non-isotropic behavior of the sub-Riemannian distance, called *nilpotent approximation*. This approximation is called nilpotent in the sense that the vector fields F_1 and F_2 can be approximated (using new coordinates, called *privileged coordinates*) by vector fields $\hat{F}_1$ and $\hat{F}_2$ which generate a nilpotent Lie algebra. The nilpotent approximation together with the accompanying privileged coordinates constitutes the basis for the infinitesimal calculus adapted to the particular structure of the (nonholonomic) control system modeling the Purcell swimmer. We refer the reader for these constructs for instance to [21].

5.6.1 Computations of the nilpotent approximation

Let us denote $D = \text{span}\{\hat{F}_1, \hat{F}_2\}$, $D_1 = D$, $D_2 = \text{span}\{D_1 \cup [D_1, D_2]\}$ and $D_3 = \text{span}\{D_2 \cup [D_1, D_2]\}$. At the point x_0 we have a $(2, 3, 5)-$distribution corresponding to the respective rank of D_1, D_2 and D_3.

We write the control system as $\dot{x} = Fu = \sum_{i=1}^{2} u_i F_i$.

5.6.1.1 Feedback group

The pseudo-group $\mathcal{G} = (\varphi, \beta)$ is defined by the actions :

- local diffeomorphism φ :
  let $\dot{x} = X(x)$ and $x = \varphi(y)$.
  The action of φ on a vector field X is $\dot{y} = (\varphi * X)(y) = \left[\frac{\partial \varphi}{\partial y}^{-1} X \, o \, \varphi\right](y)$,
  $\varphi * F = (\varphi * F_1, \varphi * F_2)$.

- feedback β :
  $u = \beta(x)v$ where β is a 2×2 invertible matrix. The action of β transforms F into $F\beta$.

5.6.1.2 Computations

Let us define the variables x_i, for $i = 1, \cdots, 5$, as $x_1 = \alpha_1$, $x_2 = \alpha_2$, $(x_3, x_4) = \mathbf{x}$, $x_5 = \theta$. In the rest of the computations, we set $L = 1$, $L_2 = 2$, $\xi = 1$, $\eta = 2$.
Hence, the 2-jets of F_1 and F_2 at zero are expressed by

$$\begin{aligned} F_1(x) = &\frac{\partial}{\partial x_1} + \left(-\frac{1}{6}\, x_5 - \frac{4}{27}\, x_1 - \frac{2}{27}\, x_2\right) \frac{\partial}{\partial x_3} \\ &+ \left(\frac{1}{6} - \frac{1}{12}\, {x_5}^2 - \frac{2}{27}\, x_5\, x_2 - \frac{4}{27}\, x_5\, x_1 - \frac{1}{27}\, {x_1}^2 - \frac{1}{27}\, x_1 x_2 - \frac{1}{36}\, {x_2}^2\right) \frac{\partial}{\partial x_4} \\ &+ \left(-\frac{7}{27} + \frac{2}{81}\, {x_1}^2 - \frac{2}{81}\, x_1 x_2 - \frac{5}{162}\, {x_2}^2\right) \frac{\partial}{\partial x_5} + O(|x|^3) \end{aligned}$$

$$\begin{aligned} F_2(x) = &\frac{\partial}{\partial x_2} + \left(\frac{1}{6}\, x_5 + \frac{4}{27}\, x_2 + \frac{2}{27}\, x_1\right) \frac{\partial}{\partial x_3} \\ &+ \left(-\frac{1}{6} + \frac{1}{12}\, {x_5}^2 + \frac{4}{27}\, x_5\, x_2 + \frac{2}{27}\, x_5\, x_1 + \frac{1}{36}\, {x_1}^2 + \frac{1}{27}\, x_1 x_2 + \frac{1}{27}\, {x_2}^2\right) \frac{\partial}{\partial x_4} \\ &+ \left(-\frac{7}{27} - \frac{5}{162}\, {x_1}^2 - \frac{2}{81}\, x_1 x_2 + \frac{2}{81}\, {x_2}^2\right) \frac{\partial}{\partial x_5} + O(|x|^3) \end{aligned}$$

The normal forms of these mappings (see [111]) are

$$(\varphi * F_1) = \tfrac{\partial}{\partial x_1} + O(|x|^3), \quad (\varphi * F_2) = \tfrac{\partial}{\partial x_2} + x_1 \tfrac{\partial}{\partial x_3} + x_3 \tfrac{\partial}{\partial x_4} + x_1^2 \tfrac{\partial}{\partial x_5} + O(|x|^3). \quad (5.3)$$

We introduce the weights 1 for x_1, x_2, 2 for x_3 and 3 for x_4, x_5. If x_i is of order p, $\frac{\partial}{\partial x_i}$ is of order $-p$ to define the nilpotent normal form of order -1.
We write $\varphi = \varphi_N \; o \; ... \; o \; \varphi_1 : \mathbb{R}^5 \to \mathbb{R}^5$. We shall employ $N = 13$ steps. At each step i, for $i = 1, ..., N$, of the computations we shall use the following notation :

. $x = (x_1, x_2, x_3, x_4, x_5)$ are the old local coordinates and $y = (y_1, y_2, y_3, y_4, y_5)$ the new ones resulting from the change of variables φ_i,

. $x_j = \varphi_i^{(j)}(y_j) : \mathbb{R} \to \mathbb{R}$ denoting the j^{th} component of φ_i for some $j \in \{1, ..., 5\}$. The other components $\varphi_i^{(k)}$, $k \neq j$ are the identity transformations.

The successive change of variables are given by

1. $x_5 = \varphi_1^{(5)}(y_5) = y_5 - \frac{7}{27} y_1$,
2. $x_3 = \varphi_2^{(3)}(y_3) = y_3 - \frac{1}{6} y_5 y_1 - \frac{17}{324} y_1^2 - \frac{2}{27} y_2 y_1$,
3. $x_4 = \varphi_3^{(4)}(y_4) = y_4 + \frac{1}{6} y_1 - \frac{37}{3\times 8748} y_1^3$,
4. $x_5 = \varphi_4^{(5)}(y_5) = y_5 + \frac{2}{24} y_1^3 - \frac{2}{162}$,
5. $x_5 = \varphi_5^{(5)}(y_5) = y_5 - \frac{7}{27} y_2$,
6. $x_3 = \varphi_6^{(3)}(y_3) = \frac{5}{81} y_3 + \frac{17}{324} y_2^2 + \frac{1}{6} y_5 y_2$,
7. $x_4 = \varphi_7^{(4)}(y_4) = y_4 - y_3 y_2$,
8. $x_4 = \varphi_8^{(4)}(y_4) = y_4 + \frac{37}{3\times 8748} y_2^3$,
9. $x_4 = \varphi_9^{(4)}(y_4) = y_4 - 54 \times \frac{83}{8748} y_5$,
10. $x_4 = \varphi_{10}^{(4)}(y_4) = y_4 + \frac{2270}{2187} y_2 y_3 + \frac{5}{81} y_5 y_3 + \frac{83}{3\times 6561} y_2^3$,
11. $x_4 = \varphi_{11}^{(4)}(y_4) = -\frac{83}{2187} y_4$,
12. $x_5 = \varphi_{12}^{(5)}(y_5) = y_5 + \frac{1}{27} y_3 y_2 + \frac{2}{3\times 81} y_2^3$,
13. $x_5 = \varphi_{13}^{(5)}(y_5) = -\frac{1}{54} y_5 - \frac{1}{27} y_4$.

Neglecting terms of order greater than 3, we denote by $\hat{F}_1, \hat{F}_2$ the resulting vector fields.

Remark 5.1. *The construction of the diffeomorphism relates the normalized coordinates to the physical coordinates. A similar transformation details the effect on a frame.*

5.6.2 Integration of extremal trajectories

For two vector fields F and G, we use the following Lie bracket convention

$$[F, G](x) = \frac{\partial F}{\partial x}(x) G(x) - \frac{\partial G}{\partial x}(x) F(x)$$

Computing we have

$$\hat{F}_1(x) = \frac{\partial}{\partial x_1}, \qquad \hat{F}_2(x) = \frac{\partial}{\partial x_2} + x_1 \frac{\partial}{\partial x_3} + x_3 \frac{\partial}{\partial x_4} + x_1^2 \frac{\partial}{\partial x_5},$$
$$[\hat{F}_1, \hat{F}_2](x) = -\frac{\partial}{\partial x_3} - 2x_1 \frac{\partial}{\partial x_5}, \quad [[\hat{F}_1, \hat{F}_2], \hat{F}_1](x) = -2\frac{\partial}{\partial x_5},$$
$$[[\hat{F}_1, \hat{F}_2], \hat{F}_2](x) = \frac{\partial}{\partial x_4}.$$

All brackets of length greater than 3 are zero.
We introduce *the Hamiltonian lifts* related to the vector fields above:

$$H_1 = \langle p, \hat{F}_1(x)\rangle = p_1, \qquad H_2 = \langle p, \hat{F}_2(x)\rangle = p_2 + p_3x_1 + p_4x_3 + p_5x_1^2,$$
$$H_3 = \langle p, [\hat{F}_1, \hat{F}_2](x)\rangle = -p_3 - 2x_1p_5, \quad H_4 = \langle p, [[\hat{F}_1, \hat{F}_2], \hat{F}_1](x)\rangle = -2p_5,$$
$$H_5 = \langle p, [[\hat{F}_1, \hat{F}_2], \hat{F}_2](x)\rangle = p_4.$$

We recall the following relation for the Poisson brackets of two lifting Hamiltonians H_F and H_G of vector fields F and G. If

$$H_F = \langle p, F(x)\rangle, \quad H_G = \langle p, G(x)\rangle,$$

are the Hamiltonian lifts of vector fields of F and G, then we have

$$\{H_F, H_G\} = \langle p, [F, G](x)\rangle.$$

We consider the SR-Cartan flat case [111], [51]

$$\dot{x} = \sum_{i=1}^{2} u_i\hat{F}_i, \quad \min_u \int_0^T (u_1^2 + u_2^2)dt.$$

Normal case. The pseudo Hamiltonian is

$$\mathcal{H} = \sum_i u_iH_i - \frac{1}{2}(u_1^2 + u_2^2).$$

The Pontryagin maximum principle [107] gives $u_i = H_i$.
Hence, the true Hamiltonian is

$$H = \frac{1}{2}(H_1^2 + H_2^2). \tag{5.4}$$

Computing we have

$$\dot{H}_1 = dH_1(\vec{H}) = \{H_1, H_2\}H_2 = \langle p, [\hat{F}_1, \hat{F}_2](x)\rangle H_2 = H_2H_3,$$

$$\dot{H}_2 = -H_3H_1, \qquad \dot{H}_3 = H_1H_4 + H_2H_5,$$
$$\dot{H}_4 = 0 \quad \text{hence} \quad H_4 = c_4, \quad \dot{H}_5 = 0 \quad \text{hence} \quad H_5 = c_5.$$

Fixing the level energy, $H_1^2 + H_2^2 = 1$ we set $H_1 = \cos(\theta)$ and $H_2 = \sin(\theta)$.

$$\dot{H}_1 = -\sin(\theta)\dot{\theta} = H_2H_3 = \sin(\theta)H_3.$$

Hence $\dot{\theta} = -H_3$ and

$$\ddot{\theta} = -(H_1c_4 + H_2c_5) = -c_4\cos(\theta) - c_5\sin(\theta) = -A\sin(\theta + \phi)$$

where A and ϕ are constants (depending only on c_4 and c_5).
By identification, we get $A\sin(\phi) = c_4$ and $A\cos(\phi) = c_5$.
Let $\psi = \theta + \phi$, we get

$$\frac{1}{2}\dot{\psi}^2 - A\cos(\psi) = B, \tag{5.5}$$

where B is a constant.
We have the two following cases :

Oscillating case

$$\dot{\psi}^2 = 4A\left(\frac{1}{2} + \frac{B}{2A} - \sin^2(\psi/2)\right).$$

We introduce $\omega^2 = A$ and $k^2 = \frac{1}{2} + \frac{B}{2A}$ with $0 < k < 1$, and we obtain [87]

$$\sin(\psi/2) = k\,\mathrm{sn}(u,k), \quad \cos(\psi/2) = \mathrm{dn}(u,k)$$

where $u = \omega t + \varphi_0$.
H_1 and H_2 are elliptic functions of the first kind. Therefore the system becomes

$$\begin{aligned} &\dot{x}_1 = H_1, && \dot{x}_2 = H_2, && \dot{x}_3 = H_2 x_1, \\ &\dot{x}_4 = H_2 x_3, && \dot{x}_5 = H_2 x_1^2. \end{aligned} \tag{5.6}$$

Parameterizing (5.6) with respect to s we have

$$\omega\frac{\mathrm{d}x_1}{\mathrm{d}s} = \cos(\vartheta\left((s-\varphi_0)/\omega\right)) = 2\,k\,\sin\left(\phi\right)\mathrm{sn}\left(s\right)\mathrm{dn}\left(s\right) + \left(2\,\mathrm{dn}^2\left(s\right) - 1\right)\cos\left(\phi\right). \tag{5.7}$$

$$\omega\frac{\mathrm{d}x_2}{\mathrm{d}s} = \sin(\vartheta\left((s-\varphi_0)/\omega\right)) = 2\,k\,\cos\left(\phi\right)\mathrm{sn}\left(s\right)\mathrm{dn}\left(s\right) + \left(1 - 2\,\mathrm{dn}^2\left(s\right)\right)\sin\left(\phi\right). \tag{5.8}$$

$$\begin{aligned} \omega^2\frac{\mathrm{d}x_3}{\mathrm{d}s} &= \omega\sin(\vartheta((s-\varphi_0)/\omega))x_1((s-\varphi_0)/\omega) \\ &= -4\,k^2\sin\left(\phi\right)\cos\left(\phi\right)\mathrm{cn}\left(s\right)\mathrm{sn}\left(s\right)\mathrm{dn}\left(s\right) + 2\,\mathrm{E}\left(s\right)\big)\sin\left(\phi\right)\cos\left(\phi\right) + \\ &\quad 2\,x_1(\varphi_0)\,k\,\cos\left(\phi\right)\mathrm{sn}\left(s\right)\mathrm{dn}\left(s\right) + \left(-2\,\mathrm{dn}^2\left(s\right) + 1\right)x_1(\varphi_0)\,\sin\left(\phi\right) + \big(-2\,s\,\mathrm{sn}\left(s\right)\mathrm{dn}\left(s\right) - \\ &\quad 4\,\mathrm{cn}\left(s\right)\mathrm{dn}^2\left(s\right) + 4\,\mathrm{sn}\left(s\right)\mathrm{dn}\left(s\right)\mathrm{E}\left(s\right) + 2\,\mathrm{cn}\left(s\right)\big)k\,\cos^2(\phi) + \big(2\,s\,\mathrm{dn}^2\left(s\right) - \\ &\quad 4\,\mathrm{dn}^2\left(s\right)\mathrm{E}\left(s\right) - s + \left(4\,\mathrm{cn}\left(s\right)\mathrm{dn}^2\left(s\right) - 2\,\mathrm{cn}\left(s\right)\right)k. \end{aligned} \tag{5.9}$$

$$\begin{aligned} \omega^3\frac{\mathrm{d}x_4}{\mathrm{d}s} &= \omega^2\sin(\vartheta((s-\varphi_0)/\omega))x_3((s-\varphi_0)/\omega) \\ &= 4\,k^4\cos^3(\phi)\,\mathrm{sn}^4\left(s\right) - 8\,k^4\cos\left(\phi\right)\mathrm{sn}^4\left(s\right) - 4\,k^2x_1(\varphi_0)\,\cos^2(\phi)\,\mathrm{cn}\left(s\right)\mathrm{sn}\left(s\right)\mathrm{dn}\left(s\right) + \\ &\quad 2\,x_3(\varphi_0)\,k\,\cos\left(\phi\right)\mathrm{sn}\left(s\right)\mathrm{dn}\left(s\right) + 4\,k^3\sin\left(\phi\right)\mathrm{sn}\left(s\right)\mathrm{dn}\left(s\right) + \big(-s^2\,\mathrm{sn}\left(s\right)\mathrm{dn}\left(s\right) - \\ &\quad 4\,s\,\mathrm{cn}\left(s\right)\mathrm{dn}^2\left(s\right) + 4\,s\,\mathrm{sn}\left(s\right)\mathrm{dn}\left(s\right)\mathrm{E}\left(s\right) + 8\,\mathrm{cn}\left(s\right)\mathrm{dn}^2\left(s\right)\mathrm{E}\left(s\right) - \\ &\quad 4\,\mathrm{sn}\left(s\right)\mathrm{dn}\left(s\right)\mathrm{E}\left(s\right)^2 + 2\,s\,\mathrm{cn}\left(s\right) - 4\,\mathrm{cn}\left(s\right)\mathrm{E}\left(s\right) - 2\,\mathrm{sn}\left(s\right)\mathrm{dn}\left(s\right)\big)k\,\sin\left(\phi\right) + \\ &\quad \big(4\,s\,\mathrm{cn}\left(s\right)\mathrm{sn}\left(s\right)\mathrm{dn}\left(s\right) - 8\,\mathrm{cn}\left(s\right)\mathrm{sn}\left(s\right)\mathrm{dn}\left(s\right)\mathrm{E}\left(s\right) + 4\,\mathrm{dn}^2\left(s\right) - 2\big)k^2\cos^3(\phi) + \big(- \\ &\quad 2\,x_3(\varphi_0)\,\mathrm{dn}^2\left(s\right) + x_3(\varphi_0)\big)\sin\left(\phi\right) + \big(s^2\,\mathrm{sn}\left(s\right)\mathrm{dn}\left(s\right) + 4\,s\,\mathrm{cn}\left(s\right)\mathrm{dn}^2\left(s\right) - \\ &\quad 4\,s\,\mathrm{sn}\left(s\right)\mathrm{dn}\left(s\right)\mathrm{E}\left(s\right) - 8\,\mathrm{cn}\left(s\right)\mathrm{dn}^2\left(s\right)\mathrm{E}\left(s\right) + 4\,\mathrm{sn}\left(s\right)\mathrm{dn}\left(s\right)\mathrm{E}\left(s\right)^2 - 2\,s\,\mathrm{cn}\left(s\right) + \\ &\quad 4\,\mathrm{cn}\left(s\right)\mathrm{E}\left(s\right)\big)k\,\sin^3(\phi) + \big(2\,s\,\mathrm{dn}^2\left(s\right) - 4\,\mathrm{dn}^2\left(s\right)\mathrm{E}\left(s\right) - s + 2\,\mathrm{E}\left(s\right)\big)x_1(\varphi_0)\,\cos^2(\phi) + \\ &\quad \big(-s^2\,\mathrm{dn}^2\left(s\right) + 4\,s\,\mathrm{dn}^2\left(s\right)\mathrm{E}\left(s\right) - 4\,\mathrm{dn}^2\left(s\right)\mathrm{E}\left(s\right)^2 + 1/2\,s^2 - 2\,s\,\mathrm{E}\left(s\right) + 2\,\mathrm{dn}^2\left(s\right) + \\ &\quad 2\,\mathrm{E}\left(s\right)^2 - 2\big)\cos^3(\phi) + \big(s^2\,\mathrm{dn}^2\left(s\right) - 4\,s\,\mathrm{dn}^2\left(s\right)\mathrm{E}\left(s\right) + 4\,\mathrm{dn}^2\left(s\right)\mathrm{E}\left(s\right)^2 - 1/2\,s^2 + \\ &\quad 2\,s\,\mathrm{E}\left(s\right) - 6\,\mathrm{dn}^2\left(s\right) - 2\,\mathrm{E}\left(s\right)^2 + 6\big)\cos\left(\phi\right) + \big(2\,s\,\mathrm{sn}\left(s\right)\mathrm{dn}\left(s\right) \end{aligned} \tag{5.10}$$

$$+4\,\mathrm{cn}\,(s)\,\mathrm{dn}^2\,(s) - 4\,\mathrm{sn}\,(s)\,\mathrm{dn}\,(s)\,\mathrm{E}\,(s) - 2\,\mathrm{cn}\,(s)\big)\cos(\phi)\,k\,x_1(\varphi_0)\,\sin(\phi) + \big(-4\,\mathrm{dn}^2\,(s) + 2\big)\,k^2\cos(\phi) + \big(4\,\mathrm{sn}^3\,(s)\,\mathrm{dn}\,(s) - 4\,\mathrm{sn}\,(s)\,\mathrm{dn}\,(s)\big)k^3\sin^3(\phi) + \big(-2\,s\,\mathrm{dn}^2\,(s) + 4\,\mathrm{dn}^2\,(s)\,\mathrm{E}\,(s) + s - 2\,\mathrm{E}\,(s)\big)x_1(\varphi_0).$$

$$\omega^3\frac{\mathrm{d}x_5}{\mathrm{d}s} = \omega^2\sin(\vartheta((s-\varphi_0)/\omega))x_1((s-\varphi_0)/\omega)^2 = -8\,k^4\sin^3(\phi)\,\mathrm{sn}^4\,(s) - 8\,k^2x_1(\varphi_0)\,\sin(\phi)\cos(\phi)\,\mathrm{cn}\,(s)\,\mathrm{sn}\,(s)\,\mathrm{dn}\,(s) + 2\,x_1(\varphi_0)^2k\,\cos(\phi)\,\mathrm{sn}\,(s)\,\mathrm{dn}\,(s) + \big(-8\,s\,\mathrm{cn}\,(s)\,\mathrm{sn}\,(s)\,\mathrm{dn}\,(s) + 16\,\mathrm{cn}\,(s)\,\mathrm{sn}\,(s)\,\mathrm{dn}\,(s)\,\mathrm{E}\,(s) - 8\,\mathrm{dn}^2\,(s) + 4\big)k^2\sin^3(\phi) + \big(4\,s\,\mathrm{dn}^2\,(s) - 8\,\mathrm{dn}^2\,(s)\,\mathrm{E}\,(s) - 2\,s + 4\,\mathrm{E}\,(s)\big)\,x_1(\varphi_0)\,\sin(\phi)\cos(\phi) + \big(-2\,s^2\,\mathrm{dn}^2\,(s) + 8\,s\,\mathrm{dn}^2\,(s)\,\mathrm{E}\,(s) - 8\,\mathrm{dn}^2\,(s)\,\mathrm{E}\,(s)^2 + s^2 - 4\,s\,\mathrm{E}\,(s) + 4\,\mathrm{E}\,(s)^2\big)\sin(\phi) + \big(-2\,\mathrm{dn}^2\,(s) + 1\big)\,x_1(\varphi_0)^2\sin(\phi) + \big(8\,s\,\mathrm{cn}\,(s)\,\mathrm{sn}\,(s)\,\mathrm{dn}\,(s) - 16\,\mathrm{cn}\,(s)\,\mathrm{sn}\,(s)\,\mathrm{dn}\,(s)\,\mathrm{E}\,(s)\big)\,k^2\sin(\phi) + \big(2\,s^2\,\mathrm{sn}\,(s)\,\mathrm{dn}\,(s) + 8\,s\,\mathrm{cn}\,(s)\,\mathrm{dn}^2\,(s) - 8\,s\,\mathrm{sn}\,(s)\,\mathrm{dn}\,(s)\,\mathrm{E}\,(s) - 16\,\mathrm{cn}\,(s)\,\mathrm{dn}^2\,(s)\,\mathrm{E}\,(s) + 8\,\mathrm{sn}\,(s)\,\mathrm{dn}\,(s)\,\mathrm{E}\,(s)^2 - 4\,s\,\mathrm{cn}\,(s) + 8\,\mathrm{cn}\,(s)\,\mathrm{E}\,(s)\big)k\,\cos^3(\phi) + \big(8\,\mathrm{sn}^3\,(s)\,\mathrm{dn}\,(s) - 8\,\mathrm{sn}\,(s)\,\mathrm{dn}\,(s)\big)k^3\cos^3(\phi) + \big(-4\,s\,\mathrm{sn}\,(s)\,\mathrm{dn}\,(s) - 8\,\mathrm{cn}\,(s)\,\mathrm{dn}^2\,(s) + 8\,\mathrm{sn}\,(s)\,\mathrm{dn}\,(s)\,\mathrm{E}\,(s) + 4\,\mathrm{cn}\,(s)\big)x_1(\varphi_0)\,k\,\cos^2(\phi) + \big(-8\,s\,\mathrm{cn}\,(s)\,\mathrm{dn}^2\,(s) - 8\,\mathrm{cn}\,(s)\,\mathrm{E}\,(s) + 4\,s\,\mathrm{cn}\,(s) - 8\,\mathrm{cn}\,(s)\,\mathrm{E}\,(s)\big)k\,\cos(\phi) + \big(-8\,\mathrm{sn}^3\,(s)\,\mathrm{dn}\,(s) + 8\,\mathrm{sn}\,(s)\,\mathrm{dn}\,(s)\big)k^3\cos(\phi) + \big(2\,s^2\,\mathrm{dn}^2\,(s) - 8\,s\,\mathrm{dn}^2\,(s)\,\mathrm{E}\,(s) + 8\,\mathrm{dn}^2\,(s)\,\mathrm{E}\,(s)^2 - s^2 + 4\,s\,\mathrm{E}\,(s) - 4\,\mathrm{dn}^2\,(s) - 4\,\mathrm{E}\,(s)^2 + 4\big)\sin^3(\phi) + \big(8\,\mathrm{cn}\,(s)\,\mathrm{dn}^2\,(s) - 4\,\mathrm{cn}\,(s)\big)x_1(\varphi_0)\,k. \tag{5.11}$$

Proposition 5.2. *The solution $x(s)$ of the system (5.6) can be expressed as a polynomial function of $(s, \mathrm{sn}(s), \mathrm{cn}(s), \mathrm{dn}(s), \mathrm{E}(s))$.*

Proof. Integrating equations (5.7) to (5.11) thanks to formulae (5.12) gives the result. □

Remark 5.3. *[87]*

- sn, cn *are* $4K$*-periodics,*
- dn *is* $2K$*-periodic,*
- $E(s) = \frac{E}{k}s + Z(s)$ *where* E, K *are complete integrals and* Z *is the* $2K$*-periodic zeta function.*

The next step is to compute the x variables using quadratures in the oscillating case. Since $x(0) = 0$, solutions depend upon 4 independent parameters $H_i(0)$ for $i = 1, ..., 5$ coupled with the relation $H_1(t=0)^2 + H_2(t=0)^2 = 1$.
To integrate the equations (5.7)-(5.11) explicitly, we use the following primitive functions (see [87])

$$\begin{aligned}
&\int \mathrm{dn}^2(s)\mathrm{d}s = E(s), \quad \int \mathrm{cn}(s)\,\mathrm{dn}(s)\mathrm{d}s = \mathrm{sn}(s), \quad \int \mathrm{cn}(s)\,\mathrm{sn}(s)\,\mathrm{dn}(s)\mathrm{d}s = -\frac{1}{2}\,\mathrm{cn}(s)^2,\\
&\int \mathrm{cn}(s)\mathrm{d}s = \frac{1}{k}\arctan\left(k\frac{\mathrm{sn}(s)}{\mathrm{dn}(s)}\right), \quad \int s\,\mathrm{sn}(s)\,\mathrm{dn}(s)\mathrm{d}s = \frac{1}{k}\arctan\left(k\frac{\mathrm{sn}(s)}{\mathrm{dn}(s)}\right) - s\,\mathrm{cn}(s),\\
&\int E(s)\,\mathrm{sn}(s)\,\mathrm{dn}(s)\mathrm{d}s = -E(s)\,\mathrm{cn}(s) + \frac{1}{2k}\arctan\left(k\frac{\mathrm{sn}(s)}{\mathrm{dn}(s)}\right) + \frac{1}{2}\,\mathrm{dn}(s)\,\mathrm{sn}(s),
\end{aligned} \tag{5.12}$$

$$\int \mathrm{cn}(s)\,\mathrm{dn}^2(s)\mathrm{d}s = \frac{1}{2k}\arctan\left(k\frac{\mathrm{sn}(s)}{\mathrm{dn}(s)}\right) + \frac{1}{2}\,\mathrm{dn}(s)\,\mathrm{sn}(s),$$
$$\int E(s)\,\mathrm{dn}^2(s)\mathrm{d}s = \frac{1}{2}E(s)^2, normal-form \quad \int \mathrm{cn}^2(s)\mathrm{d}s = \frac{E(s)+(k^2-1)s}{k^2},$$
$$\int \mathrm{sn}^4(s)\mathrm{d}s = \frac{1}{3k^4}\left(k^2\,\mathrm{sn}(s)\,\mathrm{dn}(s)\,\mathrm{cn}(s) + (2+k^2)s - 2(k^2+1)E(s)\right),$$
$$\int E(s)\,\mathrm{dn}(s)\,\mathrm{sn}(s)\,\mathrm{cn}(s)\mathrm{d}s = \frac{1}{6k^2}\big((1-2k^2)E(s) + (k^2-1)s$$
$$+ k^2\,\mathrm{dn}(s)\,\mathrm{sn}(s)\,\mathrm{cn}(s) + 3k^2\,\mathrm{sn}^2(s)E(s)\big),$$
$$\int E(s)^2\,\mathrm{dn}(s)\,\mathrm{sn}(s)\mathrm{d}s = -\,\mathrm{cn}(s)E(s)^2 + 2\int E(s)\,\mathrm{dn}(s)^2\,\mathrm{cn}(s)\mathrm{d}s$$
$$= -\,\mathrm{cn}(s)E(s)^2 + E(s)\,\mathrm{dn}(s)\,\mathrm{sn}(s) - 1/3\,\mathrm{cn}(s)(-3+2k^2+k^2\,\mathrm{sn}^2(s)) + \int E(s)\,\mathrm{cn}(s)\mathrm{d}s,$$
$$\int \mathrm{sn}^3(s)\,\mathrm{dn}(s)\mathrm{d}s = -1/3\,\mathrm{cn}(s)(2+\mathrm{sn}^2(s)), \quad \int s^2\,\mathrm{dn}(s)\,\mathrm{sn}(s)\mathrm{d}s = -s^2\,\mathrm{cn}(s) + 2\int s\,\mathrm{cn}(s)\mathrm{d}s,$$
$$\int s\,\mathrm{dn}^2(s)\,\mathrm{cn}(s)\mathrm{d}s = 1/2(\mathrm{dn}(s)\,\mathrm{sn}(s) + \mathrm{cn}(s) + \int s\,\mathrm{cn}(s)\mathrm{d}s),$$
$$\int s\,\mathrm{sn}(s)\,\mathrm{cn}(s)\,\mathrm{dn}(s)\mathrm{d}s = \frac{1}{2}\left(\frac{E(s)+(k^2-1)s}{k^2} - s\,\mathrm{cn}^2(s)\right),$$
$$\int sE(s)\,\mathrm{sn}(s)\,\mathrm{dn}(s)\mathrm{d}s = s(-E(s)\,\mathrm{cn}(s) + 1/2\,\mathrm{dn}(s)\,\mathrm{sn}(s)) + 1/2\,\mathrm{cn}(s) + 1/2\int s\,\mathrm{cn}(s) + \int E(s)\,\mathrm{cn}(s).$$

The final expressions of the solution $(x_i(s))_{i=1,\dots,5}$ of (5.6). (we supply a MAPLE code to check the correctness of the expressions)

$$\omega x_1(s) = x_1(\varphi_0) - 2k\sin(\phi)\,\mathrm{cn}(s) + (-s + 2\,\mathrm{E}(s))\cos(\phi)\,. \tag{5.13}$$

$$\omega x_2(s) = -x_2(\varphi_0) - 2k\cos(\phi)\,\mathrm{cn}(s) + (s - 2\,\mathrm{E}(s))\sin(\phi)\,. \tag{5.14}$$

$$\begin{aligned}\omega^2 x_3(s) = {} & x_3(\varphi_0) - \sin(2\phi)(\mathrm{sn}(s))^2k^2 + k^2\sin(2\phi) - 1/4\sin(2\phi)s^2 + \\ & \cos(2\phi)\,\mathrm{cn}(s)ks - 2kx_1(\varphi_0)\cos(\phi)\,\mathrm{cn}(s) - 2\,\mathrm{E}(s)\,\mathrm{cn}(s)k + s\,\mathrm{cn}(s)k - \\ & \sin(2\phi)(\mathrm{E}(s))^2 - 2x_1(\varphi_0)\sin(\phi)\,\mathrm{E}(s) + \sin(2\phi)s\,\mathrm{E}(s) + 2\,\mathrm{dn}(s)k\,\mathrm{sn}(s) + \\ & x_1(\varphi_0)\sin(\phi)s - 2\cos(2\phi)\,\mathrm{cn}(s)\,\mathrm{E}(s)k.\end{aligned} \tag{5.15}$$

$$\begin{aligned}\omega^3 x_4(s) = {} & x_4(\varphi_0) - 2\cos^3(\phi)sk^2 + 2k^2x_1(\varphi_0)\cos^2(\phi) + 4\cos^3(\phi)\,\mathrm{E}(s)k^2 + \\ & x_3(\varphi_0)\sin(\phi)s - \cos^3(\phi)s^2\,\mathrm{E}(s) + 2\cos^3(\phi)s(\mathrm{E}(s)^2 + \cos(\phi)s^2\,\mathrm{E}(s) - \\ & 2x_3(\varphi_0)\sin(\phi)\,\mathrm{E}(s) - 1/6\cos(\phi)s^3 - 4/3\cos^3(\phi)\,\mathrm{E}(s)^3 - \\ & 1/2x_1(\varphi_0)\cos^2(\phi)s^2 - 2x_1(\varphi_0)\cos^2(\phi)\,\mathrm{E}(s)^2 - 2\cos(\phi)s\,\mathrm{E}(s)^2 - \\ & 2x_1(\varphi_0)s\,\mathrm{E}(s) + k\sin(\phi)\,\mathrm{cn}(s)s^2\cos^2(\phi) + 2\cos^3(\phi)sk^2\,\mathrm{sn}(s)^2 - \\ & 2/3\cos(\phi)\,\mathrm{E}(s) + 4/3k^3\,\mathrm{cn}(s)\,\mathrm{sn}(s)^2\sin(\phi)\cos^2(\phi) + 2k\sin(\phi)\,\mathrm{cn}(s) + \\ & 2/3\cos(\phi)s - 8/3\cos(\phi)k^2\,\mathrm{dn}(s)\,\mathrm{sn}(s)\,\mathrm{cn}(s) - 8/3k^3\sin(\phi)\,\mathrm{cn}(s) + \\ & 4/3\,\mathrm{E}(s)k^2\cos(\phi) - 2/3sk^2\cos(\phi) - 4\cos^3(\phi)k^2\,\mathrm{sn}(s)^2\,\mathrm{E}(s) + \\ & 2x_1(\varphi_0)\cos^2(\phi)s\,\mathrm{E}(s)\end{aligned} \tag{5.16}$$

$$
\begin{aligned}
&-2x_3(\varphi_0)k\cos(\phi)\,\mathrm{cn}(s) + 1/2x_1(\varphi_0)s^2 - 4/3k^3\sin(\phi)\,\mathrm{cn}(s)\cos^2(\phi) - \\
&2k\sin(\phi)\,\mathrm{cn}(s)x_1(\varphi_0)\cos(\phi)s + 4k\sin(\phi)\,\mathrm{cn}(s)x_1(\varphi_0)\cos(\phi)\,\mathrm{E}(s) + \\
&1/6\cos^3(\phi)s^3 + 4/3\cos(\phi)(\mathrm{E}(s)^3 - 4/3k^3\,\mathrm{cn}(s)\,\mathrm{sn}(s)^2\sin(\phi) - \\
&2k^2x_1(\varphi_0)\cos^2(\phi)\,\mathrm{sn}(s)^2 + 2x_1(\varphi_0)\,\mathrm{E}(s)^2 - 4k\sin(\phi)\,\mathrm{cn}(s)s\,\mathrm{E}(s)\cos^2(\phi) + \\
&4k\sin(\phi)\,\mathrm{cn}(s)\,\mathrm{E}(s)^2\cos^2(\phi).
\end{aligned}
$$

$$
\begin{aligned}
\omega^3 x_5(s) = {} & x_5(\varphi_0) + -4k^2x_1(\varphi_0)\sin(\phi)\cos(\phi)\,\mathrm{sn}(s)^2 - 4/3s\sin(\phi) + \\
& 4\cos^2(\phi)\sin(\phi)sk^2\,\mathrm{sn}(s)^2 - 8\cos^2(\phi)\sin(\phi)k^2\,\mathrm{sn}(s)^2\,\mathrm{E}(s) + \\
& 4x_1(\varphi_0)\cos^2(\phi)sk\,\mathrm{cn}(s) - 8x_1(\varphi_0)\cos^2(\phi)\,\mathrm{E}(s)k\,\mathrm{cn}(s) + \\
& 8k\cos(\phi)\,\mathrm{E}(s)\,\mathrm{sn}(s)\,\mathrm{dn}(s) - 4k\cos(\phi)s\,\mathrm{sn}(s)\,\mathrm{dn}(s) + \\
& 8k\cos^3(\phi)\,\mathrm{cn}(s)s\,\mathrm{E}(s) + 4x_1(\varphi_0)\sin(\phi)\cos(\phi)s\,\mathrm{E}(s) + \\
& 4k^2x_1(\varphi_0)\sin(\phi)\cos(\phi) + 8\cos^2(\phi)\sin(\phi)\,\mathrm{E}(s)k^2 - 8/3\sin(\phi)\,\mathrm{E}(s)k^2 - \\
& 4\cos^2(\phi)\sin(\phi)sk^2 - 2k\cos^3(\phi)\,\mathrm{cn}(s)s^2 - 8k\cos^3(\phi)\,\mathrm{cn}(s)\,\mathrm{E}(s)^2 + \\
& 4\sin(\phi)\cos^2(\phi)s\,\mathrm{E}(s)^2 - 2\sin(\phi)\cos^2(\phi)s^2\,\mathrm{E}(s) - x_1(\varphi_0)\cos(\phi)\sin(\phi)s^2 - \\
& 2x_1(\varphi_0)^2k\cos(\phi)\,\mathrm{cn}(s) - 4x_1(\varphi_0)\sin(\phi)\cos(\phi)(\mathrm{E}(s)^2 + 4k\cos(\phi)\,\mathrm{cn}(s) - \\
& 8k^3\cos(\phi)\,\mathrm{cn}(s) - 2x_1(\varphi_0)^2\sin(\phi)\,\mathrm{E}(s) + 1/3\sin(\phi)\cos^2(\phi)s^3 - \\
& 8/3\sin(\phi)\cos^2(\phi)\,\mathrm{E}(s)^3 + x_1(\varphi_0)^2\sin(\phi)s - 8/3k^3\cos^3(\phi)\,\mathrm{cn}(s)\,\mathrm{sn}(s)^2 + \\
& 4/3\,\mathrm{E}(s)\sin(\phi) + 4/3\sin(\phi)sk^2 - 8/3k^2\,\mathrm{dn}(s)\,\mathrm{sn}(s)\,\mathrm{cn}(s)\sin(\phi) + \\
& 4x_1(\varphi_0)k\,\mathrm{sn}(s)\,\mathrm{dn}(s) + 8/3k^3\cos^3(\phi)\,\mathrm{cn}(s).
\end{aligned}
\tag{5.17}
$$

Rotating case

We can perform the same computations as in the oscillating case.

Abnormal case. According to [33], we consider the minimal time problem for the single-input affine system

$$\dot{x}(t) = \hat{F}_1(x(t)) + u(t)\hat{F}_2(x(t))$$

where u is a scalar control.

Denoting $x(.)$ a reference minimum time trajectory, since we consider abnormal extremals, it follows from the Pontryagin maximum principle that along the extremal lift of $x(.)$, there must hold $H_2(x(.),p(.))=0$ and differentiating with respect to t, $\{H_1,H_2\}(x(.),p(.)) = 0$ must hold too. Thanks to a further derivation, the extremals associated with the controls

$$u_a(x,p) = \frac{\{H_1,\{H_2,H_1\}\}(x,p)}{\{H_2,\{H_1,H_2\}\}(x,p)} = \frac{2p_5}{p_4}$$

satisfy the constraints $H_2 = \{H_1,H_2\} = 0$ along $(x(.),p(.))$ and are solutions of

$$\dot{x} = \frac{\partial H_a}{\partial p}, \quad \dot{p} = -\frac{\partial H_a}{\partial x}$$

where H_a is the true Hamiltonian

$$H_a(x,p) = H_1(x,p) + u_a H_2(x,p) = p_1 + 2\,\frac{p_5\,\left(p_2 + p_3\,x_1 + p_4\,x_3 + p_5\,{x_1}^2\right)}{p_4}.$$

From the transversality conditions of the Pontryagin maximum principle, the constraint $H_1(x(.), p(.)) = 0$ must hold too. The extremal system subject to the constraints $H_1 = H_2 = \{H_1, H_2\} = 0$ is integrable and solutions can be written as

$$
\begin{aligned}
&x_1(t) = t + x_1(0), \qquad x_2(t) = 2\,p_5(0)/p_4(0)t + x_2(0),\\
&x_3(t) = p_5(0)/p_4(0)t^2 + 2\,p_5(0)x_1(0)/p_4(0)t + x_3(0),\\
&x_4(t) = 2/3\,p_5(0)^2/p_4(0)^2t^3 - 2\,p_5(0)/p_4(0)^2\left(p_5(0)\,x_1(0)^2 + p_3(0)\,x_1(0) + p_2(0)\right)t\\
&\qquad - p_5(0)\,p_3(0)/p_4(0)^2\,t^2 + x_4(0),\\
&x_5(t) = 2/3\,p_5(0)/p_4(0)\,t^3 + \left(4\,p_5(0)\,x_1(0) + p_3(0)\right)/p_4(0)t^2\\
&\qquad + 2\left(2\,p_5(0)\,x_1(0)^2 + p_3(0)\,x_1(0) + x_3(0)\,p_4(0) + p_2(0)\right)/p_4(0)t + x_5(0),\\
&p_1(t) = \left(-2\,p_5(0)\,p_3(0) - 4\,p_5(0)^2x_1(0)\right)/p_4(0)t + p_1(0),\\
&p_2(t) = p_2(0), \qquad p_3(t) = -2\,p_5(0)\,t + p_3(0), \qquad p_4(t) = p_4(0), \qquad p_5(t) = p_5(0)
\end{aligned}
$$

with $(x_1(0), x_2(0), x_3(0), x_4(0), x_5(0), p_1(0), p_2(0), p_3(0), p_4(0), p_5(0))$ are constants satisfying

$$p_1(0) = 0,\ p_2(0) = p_5(0)x_1(0)^2 - p_4(0)x_3(0),\ p_3(0) = -2p_5(0)x_1(0).$$

5.7 Numerical results

This section presents the numerical simulations performed on the Purcell swimmer problem. Simulations are obtained by applying both direct and indirect methods, and using the solvers Bocop and HamPath. We use the multipliers from the solutions of the direct method to initialize the costate variables in the indirect approach. We show the optimal trajectories obtained for the nilpotent approximation and the true mechanical system.

Bocop. Bocop (`www.bocop.org`, [26]) implements a so-called direct transcription method. Namely, a time discretization is used to rewrite the optimal control problem as a finite dimensional optimization problem (i.e nonlinear programming), solved by an interior point method (Ipopt). We recall below the optimal control problem, formulated with the state $q = (\alpha_1, \alpha_2, x, y, \theta)$ and control $u = (\dot\alpha_1, \dot\alpha_2)$

$$
\begin{cases}
\min\ \int_0^T E(u(t))dt\\
\dot q(t) = F_1(q(t))\,u_1(t) + F_2(q(t))\,u_2(t)\\
\alpha_{1|2}(t) \in [-a, a]\\
x(0) = y(0) = 0,\ x(T) = x_f\\
y(T) = y_f,\ \theta(T) = \theta(0),\ \alpha_{1|2}(T) = \alpha_{1|2}(0)
\end{cases}
\tag{5.18}
$$

HamPath. The HamPath software (`www.hampath.org`, [55]) is based upon indirect methods to solve optimal control problems using simple shooting methods and testing the local optimality of the solutions.
More precisely two purposes are achieved with HamPath:

- *Shooting equations:* to compute periodic trajectories of the Purcell swimmer, we consider the true Hamiltonian H given by the Pontryagin maximum principle and the transversality conditions associated with. The normal and regular minimizing curves are the projection of extremals solutions of the boundary two values problem

$$\begin{cases} \dot{q} = \frac{\partial H}{\partial p}, \qquad \dot{p} = -\frac{\partial H}{\partial q}, \\ x(0) = x_0, \quad x(T) = x_f, \quad y(0) = 0, \quad y(T) = y_f \\ \alpha_{1|2}(T) = \alpha_{1|2}(0), \quad \theta(T) = \theta(0), \\ p_{\alpha_{1|2}}(T) = p_{\alpha_{1|2}}(0), \quad p_\theta(T) = p_\theta(0). \end{cases} \tag{5.19}$$

  where $q = (x, y, \alpha_1, \alpha_2, \theta)$, $p = (p_x, p_y, p_{\alpha_1}, p_{\alpha_2}, p_\theta)$ and $T > 0$ is fixed.
  Due to the sensitivity of the initialization of the shooting algorithm, the latter is initialized with direct methods namely the BOCOP toolbox.

- *Local optimality:* to show that the normal stroke is optimal we perform a rank test on the subspaces spanned by solutions of the variational equation with suitable initial conditions [33].

5.7.1 Nilpotent approximation

Notation: state $x = (x_1, x_2, x_3, x_4, x_5)$, costate $p = (p_1, p_2, p_3, p_4, p_5)$, $\hat{F}_1, \hat{F}_2$ the normal form given by (5.3), and H_1, H_2 are the respective Hamiltonian lifts.

Normal case. In the normal case, we consider the extremal system given by the true Hamiltonian given by (5.4). We compute the optimal trajectories with HAMPATH, and show the state and adjoint variables as functions of time on Fig.5.2. We also illustrate the conjugate points computed according to the algorithm in [38], as well as the smallest singular value for the rank test.

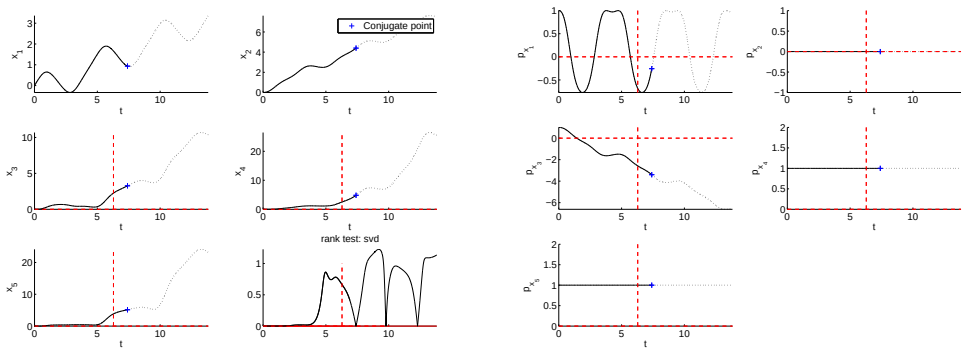

Figure 5.2: Nilpotent approximation (normal case): state, adjoint variables and first conjugate point (blue cross), with the smallest singular value of the rank test.

Property on the first conjugate point. Let us consider the fixed energy level $H_1(x(0),p(0))^2+H_2(x(0),p(0))^2=1$ along the extremals and the initial state $x(0)=0$. We take a large number of random initial adjoint vectors $p(0)$ and numerically integrate the extremal system. For each normal extremal, we compute the first conjugate time t_{1c}, the pulsation $\omega=(p_4(0)^2+4\,p_5(0)^2)^{1/4}$, and the complete elliptic integral $K(k)$, where k is the amplitude

$$k=\frac{1}{2}\sqrt{\frac{2\sqrt{p_4(0)^2+4\,p_5(0)^2}+p_3(0)^2-2\,p_1(0)\,p_4(0)-4\,p_5(0)\,p_2(0)-4\,p_5(0)\,p_4(0)\,x_3(0)}{\sqrt{p_4(0)^2+4\,p_5(0)^2}}}.$$

Let $\gamma(.)$ be a normal extremal starting at $t=0$ from the origin and defined on $[0,+\infty[$. As illustrated on Fig.5.3, there exist a first conjugate point along γ corresponding to a conjugate time t_{1c} satisfying the inequality:

$$0.3\omega t_{1c}-0.4<K(k)<0.5\omega t_{1c}-0.8.$$

Remark 5.4. *In section 5.6.2 $u=\omega t+\varphi_0$ is the normalized parametrization of the solutions.*

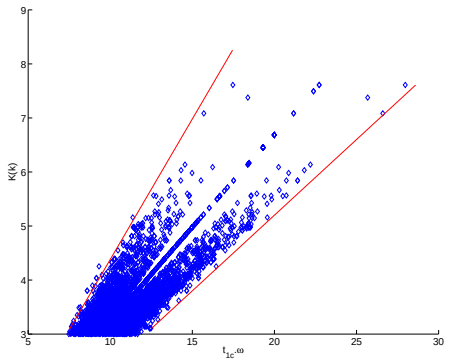

Figure 5.3: Normal extremals with constant energy $H_1^2+H_2^2=1$. The first conjugate point on the elliptic integral $K(k,\omega t_c)$ satisfies $0.3\omega t_{1c}-0.4<K(k)<0.5\omega t_{1c}-0.8$. Illustration for random initial costate $p(0)$.

Abnormal case. Fig.5.4 illustrates the time evolution of the state variables. We check the second order optimality conditions thanks to the algorithm given in [33]. The determinant test and smallest singular value for the rank condition both indicate that there is no conjugate time for abnormal extremals (Fig.5.5).

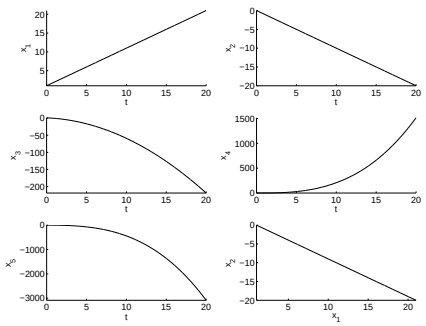

Figure 5.4: Abnormal case: state variables for $x(0) = (1, 0, 1, 0, 0)$, $p(0) = (0, 0, -2, 1, 1)$.

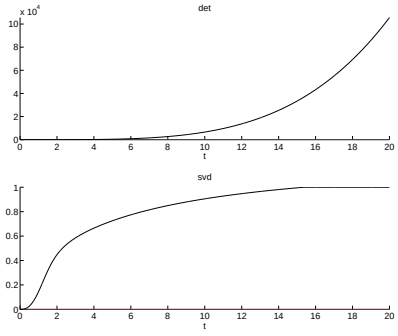

Figure 5.5: Abnormal case: the second order sufficient condition indicates there is no conjugate point.

5.7.2 True mechanical system

We now consider the optimal control problem (5.18) consisting in minimizing either the mechanical energy (5.2) or the criterion $|u|^2$.

Direct method. In the first set of simulations performed by BOCOP, we set $T = 10$, $x_f = 0.5$, and the bounds $a = 3$ large enough so that the solution is actually unconstrained. The state and control variables for the optimal trajectory are shown on Fig.5.6, 5.7 and 5.8, and we observe that the trajectory is actually a sequence of identical strokes. Fig.5.9 shows the phase portrait for the shape angles α_1, α_2, which is an ellipse. The constant energy level satisfied by the optimal trajectory means the phase portrait of the controls is a circle for the $|u|^2$ criterion, but not for the energy criterion. The adjoint variables (or more accurately in this case, the multipliers associated with the discretized dynamics) are shown on Fig.5.10-5.11.

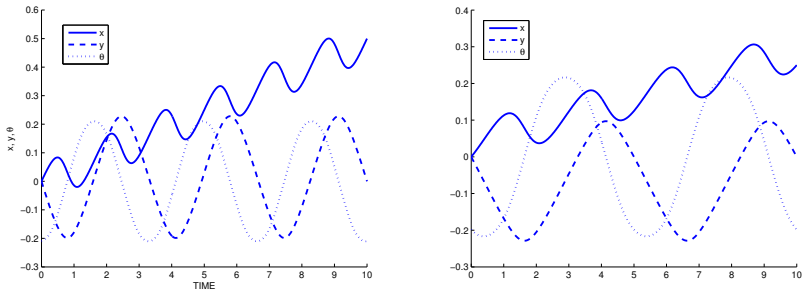

Figure 5.6: Optimal trajectory for $|u|^2$ and energy criterion - state variables x, y, θ

Indirect method. Now we use the multipliers from the BOCOP solutions to initialize the shooting algorithm of HAMPATH. Fig.5.12-5.13 and Fig.5.14-5.15 represent respectively an non intersecting curve and an eight shape curve with the same

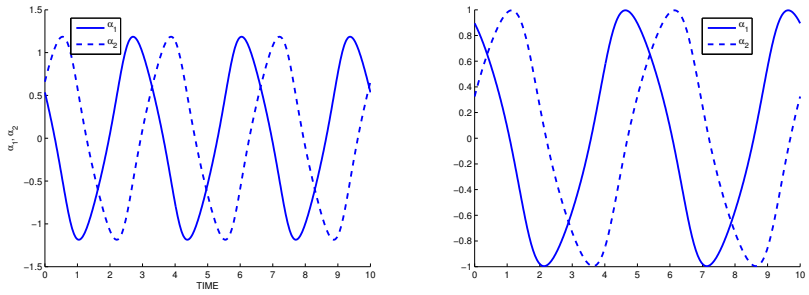

Figure 5.7: Optimal trajectory for $|u|^2$ and energy criterion - state variables α_1, α_2

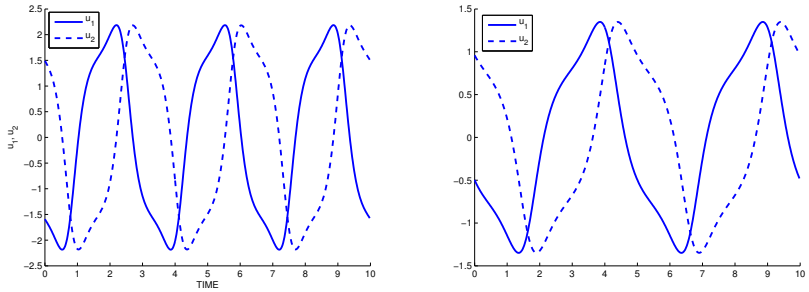

Figure 5.8: Optimal trajectory for $|u|^2$ and energy criterion - control variables

boundary values. Fig.5.16-5.17 shows another eight shape curve obtained for different boundary values. In this three cases, we check the second order optimality conditions according to [38] and observe that there is no conjugate point on $[0, T]$ where $T = 2\pi$.

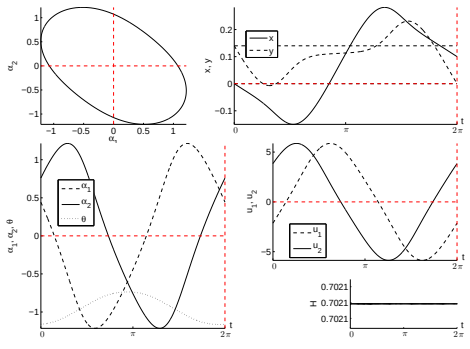

Figure 5.12: Non self-intersecting solution for the $|u|^2$ criterion ($x_0 = 0$, $y_0 = 0.14$, $x_f = 0.1$, $y_f = 0$).

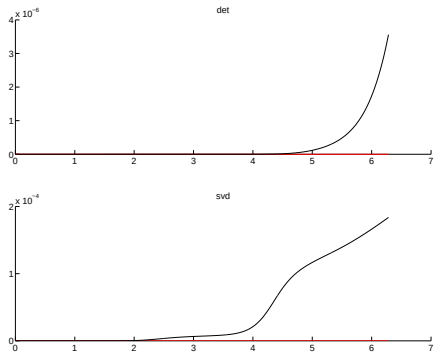

Figure 5.13: Second order conditions: no conjugate time $t_{1c} \in [0, 2\pi]$.

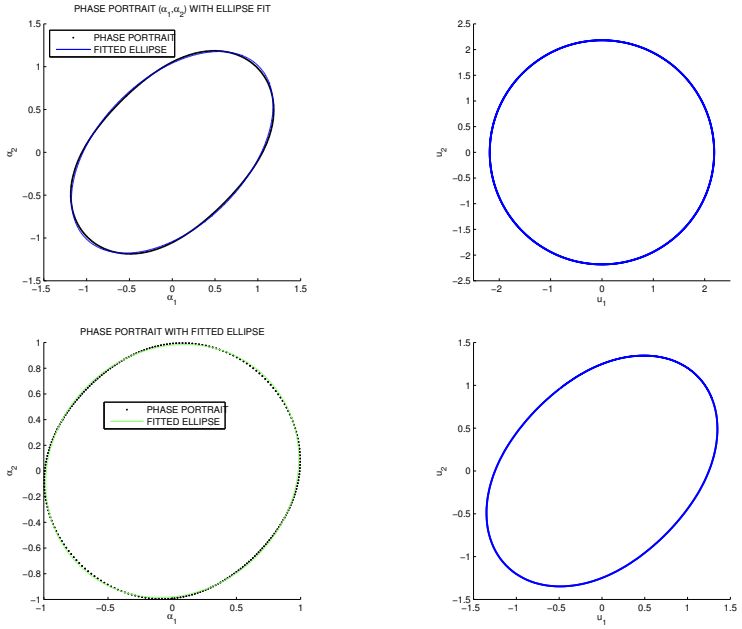

Figure 5.9: Optimal trajectory for $|u|^2$ and energy criterion - Phase portrait (ellipse) and controls

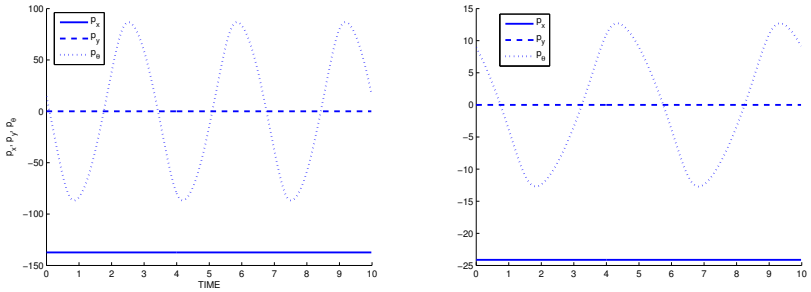

Figure 5.10: Optimal trajectory for $|u|^2$ and energy criterion - adjoint variables

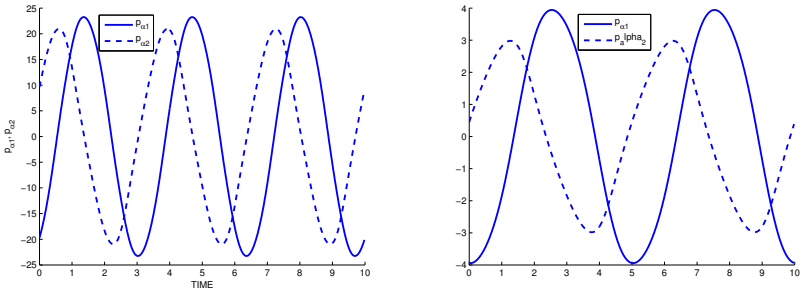

Figure 5.11: Optimal trajectoryfor $|u|^2$ and energy criterion - adjoint variables $p_{\alpha_1}, p_{\alpha_2}$

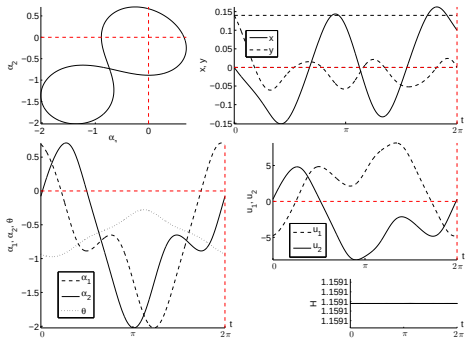

Figure 5.14: Solution `8-SONE` for the $|u|^2$ criterion ($x_0 = 0$, $y_0 = 0.14$, $x_f = 0.1$, $y_f = 0$).

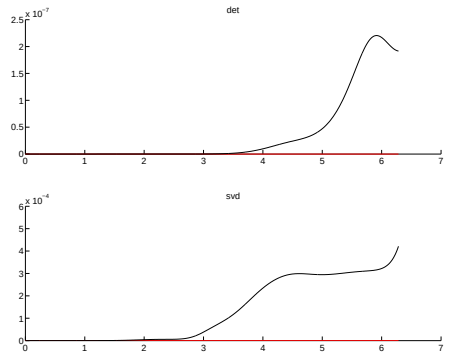

Figure 5.15: Second order conditions: no conjugate time $t_{1c} \in [0, 2\pi]$.

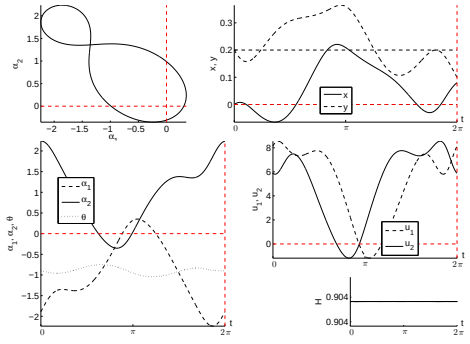

Figure 5.16: Solution `8-NOSE` for the $|u|^2$ criterion ($x_0 = 0$, $y_0 = 0.2$, $x_f = 0.08$, $y_f = 0.1$).

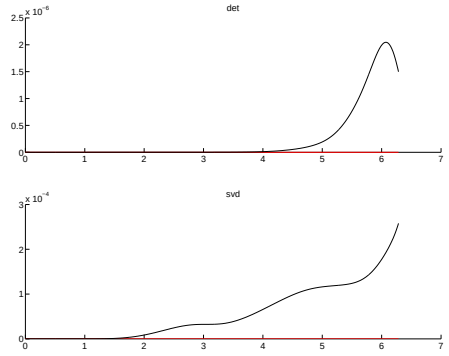

Figure 5.17: Second order conditions: no conjugate time $t_{1c} \in [0, 2\pi]$.

5.7.3 The Purcell swimmer in a round swimming pool

Clearly, due to the symmetry with respect to the initial orientation of the body, we have the following result.

Lemma 5.5. *If $\alpha(t)$, $\theta(t)$, $\overline{x}(t)$, $\overline{y}(t)$ is an extremal solution associated to $u(.)$ with $\theta(0) = 0$, then*

$$x(t) = \cos(\theta_0)\overline{x}(t) - \sin(\theta_0)\overline{y}(t),$$
$$y(t) = \sin(\theta_0)\overline{x}(t) + \cos(\theta_0)\overline{y}(t)$$

is the solution associated with $u(.)$ with $\theta(0) = \theta_0$, $(x(0), y(0)) = (x_0, y_0)$ and with the same cost ($|u|^2$ criterion or energy case).

Remark 5.6. *This leads to define a one parameter family of isocost extremals starting from any point. Practically this justify the following numerical computation.*

Minimizers having the circle as a right end-point constraint.
We present now simulations of the following boundary value problem

$$\begin{cases} \dot{q} = \frac{\partial H}{\partial p}, \qquad \dot{p} = -\frac{\partial H}{\partial q}, \\ x(0) = 0, \quad y(0) = 0, \quad x(T)^2 + y(T)^2 - R^2 = 0, \\ \alpha_{1|2}(T) = \alpha_{1|2}(0), \quad \theta(T) = \theta(0), \\ p_{\alpha_{1|2}}(T) = p_{\alpha_{1|2}}(0), \quad p_\theta(T) = p_\theta(0), \\ p_x(T)y(T) - p_y(T)x(T) = 0. \end{cases} \tag{5.20}$$

where $H(q,p)$ is the true Hamiltonian for the $|u|^2$ criterion, $q = (x, y, \alpha_1, \alpha_2, \theta)$, $p = (p_x, p_y, p_{\alpha_1}, p_{\alpha_2}, p_\theta)$ and $T > 0$ is fixed.

For numerical simulations we set $T = 2\pi$ and $R = 0.1$. Fig.5.18-5.19 show an optimal trajectory, with the test rank for the second order optimality conditions indicating that there is no conjugate time. Fig.5.20 represents the projection in the plane (x, y) of two trajectories for different initial conditions, with the end-point circle constraint drawn in black line.

It turns out that this problem has a particular symmetry, which, taking the initial position angle θ_0 as a parameter, allows to embed minimizers in a (one-parameter) family of minimizers. As a particular consequence we obtain the non-uniqueness of minimizers.

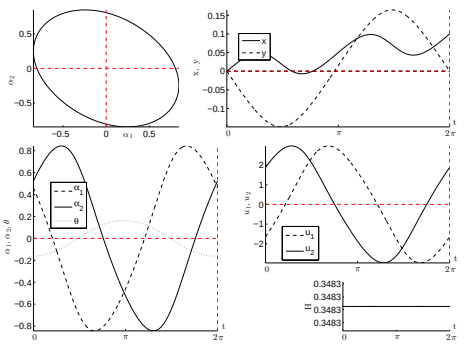

Figure 5.18: Circle end-point constraint: Optimal trajectory - state and control variables

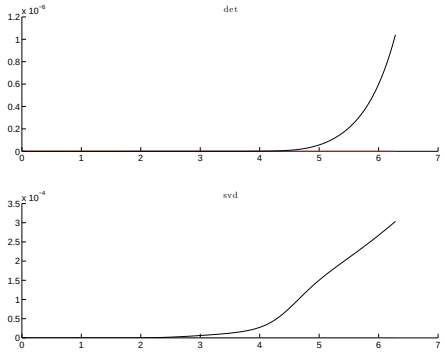

Figure 5.19: Determinant and smallest singular value problem of the rank condition.

5.8 Conclusions and future work

In the present paper we focus on some aspects related to first and second order optimality conditions applied to a mathematical model of the Purcell Three-link swimmer. Combining numerical methods with a geometrical approach we investigate crucial features of this model, as its nilpotent approximation, the integrability of extremals, the periodicity of minimizers, providing and estimate of conjugate points for both normal and abnormal extremals. This model exhibits particular

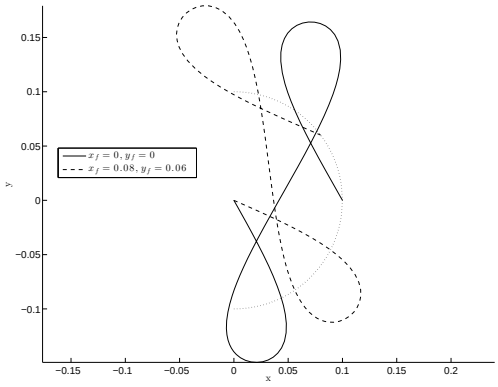

Figure 5.20: Circle end-point constraint: projections of two trajectories in the plane (x, y).

properties (such as symmetries) which make it a very good *case study* to investigate further (non-trivial) features concerning second order optimality conditions, when non-unique minimizers occur.

Chapter 6

Optimal strokes at low Reynolds number: a geometric and numeric study using the Copepod and Purcell swimmers.

Contents

6.1 Description of the article: Optimal strokes at low Reynolds number for the Copepod and the Purcell swimmers 60

6.2 Optimal strokes at low Reynolds number: a geometric and numeric study using the Copepod and Purcell swimmers. . 62

6.3 Introduction 62

6.4 Generalities 64

6.4.1 The mathematical model 64

6.4.2 Elements of sub-Riemannian geometry 66

6.4.3 `Bocop` and `HamPath` software 69

6.5 The Copepod swimmer 70

6.5.1 Abnormal curves in the copepod swimmer 71

6.5.2 The normal case 73

6.6 The Three-Link Purcell swimmer 81

6.6.1 Symmetry properties 81

6.6.2 Nilpotent approximation 82

6.6.3 Numerical results 89

6.6.4 Sufficient second order conditions for the Purcell strokes . . . 94

6.7 Conclusion 97

6.1 Description of the contributions of the article: Optimal strokes at low Reynolds number: a geometric and numeric study using the Copepod and Purcell swimmers.

The aim of this article is to made a comparative study of the Copepod and Purcell swimmers.

First of all, normal and abnormal strokes are computed using the maximum principle and will be related with geometric stroke described by D. Takagi.

Abnormal strokes will form a triangle corresponding to the boundary of the physical domain.

Variety of planar periodic curves such as simple loops, eight curves, limaçons or curves with multiple intersections are solutions as normal strokes. Note that such curves are numerically generated not using the nilpotent approximation which is not suitable to describe such families of curves. Moreover it allow to take into account state constraints using the `Bocop` and `HamPath` software. More precisely, the `Bocop` software is suitable to compute creeping curves with respect to the constraints. Finally, conjugate points computations allow to select only simple loops as candidates as minimizers and numeric computations allow to determine on each energy level a simple loop as candidate for optimality. They are all solutions of the optimal control problem where the displacement is fixed. Using the concept of geometric efficiency, the abnormal triangle is shown to be not optimal and only remains a simple loop solution to the optimality problem (see Fig.6.1 and Table 6.1) The only simple loop solution of the maximum principle using the transversality condition associated with the problem of minimizing the efficiency is computed and given in Fig.6.2

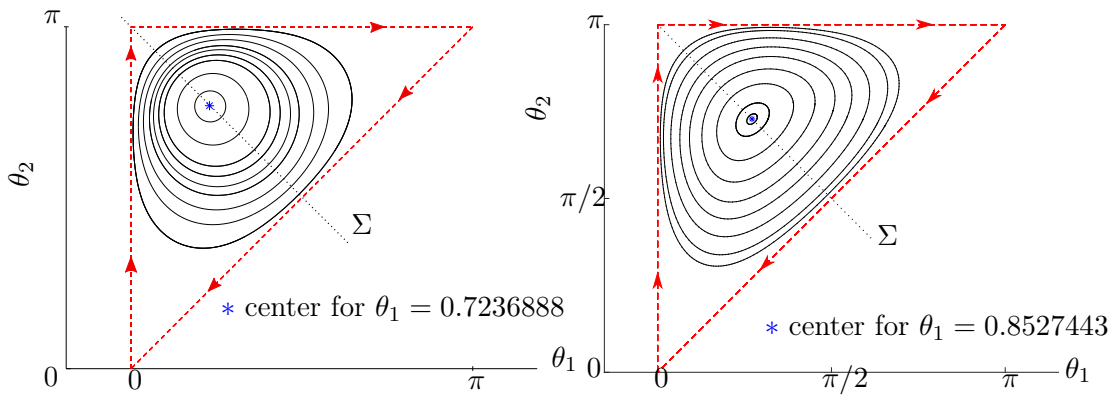

Figure 6.1: One parameter family of geodesic strokes for the Copepod swimmer for the euclidean cost (left) and for the mechanical cost (6.2) (right)

.

Types of γ	$x(T)$	$L(\gamma)$	$x(T)/L(\gamma)$
Abnormal	2.74×10^{-1}	4.93	5.56×10^{-2}
Simple loop (**Optimal Stroke** Fig.6.2)	2.28×10^{-1}	2.56	$\mathbf{8.90 \times 10^{-2}}$
Simple loop (Small Amplitude)	1.50×10^{-1}	1.86	8.06×10^{-2}
Simple loop (Close to the abnormal)	2.59×10^{-1}	3.02	8.58×10^{-2}
Limaçon	2.50×10^{-1}	3.35	7.46×10^{-2}

Table 6.1: Value of the geometric efficiency for abnormal solution and different normal strokes for the Copepod swimmer.

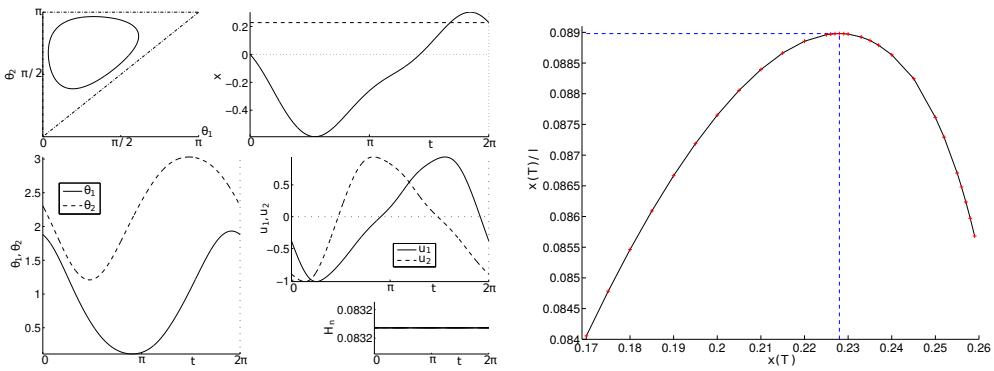

Figure 6.2: *(left)* Optimal stroke of the Copepod swimmer for the geometric efficiency, obtained by the transversality conditions of the maximum principle,
(right) Efficiency of simple loops with respect to the displacement of the Copepod swimmer.

The second study concerns the Purcell swimmer. We complete our preliminary results of the paper presented in Chapter 5. More precisely, numerical continuation methods, initialized by the nilpotent approximation, are used to generate simple curves as candidates to optimal strokes. Also an important contribution of this paper is to deal with sufficient optimality conditions taking into account the non uniqueness of minimizers associated with symmetries. For this purpose, we implement numerically the conditions given by [62]. Note that this algorithm was also implemented for the (simpler) Copepod swimmer.

6.2 Optimal strokes at low Reynolds number: a geometric and numeric study using the Copepod and Purcell swimmers.

Authors: P. Bettiol[1],
B. Bonnard[2],
J. Rouot[3].

In this article, we make a comparative geometric and numeric analysis of the optimal strokes at low Reynolds number using two specific rigid links swimmers: the Copepod swimmer, a symmetric swimmer introduced recently [119] and the historical three-link Purcell swimmer [109] where the cost to minimize is the mechanical power dissipated by the fluid viscous drag forces. This leads to a sub-Riemannian problem which can be analyzed in this rich framework. In particular nilpotent approximation can be used to compute strokes with small amplitudes and they can be continued numerically to compute more general strokes. The concept of geometric efficiency corresponding to the ratio between the displacement and the length of the stroke is introduced to analyze the global optimality. The role of both abnormal and normal strokes is described, in particular in the symmetric case, in relation with observed motions of the micro-organisms. Moreover C^1-optimality is studied using the concept of conjugate and focal points, depending upon their respective shapes. In parallel direct and indirect numerical schemes implemented in the `Bocop` (`www.bocop.org` [26]) and `HamPath` (`www.hampath.org` [55]) software allow to perform numerical simulations, crucial to complete the theoretical study and to evaluate the optimal solutions.

6.3 Introduction

Swimming models at low Reynolds numbers applicable to micro-organisms and restricting to rigid links have been introduced in the fifties [109] and assuming that the displacement is performed minimizing the mechanical energy dissipated by the drag forces, the optimal strokes can be determined in the framework of SR-geometry. This area has recently produced a lot of useful results in our study, e.g. the concept of nilpotent approximation [21] and explicit computations of the spheres with small radius [34, 1] applicable to parameterize and analyze strokes with small amplitudes.

[1]Laboratoire de Mathématiques, Unité CNRS UMR 6205, Université de Bretagne Occidentale, 6, Avenue Victor Le Gorgeu, 29200 Brest, piernicola.bettiol@univ-brest.fr
[2]Inria Sophia Antipolis et Institut de Mathématiques de Bourgogne, 9 avenue Savary, 21078 Dijon, bernard.bonnard@u-bourgogne.fr
[3]Inria Sophia Antipolis, 2004 route des lucioles, F-06902 Sophia Antipolis, jeremy.rouot@inria.fr

Moreover the role of normal and abnormal geodesics [99, 39] and smoothness of the minimizers [110], computations of conjugate points in relation with C^1-optimality (for the fixed initial and final points problem) in the normal and abnormal case [34, 1] are important issues in our specific problem.
Also the concept of optimal strokes is related to *periodic* optimal control and is connected to the standard problem of finding periodic solutions of Hamiltonian vector fields. This problem was introduced by Poincaré in relation with the N-body problem [106] and well studied by this seminal contributor using continuation and variational methods: existence of one-parameter family of periodic trajectories emanating from an equilibrium point [105], direct methods to compute periodic solutions, in relation with the class of homotopy associated with the topology induced by collisions. All contributions valuable to direct and indirect numerical schemes like in the `Bocop` and `HamPath` software [26, 55], and understanding the shape of the optimal strokes, related to the singular configurations of the n-link swimmer.

periodic solutions whose optimality can be analyzed C^1-locally, which corresponds to the notion of weak minimizers, using the concept of conjugate points [34, 2], the concept of focal points taking into account non-uniqueness of minimizers [62] or globally with the notion of geometric efficiency, a simplification of the concept of efficiency of a swimmer [119]. More precisely our article will solve the following questions in relation with the swimmer problem.

First of all, considering the problem of fixing a displacement of a given stroke, the necessary optimality conditions related to the notion of conjugate points are applicable to select only simple loop strokes as candidate to optimality (in the normal case) [33]. Such necessary conditions being complemented by sufficient conditions [62] taking into account non-uniqueness of minimizers in our problem in relation with symmetry properties. In particular, it will be a non academic test bed to the conditions mentioned previously. Secondly the problem leads to analyze the following practical problem. Parameterizing by arc-length using the metric defined by the mechanical energy (or any other metric) allows to formulate the problem as a time minimal control problem. Assuming that the distance is achieved by a sequence of n-strokes (n being not fixed) then the concept of geometric efficiency and the analysis of the corresponding optimal problem, allow to find the optimal solution.

Another very interesting question raises by the swimmer problem is the role of abnormal strokes. In particular, in this article using the Copepod swimmer and the concept of efficiency, the triangular abnormal stroke [119] is shown to be non optimal since a better policy is to reproduce twice a smooth stroke, producing the same displacement. Although this policy is not C^0-closed from the abnormal stroke, it opens a new road to deal with non smooth abnormal geodesics in SR-geometry.

Finally, a contribution of this article is to gather nilpotent approximation in SR-geometry and numeric continuation methods useful in particular for the Purcell swimmer to compute strokes of larger amplitudes starting from strokes with small amplitudes. This method being crucial due to the complexity of the Purcell dynamics [104].

The organization of this article is the following. In section 6.4, due to space restrictions, we briefly present the concepts and results needed in our study. First of all the model [74] of swimming at low Reynolds number is specialized to the case of a n-links swimmer is standard and leads easily to the dynamical model and the explicit form of the equations [104]. Secondly we recall elements of SR-geometry and introduce the concept of geometric efficiency. Finally the two software (`Bocop` and `HamPath`) and their use in our numerical computations are presented. The section 6.5 presents the combination of our geometric and numeric analysis to determine optimal strokes of the Copepod swimmer. This case is very important in our study: it is a model of swimmers of an abundant variety of zooplankton which can be observed, it will be used in the future to design a micro-robot to validate our computations. Moreover the model leads to tractable Lie brackets computations, state constraints form a triangle and has a nice geometric interpretation. As a dynamical model it is sufficiently complex to generate a variety of different strokes in accordance with the classification of periodic planar curves [23]. Finally C^1-optimality can be analyzed using the concept of conjugate points and focal point conditions related to periodicity. The concept of geometric efficiency allows to finalize the study. The section 6.6 is devoted to the three-link Purcell swimmer. The nilpotent approximation is determined to evaluate analytically the strokes with small amplitudes, thanks to integrability. Numeric computations using `Bocop` and `HamPath` software allow to compute more general strokes and to test their optimality with dedicated algorithms to compute conjugate points in the normal and abnormal case. Again, to deal with non unicity of minimizers, in relation with symmetries, we present a solution to the Purcell case.

6.4 Generalities

6.4.1 The mathematical model

In this section, we present briefly the mathematical models, the complete equations in the case of n-links can being explicitly given [104]. The two swimmers are represented in Fig.6.3, with the corresponding state variables:

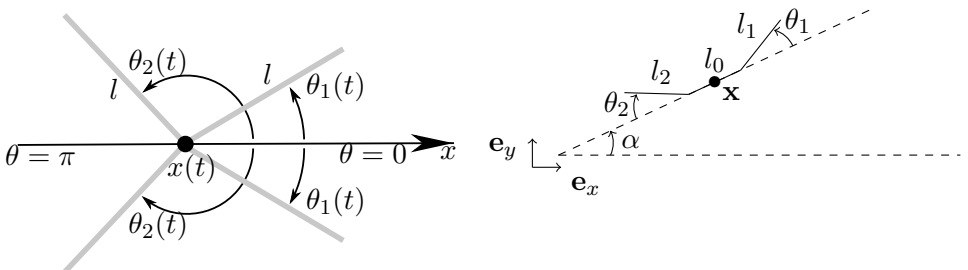

Figure 6.3: *(left)* Copepod swimmer, *(right)* Purcell swimmer.

Copepod swimmer: it is formed by gluing together two scallops. Each pair of symmetric links have their length normalized to $l = 1$.
The swimming velocity at x is given by [119]:

$$\dot{x} = \frac{\dot{\theta}_1 \sin(\theta_1) + \dot{\theta}_2 \sin(\theta_2)}{2 + \sin^2(\theta_1) + \sin^2(\theta_2)} \tag{6.1}$$

and the controls are the angular velocities

$$\dot{\theta}_1 = u_1, \quad \dot{\theta}_2 = u_2.$$

The mechanical power is given by a positive quadratic form $\dot{q}^\intercal M(q)\dot{q}$, $q = (x, \theta)$ where

$$M = \begin{pmatrix} 2 - 1/2(\cos^2(\theta_1) + \cos^2(\theta_2)) & -1/2\sin(\theta_1) & -1/2\sin(\theta_2) \\ -1/2\sin(\theta_1) & 1/3 & 0 \\ -1/2\sin(\theta_2) & 0 & 1/3 \end{pmatrix}$$

and using (6.1) this amounts to minimize the quadratic cost:

$$\int_0^T \left(a(q)u_1^2 + 2b(q)u_1u_2 + c(q)u_2^2\right) \mathrm{d}t \tag{6.2}$$

with

$$\begin{aligned} a &= \frac{1}{3} - \frac{\sin^2\theta_1}{2(2 + \sin^2\theta_1 + \sin^2\theta_2)}, \\ b &= -\frac{\sin\theta_1 \sin\theta_2}{2(2 + \sin^2\theta_1 + \sin^2\theta_2)}, \\ c &= \frac{1}{3} - \frac{\sin^2\theta_2}{2(2 + \sin^2\theta_1 + \sin^2\theta_2)}. \end{aligned}$$

Purcell swimmer: this model is much more complex. Denoting $q = (x, y, \alpha, \theta_1, \theta_2)$ it takes the form:

$$\begin{aligned} \begin{pmatrix} \dot{x} \\ \dot{y} \\ \dot{\alpha} \end{pmatrix} &= \frac{1}{\Delta G} \mathcal{R}_\alpha \begin{pmatrix} g_{11} & g_{12} \\ g_{21} & g_{22} \\ g_{31} & g_{32} \end{pmatrix} \begin{pmatrix} \dot{\theta}_1 \\ \dot{\theta}_2 \end{pmatrix}, \\ \dot{\theta} &= u = S(\theta)\tau, \end{aligned} \tag{6.3}$$

where $\mathcal{R}_\alpha$ is the rotation matrix

$$\mathcal{R}_\alpha = \begin{pmatrix} \cos(\alpha) & -\sin(\alpha) & 0 \\ \sin(\alpha) & \cos(\alpha) & 0 \\ 0 & 0 & 1 \end{pmatrix}$$

and $g_{ij}(\theta)$, $\Delta G(\theta)$ and $S(\theta)$ are detailed [104]. Again the cost function u is minimizing the expanded mechanical power

$$\int_0^T \tau \cdot u \, \mathrm{d}t. \tag{6.4}$$

We use the following terminology.

Definition 6.1. *The two angular variables $\theta = (\theta_1, \theta_2)$ are called the shape variables. A stroke of period T consists of a periodic motion in the shape variables.*

State constraints. Note that the design of the corresponding system will produce state constraints:

- Copepod case. One has:

$$\theta_1, \theta_2 \in [0, \pi],\ \theta_1 \leq \theta_2.$$

- Purcell case. They depend upon the assumption about the length l_0 of the body and the respective lengths l_1, l_2 of the leg and the arms. We shall perform our computations assuming $l_0 = 2$ and $l_1 = l_2 = 1$. Hence we have the amplitude bounds: $\theta_1, \theta_2 \in [-\pi, \pi]$.

6.4.2 Elements of sub-Riemannian geometry

The optimal control problem is written

$$\dot{q} = \sum_{i=1}^{2} u_i G_i(q), \quad \min_{u(.)} \int_0^T (u^\intercal R(q) u)\, \mathrm{d}t, \tag{6.5}$$

where the set of admissible controls $\mathcal{U}$ is the set of bounded measurable mappings. Note that T can be fixed to 2π. The *length* of a admissible trajectory γ of (6.5) associated with a control u is

$$l(\gamma) = \int_0^T (u^\intercal R(\gamma) u)^{1/2}\, \mathrm{d}t$$

Using the standard concepts of sub-Riemannian geometry [78], we introduce the following.

Definition 6.2. *Let D be the distribution* $\mathrm{span}\{G_1, G_2\}$. *Using a feedback transformation $u = \beta(q)v$, we may choose locally an orthonormal frame $F = (F_1, F_2)$ such that the cost function reduces to $v^\intercal v$. Near a point q_0, one can choose the so-called privileged coordinates so that the distribution D can be approximated by a nilpotent distribution denoted $\widehat{D} = \mathrm{span}\{\widehat{G_1}, \widehat{G_2}\}$. Similarly, one can choose an nilpotent orthonormal frame denoted $\{\widehat{F_1}, \widehat{F_2}\}$ to approximate the SR-problem.*

Note that this approximation step is particularly important in the Purcell case where the complexity of the model leads to non realizable analytic computations.

6.4.2.1 Maximum Principle and computations of geodesic equations

The Maximum Principle is used to compute the geodesic equations. We write $z = (q, p)$ the symplectic coordinates and $H_F(z) = p \cdot F(q)$ the Hamiltonian lift of the

vector field F. Assuming that $\{F_1, F_2\}$ forms an orthonormal frame, the pseudo-Hamiltonian takes the form:

$$H(z,u) = \sum_{i=1}^{2} u_i H_i(z) + \lambda_0 \sum_{i=1}^{2} u_i^2$$

where H_i is the Hamiltonian lift of F_i and λ_0 is a constant which can be normalized to $\lambda_0 = -1/2$ (*normal case*) or $\lambda_0 = 0$ (*abnormal case*). Using the condition: $\frac{\partial H}{\partial u} = 0$ one gets the two cases.

- Normal case: We get $u_i = H_i$ and plugging such u_i into H leads to the true Hamiltonian in the normal case: $H_n = \frac{1}{2}\sum_{i=1}^{2} H_i^2$. The corresponding solutions are called *normal extremals* and their projections on the q-space are called *normal geodesics*.
- Abnormal case: We get the constraints $H_i(z) = 0$, $i = 1, 2$. The corresponding solutions are called *abnormal extremals* and their projections are called *abnormal geodesics*.
- A normal geodesic is called strict if it is not the projection of an abnormal extremal.

This leads to the following concepts.

Definition 6.3. *Assuming arc-length parameterization $H_n = 1/2$, the exponential mapping is:* $\exp_{q_0} : (t, p(0)) \to \Pi(\exp(t\overrightarrow{H_n}(z(0))))$, *with* $z(0) = (q_0, p(0))$ *and* Π *is the projection:* $z \mapsto q$. *A conjugate time (normal case) is a time* t_c *such that the function* $\exp_{q_0}$ *is not of full rank at* t_c *and the corresponding point is called a conjugate point along the geodesic with initial condition* $z(0)$. *We denote* t_{1c} *the first conjugate point.*

6.4.2.2 Concepts of SR-geometry adapted to the swimmer problem

Two aspects of the problem are the state constraints, which will not be theoretically studied in this article, and the boundary conditions related to strokes, which will be introduced next in relation with periodic optimal control. First of all, we recall the necessary optimality conditions [62].

Proposition 6.4. *Let* $\bar{q} = (q, q^0)$ *and consider the cost extended system denoted* $\dot{\bar{q}}(t) = F(\bar{q}(t), u(t))$*:*

$$\dot{q} = \sum_{i=1}^{2} u_i G_i(q)$$
$$\dot{q}^0 := L(q,u), \quad q^0(0) = 0$$

and the problem $\min g(\bar{q}(0), \bar{q}(T))$ *for* $u \in U$ *(U is the control domain) and with the boundary condition* $(\bar{q}(0), \bar{q}(T)) \in C$ *where* C *is a closed set and* T *is fixed.*

Introducing $H(\bar{q},\bar{p},u)=\bar{p}\cdot F(\bar{q},u)=p\cdot\sum_{i=1}^{2}u_iG_i(q)+p_0L(q,u)$, $\bar{p}=(p,p_0)$, $\lambda\geq 0,(\bar{p},\lambda)\neq 0$. *Then if* $(\bar{q}^*,u^*)$ *is optimal on* $[0,T]$, *there exists* $\bar{p}^*$ *such that the following necessary conditions are satisfied:*

$$\dot{\bar{q}}^*=\frac{\partial H}{\partial\bar{p}},\quad \dot{\bar{p}}^*=-\frac{\partial H}{\partial\bar{q}}\qquad a.e.$$
$$H(\bar{q}^*,\bar{p}^*,u^*)=\max_{u\in U}H(\bar{q}^*,\bar{p}^*,u)\qquad a.e\ .$$

Moreover $\max_{u\in U}H$ *is constant and the following transversality conditions hold:*

$$(\bar{p}^*(0),-\bar{p}^*(T))\in\lambda\nabla_{\bar{q}(0),\bar{q}(T)}g(\bar{q}^*(0),\bar{q}^*(T))+N_C(\bar{q}^*(0),\bar{q}^*(T)) \tag{6.6}$$

where N_C *is the normal cone.*

Applied to periodic optimal control this lead to the following geometric conditions deduced from the transversality conditions, considering separately periodic conditions and efficiency cost.

Boundary conditions associated with periodicity. We split the state variable q into (q_1,q_2) where q_2 represents the periodic part of q. Let $p=(p_1,p_2)$ be the associated splitting of the adjoint vector. Assuming periodic conditions: $q_2(0)=q_2(T)$ the Maximum Principle leads to the condition:

$$p_2(0)=p_2(T) \tag{6.7}$$

Definition 6.5. *A normal (resp. abnormal) stroke is a stroke corresponding to a normal (resp. abnormal) extremal. A piecewise smooth abnormal stroke is a piecewise smooth stroke such that each smooth sub-arc corresponds to an abnormal arc.*

Shooting equation. To define the *shooting equation*, one restricts the flow to normal extremals, solution of $\overrightarrow{H_n}$, with the following boundary conditions associated with the state variables splitting:

- $q_1(0)=q_{10},q_1(T)=q_{1T}$ where q_{10},q_{1T} are fixed,
- $q_2(0)=q_2(T)$, $p_2(0)=p_2(T)$

In the framework of SR-geometry and in relation with the underlying fixed endpoints we have the following two properties [34, 1].

Property 6.6. *The shooting mapping fails to be locally injective due to the existence of conjugate points.*

Property 6.7. *The shooting mapping is defined on the cylinder and it fails to be proper due to the existence of abnormal extremals.*

Finally in relation with the problem we introduce the following concept.

Definition 6.8. *The geometric efficiency $\mathcal{E}$ of a stroke γ is defined as*

- *Copepod swimmer:* $\mathcal{E} = x(T)/l(\gamma)$,
- *Purcell swimmer:* $\mathcal{E} = \sqrt{x(T)^2 + y(T)^2}/l(\gamma)$

that is the ratio between the euclidean displacement along (part of) the state variable and the sub-Riemannian length of the stroke.

In relation with the problem of maximizing the efficiency one introduces the following additional geometric necessary conditions.

Geometric optimality conditions and efficiency. Denoting $\bar{q} = (q, q^0)$ one introduces the cost extended system:

$$\dot{q} = \sum_{i=1}^{2} u_i G_i(q)$$
$$\dot{q}^0 := L(q,u) \quad q^0(0) = 0$$

and maximizing the efficiency leads to $\min g(q(T), q^0(T))$ with $g = -\mathcal{E}$. If $A(\bar{q}(0), T)$ is the accessibility set from $(\bar{q}(0) = q(0), 0)$ at time T and if $(\bar{q}^*, \bar{p}^*, \bar{u}^*)$ is an optimal solution the geometric optimality conditions are

$$\bar{q}^*(T) \in \partial A(\bar{q}(0), T)$$

and the transversality condition (6.6) gives

$$\bar{p}^*(T) = \lambda \nabla_{\bar{q}} g(\bar{q}^*).$$

6.4.2.3 General concepts in SR-Geometry

Finally we recall the standard concepts of SR-geometry related to the problem with fixed extremities. Having fixed $q(0) = q_0$, the *conjugate locus* $\mathcal{C}(q_0)$ is the set of first conjugate points considering all normal geodesics emanating from q_0. The *cut locus* $C_\Sigma(q_0)$ is the set of points where a (normal or abnormal) geodesic emanating from q_0 ceases to be optimal. The *sphere* $S(q_0, r)$ is formed by the set of points at SR-distance r from q_0.

6.4.3 `Bocop` and `HamPath` software

- `Bocop` . The so-called *direct* approach transforms an infinite dimensional control problem into a finite dimensional optimization problem. This is done by a discretization in time applied to the state space, control variables and the dynamics. This method can take into account control and state variables constraints. It is in general less precise than the *indirect* method based on the Maximum Principle, but more robust with respect to the initialization. It will be used to compute optimal strokes satisfying the state constraints and also as a complementary method to initialize the shooting of the *indirect* method implemented in `HamPath` .

- `HamPath` . This software is based on indirect methods and solve the shooting equation and differential continuation (homotopy) methods and computation of the solutions of the variational equation to check second order conditions of local optimality (conjugate points computations). Having found a stroke using nilpotent approximations and explicit computations (for small amplitudes) or more general solution using `Bocop` , a continuation is performed mainly using as parameter the displacement.

6.5 The Copepod swimmer

We start recalling two types of strokes [119] employing geometric arguments. These strokes will constitute two important reference cases for our analysis of the Copepod model and which will contribute the motivation of our study.

First case (Fig.6.4) The two legs are paddling in sequence followed by a recovery stroke performed in unison. In this case, the first step is to steer θ_1 follows by θ_2 from 0 to π, while the unison sequence corresponds to a displacement from π to 0 with the constraint $\theta_1 = \theta_2$. Note it corresponds to a *triangle stroke* and moreover θ_1 and θ_2 stay in the boundary of the domain.

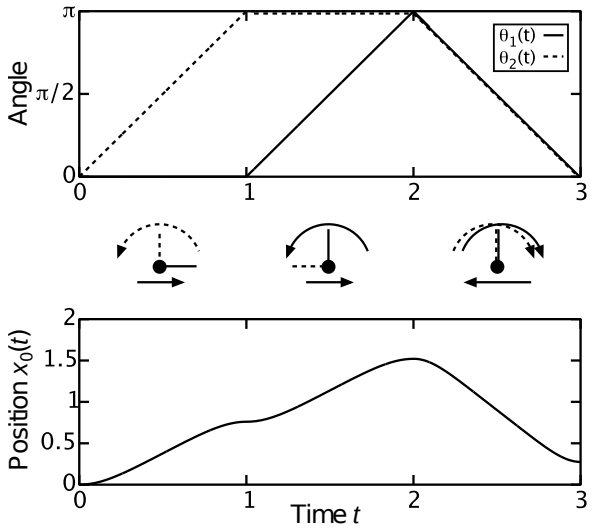

Figure 6.4: Two legs paddling in sequence. The legs perform power strokes in sequence and then a recovery stroke in unison, each stroke sweeping an angle π.

Second case (Fig.6.5) The two legs are assumed to oscillate sinusoidally with period 2π according to

$$\theta_1 = \Phi_1 + a\cos(t), \quad \theta_2 = \Phi_2 + a\cos(t + k_2)$$

with $a = \pi/4$, $\Phi_1 = \pi/4$, $\Phi_2 = 3\pi/4$ and $k_2 = \pi/2$, such parameters being chosen to optimize this efficiency. Assuming $x(0) = 0$, this produces a displacement $x(2\pi) = 0.2$.
Parameters a, Φ_1, Φ_2 and k are designed to maximize the efficiency.

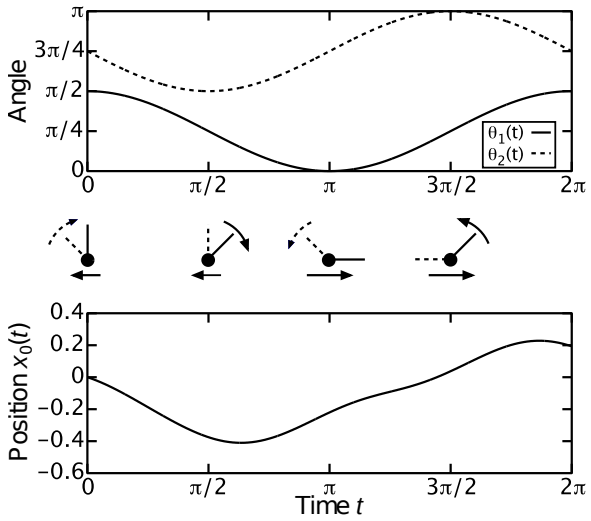

Figure 6.5: Two legs oscillating sinusoidally according to $\theta_1 = \pi/4 + a\cos t$ and $\theta_2 = 3\pi/4 + a\cos(t + \pi/2)$, where $a = \pi/4$ is the amplitude. The second leg (blue) oscillates about $\Phi_2 = 3\pi/4$, while the first leg (red) oscillates about $\Phi_1 = \pi/4$ with a phase lag of $\pi/2$. The swimmer position x translates about a fifth of the leg length after one cycle.

6.5.1 Abnormal curves in the copepod swimmer

With $q = (x, \theta_1, \theta_2) \in \mathbb{R}^3$, the dynamics given by the control system

$$\dot{q}(t) = \sum_{i=1}^{2} u_i(t) G_i(q(t)).$$

The Lie bracket of two vectors fields F, G is computed with the convention

$$[F, G](q) = \frac{\partial F}{\partial q}(q)G(q) - \frac{\partial G}{\partial q}(q)F(q).$$

Denoting $p = (p_1, p_2, p_3)$ the adjoint vector associated with q, $z = (q, p)$ and if H_F, H_G are the Hamiltonian lifts $p \cdot F, p \cdot G$, one has:

$$\{H_F, H_G\}(z) = \mathrm{d}H_F(\overrightarrow{H}_G)(z) = p \cdot [F, G](q).$$

Denoting $D = \mathrm{span}\{G_1, G_2\}$, the distribution associated with the control system, one needs to recall basic facts about the classification of such two-dimensional distributions, in relation with abnormal curves [128].

Local classification of two-dimensional distributions in dimension three and abnormal curves. Denoting $H_i(z) = p \cdot G_i(q)$ $i = 1, 2$ the Hamiltonian lifts, abnormal curves are defined by

$$H_1(z) = H_2(z) = 0$$

and differentiating with respect to time and using the dynamics

$$\frac{\mathrm{d}z}{\mathrm{d}t} = \sum_{i=1}^{2} u_i \overrightarrow{H}_i(z)$$

we obtain the relations

$$\begin{aligned} &\{H_1, H_2\}(z) = 0 \\ &u_1 \left\{\{H_1, H_2\}, H_1\right\}(z) + u_2 \left\{\{H_1, H_2\}, H_2\right\}(z) = 0 \end{aligned}$$

defining the corresponding abnormal controls. Next, we present only the two stable models related to our study.

Contact case. We say that q_0 is a *contact point* if $\mathrm{span}\{G_1, G_2, [G_1, G_2]\}$ is of dimension 3 at q_0. At a contact point, identified with 0, there exists a system of local coordinates $q = (x, y, z)$ such that

$$D = \ker(\alpha), \qquad \alpha = \mathrm{d}z + (x\mathrm{d}y - y\mathrm{d}x).$$

with the corresponding nilpotent frame

$$\widehat{G_1} = \frac{\partial}{\partial x} + y\frac{\partial}{\partial z}, \widehat{G_2} = \frac{\partial}{\partial y} - x\frac{\partial}{\partial z}$$

Taking $\widehat{G_1}, \widehat{G_2}$ as an orthonormal frame, this leads to the *Heisenberg model* in SR-geometry. Observe that $\mathrm{d}\alpha = -2\,\mathrm{d}y \wedge \mathrm{d}x$ (Darboux form) and that $\frac{\partial}{\partial z}$ is the characteristic direction of $\mathrm{d}\alpha$.

The Martinet case. A point q_0 is a *Martinet point* if at q_0 we have the following property: $[G_1, G_2] \in D = \mathrm{span}\{G_1, G_2\}$ but $\{[[G_1, G_2], G_1], [[G_1, G_2], G_2]\} \not\subseteq D$. Then, there exist local coordinates $q = (x, y, z)$ near q_0 (which can be identified as 0 in these new coordinates) such that

$$D = \ker \omega, \qquad \text{where } \omega := \mathrm{d}z - \frac{y^2}{2}\mathrm{d}x,$$

and the corresponding nilpotent frame takes the form

$$\widehat{G_1} = \frac{\partial}{\partial x} + \frac{y^2}{2}\frac{\partial}{\partial z}, \widehat{G_2} = \frac{\partial}{\partial y}.$$

Moreover, we obtain

$$\widehat{G_3} = [\widehat{G_1}, \widehat{G_2}] = y\frac{\partial}{\partial z}, \ [[\widehat{G_1}, \widehat{G_2}], \widehat{G_1}] = 0, \ [[\widehat{G_1}, \widehat{G_2}], \widehat{G_2}] = \frac{\partial}{\partial z}. \tag{6.8}$$

The surface $\Sigma : y = 0$ where $\widehat{G_1}, \widehat{G_2}, [\widehat{G_1}, \widehat{G_2}]$ are linearly dependent is called the *Martinet surface* and is foliated by abnormal curves, solutions of $\frac{\partial}{\partial x}$. In particular, through the origin it corresponds to the curve $t \to (t, 0, 0)$. Taking $\widehat{G_1}, \widehat{G_2}$ as an orthonormal frame, it corresponds to the so-called *flat Martinet case*.

Computation in the Copepod case. One has

$$G_i = \frac{\sin(\theta_i)}{\Delta}\frac{\partial}{\partial x} + \frac{\partial}{\partial \theta_i},\ i = 1, 2 \ \text{ where } \Delta := 2 + \sin^2(\theta_1) + \sin^2(\theta_2). \tag{6.9}$$

As a consequence we obtain

$$G_3 = [G_1, G_2] = f(\theta_1, \theta_2)\frac{\partial}{\partial x} \quad \text{and} \quad [[G_1, G_2], G_i] = \frac{\partial f}{\partial \theta_i}(\theta_1, \theta_2)\frac{\partial}{\partial x},\ \text{for } i = 1, 2. \tag{6.10}$$

where

$$f(\theta_1, \theta_2) := \frac{2\sin(\theta_1)\sin(\theta_2)(\cos(\theta_1) - \cos(\theta_2))}{\Delta^2}. \tag{6.11}$$

We immediately deduce the following result

Lemma 6.9. *The Martinet surface Σ for the Copepod swimmer is given by the equation $\sin(\theta_1)\sin(\theta_2)(\cos(\theta_1) - \cos(\theta_2)) = 0$. The vector fields G_1, G_2 and $[G_1, G_2]$ are coplanar on Σ, which corresponds to the following values of θ_1 and θ_2:*

- *$\theta_1 = 0$ or π, $\theta_2 = 0$ or π, $\theta_1 = \theta_2$.*

Σ contains the boundary of the physical domain: $\theta_1, \theta_2 \in [0, \pi], \theta_1 \leq \theta_2$, and the edges (with excluded vertices) of the triangle are Martinet points. The associated adjoint vector can be normalized to $p = \left(1, \frac{\sin(\theta_1)}{\Delta}, \frac{\sin(\theta_2)}{\Delta}\right)$. Thus the triangle is an abnormal stroke.

Remark 6.10. *The previous lemma provides the interpretation of the policy represented in Fig.6.4 which corresponds exactly to the abnormal stroke. Notice that it provides in the $(\theta_1, \theta_2)-$plane the boundary of the physical domain for the Copepod model. A recent contribution [75] proves that such an abnormal curve with corners cannot be optimal (not taking into account a state constraints). Our related analysis with the concept of efficiency will be interesting in the framework of SR-geometry.*

6.5.2 The normal case

In the previous section we have discussed the abnormal case, which provide strokes having necessarily a "triangular" shape.

The "Second case" (cf Fig.6.5) suggests to investigate also strokes which can be described in terms of smooth (trigonometric) functions. This requires dealing with the class of normal extremals. We shall consider both the situations in which we minimize the mechanical energy and the simplified (SR-type) cost where G_1, G_2 are assumed orthonormal. We first provide a feedback transformation which (locally) reduces the mechanical energy to a sum of squares (construction of an orthonormal frame).

6.5.2.1 Mechanical energy

For the SR-problem an orthonormal frame can be established as follows. Using the following feedback transformation

$$\begin{pmatrix} u_1 \\ u_2 \end{pmatrix} = \begin{pmatrix} \cos(\alpha) & \sin(\alpha) \\ -\sin(\alpha) & \cos(\alpha) \end{pmatrix} \begin{pmatrix} v_1 \\ v_2 \end{pmatrix}$$

where $\alpha = \arctan\left(\frac{2\sin(\theta_1)\sin(\theta_2)}{\sin^2(\theta_2)-\sin^2(\theta_1)}\right) = \begin{cases} \arctan\left(\frac{\sin(\theta_1)}{\sin(\theta_2)}\right) & \text{if } \sin(\theta_1) \leq \sin(\theta_2) \\ -\arctan\left(\frac{\sin(\theta_2)}{\sin(\theta_1)}\right) & \text{if } \sin(\theta_1) > \sin(\theta_2) \end{cases}$,
the mechanical energy can be written as

$$\begin{cases} \delta_1 v_1^2 + \delta_2 v_2^2 & \text{if } \sin(\theta_1) \leq \sin(\theta_2) \\ \delta_2 v_1^2 + \delta_1 v_2^2 & \text{if } \sin(\theta_1) > \sin(\theta_2) \end{cases}$$

in which $\delta_1 = \frac{1}{3}$, $\delta_2 = \frac{1}{6}\frac{4-\sin^2(\theta_1)-\sin^2(\theta_2)}{2+\sin^2(\theta_1)+\sin^2(\theta_2)}$.
Introducing

$$\begin{cases} w_1 = \delta_1 v_1,\ w_2 = \delta_2 v_2 & \text{if } \sin(\theta_1) \leq \sin(\theta_2) \\ w_1 = \delta_2 v_1,\ w_2 = \delta_1 v_2 & \text{if } \sin(\theta_1) > \sin(\theta_2) \end{cases}$$

the mechanical energy takes the form $w_1^2 + w_2^2$.

We shall not use this reduction to make our numerical simulations and we use directly the normal Hamiltonian associated with the metric $a(q)u_1^2 + 2b(q)u_1u_2 + c(q)u_2^2$ which is (with $\lambda_0 = -1/2$)

$$H_n(q,p) = \frac{1}{2}\left(a(q)u_1^2 + 2b(q)u_1u_2 + c(q)u_2^2\right), \tag{6.12}$$

where the optimal controls u_1, u_2 are computed according to

$$\begin{cases} H_1(q,p) = a(q)u_1 + b(q)u_2, \\ H_2(q,p) = b(q)u_1 + c(q)u_2 \end{cases}$$

6.5.2.2 Simplified cost

Note that if the cost is simplified to $\int_0^T (u_1^2 + u_2^2)\mathrm{d}t$, some geometric computations can be made, in relation with the Heisenberg case (assuming G_1, G_2 orthonormal) and which can be used in the numerical implementation, in particular to compute strokes with small amplitudes. In this case,

$$H_n = \frac{1}{2}\left(H_1^2 + H_2^2\right)$$

and straightforward computations inside the abnormal triangle are the following using the Poincaré coordinates (q, H), $H = (H_1, H_2, H_3)$ and $H_i = p \cdot G_i(q)$. Indeed:

$$\dot{H}_1 = \mathrm{d}H_1(\vec{H}_n) = \{H_1, H_2\}H_2 = H_2H_3,$$
$$\dot{H}_2 = \mathrm{d}H_2(\vec{H}_n) = \{H_2, H_1\}H_1 = -H_1H_3,$$

Moreover

$$\dot{H}_3 = \mathrm{d}H_3(\vec{H_n}) = \{H_3, H_1\}H_1 + \{H_3, H_2\}H_2,$$

with

$$\{H_3, H_1\}(z) = p \cdot [[G_1, G_2], G_1](q) \text{ and } \{H_3, H_2\}(z) = p \cdot [[G_1, G_2], G_2](q).$$

At a contact point, G_1, G_2, G_3 form a frame, therefore we obtain

$$[[G_1, G_2], G_1](q) = \sum_{i=1}^{3} \lambda_i(q) G_i(q)$$

where $\lambda_1 = \lambda_2 = 0$, $\frac{\partial f}{\partial \theta_1} = \lambda_3 f$.
Similarly,

$$[[G_1, G_2], G_2](q) = \sum_{i=1}^{3} \lambda_i'(q) G_i(q),$$

with

$$\lambda_1' = \lambda_2' = 0, \qquad \frac{\partial f}{\partial \theta_2} = \lambda_3' f.$$

We conclude that

$$\begin{aligned} &\dot{H}_1 = H_2 H_3, \quad \dot{H}_2 = -H_1 H_3, \\ &\dot{H}_3 = H_3 \left(\lambda_3 H_1 + \lambda_3' H_2\right). \end{aligned} \tag{6.13}$$

The associated one dimensional distribution can be analyzed setting $\mathrm{d}s = H_3 \mathrm{d}t$ and we obtain

$$\frac{\mathrm{d}H_1}{\mathrm{d}s} = H_2, \qquad \frac{\mathrm{d}H_2}{\mathrm{d}s} = -H_1, \qquad \frac{\mathrm{d}H_3}{\mathrm{d}s} = \lambda_3 H_1 + \lambda_3' H_2. \tag{6.14}$$

In particular, differentiating one more time the first relation of (6.14) with respect to s and using the second relation, we have the harmonic oscillator $H_1'' + H_1 = 0$. Furthermore H_3 can be analyzed using the remaining equation (6.13). Observe that with the approximation λ_3, λ_3' constant, the equation takes the form

$$\frac{\mathrm{d}H_3}{\mathrm{d}s} = A\cos(s + \rho).$$

with A, ρ constant. In those computations, we recognize the Heisenberg case, corresponding to $\lambda_3 = \lambda_3' = 0$.
Observe that when q is not a contact point (that is $G_2 = [G_1, G_2] \in \mathrm{span}\{G_1, G_2\}$, in order to deal with the Martinet case, we can choose the frame G_1', G_2' and G_3', where $G'1 = G_1, G_2' = G_2$ and $G_3' = \frac{\partial}{\partial x}$.

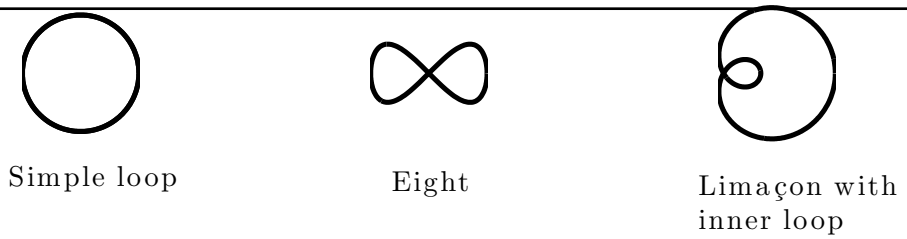

Figure 6.6: Non equivalent strokes.

6.5.2.3 Numerical results not taking into account the state constraints

The objective of this section is to investigate the two following problems:

- **Problem 1:** From the micro-local point of view, variety of the different kind of normal strokes e.g. simple loop, eight, limaçon realizable normal strokes by the Copepod swimmer in relation with the classification of planar periodic curves, [23] see Fig.6.6.
  For this study, we lift the angles $\theta_i \in S^1$ to the covering space $\mathbb{R}$.
- **Problem 2:** Compute the conjugate points along a strict normal stroke to select the candidates for optimality for the fixed endpoints problem.

Numerical methods. The period T is fixed at 2π in our simulations. We use the `HamPath` software [55] at two levels:

1. The shooting equations associated with the problem are

$$\begin{array}{llll} x(0) = 0, & & x(2\pi) = x_f, & \\ \theta_j(0) = \theta_j(2\pi) & j = 1,2, & p_k(0) = p_k(2\pi) & k = 2,3. \end{array} \tag{6.15}$$

2. We consider a normal stroke and we test its optimality by showing the non-existence of conjugate points using the variational equation to compute Jacobi fields. Recall that [34] given a reference curve $(q(t), p(t))$ solution of $\overrightarrow{H_n}$, a time $t_c \in]0, 2\pi]$ is a conjugate time if there exists a Jacobi field $\delta z = (\delta q, \delta p)$, that is a non-zero solution of the variational equation

$$\dot{\delta z}(t) = \frac{\partial \vec{H}_n}{\partial z}(q(t), p(t))\delta z(t) \tag{6.16}$$

such that $\delta q(0) = \delta q(t_c) = 0$. We denote $\delta z_i = (\delta q_i, \delta p_i)$, $i = 1...3$, three linearly independent solutions of (6.16) with initial condition $\delta q(0) = 0$. At time t_c we have the following rank condition

$$\text{rank}\{\delta q_1(t_c), \delta q_2(t_c), \delta q_3(t_c)\} < 3. \tag{6.17}$$

Remark 6.11. *Note the following result coming from [2, 38, 126].*

Proposition 6.12. *A necessary optimality condition for a strict normal stroke to provide a weak minimizer is the non-existence of a conjugate point on* $]0, 2\pi[$.

Complexity of optimal policies. Fig.6.7 illustrates four different strokes not taking into account the state constraints confirming the complexity of the model. This can be regarded as examples covering the generic classification of periodic planar curves [23]. Conjugate points are also computed to check the second order optimality conditions. There are no conjugate points on $]0, 2\pi]$ just in the case of the simple loop, but they do appear for the limaçon case, the eight case. Further simulations, taking into account more complicated shapes (combining two "eights") for instance) confirm the presence of conjugate points on $]0, 2\pi[$. *Hence, the only candidates for optimality are the simple loops.*

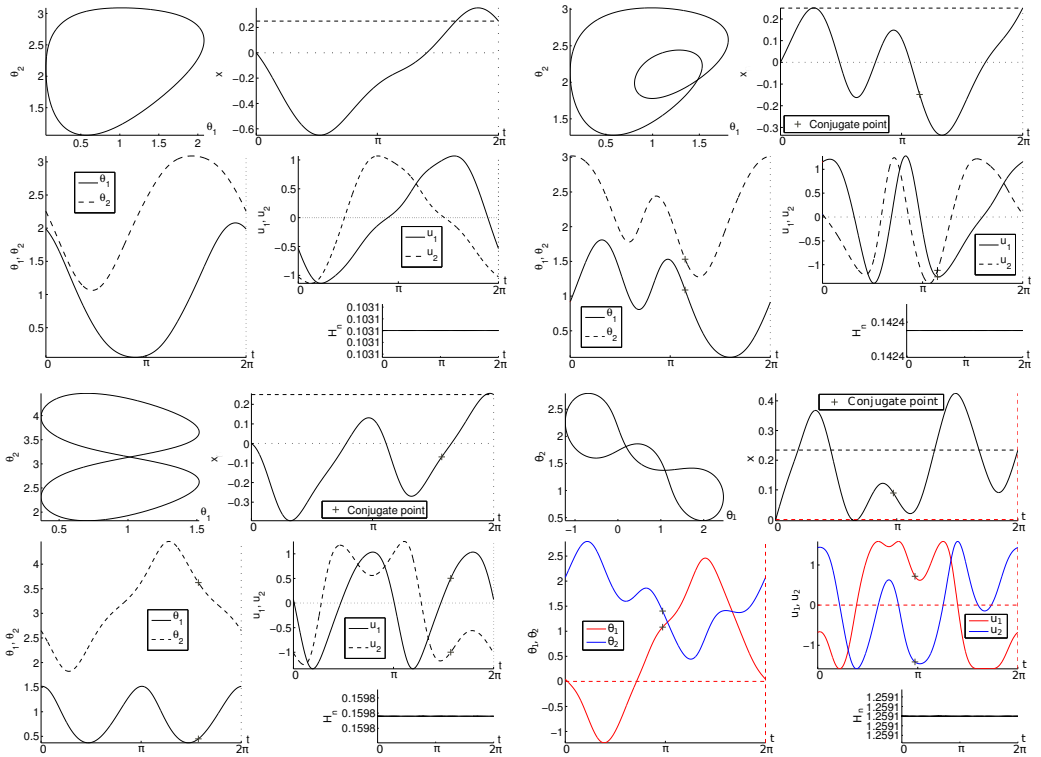

Figure 6.7: Normal strokes: simple loop (left), limaçon with inner loop (right) and eight case, and a two self-intersecting case (bottom). First conjugate points on $[0, 2\pi]$ appear with a cross except for the simple loop stroke.

6.5.2.4 Optimal curves circumscribed in the triangle of constraints

We use a combination of the `Bocop` and `HamPath` software.

- `Bocop`: This software is useful when we look for extremals whose state variables have to be confined in a given set, satisfying some state constraints. Fig.6.8 describes a single loop tangent to the boundary which is used to initialize the shooting algorithm of the `HamPath` software.

- `HamPath`: This software cannot be directly applied to compute the optimal solution using the Maximum Principle with state constraints, due to the

complexity of the different principles [38].

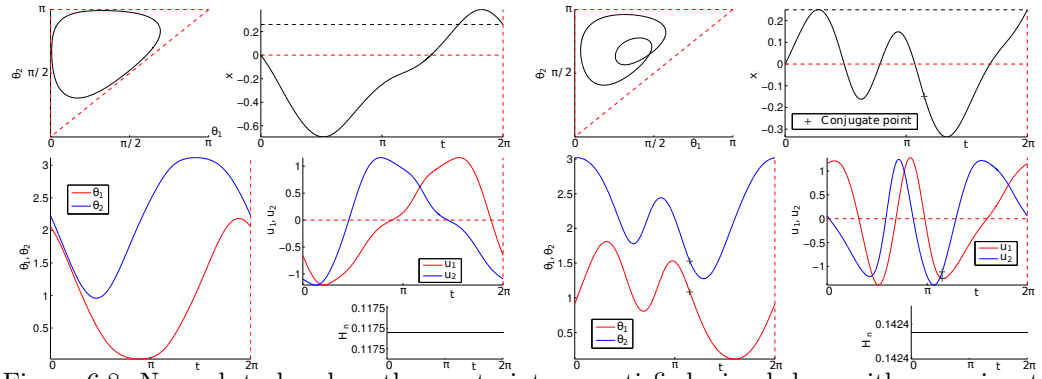

Figure 6.8: Normal stroke where the constraints are satisfied: simple loop with no conjugate point on $[0, T]$ (left) and limaçon with inner loop with one conjugate point on $[0, T]$ (right).

Fixing the energy level $H_n = 1/2$, the domain of the exponential map is not compact (it turns out to be a cylinder) and the shooting problem, consisting in finding an initial adjoint vector, is ill-conditioned when we compute normal extremals near the abnormal extremal. Fig.6.9 highlights this fact by representing the norm of the initial adjoint vector $p = (p_1, p_2, p_3)$ for different displacements, showing that the exponential map is non proper.

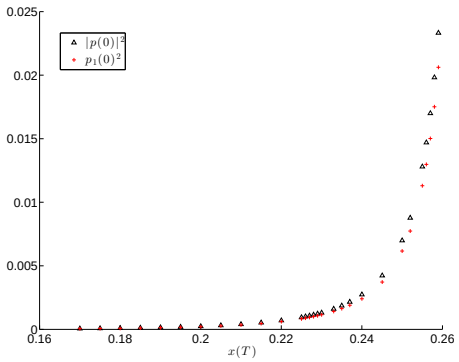

Figure 6.9: Norm of the initial adjoint vector $p = (p_1, p_2, p_3)$ and value of $p_1(0)^2$ for normal strokes such that $H_n = 1/2$ and having different displacements, illustrating the non properness of the exponential mapping.

Second order sufficient conditions for the Copepod strokes The aim of this section is to check second order sufficient conditions for normal extremals represented by simple loop strokes of the Copepod swimmer. We shall employ here particular second order sufficient conditions which can be used in presence of non-uniqueness of minimizers [62]. We provide a short introduction of these results in the Appendix.

We consider the optimal control problem in which we minimize the cost (6.2) over trajectories satisfying (6.1) and such that

$$x(0) = 0, \quad x(T) = x_T, \quad \theta_j(0) = \theta_j(T) \;\; j = 1, 2. \tag{6.18}$$

Proposition 6.13. *Take $I = (-\varepsilon, \varepsilon)$ for some $\varepsilon > 0$, and let $(\bar{q}(.), p(.), \bar{u}(.))$ be a normal extremal (on $[0, T]$) where $\bar{q} = (\bar{x}, \bar{\theta}_1, \bar{\theta}_2)$, $p = (p_1, p_2, p_3)$ and $\bar{u} = (\bar{u}_1, \bar{u}_2)$. Write $\bar{\theta}_j(.)$, $j = 1, 2$, $p(.)$, $\bar{x}(.)$ and $\bar{u}(.)$ their corresponding periodic extensions. For all $a \in I$ and $t \in [0, T]$, we define $q^a(.) = (x^a(.), \theta_1^a(.), \theta_2^a(.))$ where*

$$\begin{aligned} &\theta_j^a(t) = \bar{\theta}_j(t + a), \quad u_j^a(t) = \bar{u}_j(t + a) \quad \text{for } j = 1, 2, \\ &x^a(t) = \bar{x}(t + a) - \bar{x}(a), \quad p^a(t) = (p_1(t), p_2(t + a), p_3(t + a)). \end{aligned}$$

Then the normal extremal $(\bar{q}(.), p(.), \bar{u}(.))$ is continuously embedded in the family of extremals $(q^a(.), p^a(.), u^a(.))_{a \in I}$.

In what follows, we denote by $(\bar{q}, \bar{u})$ the simple loop of Fig.6.8 *(left)* with associated adjoint vector p and satisfying (6.18).

Numerical result: *The simple loop $(\bar{q}, \bar{u})$ is weak-locally optimal.*
To confirm this claim, we refer the reader to [62].

1. First, we shall invoke the second order test provided by 2.13. Conditions (F1)-(F4), which ensures that the normal extremal $(\bar{q}, \bar{u}, p)$ is embedded in a family of normal extremals and assumptions (H1)-(H4) required by 2.13 are satisfied owing to the data of control system (6.2)-(6.1) and Prop.6.13. Numerical arguments allow to conclude that there is no conjugate point on $[0, T]$ for the normal extremal $(\bar{q}(.), p, \bar{u}(.))$ (cf Sec.6.5.2.3). It implies that the Riccati equation (2.9) associated with the accessory problem has a global symmetric solution.

2. Using the *Isoda* integrator from the FORTRAN library *odepack*, the computation of the matrix $\mathcal{W}$, defined in (2.11), yields

$$\mathcal{W} = \begin{pmatrix} 573.04 & -146.59 & -134.55 & -573.04 & 160.65 & 127.23 \\ -146.59 & 37.588 & 34.681 & 146.59 & -41.082 & -32.581 \\ -134.55 & 34.681 & 30.481 & 134.55 & -37.698 & -29.925 \\ -573.04 & 146.59 & 134.55 & 573.04 & -160.65 & -127.23 \\ 160.65 & -41.082 & -37.698 & -160.65 & 46.532 & 34.579 \\ 127.23 & -32.581 & -29.926 & -127.23 & 34.579 & 29.901 \end{pmatrix}.$$

   Consider the linear subspace

$$\mathcal{L}_s = \{ (y_0, y_T) \in \mathbb{R}^3 \times \mathbb{R}^3 \mid \nabla_{q_0, q_T} m(q_0, q_T) \begin{pmatrix} y_0 & y_T \end{pmatrix}^\intercal = 0 \}.$$

   where $m(q_0, q_T) = (x(0), x(T), \theta_1(0) - \theta_1(T), \theta_2(0) - \theta_2(T))^\intercal$.
   We introduce the matrix M_s such that $\ker(\nabla_{q_0, q_T} m(q_0, q_T)) = \mathrm{Im}(M_s)$. Standard second order sufficient conditions of 2.12 lead to check that $\mathcal{W}$ is definite-positive on $\mathcal{L}_s$. This is equivalent to check that $\mathcal{W}_s = M_s^\intercal (\mathcal{W}^\intercal + \mathcal{W}) M_s$ is

positive-definite. Due to the non-uniqueness of the extremal $(\bar{q}, p, \bar{u})$, $\mathcal{W}_s$ is not definite-positive (see Table 6.2).

For the refined second order sufficient conditions of 2.13, we consider the vector

$$\begin{aligned}\Gamma &= \begin{pmatrix} 0 & \dot{x}_2(0) & \dot{x}_3(0) & 0 & \dot{x}_2(0) & \dot{x}_3(0) \end{pmatrix}^\intercal \\ &= \begin{pmatrix} 0 & -0.53460 & -1.0257 & 0 & -0.53460 & -1.0257 \end{pmatrix}^\intercal,\end{aligned}$$

the linear subspace

$$\mathcal{L}_r = \mathcal{L}_s \cap \{(y_0, y_T) \in \mathbb{R}^3 \times \mathbb{R}^3 \mid \Gamma^\intercal \begin{pmatrix} y_0 & y_T \end{pmatrix}^\intercal = 0\}$$

and the matrix M_r such that $\ker \begin{pmatrix} \nabla_{q_0,q_T} m(q_0, q_T) & \Gamma^\intercal \end{pmatrix}^\intercal = \mathrm{Im}(M_r)$, hence $M_r^\intercal = \begin{pmatrix} 0 & -\dot{x}_3(0) & \dot{x}_2(0) & 0 & -\dot{x}_3(0) & \dot{x}_2(0) \end{pmatrix}$.
Numerical simulations confirm that $\mathcal{W}_r = M_r^\intercal(\mathcal{W}^\intercal + \mathcal{W})M_r$ is positive-definite and taking different absolute and relative tolerances for the integrator, $\mathcal{W}_s$ has zero eigenvalue associated with the vector Γ (see Table 6.2).

Absolute and relative tolerance	(Standard condition) Spec($\mathcal{W}_s$)	(Refined condition) Spec($\mathcal{W}_r$)
10^{-5}	$6.8981e-4$ 3.4200	22.553
10^{-10}	$-9.1247e-7$ 3.4200	22.555

Table 6.2: The standard second order sufficient conditions fail: $\mathcal{W}_s$ has zero eigenvalue and the refined second order sufficient conditions are satisfied: $\mathcal{W}_r$ is positive-definite.

Comparisons of the geometric efficiency of the strokes. To compare normal and abnormal solutions corresponding to different displacements, in Fig.6.10 we represent the ratio $\mathcal{E} = x/l$ concerning solutions obtained for a given displacement x and l is the length of the stroke (this quantity does not depend upon the parameterization).
For the triangle, a displacement along the vertical or horizontal edge gives $x = \frac{2\sqrt{3}}{3} arctanh\left(\frac{\sqrt{3}}{3}\right)$ and along the hypotenuse $x = -\sqrt{2} arctanh\left(\frac{\sqrt{2}}{2}\right)$ and the total displacement is $2.742.10^{-1}$.
The length of a normal stroke γ is $l(\gamma) = \int_0^{2\pi} \sqrt{\dot{q} \cdot \dot{q}} dt$ and is given by $2\pi\sqrt{2H_n}$ where H_n is the energy level. The efficiency curve is displayed in Fig.6.10 where the normal strokes corresponding to the maximal efficiency is also represented.
Note that the geometric efficiency $\mathcal{E}$ here introduced is different from the concept of efficiency employed in some previous papers [53].
Observe that from computations above obtained for the abnormal stroke, the efficiency turns out to be 5.56×10^{-2}. This result will be compared with the efficiency of normal strokes (cf Fig.6.10) establishing the optimality of normal strokes (in terms of efficiency).

Conclusions. From our analysis we deduce that the (triangle) abnormal stroke is not optimal. Indeed, one can choose a normal stroke (inside the triangle) such that the displacement is $\bar{x}/2$ with $\bar{x} = 2.742$ and the length is less than $\bar{l}/2$ where $\bar{l}$ is the length of the triangle. Applying twice the normal stroke, we obtain the same displacement $\bar{x}$ than with the abnormal stroke but with a length $< \bar{l}$.

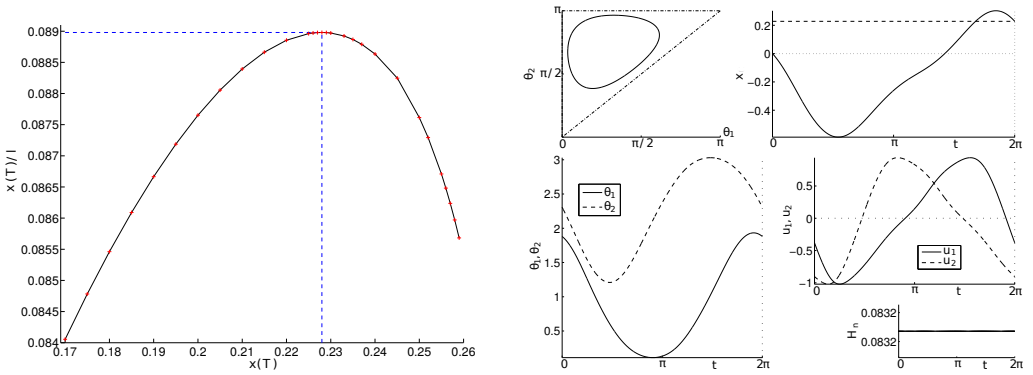

Figure 6.10: Efficiency curve (left) and the corresponding minimizing curve with the best performance (right). Note that the efficiency of the abnormal curve is $\mathbf{5.56e^{-2}}$ vs of order $\mathbf{8.89e^{-2}}$ for normal strokes.

6.6 The Three-Link Purcell swimmer

The controlled dynamics of the Purcell swimmer, briefly recalled in the introduction, is linear with respect to the control [104]

$$\dot{q} = u_1 F_1(q) + u_2 F_2(q) \text{ where } q = (\theta_1, \theta_2, x, y, \alpha) \tag{6.19}$$

where we minimize the mechanical energy given by (6.4).

6.6.1 Symmetry properties

First of all due to the structure of the equations (6.3) we have the following.

Lemma 6.14. *Let $\bar{q}(t) = (\bar{\theta}_1(t), \bar{\theta}_2(t), \bar{x}(t), \bar{y}(t), \bar{\alpha}(t))$ and $q(t) = (\theta_1(t), \theta_2(t), x(t), y(t), \alpha(t))$ be the solutions associated with $u(.)$ with respective initial conditions $(\theta_{10}, \theta_{20}, 0, 0, 0)$ and $(\theta_{10}, \theta_{20}, 0, 0, \alpha_0)$ then*

$$\begin{aligned} &\bar{\theta}_j(t) = \theta_j(t) \quad j = 1, 2, \quad \alpha(t) = \bar{\alpha}(t) + \alpha_0, \\ &x(t) = \cos(\alpha_0)\bar{x}(t) - \sin(\alpha_0)\bar{y}(t), \\ &y(t) = \sin(\alpha_0)\bar{x}(t) + \cos(\alpha_0)\bar{y}(t). \end{aligned} \tag{6.20}$$

Proof. We denote $A = \begin{pmatrix} 0 & -1 \\ 1 & 0 \end{pmatrix}$, $e^{At} = \begin{pmatrix} \cos(t) & -\sin(t) \\ \sin(t) & \cos(t) \end{pmatrix}$ and using (6.3), one has:

$$\frac{\mathrm{d}}{\mathrm{d}t} \begin{pmatrix} x(t) \\ y(t) \\ \alpha(t) \end{pmatrix} = \begin{pmatrix} \cos(\alpha) & -\sin(\alpha) & 0 \\ \sin(\alpha) & \cos(\alpha) & 0 \\ 0 & 0 & 1 \end{pmatrix} \begin{pmatrix} f_1(t) \\ f_2(t) \\ f_3(t) \end{pmatrix}$$

where $f_i(t)$, $i = 1 \dots 3$ are obtained integrating the θ-dynamics corresponding to $u(.)$ and with $\theta(0) = \theta_0$ and is independent of the (α, x, y)-variables.
One has

$$\alpha(t) = \int_0^t f_3(s)\mathrm{d}s + \alpha_0$$

and denoting $X = (x, y)^\intercal$, $\bar{X} = (\bar{x}, \bar{y})^\intercal$ and $V = (f_1, f_2)^\intercal$,

$$\begin{aligned}\frac{\mathrm{d}X}{\mathrm{d}t} &= e^{A\alpha(t)}V(t)\\ &= e^{A(\alpha_0+\int_0^t f_3(s)\mathrm{d}s)}V(t)\\ &= e^{A\alpha_0}e^{A\int_0^t f_3(s)\mathrm{d}s}V(t)\\ &= e^{A\alpha_0}\frac{\mathrm{d}\bar{X}}{\mathrm{d}t}\end{aligned}$$

Hence, integrating, one gets the remaining equation (6.20) that is

$$X(t) = e^{A\alpha_0}\bar{X}(t).$$

□

Lemma 6.15. *Let H_n be the extremal normal Hamiltonian associated with any quadratic cost $\int_0^{2\pi}(a(q)u_1^2 + 2b(q)u_1u_2 + c(q)u_2^2)\mathrm{d}t$. Denoting $(p_\theta, p_x, p_y, p_\alpha)$ the adjoint components, we have the following first integrals*

$$I_1 = p_x,\ I_2 = p_y,\ I_3 = H_n,\ I_4 = (p_x y - p_y x) - p_\alpha$$

Proof. The proof results from straightforward computations. □

Corollary 6.16. *Consider the shooting conditions*
- *θ, α 2π-periodic,*

can be completed considering • *p_θ, p_α 2π-periodic,* • *$(p_x y - x p_y)(2\pi) = 0$ i.e. $(p_x, p_y)(2\pi)$ normal to $S(r)$*

Observe that, since $I_4 = (p_x y - x p_y) - p_\alpha$ is a first integral, at $t = 0$ and $t = 2\pi$ we have $p_x y - p_y x = 0$, we deduce $p_\alpha(0) = p_\alpha(2\pi)$. Hence the assertion above p_α is 2π-periodic is equivalent to p is normal to $S(r)$ and one of the conditions can be relaxed and be replaced by $\alpha(0) = 0$ to determine the solution.

6.6.2 Nilpotent approximation

Due to the mathematical complexity of the model, the nilpotent approximation will play a crucial role in our analysis. First of all, owing to the integrability of the associated normal extremals in the class of elliptic functions, it will allow to make a micro-local analysis of the different kind of strokes and to estimate the conjugate points using a proper time rescaling. Secondly, the abnormal extremals forming piecewise smooth strokes can be easily computed in this approximation and their optimality studied using the corresponding concept of conjugate point.

6.6.2.1 The flat nilpotent model

There is a unique nilpotent model associated with a 2-dimensional distribution with grow vector $(2,3,5)$ which is described next [51, 111].

Definition 6.17. *We call the flat Cartan model the 2-dimensional distribution in dimension five defined by the two vector fields:*

$$\hat{F}_1(\hat{q}) = \frac{\partial}{\partial \hat{q}_1},\ \hat{F}_2(\hat{q}) = \frac{\partial}{\partial \hat{q}_2} + \hat{q}_1\frac{\partial}{\partial \hat{q}_3} + \frac{\partial}{\partial \hat{q}_4} + \hat{q}_1^2\frac{\partial}{\partial \hat{q}_5}.$$

where $\hat{q} = (\hat{q}_1, \hat{q}_2, \hat{q}_3, \hat{q}_4, \hat{q}_5)$ will be the privileged coordinates with the following weights: 1 for $\hat{q}_1, \hat{q}_2$, 2 for $\hat{q}_3$ and 3 for $\hat{q}_4, \hat{q}_5$.

6.6.2.2 Computations of the nilpotent approximation

The Purcell system (6.3) can be written as a control system of the form $\dot{q} = Fu = \sum_{i=1}^{2} u_i F_i$, where the two vectors fields F_1, F_2 have a complicated expression, which can be found in literature [104]. The nilpotent approximation is computed at $q_0 = 0$ and will provide a nilpotent approximation of the SR-problem for the simplified cost $\int_0^{2\pi}(u_1^2 + u_2^2)\mathrm{d}t$ which is sufficient in our theoretical analysis. Assuming that the lengths of the three links are $l_0 = 2, l_1 = l_2 = 1$, the two-jets of F_1 and F_2 at $q = 0$ are

$$\begin{aligned} F_1(q) = {} & \frac{\partial}{\partial q_1} + \left(-\frac{1}{6}\,q_5 - \frac{4}{27}\,q_1 - \frac{2}{27}\,q_2\right)\frac{\partial}{\partial q_3} \\ & + \left(\frac{1}{6} - \frac{1}{12}\,{q_5}^2 - \frac{2}{27}\,q_5\,q_2 - \frac{4}{27}\,q_5\,q_1 - \frac{1}{27}\,{q_1}^2 - \frac{1}{27}\,q_1q_2 - \frac{1}{36}\,{q_2}^2\right)\frac{\partial}{\partial q_4} \\ & + \left(-\frac{7}{27} + \frac{2}{81}\,{q_1}^2 - \frac{2}{81}\,q_1q_2 - \frac{5}{162}\,{q_2}^2\right)\frac{\partial}{\partial q_5} + O(|q|^3). \end{aligned}$$

$$\begin{aligned} F_2(q) = {} & \frac{\partial}{\partial q_2} + \left(\frac{1}{6}\,q_5 + \frac{4}{27}\,q_2 + \frac{2}{27}\,q_1\right)\frac{\partial}{\partial q_3} \\ & + \left(-\frac{1}{6} + \frac{1}{12}\,{q_5}^2 + \frac{4}{27}\,q_5\,q_2 + \frac{2}{27}\,q_5\,q_1 + \frac{1}{36}\,{q_1}^2 + \frac{1}{27}\,q_1q_2 + \frac{1}{27}\,{q_2}^2\right)\frac{\partial}{\partial q_4} \\ & + \left(-\frac{7}{27} - \frac{5}{162}\,{q_1}^2 - \frac{2}{81}\,q_1q_2 + \frac{2}{81}\,{q_2}^2\right)\frac{\partial}{\partial q_5} + O(|q|^3) \end{aligned}$$

(In these expressions we are taking the standard normalization $c_t = 1, c_n = 2c_t$ of the respective tangential and normal drag coefficients [104]).
We compute the local diffeomorphism φ to reduce F_1, F_2 to the nilpotent approximation $\hat{F}_1, \hat{F}_2$ using the sequence $\varphi = \varphi_N\ o\ ...\ o\ \varphi_1 : \mathbb{R}^5 \to \mathbb{R}^5$, where $N = 13$ and each φ_i is a simple change of coordinates that we describe below.
At each step i, we denote $q = (q_1, q_2, q_3, q_4, q_5)$ the old local coordinates and $Q = (Q_1, Q_2, Q_3, Q_4, Q_5)$ the new ones: $q = \varphi_i(Q)$ and each φ_i has only one non trivial component, the other components being the identity transformation are not specified.

1. $q_5 = \varphi_1^{(5)}(Q_5) = Q_5 - \frac{7}{27}Q_1$,
2. $q_3 = \varphi_2^{(3)}(Q_3) = Q_3 - \frac{1}{6}Q_5Q_1 - \frac{17}{324}Q_1^2 - \frac{2}{27}Q_2Q_1$,

3. $q_4 = \varphi_3^{(4)}(Q_4) = Q_4 + \frac{1}{6}Q_1 - \frac{37}{26244}Q_1^3$,
4. $q_5 = \varphi_4^{(5)}(Q_5) = Q_5 + \frac{2}{24}Q_1^3 - \frac{2}{162}$,
5. $q_5 = \varphi_5^{(5)}(Q_5) = Q_5 - \frac{7}{27}Q_2$,
6. $q_3 = \varphi_6^{(3)}(Q_3) = \frac{5}{81}Q_3 + \frac{17}{324}Q_2^2 + \frac{1}{6}Q_5Q_2$,
7. $q_4 = \varphi_7^{(4)}(Q_4) = Q_4 - Q_3Q_2$,
8. $q_4 = \varphi_8^{(4)}(Q_4) = Q_4 + \frac{37}{26244}Q_2^3$,
9. $q_4 = \varphi_9^{(4)}(Q_4) = Q_4 - \frac{4482}{8748}Q_5$,
10. $q_4 = \varphi_{10}^{(4)}(Q_4) = Q_4 + \frac{2270}{2187}Q_2Q_3 + \frac{5}{81}Q_5Q_3 + \frac{83}{19683}Q_2^3$,
11. $q_4 = \varphi_{11}^{(4)}(Q_4) = -\frac{83}{2187}Q_4$,
12. $q_5 = \varphi_{12}^{(5)}(Q_5) = Q_5 + \frac{1}{27}Q_3Q_2 + \frac{2}{243}Q_2^3$,
13. $q_5 = \varphi_{13}^{(5)}(Q_5) = -\frac{1}{54}Q_5 - \frac{1}{27}Q_4$.

This leads to a complicated transformation whose role is to relate the privileged coordinates to the physical coordinates $(\theta_1, \theta_2, x, y, \alpha)$ in particular we have:

Lemma 6.18. *The shape variables $\theta = (\theta_1, \theta_2)$ corresponds to the $(\hat{q}_1, \hat{q}_2)$ coordinates.*

6.6.2.3 Integration of normal extremal trajectories

Computing with (6.17), one has

$$\hat{F}_1(\hat{q}) = \frac{\partial}{\partial \hat{q}_1}, \qquad \hat{F}_2(\hat{q}) = \frac{\partial}{\partial \hat{q}_2} + \hat{q}_1\frac{\partial}{\partial \hat{q}_3} + \hat{q}_3\frac{\partial}{\partial \hat{q}_4} + \hat{q}_1^2\frac{\partial}{\partial \hat{q}_5},$$
$$[\hat{F}_1, \hat{F}_2](\hat{q}) = -\frac{\partial}{\partial \hat{q}_3} - 2\hat{q}_1\frac{\partial}{\partial \hat{q}_5}, \quad [[\hat{F}_1, \hat{F}_2], \hat{F}_1](\hat{q}) = -2\frac{\partial}{\partial \hat{q}_5},$$
$$[[\hat{F}_1, \hat{F}_2], \hat{F}_2](\hat{q}) = \frac{\partial}{\partial \hat{q}_4}.$$

All brackets of length greater than 3 are zero.
Write $\hat{z} = (\hat{q}, \hat{p})$. Introducing the Hamiltonian lifts, one has:

$$H_1(\hat{z}) = \hat{p} \cdot \hat{F}_1(\hat{q}) = \hat{p}_1, \qquad H_2(\hat{z}) = \hat{p} \cdot \hat{F}_2(\hat{q}) = \hat{p}_2 + \hat{p}_3\hat{q}_1 + \hat{p}_4\hat{q}_3 + \hat{p}_5\hat{q}_1^2,$$
$$H_3(\hat{z}) = \hat{p} \cdot [\hat{F}_1, \hat{F}_2](\hat{q}) = -\hat{p}_3 - 2\hat{q}_1\hat{p}_5, \quad H_4(\hat{z}) = \hat{p} \cdot [[\hat{F}_1, \hat{F}_2], \hat{F}_1](\hat{q}) = -2\hat{p}_5,$$
$$H_5(\hat{z}) = \hat{p} \cdot [[\hat{F}_1, \hat{F}_2], \hat{F}_2](\hat{q}) = \hat{p}_4.$$

The SR-Cartan flat case is

$$\dot{\hat{q}} = \sum_{i=1}^{2} u_i \hat{F}_i, \quad \min_u \int_0^{2\pi} (u_1^2 + u_2^2)\mathrm{d}t.$$

and the normal Hamiltonian takes the form

$$H_n = \frac{1}{2}(H_1^2 + H_2^2). \tag{6.21}$$

More precisely, using the Poincaré coordinates, the control system is written

$$\begin{aligned} &\dot{\hat{q}}_1 = H_1, \qquad &&\dot{\hat{q}}_2 = H_2, \qquad &&\dot{\hat{q}}_3 = H_2\hat{q}_1, \\ &\dot{\hat{q}}_4 = H_2\hat{q}_3, \qquad &&\dot{\hat{q}}_5 = H_2\hat{q}_1^2. \end{aligned} \tag{6.22}$$

Deriving with respect to the time variable, we have

$$\begin{aligned} &\dot{H}_1 = \mathrm{d}H_1(\vec{H}) = \{H_1, H_2\}H_2 = \hat{p}\cdot[\hat{F}_1, \hat{F}_2](\hat{q})H_2 = H_2H_3, \\ &\dot{H}_2 = -H_3H_1, \qquad &&\dot{H}_3 = H_1H_4 + H_2H_5, \\ &\dot{H}_4 = 0 \quad \text{hence} \quad H_4 = c_4, \quad &&\dot{H}_5 = 0 \quad \text{hence} \quad H_5 = c_5. \end{aligned}$$

Fixing the level energy, $H_1^2 + H_2^2 = 1$ we set $H_1 = \cos(\theta)$ and $H_2 = \sin(\theta)$.

$$\dot{H}_1 = -\sin(\theta)\dot{\theta} = H_2H_3 = \sin(\theta)H_3.$$

Hence $\dot{\theta} = -H_3$ and

$$\ddot{\theta} = -(H_1c_4 + H_2c_5) = -c_4\cos(\theta) - c_5\sin(\theta) = -\omega^2\sin(\theta+\phi)$$

where ω and ϕ are constant. More precisely, we have

$$\omega = \left(\hat{p}_4(0)^2 + 4\hat{p}_5(0)^2\right)^{1/4}, \quad \phi = \arctan\left(\frac{-2\,\hat{p}_5(0)}{\hat{p}_4(0)}\right).$$

Taking $\psi = \theta + \phi$, we get

$$\frac{1}{2}\dot{\psi}^2 - \omega^2\cos(\psi) = B, \tag{6.23}$$

where B is the constant

$$B = 1/2\ \left(\hat{p}_3(0) + 2\,\hat{q}_1(0)\hat{p}_5(0)\right)^2 - \hat{p}_1(0)\,\hat{p}_4(0) - 2\,\hat{p}_5(0)\,\hat{p}_2(0) - 2\,\hat{p}_5(0)\,\hat{p}_4(0)\,\hat{x}_3(0).$$

We distinguish the following two cases.

- *Oscillating case.* We introduce $k^2 = \frac{1}{2} + \frac{B}{2\omega^2}$ with $0 < k < 1$ so that (6.23) becomes

  $$\dot{\psi}^2 = 4\omega^2\left(k^2 - \sin^2(\frac{\psi}{2})\right)$$

  and we obtain [87]

  $$\sin(\psi/2) = k\,\mathrm{sn}(u,k), \quad \cos(\psi/2) = \mathrm{dn}(u,k)$$

  where $u = \omega t + \varphi_0$.
  H_1 and H_2 are elliptic functions of the first kind and $\hat{q}_1, \hat{q}_2$, solutions of

(6.22), are expressed as

$$\begin{aligned}\hat{q}_1(u) &= \hat{q}_{10} + \frac{1}{\omega}\Big[-2\,k\,\sin(\phi)\,\mathrm{cn}(u) + (-u + 2\,E(u))\cos(\phi)\Big] \\ \hat{q}_2(u) &= \hat{q}_{20} + \frac{1}{\omega}\Big[-2\,k\,\cos(\phi)\,\mathrm{cn}(u) + (u - 2\,E(u))\sin(\phi)\Big]\end{aligned} \tag{6.24}$$

where $\hat{q}_{10}$ and $\hat{q}_{20}$ are constant, and $E(.)$ is the elliptic integral of the second kind [87].

- *Rotating case.* We introduce $k^2 = \frac{2\omega^2}{B+\omega^2}$ with $0 < k < 1$ so that (6.23) becomes

$$\dot{\psi}^2 = \frac{4\omega^2}{k^2}\left(1 - k^2\sin^2(\frac{\psi}{2})\right).$$

and we obtain [87]

$$\sin(\psi/2) = \mathrm{sn}(\frac{u}{k}, k), \quad \cos(\psi/2) = \mathrm{cn}(\frac{u}{k}, k)$$

where $u = \omega t + \varphi_0$.
H_1 and H_2 are elliptic functions of the first kind and $\hat{q}_1, \hat{q}_2$ solutions of (6.22) are expressed as

$$\begin{aligned}\hat{q}_1(u) = \hat{q}_{10} + \frac{1}{\omega}\Bigg[&\Big(1 - \frac{2}{k^2} + 2\,\frac{\mathrm{E}(k)}{k^2\,\mathrm{K}(k)}\Big)\cos(\phi)\,u \\ &+ \frac{2}{k}\left(\cos(\phi)\,\mathrm{Z}\left(\frac{u}{k}\right) - \sin(\phi)\,\mathrm{dn}\left(\frac{u}{k}\right)\right)\Bigg] \\ \hat{q}_2(u) = \hat{q}_{20} + \frac{1}{\omega}\Bigg[&\Big(\frac{2}{k^2} - 1 - 2\,\frac{\mathrm{E}(k)}{k^2\,\mathrm{K}(k)}\Big)\sin(\phi)\,u \\ &- \frac{2}{k}\left(\sin(\phi)\,\mathrm{Z}\left(\frac{u}{k}\right) + \cos(\phi)\,\mathrm{dn}\left(\frac{u}{k}\right)\right)\Bigg]\end{aligned} \tag{6.25}$$

where $\hat{q}_{10}$ and $\hat{q}_{20}$ are constant, $K(k), E(k)$ are respectively the complete elliptic integrals of the first and second kind, $Z(.)$ is the Jacobi's Zeta function.

6.6.2.4 Computations of strokes with small amplitudes using the nilpotent approximation

We recall that the physical variables q are related to $\hat{q}$ using the transformation φ. The adjoint variables p are obtained by a Mathieu transformation associated with φ. Strokes with small amplitudes such that $q(0) = 0$ are computed from the nilpotent approximation in the following ways:

- *Oscillating case:*

The modulus k can be expressed as

$$k(\hat{p}(0)) = \frac{1}{2}\sqrt{\frac{2\sqrt{\hat{p}_4(0)^2+4\,\hat{p}_5(0)^2}+\hat{p}_3(0)^2-2\,\hat{p}_1(0)\,\hat{p}_4(0)-4\,\hat{p}_5(0)\,\hat{p}_2(0)}{\sqrt{\hat{p}_4(0)^2+4\,\hat{p}_5(0)^2}}} \tag{6.26}$$

and computing $k(\hat{p}(0))$ such that the linear terms of $\theta_1(t) = \hat{q}_1(\omega t+\varphi_0), \theta_2(t) = \hat{q}_2(\omega t+\varphi_0)$ of (6.24) vanish leads to periodic strokes with eight shapes of period

$$T = \frac{4\,K(k)}{\left(\hat{p}_4(0)^2+4\,\hat{p}_5(0)^2\right)^{1/4}}.$$

The constant $\hat{q}_{10}, \hat{q}_{20}$ are chosen such that $\theta(0) = 0$. The initial adjoint vector $p(0)$ has to check the conditions $H_1(\hat{q}(0),\hat{p}(0))^2 + H_2(\hat{q}(0),\hat{p}(0))^2 = 1$, $k(\hat{p}(0)) \in (0,1)$ and $\hat{p}_4(0)^2+4\,\hat{p}_5(0)^2 \neq 0$. We integrate numerically the stroke in the physical variables starting from $(q(0) = 0, p(0))$ and compute the first conjugate points on $[0,T]$ (see Fig.6.12).

- *Rotating case:* The modulus k can be expressed as

$$k(\hat{p}(0)) = 2\sqrt{\frac{\sqrt{\hat{p}_4(0)^2+4\,\hat{p}_5(0)^2}}{2\sqrt{\hat{p}_4(0)^2+4\,\hat{p}_5(0)^2}+\hat{p}_3(0)^2-2\,\hat{p}_1(0)\,\hat{p}_4(0)-4\,\hat{p}_5(0)\,\hat{p}_2(0)}} \tag{6.27}$$

We have $\theta_1(t) = \hat{q}_1(\omega t+\varphi_0), \theta_2(t) = \hat{q}_2(\omega t+\varphi_0)$ where $\hat{q}_1, \hat{q}_2$ are explicitly written in (6.25). We choose $p(0)$ so that $H_1(\hat{q}(0),\hat{p}(0))^2+H_2(\hat{q}(0),\hat{p}(0))^2 = 1$, $k(\hat{p}(0)) \in (0,1)$ and such that the denominator of $k(\hat{p}(0))$ is nonzero.
As $k(\hat{p}(0))$ tends to 0, the linear terms of $\hat{q}_1(u), \hat{q}_2(u)$ of (6.25) tend to 0. This is the case when $\hat{p}_4(0) \to 0$ and $\hat{p}_5(0) \to 0$, and the equation (6.23) becomes

$$\dot{\theta}^2 = \hat{p}_3(0)^2, \tag{6.28}$$

hence $\ddot{\theta} = 0$ and this case is treated below as the degenerated case.

- *Degenerated case:* We have

$$\ddot{\theta} = 0, \quad \dot{\theta}^2 = \hat{p}_3(0)^2,$$

hence $\theta(t) = \pm\hat{p}_3(0)\,t+\theta_0$ where θ_0 is a constant and the strokes are given by

$$\hat{q}_1(t) = \hat{q}_{10}+\frac{1}{\pm\hat{p}_3(0)}\sin(\pm\hat{p}_3(0)\,t+\theta_0),\ \hat{q}_2(t) = \hat{q}_{20}-\frac{1}{\pm\hat{p}_3(0)}\cos(\pm\hat{p}_3(0)\,t+\theta_0).$$

Abnormal case. We consider the minimal time problem for the single-input affine system [33]

$$\dot{\hat{q}}(t) = \hat{F}_1(\hat{q}(t)) + u(t)\hat{F}_2(\hat{q}(t))$$

where u is a scalar control.
Denoting $\hat{q}(.)$ a reference minimum time trajectory, since we consider abnormal

extremals, it follows from the Pontryagin maximum principle that along the extremal lift of $\hat{q}(.)$, there must hold $H_2(\hat{q}(.),\hat{p}(.))=0$ and differentiating with respect to t, $\{H_1,H_2\}(\hat{q}(.),\hat{p}(.))=0$ must hold too. Thanks to a further derivation, the extremals associated with the controls

$$u_a(\hat{q},\hat{p})=\frac{\{H_1,\{H_2,H_1\}\}(\hat{q},\hat{p})}{\{H_2,\{H_1,H_2\}\}(\hat{q},\hat{p})}=\frac{2\hat{p}_5}{\hat{p}_4}$$

satisfy the constraints $H_2=\{H_1,H_2\}=0$ along $(\hat{q}(.),\hat{p}(.))$ and are solutions of

$$\dot{\hat{q}}=\frac{\partial H_a}{\partial \hat{p}},\quad \dot{\hat{p}}=-\frac{\partial H_a}{\partial \hat{q}}$$

where H_a is the true Hamiltonian

$$H_a(\hat{q},\hat{p})=H_1(\hat{q},\hat{p})+u_aH_2(\hat{q},\hat{p})=\hat{p}_1+2\,\frac{\hat{p}_5\,\left(\hat{p}_2+\hat{p}_3\,\hat{q}_1+\hat{p}_4\,\hat{q}_3+\hat{p}_5\,\hat{q}_1^2\right)}{\hat{p}_4}.$$

From the Pontryagin maximum principle, the constraint $H_1(\hat{q}(.),\hat{p}(.))=0$ must hold too. The extremal system subject to the constraints $H_1=H_2=\{H_1,H_2\}=0$ is integrable and solutions can be written as

$$\begin{aligned}
\hat{q}_1(t)&=t+\hat{q}_1(0),\qquad \hat{q}_2(t)=2\,\frac{\hat{p}_5(0)\,t}{\hat{p}_4(0)}+\hat{q}_2(0),\\
\hat{q}_3(t)&=\frac{\hat{p}_5(0)\,t^2}{\hat{p}_4(0)}+2\,\frac{\hat{p}_5(0)\,\hat{q}_1(0)\,t}{\hat{p}_4(0)}+\hat{q}_3(0),\\
\hat{q}_4(t)&=2/3\,\frac{\hat{p}_5(0)^2t^3}{\hat{p}_4(0)^2}-2\,\frac{\hat{p}_5(0)\,\left(\hat{p}_5(0)\,\hat{q}_1(0)^2+\hat{p}_3(0)\,\hat{q}_1(0)+\hat{p}_2(0)\right)t}{\hat{p}_4(0)^2}\\
&\quad-\frac{\hat{p}_5(0)\,\hat{p}_3(0)\,t^2}{\hat{p}_4(0)^2}+\hat{q}_4(0),\\
\hat{q}_5(t)&=2/3\,\frac{\hat{p}_5(0)\,t^3}{\hat{p}_4(0)}+\frac{\left(4\,\hat{p}_5(0)\,\hat{q}_1(0)+\hat{p}_3(0)\right)t^2}{\hat{p}_4(0)}\\
&\quad+2\,\frac{\left(2\,\hat{p}_5(0)\,\hat{q}_1(0)^2+\hat{p}_3(0)\,\hat{q}_1(0)+\hat{q}_3(0)\,\hat{p}_4(0)+\hat{p}_2(0)\right)t}{\hat{p}_4(0)}+\hat{q}_5(0),\\
\hat{p}_1(t)&=\left(-2\,\frac{\hat{p}_5(0)\,\hat{p}_3(0)}{\hat{p}_4(0)}-4\,\frac{\hat{p}_5(0)^2\hat{q}_1(0)}{\hat{p}_4(0)}\right)t+\hat{p}_1(0),\\
\hat{p}_2(t)&=\hat{p}_2(0),\qquad \hat{p}_3(t)=-2\,\hat{p}_5(0)\,t+\hat{p}_3(0),\qquad \hat{p}_4(t)=\hat{p}_4(0),\qquad \hat{p}_5(t)=\hat{p}_5(0)
\end{aligned}$$

with $(\hat{q}_1(0),\hat{q}_2(0),\hat{q}_3(0),\hat{q}_4(0),\hat{q}_5(0),\hat{p}_1(0),\hat{p}_2(0),\hat{p}_3(0),\hat{p}_4(0),\hat{p}_5(0))$ are constant satisfying

$$\hat{p}_1(0)=0,\ \hat{p}_2(0)=\hat{p}_5(0)\hat{q}_1(0)^2-\hat{p}_4(0)\hat{q}_3(0),\ \hat{p}_3(0)=-2\hat{p}_5(0)\hat{q}_1(0).$$

Remark 6.19. *The θ-projection abnormals are straight lines and will form triangular strokes.*

6.6.3 Numerical results

6.6.3.1 Computations of conjugate points

Normal case. In the normal case, we consider the extremal system given by the true Hamiltonian given by (6.21). In section 6.6.2.3, we described three types of extremals. For each case, we have computed solutions using `HamPath` , representing the control, state and adjoint variables as functions of time (see Fig.6.11, Fig.6.12, Fig.6.13). We also illustrate the conjugate points evaluated according to the algorithm [38], as well as the smallest singular value for the rank test.

Property on the first conjugate point. For the normal extremals in the oscillating case and the rotating case presented in section 6.6.2.3, we take a large number of random initial adjoint vectors $\hat{p}(0)$ such that $H_1(\hat{q}(0),\hat{p}(0))^2 + H_2(\hat{q}(0),\hat{p}(0))^2 = 1$ and such that $0 < k(\hat{p}(0)) < 1$ where k is given by (6.26) for the oscillating case and by (6.27) for the rotating case. Then we numerically integrate the extremal system. We compute the first conjugate time t_{1c}, the pulsation $\omega = (\hat{p}_4(0)^2 + 4\,\hat{p}_5(0)^2)^{1/4}$, and the complete elliptic integral $K(k)$, where k is the modulus given by (6.26) in the oscillating case or by (6.27) in the rotating case.

Let $\gamma(.)$ be a normal extremal starting at $t = 0$ from the origin and defined on $[0, +\infty[$. As illustrated on Fig.6.14, there exists a first conjugate point along γ corresponding to a conjugate time t_{1c} satisfying the inequalities:

$$0.34\,\omega\,t_{1c} - 0.4 < K(k) < 0.53\,\omega\,t_{1c} - 0.8 \text{ for the oscillating case,}$$
$$0.33\,\omega\,t_{1c} + 0.16 < K(k) < 0.55\,\omega\,t_{1c} - 1.27 \text{ for the rotating case.}$$

Abnormal case. Fig.6.15 illustrates the time evolution of the state variables. We check numerically the second order optimality conditions [33]. Both the determinant test and the smallest singular value for the rank condition indicate that there is no conjugate time for abnormal extremals (Fig.6.16).

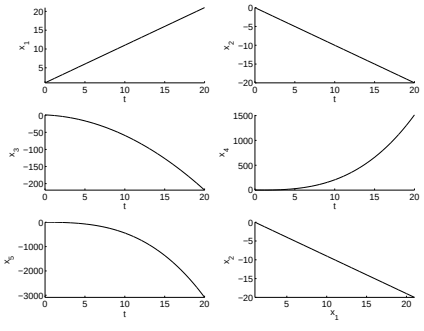

Figure 6.15: Abnormal case: state variables for $\hat{q}(0) = (1,0,1,0,0)$, $\hat{p}(0) = (0,0,-2,1,1)$.

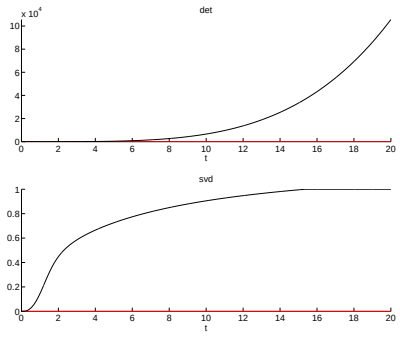

Figure 6.16: Abnormal case: the second order sufficient condition indicates there is no conjugate point.

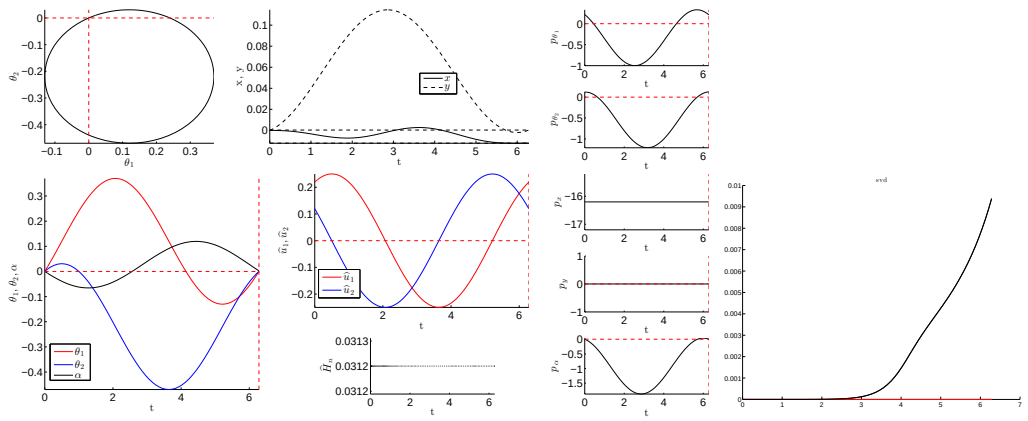

Figure 6.11: *(left)* Control, state and adjoint physical variables in the degenerated case of the nilpotent approximation with an simple loop. *(right)* SVD test of conjugate points (no conjugate point on $[0, 2\pi]$).

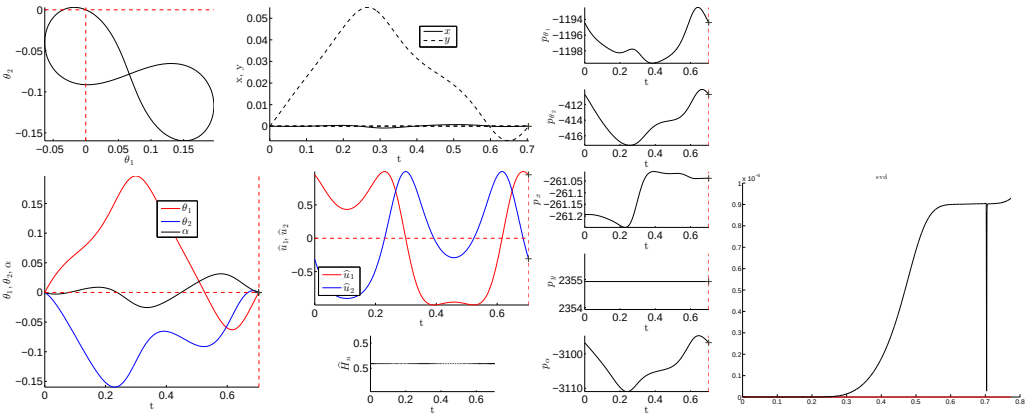

Figure 6.12: *(left)* Control, state and adjoint physical variables in the oscillating case of the nilpotent approximation with an eight shape. *(right)* SVD test of conjugate points (the cross stands for the first conjugate point).

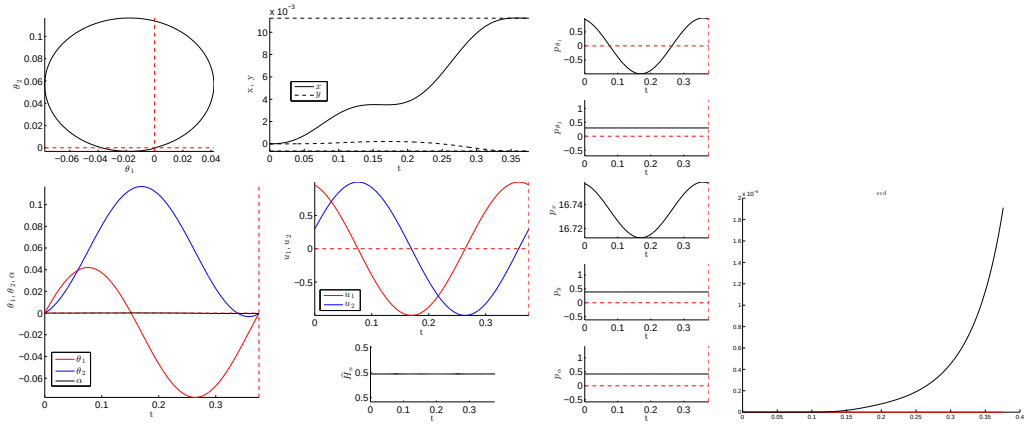

Figure 6.13: *(left)* Control, state and adjoint physical variables in the rotating case of the nilpotent approximation ($k = 0.115$). *(right)* SVD test of conjugate points.

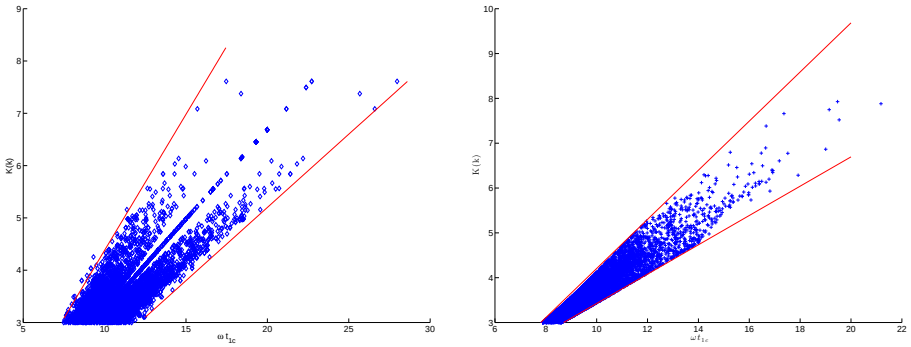

Figure 6.14: Conjugate points of normal extremals with constant energy $H_1^2 + H_2^2 = 1$ in the oscillating case *(left)* and in the rotating case *(right)*.

6.6.3.2 Computations of optimal strokes using a discrete numerical homotopy

Method.

- The analytical expressions of $\theta_1(t), \theta_2(t)$, given for the degenerated case and for the oscillating case in section 6.6.2.3, allow us to compute strokes with small amplitudes of the nilpotent model. Besides, SVD test for conjugate points is also illustrated (see Fig.6.11 and Fig.6.12) showing that the simple loop have no conjugate points on $[0, T]$ while the eight stroke have a first conjugate point on $[0, T]$.

- The previous solutions are used to compute strokes for the Purcell swimmer with the $\int_0^T (u_1^2 + u_2^2)\mathrm{d}t$ cost. More precisely, the initial adjoint vector $\hat{p}(0)$ of the nilpotent model gives a good initialization of the shooting algorithm used by `HamPath` to solve the following boundary value problem.

$$\begin{cases} \dot{q} = \frac{\partial \tilde{H}_n}{\partial p}, \quad \dot{p} = -\frac{\partial \tilde{H}_n}{\partial q}, \\ \theta_j(T) = \theta_j(0) \quad j = 1, 2, \\ x(0) = y(0) = \alpha(0) = 0, \\ x(T)^2 + y(T)^2 = c_1,\ \alpha(T) = c_2, \\ p_{\theta_j}(T) = p_{\theta_j}(0) \quad j = 1, 2, p_\alpha(0) = p_\alpha(T) \end{cases} \tag{6.29}$$

  where T, c_1, c_2 are fixed constants and $\tilde{H}_n$ is the normal Hamiltonian associated with the $\int_0^T (u_1^2 + u_2^2)\mathrm{d}t$ cost.
  Then, with T fixed to 2π and c_2 to 0, we perform a discrete homotopy on the radius c_1 to obtain stroke with larger amplitudes (see Fig.6.17).

  Fig.6.18 (resp. Fig.6.19) illustrates state and adjoint variables for a simple loop stroke (resp. eight stroke) solution of (6.29) and it is obtained from $\hat{p}(0)$ given by the degenerated case (resp. oscillating case). There are no conjugate points on $[0, 2\pi]$ for the simple loop case, but a conjugate points does appear for the eight case.

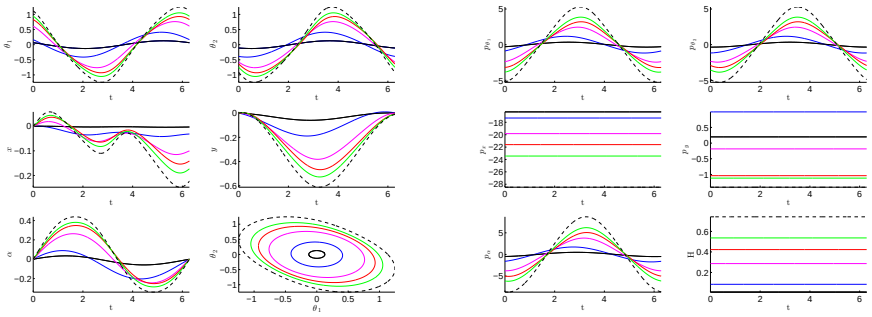

Figure 6.17: One parameter family of simple loop strokes of the Purcell swimmer with the $\int_0^T (u_1^2 + u_2^2)\mathrm{d}t$ cost. The continuation is performed on the constant c_1 where we fixed $T = 2\pi$ and $c_2 = 0$.

- Let consider the following optimal control problem

$$\begin{cases} \dot{q} = \frac{\partial H_n}{\partial p}, \quad \dot{p} = -\frac{\partial H_n}{\partial q}, \\ \theta_j(T) = \theta_j(0) \quad j = 1, 2, \\ x(0) = y(0) = \alpha(0) = 0, \\ x(T)^2 + y(T)^2 = c_1,\ \alpha(T) = c_2, \\ p_{\theta_j}(T) = p_{\theta_j}(0) \quad j = 1, 2, p_\alpha(0) = p_\alpha(T) \end{cases} \tag{6.30}$$

  where $H_n = \frac{1}{2}\left(a(q)u_1^2 + 2b(q)u_1u_2 + c(q)u_2^2\right)$ is the true Hamiltonian associated with the mechanical cost, and u_1, u_2 are the optimal controls.
  We take an extremal of (6.29) to initialize a discrete homotopy with parameter $\lambda \in [0, 1]$, of the following optimal control problem

$$\begin{cases} \dot{q} = \frac{\partial H_\lambda}{\partial p}, \quad \dot{p} = -\frac{\partial H_\lambda}{\partial q}, \\ \theta_j(T) = \theta_j(0) \quad j = 1, 2, \\ x(0) = y(0) = \alpha(0) = 0, \\ x(T)^2 + y(T)^2 = c_1,\ \alpha(T) = c_2, \\ p_{\theta_j}(T) = p_{\theta_j}(0) \quad j = 1, 2, p_\alpha(0) = p_\alpha(T) \end{cases} \tag{6.31}$$

  where $H_\lambda = \lambda H_n + (1 - \lambda)\tilde{H}_n$. When λ reaches the value 1, we obtain an extremal of (6.30).
  Since the latter homotopy is discrete, we may not follow a unique branch and obtain many kind of strokes: Fig.6.20, Fig.6.21 and Fig.6.22 are three different strokes solutions of (6.30) and the SVD rank condition show that the only candidates for optimality are the simple loops.

  Then we perform a second homotopy on the radius c_1 to have a one-parameter family of strokes. Fig.6.23 and Fig.6.24 represent two one-parameter families of solutions of (6.30) corresponding respectively to the strokes of Fig.6.20 and Fig.6.21. To compare these two families of strokes, we compute in Fig.6.25 their geometric efficiencies and we conclude that for a given radius $r = c_1$, the corresponding stroke of the family 1 is more efficient.

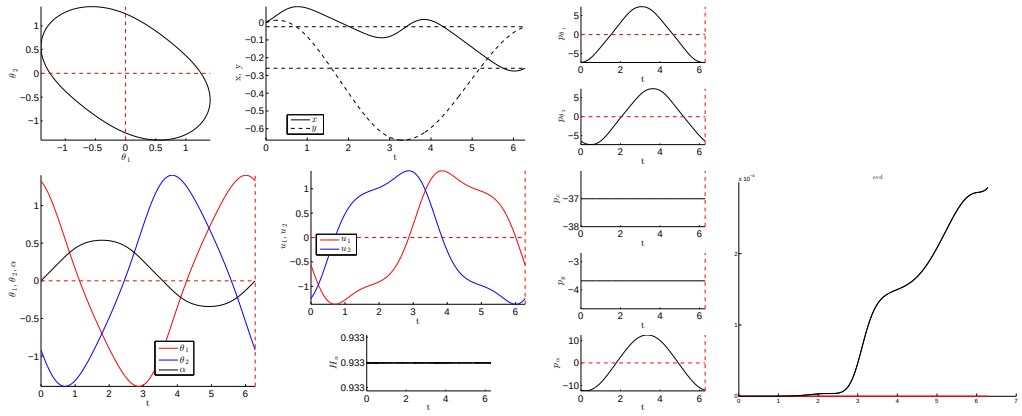

Figure 6.18: *(left)* Simple loop stroke for the Purcell swimmer minimizing the cost $\int_0^T (u_1^2 + u_2^2)\mathrm{d}t$, taking $T = 2\pi$, $c_1 = 0.068$, $c_2 = 0$ and imposing the periodicity on α. *(right)* Test of conjugate points (no conjugate point on $[0, 2\pi]$).

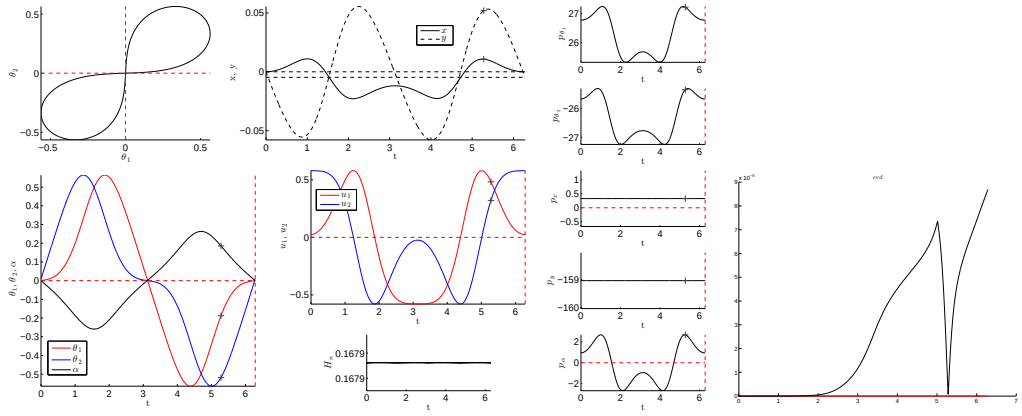

Figure 6.19: *(left)* Eight stroke for the Purcell swimmer minimizing the cost $\int_0^T (u_1^2 + u_2^2)\mathrm{d}t$, taking $T = 2\pi$, $c_1 = 4.6e{-}4$, $c_2 = 0$ and imposing the periodicity on α. *(right)* Test of conjugate points (the cross stands for the first conjugate point).

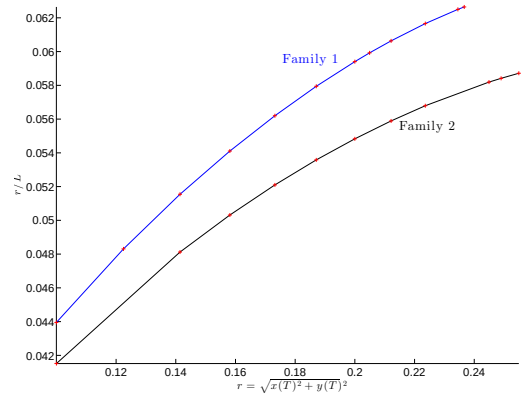

Figure 6.25: Comparison of the efficiency between the two families of strokes for the true mechanical cost.

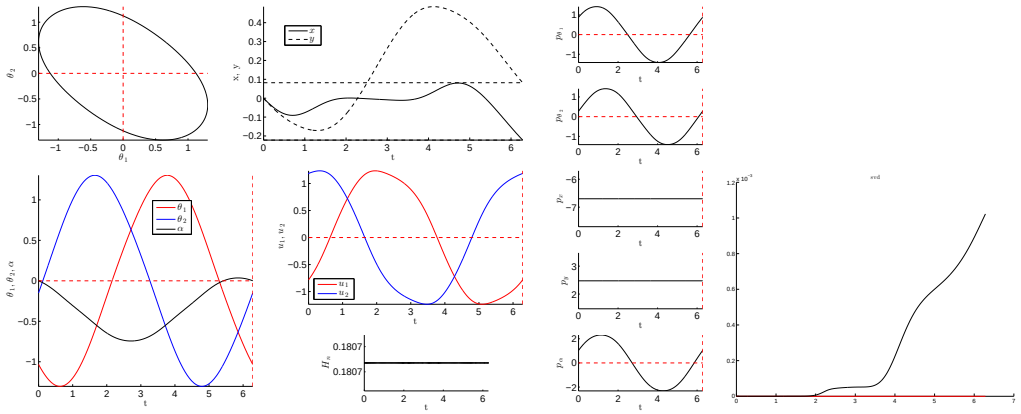

Figure 6.20: *(left)* State and adjoint variables for the Purcell swimmer minimizing the mechanical cost, taking $T = 2\pi$, $c_1 = 0.058$ and $c_2 = 0$. *(right)* Test of conjugate points (no conjugate point on $[0, 2\pi]$).

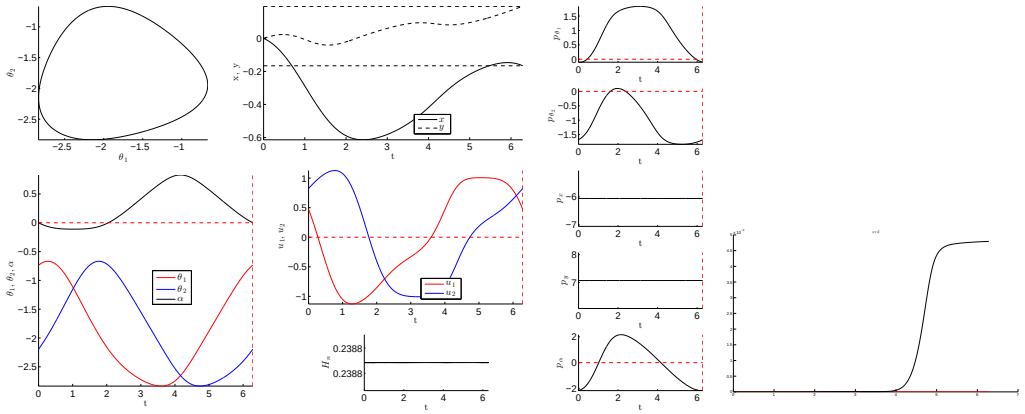

Figure 6.21: *(left)* State and adjoint variables for the Purcell swimmer minimizing the mechanical cost, taking $T = 2\pi$, $c_1 = 0.065$ and $c_2 = 0$. *(right)* Test of conjugate points (no conjugate point on $[0, 2\pi]$).

- Result of the continuation: two one-parameter families of simple loop for the mechanical cost appear and their respective efficiency is compared in Fig.6.25. Note that the efficiency increases with the radius of the circle c_1.

6.6.4 Sufficient second order conditions for the Purcell strokes

The lemma 6.14 gives one symmetry for the Purcell swimmer. We present here an additional symmetry: any time translation of the shape variables (θ_1, θ_2) and the orientation variable α is also a stroke and has the same cost. The presence of these symmetries need particular second order sufficient conditions [62] (see the Appendix for a brief summary). For this purpose, we provide numerical results on second order sufficient conditions for normal extremals of the Purcell swimmer.
We consider the optimal control problem in which we minimize the cost (6.4) over

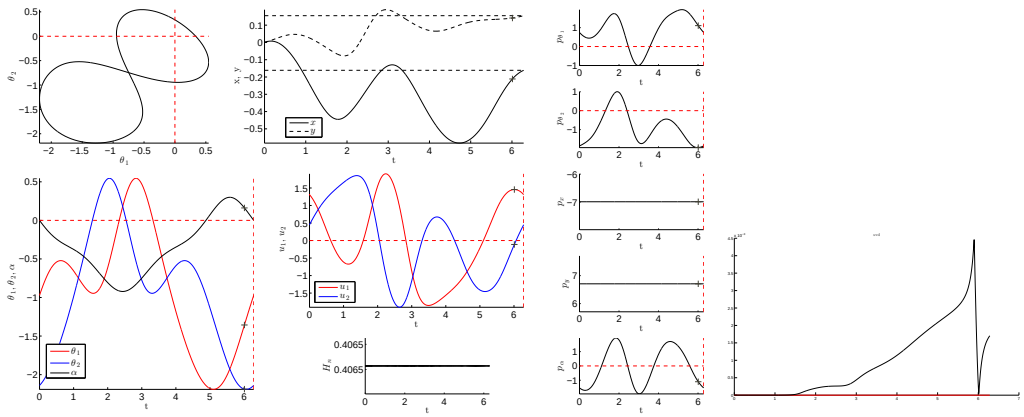

Figure 6.22: *(left)* State and adjoint variables for the Purcell swimmer minimizing the mechanical cost, taking $T = 2\pi$, $c_1 = 0.05$ and $c_2 = 0$. *(right)* Test of conjugate points (the cross stands for the first conjugate point).

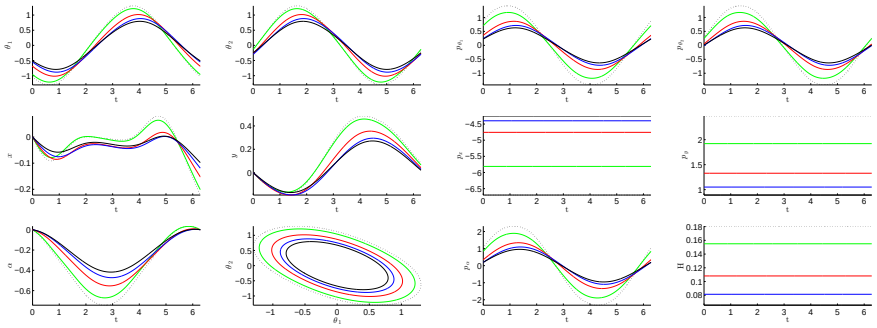

Figure 6.23: Family 1 of strokes for the Purcell swimmer minimizing the mechanical cost. We fixed $T = 2\pi$ and $c_2 = 0$ and the family of strokes is obtained by a continuation on c_1.

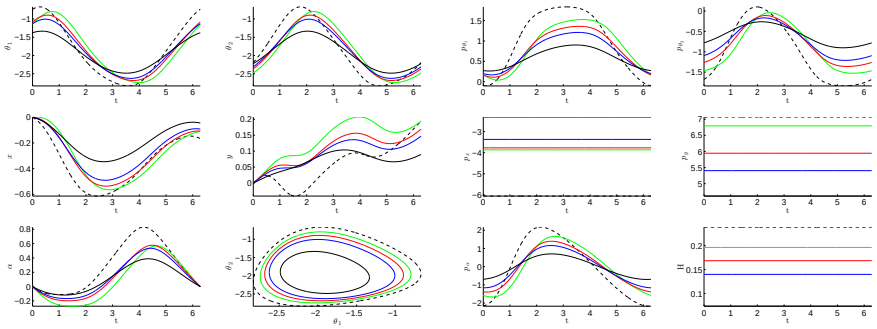

Figure 6.24: Family 2 of strokes for the Purcell swimmer minimizing the mechanical cost. We fixed $T = 2\pi$ and $c_2 = 0$ and each family of strokes is obtained by a continuation on c_1.

trajectories satisfying (6.3) and such that

$$\begin{aligned} &\theta_j(0) = \theta_j(T) \quad j = 1, 2, \quad \alpha(0) = \alpha(T), \\ &x(0) = 0,\ y(0) = 0,\ x(T)^2 + y(T)^2 = r \text{ (r is fixed)} . \end{aligned} \tag{6.32}$$

Proposition 6.20. *Take $a = (\phi, \sigma) \in I = (-\varepsilon, \varepsilon)^2$ for some $\varepsilon > 0$. Let $(\bar{q}, \bar{u}, p)$ where $\bar{q} = (\bar{\theta}_1, \bar{\theta}_2, \bar{x}, \bar{y}, \bar{\alpha})$ and $\bar{u} = (\bar{u}_1, \bar{u}_2)$ be a normal extremal. Write $\bar{\theta}_j(.)$, $j = 1, 2$, $p(.)$, $\bar{x}(.)$, $\bar{y}(.)$ and $\bar{u}(.)$ their corresponding periodic extensions.*
For all $a \in I$ and $t \in [0, T]$, we define $q^a(.) = (\theta_1^a(.), \theta_2^a(.), x^a(.), y^a(.), \alpha^a(.))$ where

$$\begin{aligned} &u_j^a(t) = \bar{u}_j(t+\sigma),\ \theta_j^a(t) = \bar{\theta}_j(t+\sigma) \quad j = 1, 2, \\ &x^a(t) = \cos(\phi)\,(\bar{x}(t+\sigma) - \bar{x}(\sigma)) - \sin(\phi)\,(\bar{y}(t+\sigma) - \bar{y}(\sigma)), \\ &y^a(t) = \sin(\phi)\,(\bar{x}(t+\sigma) - \bar{x}(\sigma)) + \cos(\phi)\,(\bar{y}(t+\sigma) - \bar{y}(\sigma)), \\ &\alpha^a(t) = \bar{\alpha}(t+\sigma) + \phi. \end{aligned} \tag{6.33}$$

Then the normal extremal $(\bar{q}(.), p(.), \bar{u}(.))$ is continuously embedded in the family of extremals $(q^a(.), p^a(.), u^a(.))_{a \in I}$ where $p^a(.)$ is the adjoint vector associated with $(q^a(.), u^a(.))$.

We apply the algorithm [62] to the simple loop of Fig.6.21 satisfying (6.32) with associated adjoint vector p and we have the following result.

Numerical result: *The simple loop $(\bar{q}, \bar{u})$ is weak-locally optimal.*
To confirm this claim, we refer the reader to [62].

1. The Purcell model verifies the conditions (F1)-(F4), which ensures that the normal extremal $(\bar{q}, \bar{u}, p)$ is embedded in a family of normal extremals and assumptions (H1)-(H4) required by 2.13 are satisfied. Owing to the fact that there is no conjugate points for the normal extremal $(\bar{q}(.), p, \bar{u}(.))$ (cf Section 6.6.3.2), the Riccati equation (2.9) has a global symmetric solution.

2. Using the *Isoda* integrator from the FORTRAN library *odepack*, the computation of the matrix $\mathcal{W}$, defined in (2.11), yields

$$\mathcal{W} = \begin{pmatrix} 36.7491 & -12.3797 & -90.3501 & -38.4486 & 45.9572 & -20.9543 & 12.3334 & 90.3501 & 38.4486 & -22.0849 \\ -12.3797 & 12.7351 & 63.8598 & -2.19107 & -4.48021 & 5.29771 & -14.0060 & -63.8598 & 2.19107 & -7.52291 \\ -90.3501 & 63.8598 & 356.119 & 72.4282 & -72.3005 & 50.6364 & -65.6286 & -356.119 & -72.4282 & 5.46840 \\ -38.4486 & -2.19107 & 72.4283 & 155.119 & -58.0160 & 27.2663 & -1.54193 & -72.4283 & -155.119 & 30.3765 \\ 45.9572 & -4.48021 & -72.3005 & -58.0160 & 74.6500 & -29.6527 & 3.10041 & 72.3005 & 58.0160 & -51.0282 \\ -20.9543 & 5.29771 & 50.6364 & 27.2663 & -29.6527 & 11.6627 & -5.47480 & -50.6364 & -27.2663 & 15.3254 \\ 12.3334 & -14.0060 & -65.6286 & -1.54192 & 3.10041 & -5.47479 & 15.7573 & 65.6286 & 1.54192 & 9.86428 \\ 90.3501 & -63.8598 & -356.119 & -72.4282 & 72.3005 & -50.6364 & 65.6286 & 283.095 & 72.4282 & -5.46840 \\ 38.4486 & 2.19107 & -72.4283 & -155.119 & 58.0160 & -27.2663 & 1.54193 & 72.4283 & 82.0946 & -30.3765 \\ -22.0850 & -7.52291 & 5.46840 & 30.3766 & -51.0282 & 15.3254 & 9.86428 & -5.46840 & -30.3766 & 44.9320 \end{pmatrix}.$$

   We set

$$\mathcal{L}_s = \{\, (y_0, y_T) \in \mathbb{R}^5 \times \mathbb{R}^5 \mid \nabla_{q_0, q_T} m(q_0, q_T)\ (y_0 \quad y_T)^\intercal = 0 \,\}$$

   where $m(q_0, q_T) = (\theta_1(0) - \theta_1(T), \theta_2(0) - \theta_2(T), x(0), y(0), \alpha(0) - \alpha(T), x(T)^2 + y(T)^2 - r)$.
   We take the matrix N_s such that $\ker(\nabla_{q_0, q_T} m(q_0, q_T)) = \mathrm{Im}(N_s)$.

   Now from the symmetry described in Prop.6.20, we define

$$\Gamma_\phi = \begin{pmatrix} \nabla_\phi q^a(0) \\ \nabla_\phi q^a(T) \end{pmatrix}_{\phi=0},\ \Gamma_\sigma = \begin{pmatrix} \nabla_\sigma q^a(0) \\ \nabla_\sigma q^a(T) \end{pmatrix}_{\sigma=0} \text{ and } \Gamma_r = (\Gamma_\phi \quad \Gamma_\sigma). \tag{6.34}$$

We consider the linear subspaces

$$\mathcal{L}_\phi = \mathcal{L}_s \cap \{(y_0, y_T) \in \mathbb{R}^5 \times \mathbb{R}^5 \mid \Gamma_\phi^\intercal \, (y_0 \quad y_T)^\intercal = 0\},$$
$$\mathcal{L}_\sigma = \mathcal{L}_s \cap \{(y_0, y_T) \in \mathbb{R}^5 \times \mathbb{R}^5 \mid \Gamma_\sigma^\intercal \, (y_0 \quad y_T)^\intercal = 0\},$$
$$\mathcal{L}_r = \mathcal{L}_s \cap \{(y_0, y_T) \in \mathbb{R}^5 \times \mathbb{R}^5 \mid \Gamma_r^\intercal \, (y_0 \quad y_T)^\intercal = 0\}$$

and the matrices N_ϕ, N_σ and N_r such that

$$\mathcal{L}_\phi = \mathrm{Im}(N_\phi), \quad \mathcal{L}_\sigma = \mathrm{Im}(N_\sigma), \quad \mathcal{L}_r = \mathrm{Im}(N_r).$$

We take two different tolerances for the integrator used to compute numerically the matrix $\mathcal{W}$. Table 6.3 shows that the matrices $\mathcal{W}_s = N_s^\intercal \left(\mathcal{W}^\intercal + \mathcal{W}\right) N_s$, $\tilde{\mathcal{W}}_\phi = N_\phi^\intercal \left(\mathcal{W}^\intercal + \mathcal{W}\right) N_\phi$ and $\tilde{\mathcal{W}}_\sigma = N_\sigma^\intercal \left(\mathcal{W}^\intercal + \mathcal{W}\right) N_\sigma$ have zero eigenvalues (whose eigenvectors are Γ_ϕ and Γ_σ). In particular, $\mathcal{W}_s$ is not definite-positive hence the standard sufficient second order conditions 2.12 fail. Also, the refined second order sufficient conditions of 2.13 are satisfied since the eigenvalues of $\mathcal{W}_r = N_r^\intercal \left(\mathcal{W}^\intercal + \mathcal{W}\right) N_r$ are positive.

Absolute and relative tolerance	(Standard condition) Spec($\mathcal{W}_s$)	Spec($\tilde{\mathcal{W}}_\phi$)	Spec($\tilde{\mathcal{W}}_\sigma$)	(Refined condition) Spec($\mathcal{W}_r$)
10^{-4}	1319.91 3.44629 $-2.61575e-5$ $-4.17860e-3$	35380.1 3.46392 $-4.18945e-3$	1366.83 $-4.10573e-4$ 14.5123	36179.7 13.8018
10^{-7}	1320.17 3.44676 $9.81190e-6$ $-5.40128e-6$	35386.9 3.46438 $-4.84724e-6$	1367.10 $9.85195e-6$ 14.5151	36186.9 13.8037

Table 6.3: The standard second order sufficient conditions fail: $\mathcal{W}_s$ has zero eigenvalues and the refined second order sufficient conditions are satisfied: $\mathcal{W}_r$ is positive-definite.

6.7 Conclusion

For further studies the program is the following.

- Nilpotent approximations are not sufficient in the Copepod case where only simple loops can be obtained and for the Purcell swimmer and moreover they are not a generic model to study the SR-balls. A more complete program is to compute higher order approximations for the contact case [1] and for the Martinet case [34] to generate generic strokes. Also it will clarify the distribution of conjugate points, crucial for the convergence of continuation methods.

- The numerical results have to be completed to compute strokes with larger amplitudes for the Purcell case and the analysis pursued to deal with different links parameters.

- A more complete analysis in relation with non smooth abnormal minimizers has to be done in order to clarify the optimality status of abnormal strokes, taking into account the state constraints and with respect to C^0-optimality.

Part II

Averaging for the orbital transfer problem with low thrust

Chapter 7

Preliminairies

In this chapter we formulate the minimal time control problem. First we start by recalling preliminaries in spatial mechanics: Kepler problem, models of some perturbations and we present some averaging theorem used in dynamical system.

Contents

8.1 Non averaged extremal system 117
8.2 Averaging extremals 119
8.2.1 Preparation for averaging 119
8.2.2 Averaged dynamic for a single frequency 121
8.2.3 Pulsation depending upon the fast angular variable 123
8.2.4 Case of several frequencies 125
8.3 Convergence theorems for the boundary value problems . . 127
8.3.1 The non averaged and averaged boundary value problem . . . 127
8.3.2 Convergence theorems 128

7.1 Controlled two-body (Newtonian) problem

We investigate the bounded motion of a satellite in $\mathbb{R}^3$ which is under the influence of a gravitational field of the Earth fixed at the origin and whose trajectory is controlled by a low-thrust engine. The acceleration of a satellite of mass m_S rotating around the Earth under the influence of gravity and engine thrust is (see [120, 57, 50])

$$\ddot{q} = -\nabla V(q) + \frac{u}{m_S}, \quad |u| < 1, \quad q, u \in \mathbb{R}^3$$

where q is the position of the satellite in an inertial frame with the origin at the Earth. The potential V is taken as a first approximation $V(q) = -\frac{\mu}{|q|}$ ($\mu > 0$ is the standard gravitational parameter of the Earth). The control u is the external force produced by the engines which have limited thrust.
In order to take into account more forces than the Newton spheric attraction, one may study a perturbed controlled two-body problem namely taking into account some perturbations caused by higher order terms in the gravitational field of the Earth and/or the lunar perturbation seen as a perturbation of the two-body problem {satellite, Earth}. These perturbations enter in the same way as the control.

7.2 Two body problem

In this section, the mass of the satellite is set to 1. The Kepler Hamiltonian is defined by

$$H(q,p) : T_0\mathbb{R}^3 \to \mathbb{R} : (q,p) \mapsto \frac{1}{2}p \cdot p - \frac{\mu}{|q|}$$

where $T_0\mathbb{R}^3 = (\mathbb{R}^3 \setminus \{0\}) \times \mathbb{R}^3$ is the phase space with coordinates (q,p). Integral curves of the Hamiltonian vector field $\overrightarrow{H}$ on $T_0\mathbb{R}^3$ satisfy

$$\begin{cases} \dot{q} = p \\ \dot{p} = -q\frac{\mu}{|q|^3} \end{cases}$$

On top of the Hamiltonian H, the angular momentum C and the eccentricity vector ϵ are other first integrals and are defined by

$$C := q \times p, \qquad \epsilon := \frac{q}{|q|} - \frac{1}{\mu}p \times C. \tag{7.1}$$

We restrict ourselves on the set

$$\mathcal{E} = \{(q,p) \in \mathbb{R}^3 \setminus \{0\} \times \mathbb{R}^3 \mid H(q,p) < 0\}$$

and it is well-known [56] that projections on the q-space of integral curves of $\overrightarrow{H}$ are ellipses if $C \neq 0$. Typically, when $C \neq 0$, the orbital elements $(a, e, i, \varpi, \Omega)$ give local coordinates on $\mathcal{E}$ and are defined by

- $\frac{1}{\mu}|C|^2 + \mu\,|\frac{\epsilon}{\sqrt{-2H}}|^2 = a > 0$ is the semi-major axis of the ellipse,
- the vector $C/|C| \in \boldsymbol{S}^2$ defines a unique oriented plane of $\mathbb{R}^3$, the orbital plane. It is located in a reference sphere by two angles. In Fig.7.1, these two angles are $(\frac{\pi}{2} - \Omega, i)$ where Ω is called the longitude of ascending node and i is called the inclination,
- $C/\sqrt{\mu a} + \epsilon \in \boldsymbol{S}^2$ is also represented by two angles (ϖ, ϕ). More precisely, this vector is measured from the ascending node to compute ϖ and from the direction of C to compute ϕ, see Fig.7.1 (the eccentricity of the ellipse is given by $|\epsilon| = e = \sin(\phi)$).

We add to $(a, e, i, \varpi, \Omega)$ an angle $v \in S^1$ to locate the position of the satellite on its orbit. This angle is represented in Fig.7.1 as the true anomaly. Other choice can be made such as the mean anomaly M, the eccentric anomaly E or the true longitude $l = \Omega + \varpi + v$ as well.

To desingularize these orbital coordinates $(a, e, i, \varpi, \Omega, M)$ – which are not well defined in the case of circular orbits, or when the orbital plane is equal to the reference plane – it is useful to consider the so-called equinoctial elements [125]

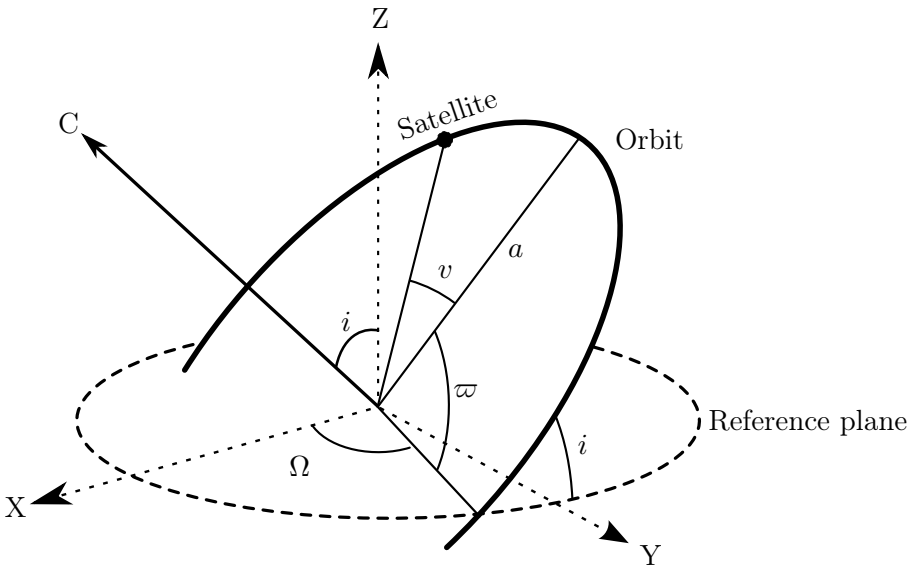

Figure 7.1: Classical orbital elements

$(P, e_x, e_y, h_x, h_y, l)$ defined from the projections of the vectors $C/\sqrt{a} + e$ and $C/|C|$ in the orbital plane and the reference plane respectively:

$$P = a\,(1 - e^2) \quad e_x = e\cos(\Omega + \varpi), \quad e_y = e\sin(\Omega + \varpi),$$
$$h_x = \tan(i/2)\cos(\Omega), \quad h_y = \tan(i/2)\sin(\Omega),$$

The expressions of the Cartesian coordinates $(q, \dot{q})$ where $q = (q_1, q_2, q_3)$ in terms of the equinoctial elements $(P, e_x, e_y, h_x, h_y, l)$ (in an inertial frame with the origin at the Earth) are (see [50])

$$\begin{aligned}
q_1 &= P/CW((1 + h_x^2 - h_y^2)\cos l + 2h_x h_y \sin l) \\
q_2 &= P/CW((1 - h_x^2 + h_y^2)\sin l + 2h_x h_y \cos l) \\
q_3 &= 2PD/CW \\
\dot{q}_1 &= 1/C\mu/P(2h_x h_y(e_x + \cos l) - (1 + h_x^2 - h_y^2)(e_y + \sin l)) \\
\dot{q}_2 &= 1/C\mu/P((1 - h_x^2 + h_y^2)(e_x + \cos l) - 2h_x h_y(e_y + \sin l)) \\
\dot{q}_3 &= 2/C\mu/P(h_x(e_x + \cos l) + h_y(e_y + \sin l))
\end{aligned} \tag{7.2}$$

where

$$W = 1 + e_x\cos l + e_y \sin l,\ D = h_x \sin l - h_y \cos l,\ C = 1 + h_x^2 + h_y^2. \tag{7.3}$$

7.3 Lagrange and Gauss equations

In this section, we recall from [50, 127, 98] the Lagrange and Gauss equations which aim to solve the dynamic equations $\ddot{q} = -q\frac{\mu}{|q|^3} + \gamma_P(q) + F_T/m_S$ where γ_P is a perturbing acceleration which derives from a potential and F_T is the force produced

by the thrust of the spacecraft. These perturbations are considered small compared with the kepler term. To obtain the time evolution of the orbital elements, we have two cases:

- the conservative case where γ_P can be derived from a scalar potential R, namely if γ_P results from gravitational interactions. The dynamic is given by the Lagrange equations.

- the non conservative case, in the sense that the work of the force F_T is non zero. The approach is to decompose F_T in a local orbital frame and to derive the Gauss equations.

7.3.1 The Lagrange equations

We assume that the perturbing force γ_P is derived from a scalar potential R, then

$$\gamma_P(q) = -\nabla R(q).$$

Then, using the orbital elements $(a, e, i, \varpi, \Omega, M)$, where M is the mean anomaly, the Lagrange equations take the form [127, 50]

$$\begin{aligned}
\frac{\mathrm{d}a}{\mathrm{d}t} &= -\frac{2}{na}\frac{\partial R}{\partial M} \\
\frac{\mathrm{d}e}{\mathrm{d}t} &= \frac{\sqrt{1-e^2}}{na^2e}\frac{\partial R}{\partial \varpi} - \frac{1-e^2}{na^2e}\frac{\partial R}{\partial M} \\
\frac{\mathrm{d}i}{\mathrm{d}t} &= \frac{1}{na^2\sin(i)\sqrt{1-e^2}}\frac{\partial R}{\partial \Omega} - \frac{\cot(i)}{na^2\sqrt{1-e^2}}\frac{\partial R}{\partial \varpi} \\
\frac{\mathrm{d}\Omega}{\mathrm{d}t} &= -\frac{1}{na^2\sin(i)\sqrt{1-e^2}}\frac{\partial R}{\partial i} \\
\frac{\mathrm{d}\varpi}{\mathrm{d}t} &= -\frac{\sqrt{1-e^2}}{na^2e}\frac{\partial R}{\partial e} + \frac{\cot(i)}{na^2\sqrt{1-e^2}}\frac{\partial R}{\partial i} \\
\frac{\mathrm{d}M}{\mathrm{d}t} &= n + \frac{2}{na}\frac{\partial R}{\partial a} + \frac{1-e^2}{na^2e}\frac{\partial R}{\partial e}
\end{aligned} \tag{7.4}$$

where n is the mean motion defined by $\mu = a^3n^2$.

In the equinoctial elements, the Lagrange equations are expressed as (see [125])

$$\begin{aligned}
\frac{\mathrm{d}P}{\mathrm{d}t} &= 2\sqrt{\frac{P}{\mu}}\left(-e_y\frac{\partial R}{\partial e_x}+e_x\frac{\partial R}{\partial e_y}+\frac{\partial R}{\partial l}\right)\\
\frac{\mathrm{d}e_x}{\mathrm{d}t} &= \frac{1}{\sqrt{\mu P}}\left(2Pe_y\frac{\partial R}{\partial P}-(1-e_x^2-e_y^2)\frac{\partial R}{\partial e_y}-\frac{e_yC}{2}(h_x\frac{\partial R}{\partial h_x}+h_y\frac{\partial R}{\partial h_y})\right.\\
&\qquad\left.+(e_x+(1+W)\cos l)\frac{\partial R}{\partial l}\right)\\
\frac{\mathrm{d}e_y}{\mathrm{d}t} &= \frac{1}{\sqrt{\mu P}}\left(-2Pe_x\frac{\partial R}{\partial P}+(1-e_x^2-e_y^2)\frac{\partial R}{\partial e_x}+\frac{e_xC}{2}(h_x\frac{\partial R}{\partial h_x}+h_y\frac{\partial R}{\partial h_y})\right.\\
&\qquad\left.+(e_y+(1+W)\sin l)\frac{\partial R}{\partial l}\right)\\
\frac{\mathrm{d}h_x}{\mathrm{d}t} &= \frac{C}{2\sqrt{\mu P}}\left(h_x(e_y\frac{\partial R}{\partial e_x}-e_x\frac{\partial R}{\partial e_y}-\frac{\partial R}{\partial l})-\frac{C}{2}\frac{\partial R}{\partial h_y}\right)\\
\frac{\mathrm{d}h_y}{\mathrm{d}t} &= \frac{C}{2\sqrt{\mu P}}\left(h_y(e_y\frac{\partial R}{\partial e_x}-e_x\frac{\partial R}{\partial e_y}-\frac{\partial R}{\partial l})+\frac{C}{2}\frac{\partial R}{\partial h_x}\right)\\
\frac{\mathrm{d}l}{\mathrm{d}t} &= \sqrt{\mu P}\left(\frac{W}{P}\right)^2+\frac{C}{2\sqrt{\mu P}}\left(h_x\frac{\partial R}{\partial h_x}+h_y\frac{\partial R}{\partial h_y}\right)
\end{aligned} \tag{7.5}$$

where C, W are given by (7.3).

7.3.2 The Gauss equations

Local frame: The perturbing force γ_P is written with respect to a local orbital frame with origin fixed at the satellite. The Gauss equations arise from a choice of coordinates of the elliptic domain once the moving frame for the perturbing force is fixed. One possibility is to choose the radial-orthoradial frame (Q, S, Z) with

$$Q=\frac{q}{|q|},\quad S=Z\wedge Q,\quad Z=\frac{q\wedge\dot{q}}{|q\wedge\dot{q}|}. \tag{7.6}$$

Another choice is the tangential-normal frame (T, N, Z) defined by

$$T=\frac{\dot{q}}{|\dot{q}|},\quad N=Z\wedge T,\quad Z=\frac{q\wedge\dot{q}}{|q\wedge\dot{q}|}. \tag{7.7}$$

If a force $X=(X_T, X_N, X_Z)$ is expressed in the (T, N, Z)-frame then the components (X_Q, X_S) in the (Q, S, Z)-frame are, in terms of the equinoctial elements

$$\begin{aligned}
X_Q &= 1/d\,((e_x\sin(l)-e_y\cos(l))X_T-(1+e_x\cos(l)+e_y\sin(l))X_N),\\
X_S &= 1/d\,((1+e_x\cos(l)+e_y\sin(l))X_T+(e_x\sin(l)-e_y\cos(l))X_N)
\end{aligned}$$

where $d=(1+2e_x\cos(l)+2e_y\sin(l)+e_x^2+e_y^2)^{1/2}$.

Gauss equations in the equinoctial coordinates: Decomposing γ_P in the radial-orthoradial frame, $\gamma_P = (\mathcal{Q}, \mathcal{S}, \mathcal{Z})$, we deduce from the change of variables (7.2) the Gauss equations in the equinoctial elements

$$\begin{aligned}
\frac{\mathrm{d}P}{\mathrm{d}t} &= \frac{2P}{W}\sqrt{\frac{P}{\mu}}\,\mathcal{S} \\
\frac{\mathrm{d}e_x}{\mathrm{d}t} &= \sqrt{\frac{P}{\mu}}\left(-\sin l\,\mathcal{Q} + (\cos l + \frac{e_x + \cos l}{W})\,\mathcal{S} - \frac{D}{W}e_y\,\mathcal{Z}\right) \\
\frac{\mathrm{d}e_y}{\mathrm{d}t} &= \sqrt{\frac{P}{\mu}}\left(-\cos l\,\mathcal{Q} + (\sin l + \frac{e_y + \sin l}{W})\,\mathcal{S} + \frac{D}{W}e_x\,\mathcal{Z}\right) \\
\frac{\mathrm{d}h_x}{\mathrm{d}t} &= \sqrt{\frac{P}{\mu}}\frac{C}{2W}\cos l\,\mathcal{Z} \\
\frac{\mathrm{d}h_y}{\mathrm{d}t} &= \sqrt{\frac{P}{\mu}}\frac{C}{2W}\sin l\,\mathcal{Z} \\
\frac{\mathrm{d}l}{\mathrm{d}t} &= \sqrt{\frac{\mu}{P}}\left(\frac{W^2}{P}\right) + \sqrt{\frac{P}{\mu}}\left(\frac{D}{W}\,\mathcal{Z}\right)
\end{aligned} \tag{7.8}$$

where C, D and W are given by 7.3.

7.4 Gravitational perturbations

In this section we present the gravitational potential of the Earth and the perturbation of the Moon on the system {Earth, satellite} which are not the only but interesting to take into account. We refer the reader to [98] for a classification of perturbations on an artificial satellite. The reference plane is taken as the equatorial plane of the Earth and the frame is assumed inertial, centered at the center of mass of the Earth. We present expression of the Earth gravitational potential and the perturbing gravitational potential of the Moon in terms of the orbital elements.

7.4.1 Gravitational potential of the Moon

We consider the lunar effect of the satellite as a perturbation of the two-body problem {satellite, Earth }. In this section, we compute the perturbing potential of the Moon and we follow the approach presented in [103] where they study the Moon motion around the Earth under the Sun perturbation. However, we consider the equatorial plane of the Earth as the plane of reference and we give computations of the potential at any orders without any assumptions on the inclination of the Moon or the satellite with the use of symbolic computations.
It is well known that the three body problem doesn't have analytical solutions. Given the perturbing gravitational potential of the Moon, the effect of the Moon on the satellite is modeled by the Lagrange equations.

The perturbing lunar gravitational potential is expressed as

$$R(q,q') = Gm_M\left(\frac{1}{|q-q'|} - \frac{q\cdot q'}{r'^3}\right) \tag{7.9}$$

where m_M is the mass of the moon and G is the gravitational constant . q (resp. q') is the position vector of the satellite (resp. the Moon) and $|q|$ (resp. $|q'|$) is denoted by r (resp. r').
The exact expression of the potential given in (7.9) is used for numerical computations. For an analytic study, it is interesting to develop R as a series of trigonometric functions expressed in terms of the mean anomalies M, M' respectively of the satellite and of the Moon.
We have,

$$R(q,q') = Gm_M\left(\frac{1}{r'\sqrt{1+\left(\frac{r}{r'}\right)^2 - 2\frac{r}{r'}\cos(\Psi)}} - \frac{r}{r'^2}\cos(\Psi)\right)$$

where Ψ is the angle between the two vectors q and q'.
Assume $r \ll r'$ (so $a \ll a'$), we develop the previous expression using Legendre polynomials P_k and the potential becomes

$$R(q,q') = \frac{Gm_M}{r'}\left(1+\sum_{k=2}^{\infty}\left(\frac{r}{r'}\right)^k P_k(\cos(\Psi))\right). \tag{7.10}$$

The first term $\frac{Gm_M}{r'}$ in R is removed since it doesn't depend on the orbital elements of the satellite and we write

$$R(q,q') = \rho\frac{G(m_T+m_M)'}{a'}\sum_{k=2}^{\infty}\left(\frac{a}{a'}\right)^k\left(\frac{r}{a}\right)^k\left(\frac{a'}{r'}\right)^{k+1}P_k(\cos(\Psi)) \tag{7.11}$$

where m_T is the mass of the Earth in $\rho = m_M/(m_T+m_M)$.

Development of the terms $\frac{r}{a}$ and $\frac{a'}{r'}$. From Vinti [123], the eccentric anomaly E is expressed in terms of the eccentricity e and the mean anomaly M as

$$E = M+\sum_{k=1}^{\infty}\frac{2}{k}J_k(ke)\sin(kM), \quad \cos(E) = -\frac{e}{2}+\sum_{k=1}^{\infty}\frac{2}{k^2}\frac{\mathrm{d}}{\mathrm{d}e}[J_k(ke)]\cos(kM) \tag{7.12}$$

where $J_m(.)$, $m\in\mathbb{Z}$ are the Bessel functions of the first kind defined as

$$J_m(z) = \frac{1}{\pi}\int_0^{\pi}\cos(m\theta - z\sin(\theta))\mathrm{d}\theta,\ z\in\mathbb{C}.$$

From the relations,

$$\frac{a}{r} = \frac{1}{n}\dot{E}, \quad \frac{r}{a} = 1-e\cos(E),$$

we have the following expansions,

$$\frac{a'}{r'} = 1 + 2\sum_{k=1}^{\infty} J_k(ke')\cos(kM'),$$
$$\frac{r}{a} = 1 + \frac{e^2}{2} - \sum_{k=1}^{\infty} \frac{2e}{k^2}\frac{\mathrm{d}}{\mathrm{d}e}[J_k(ke)]\cos(kM).$$

Development of the term $\cos(\Psi)$**.** We express the cosinus of the angle Ψ in terms of the orbital elements of the satellite and the Moon with respect to the equatorial plane. The geometry is shown in Fig.7.2. Denoting v and v' the true anomaly of the satellite and the Moon respectively, we have

$$q' = r' \begin{pmatrix} \cos(\varpi' + v') \\ \sin(\varpi' + v')\cos(i') \\ \sin(\varpi' + v')\sin(i') \end{pmatrix}$$

and using basic concept of spherical trigonometry (see [60] for similar computations), we have

$$q = r \begin{pmatrix} (\cos(\varpi)\cos(\Delta\Omega) - \sin(\varpi)\sin(\Delta\Omega)\cos(i))\cos(v) \\ \qquad -(\sin(\varpi)\cos(\Delta\Omega) + \cos(\varpi)\sin(\Delta\Omega)\cos(i))\sin(v) \\ \cos(\varpi)\sin(\Delta\Omega) - \sin(\varpi)\cos(\Delta\Omega)\cos(i))\cos(v) \\ \qquad -(\sin(\varpi)\sin(\Delta\Omega) + \cos(\varpi)\cos(\Delta\Omega)\cos(i))\sin(v) \\ \sin(\varpi)\sin(i)\cos(v) + \cos(\varpi)\sin(i)\sin(v) \end{pmatrix}.$$

Then, using the relations

$$\cos(v) = \frac{\cos(E) - e}{1 - e\cos(E)}, \quad \sin(v) = \frac{\sqrt{1-e^2}\sin(E)}{1 - e\cos(E)}$$

and the equations (7.12), we obtain $\cos(\Psi) = (q \cdot q')/(rr')$ in terms of $(a, e, i, \varpi, \Omega, M, a', e', i', \varpi', \Omega', M')$.

Perturbing gravitational potential of the Moon. Using the previous paragraphs, the potential R is represented as a series of trigonometric functions

$$R(x, M, M') = \sum_{k,m\in\mathbb{Z}} C_{k,m}(x, x')\exp(I(kM + mM')), \tag{7.13}$$

where $x = (a, e, i, \varpi, \Omega)$ and $x' = (a', e', i', \varpi', \Omega')$. The latter elements are assumed constant.

Remark 7.1. *We could avoid to assume e and e' small and the potential R would be in terms of the eccentric anomaly E (or the true anomaly v). Applying a change of variables from $(a, e, i, \varpi, \Omega)$ to (P, e_x, e_y, h_x, h_y) in R, the dynamics are obtained from the Lagrange equations 7.5. However, the development (7.13) of R in terms of the mean anomaly is interesting to analyse the secular perturbations and the short period perturbations.*

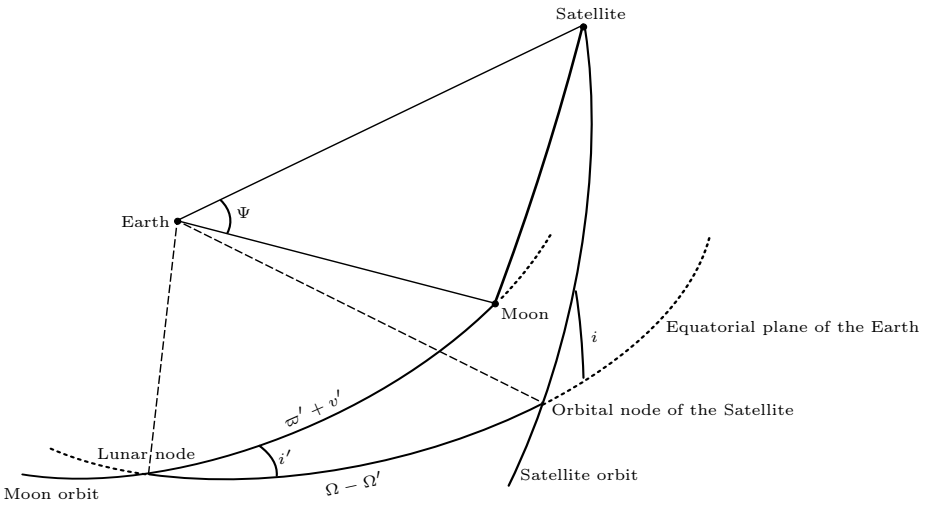

Figure 7.2: Relative position of each body

Using Maple, the computations can be done at any orders. Computations at order 2 in (7.10) with respect to $\frac{r}{r'}$ and at order 2 in (7.12) with respect to e, e' leads to the following expression to

$$\begin{aligned}
R(x,M,M') &= \rho {n'}^2 a^2/8(2+24\sin(i/2)\sin(i'/2)\cos(\Omega'-\Omega)+3(e^2+{e'}^2)-12(\sin^2(i/2)\\
&\quad+\sin^2(i'/2))+15e^2\cos(-2\Omega-2\varpi+2\varpi'+2M')+12\sin^2(i/2)\cos(2\varpi+2M)\\
&\quad+12\sin^2(i/2)\cos(2\varpi'+2M'-2\Omega)+12\sin^2(i'/2)\cos(2\varpi'+2M'-2\Omega')+6e'\cos(M')\\
&\quad+12\sin^2(i'/2)\cos(2\varpi+2\Omega+2M-2\varpi')+51{e'}^2\cos(2\varpi'+4M'-2\varpi-2\Omega-2M)\\
&\quad+21e'\cos(2\varpi'+3M'-2\varpi-2\Omega-2M)-3e'\cos(2\varpi'+M'-2\varpi-2\Omega-2M)\\
&\quad-12(\sin^2(i/2)+\sin^2(i'/2))\cos(2(\varpi'-\varpi-\Omega-M+M'))-12ee'\cos(M')\cos(M)\\
&\quad-15(e^2+{e'}^2)\cos(2(\varpi'-\varpi-\Omega-M+M'))+9{e'}^2\cos(2M')-e^2\cos(2M)-4e\cos(M)\\
&\quad-63ee'\cos(-2\varpi-2\Omega-M+2\varpi'+3M')-3ee'\cos(-2\varpi-2\Omega-3M+2\varpi'+M')\\
&\quad+9ee'\cos(-2\varpi-2\Omega-M+2\varpi'+M')+21ee'\cos(-2\varpi-2\Omega-3M+2\varpi'+3M')\\
&\quad+6\cos(-2\varpi-2\Omega-2M+2\varpi'+2M')-24\sin(i/2)\sin(i'/2)\cos(2\varpi+\Omega+2M-\Omega')\\
&\quad-24\sin(i/2)\sin(i'/2)\cos(2\varpi'+2M'-\Omega'-\Omega)+6e\cos(2\varpi'+2M'-2\varpi-2\Omega-3M)\\
&\quad+6e^2\cos(-2\varpi-2\Omega-4M+2\varpi'+2M')-18e\cos(-2\varpi-2\Omega-M+2\varpi'+2M')\\
&\quad+24\sin(i/2)\sin(i'/2)\cos(-2\varpi-\Omega-2M+2\varpi'+2M'-\Omega')+o(\alpha^2)+o(e^2)+o({e'}^2).
\end{aligned} \tag{7.14}$$

where n' is the mean motion of the Moon and satisfies ${n'}^2{a'}^3 = G(m_T + M')$. In [103], the author obtained this series where he assumes $i' = 0, \Omega' = 0, e' = 0$ and $\sin(i) \simeq i$. Besides, in his case, he has $\rho = 1$. Making these simplifications, the resulting expression of R is the same than in [103].
This development is useful to see the double averaged of the potential with respect to M and M'.

Definition 7.2. *The double averaged potential is defined by*

$$\bar{\bar{R}} = \frac{1}{(2\pi)^2}\int_0^{2\pi} R(x,M,M')\mathrm{d}M\mathrm{d}M'.$$

In our case, we obtain

$$\bar{\bar{R}} = \frac{\rho n'^2 a^2}{4}\,(1+12\sin(i/2)\sin(i'/2)\cos(\Omega'-\Omega) + 3/2(e^2+e'^2) - 6(\sin^2(i/2)+\sin^2(i'/2)) \tag{7.15}$$

Further interesting studies consist in analyzing the preponderant terms in (7.14) and to add them to the double averaged potential (7.15) to see the effects of these terms (see [52] for an interesting study).

7.4.2 Gravitational potential of the Earth

The Earth is modeled as nonspherical body such that its polar axis is a symmetry axis. Therefore, from [123], it follows

$$R_E = \frac{\mu}{r}\sum_{k=2}^{\infty} J_n \left(\frac{R_e}{r}\right)^k P_n(\sin(\vartheta))$$

where ϑ is the geocentric latitude of the satellite, P_n is a Legendre polynomial, J_n is a coefficient for the zonal harmonic and R_e is the primary equatorial radius. According to

$$r = \frac{a(1-e^2)}{1+e\cos(v)}, \quad \sin\vartheta = \sin i \sin(\varpi + v)$$

we develop R with respect to the orbital elements $(a, e, i, \varpi, \Omega, v)$ and we get, up to order 3, in $1/r$

$$R_E = \frac{\mu R_e^2 J_2}{4a^3}\left(\frac{a}{r}\right)^3 \left((-1+3\cos^2 i) + 3(1+\cos^2 i)\cos(2\varpi+2v)\right) \tag{7.16}$$

and using the development of a/r in the above paragraph 7.4.1, up to order 2 in e, we can express in terms of the mean anomaly, (see [123])

$$\begin{aligned} R_E = \frac{\mu R_e^2 J_2}{a^3}\Bigg(&\Big(-\frac{1}{4}+\frac{3}{4}\cos^2 i\Big)\Big(1+\frac{3}{2}e^2+3e\cos M+\frac{9}{2}e^2\cos 2M\Big) \\ &+\frac{3}{4}\sin^2 i\Big(-\frac{e}{2}\cos(2\varpi+M)+(1-\frac{5e^2}{2})\cos(2\varpi+2M)+\frac{7}{2}e\cos(2\varpi+3M) \\ &+\frac{17}{2}e^2\cos(2\varpi+4M)\Big)\Bigg)+\mathcal{O}(e^3). \end{aligned} \tag{7.17}$$

Definition 7.3. *The averaged potential is defined by*

$$\bar{R}_E = \frac{1}{\tau}\int_0^\tau R_E \mathrm{d}t = \frac{1}{2\pi}\int_0^{2\pi} R_E(x, M)\mathrm{d}M.$$

where τ is the period of the unperturbed orbit and $x = (a, e, i, \varpi, \Omega)$ are the orbital elements of the satellite.

For the disturbing potential of the Earth computed in (7.17), we have

$$\bar{R}_E = \frac{\mu R_e^2 J_2}{a^3}\Big(-\frac{1}{4}+\frac{3}{4}\cos^2 i\Big)\Big(1+\frac{3}{2}e^2\Big)+\mathcal{O}(e^3). \tag{7.18}$$

Remark 7.4. *As for the disturbing potential of the Moon, we could simply express R in terms of the true anomaly and we don't make any development with respect to the eccentricity e. Indeed, from (7.16), we have*

$$R_E = R_s + R_c(v)$$

where R_s is the secular part (averaged potential) and R_c the periodic part written as

$$\begin{aligned} R_s &= \frac{\mu R_e^2 J_2}{a^3}\left(-\frac{1}{4}+\frac{3}{4}\cos^2(i)\right)(1-e^2)^{-3/2},\\ R_c(v) &= \frac{\mu R_e^2 J_2}{a^3}\left(\frac{a}{r}\right)^3\left[\left(-\frac{1}{4}+\frac{3}{4}\cos^2(i)\right)\left(1-\left(\frac{r}{a}\right)^3(1-e^2)^{-3/2}\right)\right.\\ &\qquad\left.+\frac{3\sin^2(i)}{4}\cos(2(v+\omega))\right]. \end{aligned}$$

7.4.3 Problem formulation of the minimal time control problem

Periodic and autonomous perturbations are taken into account and they stand for external forces on the system. Namely these forces arise from the gravitational potential of the Earth with high order terms (see section 7.4.2) and/or the Moon gravitational interaction seen as a perturbation of the two body problem (see section 7.4.1). Besides, a three-dimensional control is exerted on the satellite with a constrained amplitude.
The controlled dynamic is written as,

$$\begin{aligned} \dot{I} &= \varepsilon F_0(I,\varphi,\varepsilon)+\varepsilon\sum_{i=1}^{3}u_i F_i(I,\varphi,\varepsilon), \quad |u|=\sqrt{u_1^2+u_2^2+u_3^2}\le 1,\\ \dot{\varphi} &= \omega(I)+\varepsilon G_0(I,\varphi,\varepsilon)+\varepsilon\sum_{i=1}^{3}u_i G_i(I,\varphi,\varepsilon) \end{aligned} \tag{7.19}$$

where

- The final time t_f is not fixed.
- $(I,\varphi)\in\mathcal{X}\times S^1$ where $\mathcal{X}$ is the manifold of elliptic keplerian orbits of dimension n (collisions are not taken into account , see section 7.2).
- F_0, G_0 are the drifts representing the uncontrolled dynamic. They model the gravitational forces of the Earth and/or the gravitational interaction of the Moon seen as a perturbation (see section 7.4).

- The case $\varepsilon = 0$ corresponds to the keplerian dynamic. This dynamic is perturbed by the action of the control u and the action of perturbing forces represented by F_0, G_0. The control engine has limited thrust which is modeled by a small parameter $\varepsilon_1 > 0$. Likewise, from the perturbations described in section 7.4, a small parameter arises from formula (7.17), namely $\varepsilon_2 = (a(0)/a')^2$ where a' the semi-major axis of the Moon's orbit and from formula (7.14), namely $\varepsilon_3 = J_2 R_e^2/a(0)^2$. Then, the small parameter ε in (7.19) may be taken as $\varepsilon = \max(\varepsilon_1, \varepsilon_2, \varepsilon_3)$.

- F_i, G_i $i = 1 \dots 3$ are the controlled vector fields decomposed in the local orbital frame (see section 7.3).

- $u_i,\ i = 1 \dots 3$ are the controls. The admissible controls are bounded mappings of $[0, t_f]$.

The initial and final phases are free and we fixed $I(0) = I_0$ and $I(t_f) = I_f$.

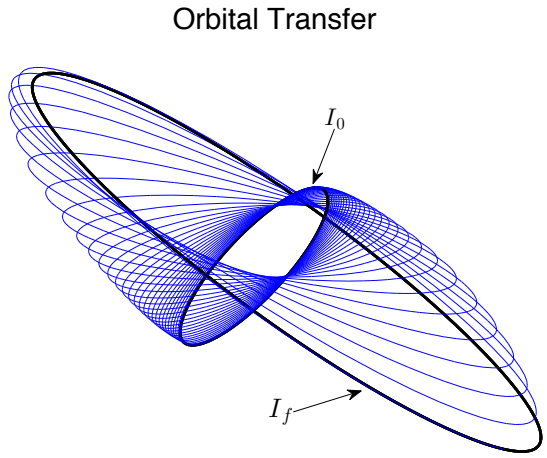

Figure 7.3: Orbital transfer between two elliptic orbits.

Remark 7.5. *The pulsation ω may depend of the fast angular variable φ. This is the case if φ is not the mean anomaly but for instance the true longitude. This point makes easier to write proofs and won't change our results (see section 8.2.3).*

7.5 Averaging principle in perturbation theory

We consider the minimal time control problem defined by the controlled dynamic and boundary conditions given in (7.19) and we are interested in solving numerically this optimal control problem by using indirect methods implemented in the `HamPath` software [55] (and see chapter 4) . Due to the fast oscillating nature of the system, the boundary value problem is not well-conditioned. It turns out that it is very difficult in practice to find a numerical zero of the shooting function based on

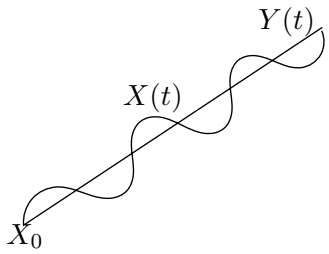

Figure 7.4: Averaging principle. The oscillations of the perturbed trajectories $X(.)$ are superimposed to the drift of the averaged trajectory $Y(.)$.

a Newton-type algorithm.
To overcome this difficulty, one may investigate several alternative methods

- use direct methods, such as the `Bocop` software [26], to have an initial guess for the Newton-type algorithm,
- use of homotopy methods [44],
- define an averaged system so that the induced problem is numerically well-conditioned and close to the non averaged problem.

We present the latter solution by recalling basic ideas about averaging principle in perturbation theory. We emphasize the idea of dividing motion into slow drift and rapid oscillations.

We start from an unperturbed integrable system whose equations of motion are

$$\begin{aligned} &\dot{X} = 0, \quad X \in U \subset \mathbb{R}^n, \\ &\dot{\psi} = \omega(X), \quad \psi \in \mathbb{T}^m. \end{aligned}$$

A small periodic perturbation of the system leads to the perturbed system

$$\begin{aligned} &\dot{X} = \varepsilon f(X, \psi, \varepsilon), \\ &\dot{\psi} = \omega(X) + \varepsilon g(X, \psi, \varepsilon) \end{aligned} \tag{7.20}$$

where f and g are 2π-periodic with respect to ψ and $\varepsilon > 0$ is small. The averaging principle consists in discarding the oscillating terms which cause only small oscillations and which are superimposed on the drift described by the averaged system.

Definition 7.6. *The average system is defined by*

$$\dot{Y} = \varepsilon \bar{f}(Y), \quad \bar{f}(Y) = 1/(2\pi)^m \int_{\mathbb{T}^m} f(Y, \psi, \varepsilon = 0) \mathrm{d}\psi. \tag{7.21}$$

The case of one frequency. When $\psi \in \mathbb{T}^1$, we have the following theorem [112].

Theorem 7.7. *The difference between the slow motion $X(t)$ in the perturbed system (7.20) and $Y(t)$ in the averaged system (7.21) remains of order 1 in ε over time $1/\varepsilon$:*

$$|X(t) - Y(t)| < c_1\varepsilon \quad \text{if } X(0) = Y(0),\ 0 \le t \le 1/\varepsilon$$

where the constant c_1 doesn't depend on ε.

We give slightly different versions of the above theorem, which we will use in the Chapter 8.

Theorem 7.8 deals with the case where the initial values of the slow variables of a family of non averaged solutions converge.

Theorem 7.8. *Assume $|\omega(X)| > R > 0$ and let $\tau > 0$ fixed.*
If

- *$(X_\varepsilon(.), \psi_\varepsilon(.))_\varepsilon$ is a family of solutions of the non averaged dynamic (7.20) on $[0, \frac{\tau}{\varepsilon}]$,*
- *$X_\varepsilon(0) \underset{\varepsilon\to 0}{\longrightarrow} X_0^0$.*

Then $t \mapsto X_\varepsilon(t/\varepsilon)$ uniformly converges to $t \mapsto Y(t)$ on $[0, \tau]$ such that

- *$Y(.)$ is a solution of the averaged system (7.21),*
- *$Y(0) = X_0^0$.*

Theorem 7.9 deals with the uniformity of the estimate with respect to the initial conditions.

Theorem 7.9 (see Theorem 2.8.9 of [112])**.** *Fix $\varepsilon, \tau_f > 0$ and let $\tau \in [0, \tau_f] \mapsto X(\tau, X_0)$ be the solution at time τ of (7.20) reparameterized in the slow time $\tau = \varepsilon t$ which was at X_0 at $\tau = 0$. Let K be a compact of $\mathbb{R}^n$ and let $L \ge 0$ be given arbitrarily. For each $X_0 \in K$, take $\widetilde{L} \le L$ such that $X(\tau, X_0)$ belongs to K for $0 \le \tau \le \widetilde{L}$.*
Then $\tau \mapsto X(\tau, X_0)$ uniformly converges on $[0, \tau_f]$ to $\tau \mapsto Y(\tau, X_0)$ such that $Y(., X_0)$ is solution on $[0, \widetilde{L}]$ of the averaged system (8.38) reparameterized in the slow time $\tau = \varepsilon t$ and with $Y(0) = X_0$.

The case of several frequencies. In the average of the vector field f with respect to the angle ψ, see (7.21), the unperturbed trajectories $\psi(.)$ should fill the whole torus for the averaged dynamics to be a reasonable approximation of the true one. It is well known [15] that this is related to the concept of resonance.

Definition 7.10. *The frequencies $\omega = (\omega_1, \ldots, \omega_m) \in \mathbb{R}^m$ are rationally commensurable if there exists $\kappa \in \mathbb{N}^m$ such that $\kappa \cdot \omega = 0$. This is the resonant case.*
The non-resonant case corresponds to the situation where we can find some positive constants c, d such that $|\kappa \cdot \omega| > 1/(c|\kappa|^d)$ for all $\kappa \in \mathbb{N}^m \setminus \{0\}$.

In our case, we have a three frequency system $(\omega_S, \omega_E, \omega_M)$ where ω_S is the frequency of the satellite, ω_E the one of the gravitational perturbation of the Earth (see section 7.4.2) and ω_M resulting from the perturbation of the Moon (see section 7.4.1). Namely, resonances may appear in an orbital transfer from a low orbit to a high orbit where the we encounter resonances from $2:1$ to $1:1$ for $\omega_S : \omega_E$. However, although it is an interesting problem to study resonances especially with the expressions of the disturbing potentials (7.14) and (7.18), our work deals with averaging in the non-resonant case.

A convergence result for the several frequency case [15]. In the case of several frequencies, we also have that, outside the resonances, the difference between the slow motion $X(t)$ in the perturbed system (7.20) and $Y(t)$ in the averaged system (7.21) remains of order 1 in ε over time $1/\varepsilon$.

Double averaging case [15]

Theorem 7.11. *Consider a two-frequency perturbed system*

$$\dot{X} = \varepsilon f(X, \psi, \varepsilon),$$
$$\dot{\psi}_1 = \omega_1(X) + \varepsilon g_1(X, \psi, \varepsilon), \quad \dot{\psi}_2 = \omega_2(X) + \varepsilon g_2(X, \psi, \varepsilon).$$

where $X \in U \subset \mathbb{R}^n$, $\psi = (\psi_1, \psi_2) \in \mathbb{T}^2$.
Under the condition

$$\left(\omega_1 \frac{\partial \omega_2}{\partial X} - \omega_2 \frac{\partial \omega_1}{\partial X}\right) f > c_2 > 0,$$

we have the approximation

$$|X(t) - Y(t)| < c_3\sqrt{\varepsilon} \quad \text{if } X(0) = Y(0),\ 0 \le t \le 1/\varepsilon.$$

An important remark is that these results hold for Cauchy problem, i.e. for dynamical systems with prescribed initial condition condition at one time. The orbital transfer problem (7.19), posed as an optimal control problem leads to a boundary value problem with mixed initial and final conditions on the slow variable. In Chapter 8, we will describe averaging methods inspired by these results for a two points boundary value problem.

Chapter 8

Averaging and Pontryagin maximum principle

In this chapter we present our approach to solve the orbital transfer problem. First, the Pontryagin maximum principle gives necessary conditions for a solution to be optimal. These solutions have to satisfy an Hamiltonian dynamic and transversality conditions. Therefore we obtain a boundary value problem on which we apply an averaging principle. The Hamiltonian system obtained is written in the standard form for the averaging method presented in Section 7.5. Finally we add the boundary value conditions and we study convergence theorems between the solutions of the non averaged boundary value problem and the averaged one.

Contents

9.1 Description of the simulated problems 133
9.1.1 Initialization of the non averaged shooting algorithm 134
9.1.2 Commented numerical results 134
9.2 Numerical conjecture 138
9.2.1 Simple averaging 138
9.2.2 Double averaging 141

8.1 Non averaged extremal system

We start by writing the Pontryagin maximum principle for the optimal control problem described by (7.19).

Theorem 8.1. *Time-minimal trajectories solution of the optimal control problem* (7.19) *are projections of solutions of the Hamiltonian system defined by*

$$H(I, p_I, \varphi, p_\varphi, \varepsilon) := p^0 + p_\varphi \omega(I) + \varepsilon K(I, p_I, \varphi, p_\varphi, \varepsilon), \quad p^0 \leq 0 \tag{8.1}$$

where

$$\begin{aligned} K &:= H_0 + \sqrt{\sum_{i=1}^{3} H_i^2}, \\ H_i(I, p_I, \varphi, p_\varphi, \varepsilon) &:= p_I F_i(I, \varphi, \varepsilon) + p_\varphi G_i(I, \varphi, \varepsilon), \quad i = 0, ..., 3. \end{aligned} \tag{8.2}$$

The extremal system is

$$\begin{aligned} \dot{I} &= \varepsilon \frac{\partial K}{\partial p_I}, \quad \dot{p}_I = -p_\varphi \omega' - \varepsilon \frac{\partial K}{\partial I}, \\ \dot{\varphi} &= \omega + \varepsilon \frac{\partial K}{\partial p_\varphi}, \quad \dot{p}_\varphi = -\varepsilon \frac{\partial K}{\partial \varphi}. \end{aligned} \tag{8.3}$$

with the boundary conditions

$$I(0) = I_0,\ I(t_f) = I_f,\ p_\varphi(0) = 0,\ p_\varphi(t_f) = 0,\ H = 0. \tag{8.4}$$

Remark 8.2. *The existence of singular extremals in the time-minimal case is covered in [32]. In our case, we have a 3D control and there are no singular extremals (they do exist singular extremals in the single-input time-minimal case) and we focus on the normal case, that it $p^0 < 0$.*

Definition 8.3. *An extremal is a quadruplet $(I(.), \varphi(.), p_I(.), p_\varphi(.))$ solution of (8.3). If moreover the transversality conditions (8.4) are satisfied, the extremal is said a BC-extremal.*

Notation 8.4. *A non averaged trajectory is denoted by (I, φ) with adjoint variables (p_I, p_φ). An averaged trajectory is denoted by J with adjoint variable p_J.*

Except for the Section 8.2.4 where we generalize the construction to several frequencies, we assume now that there is a single fast variable $\varphi \in S^1$.

Regularity of the Hamiltonian. From its expression (8.1)-(8.2), it is clear that H is as smooth as the maps ω, H_0,H_1,H_2,H_3 i.e. as smooth as the vector fields defining the control except at points where $H_1 = H_2 = H_3 = 0$.
Let us define, for $\varepsilon \geq 0$, the set

$$\begin{aligned} \Sigma_\varepsilon := \{(I, p_I, \varphi, p_\varphi) \in T\mathcal{X} \times S^1 \times \mathbb{R} \times [0,1] \\ | H_i(I, p_I, \varphi, p_\varphi, \varepsilon) = 0 \text{ for } i = 1 \dots 3.\} \end{aligned} \tag{8.5}$$

Proposition 8.5. *For any constant p_0, H defined by (8.1)-(8.2) is smooth outside the set $\{(I, p_I, \varphi, p_\varphi, \varepsilon) \mid (I, p_I, \varphi, p_\varphi) \in \Sigma_\varepsilon\}$.*

In the sequel, we will also need its projection onto the (I, p_I, p_φ) variables :

$$\pi : TX \times S^1 \times \mathbb{R} \to TX \times \mathbb{R}, \quad (I, p_I, \varphi, p_\varphi) \mapsto (I, p_I, p_\varphi) \tag{8.6}$$

and the set

$$\pi(\Sigma_\varepsilon) := \{(I, p_I, p_\varphi) \mid \exists \varphi \in S^1, (I, p_I, \varphi, p_\varphi) \in \Sigma_\varepsilon\}. \tag{8.7}$$

Note that, since the H_i's are well defined for $\varepsilon = 0$, the set Σ_0 and $\pi(\Sigma_0)$ are well defined, one has the following property.

Proposition 8.6. *For any compact K and any neighborhood W of the set $K \cap \pi(\Sigma_0)$, one has, for ε small enough,*

$$K \cap \pi(\Sigma_\varepsilon) \subset K \cap W$$

or in other words, any (I, p_I, p_φ) which is in K but not in W satisfies $(I, p_I, \varphi, p_\varphi) \notin \Sigma_\varepsilon$ for all $\varphi \in S^1$.

8.2 Averaging extremals

8.2.1 Preparation for averaging

In order to apply averaging to the differential equation (8.3), one prerequisite is to identify "fast" and "slow" variables. Among the state variables (I, φ), it is clear that I is slow, at least when the control and perturbations are "small", and that φ is a fast variable with respect to which we have to average. It is harder to decide what part is "slow" in the adjoint variables (p_I, p_φ). It would be convenient that all the adjoint vector is slow, but for instance, although p_φ is zero at final and initial time, there is no reason that the term $p_\phi\, \omega'(I)$ be small. In [120], one assumes $p_\varphi(t) = 0$ for all t without a clear justification, in a sense we will give a justification about why this is legitimate as a limit. In [63], this problem is not encountered because φ is taken as new time and no adjoint component is formally associated to it. We are able to make a clean justification of averaging in the following way: according to (8.4), the equation (8.3) can be restricted to the submanifold $\{H = 0\}$, and it is only necessary that the adjoint vector is slow *on this level set of* H; this is achieved by choosing p_0 as follows:

$$p^0 = -\varepsilon.$$

Note that

- this is somehow consistent since it is shown in [25] that if $t_f(\varepsilon)$ is the final time of a family of extremals then $\varepsilon t_f(\varepsilon)$ is bounded. Therefore, instead of minimizing the final time t_f, a natural reformulation would be to minimize, for each given ε, the cost εt_f,
- in any case, one is free to fix p_0 to any negative value, this does not change the solutions of (8.3).

We are going to show that, with this choice, the only fast variable of the dynamics restricted to $\{H = 0\}$ is φ.

Normalization on the energy level $\{H = 0\}$. Since we have fixed $p_0 = -\varepsilon < 0$, the Hamiltonian H defined by (8.1) is given by

$$H(I, p_I, \varphi, p_\varphi, \varepsilon) = -\varepsilon + p_\varphi \omega(I) + \varepsilon K(I, p_I, \varphi, p_\varphi, \varepsilon)$$

Proposition 8.7. *Let $X \subset \mathcal{X}$ be a open set with compact topological closure on which $\omega(I) > \omega_0$. Then there exists $\varepsilon_0 > 0$ and a unique continuous map $h : TX \times S^1 \times [0, \varepsilon_0] \to \mathbb{R}$ such that*

$$H(I, p_I, \varphi, p_\varphi, \varepsilon) = 0 \Longleftrightarrow p_\varphi = -\varepsilon h(I, p_I, \varphi, \varepsilon)$$

for any $(I, p_I, \varphi, p_\varphi, \varepsilon) \in T^*X \times S^1 \times \mathbb{R} \times [0, \varepsilon_0]$.
This map is Lipschitz continuous, and it is smooth away from the subset $\{(I, p_I, \varphi, \varepsilon) \mid (I, p_I, \varphi, -\varepsilon h(I, p_I, \varphi, \varepsilon)) \in \Sigma_\varepsilon\}$.

Since $\frac{\partial H}{\partial p_\varphi}(I, p_I, \varphi, p_\varphi, \varepsilon = 0) = -\omega(I) \neq 0$, this is a consequence of the inverse function theorem *locally around* $\varepsilon = 0$ on the zone where H is differentiable, but we give a self contained proof that has the advantage that it controls the domain of definition of h and works without excluding the set Σ_ε where H fails to be differentiable, and that it is *global on a compact set*.

Proof. First notice that, for all $(I, p_I, \varphi, \varepsilon) \in TX \times S^1 \times \mathbb{R} \times [0, 1]$, one has

$$|K(I, p_I, \varphi, p_\varphi^1, \varepsilon) - K(I, p_I, \varphi, p_\varphi^2, \varepsilon)| \leq k|p_\varphi^1 - p_\varphi^2| \tag{8.8}$$

with $k = \max_{i\in\{0,1,2,3\}} \sup_{(I,\varphi,\varepsilon)\in X\times S^1\times[0,1]} \|H_i(I, \varphi, \varepsilon)\|$. Indeed $\sup_{(I,\varphi,\varepsilon)\in X\times S^1\times[0,1]} H_i(I, \varphi, \varepsilon)$ is a Lipschitz constant of $p_\varphi \mapsto H_i(I, p_I, \varphi, p_\varphi, \varepsilon)$ for any $(I, p_I, \varphi, \varepsilon)$ in $TX \times S^1 \times [0, 1]$ and $(H_0, H_1, H_2, H_3) \mapsto H_0 + \sqrt{H_1^2 + H_2^2 + H_3^2}$ is Lipschitz-continuous with constant 1.
Besides, from the Proposition 8.5, H is continuous, so is h.
Therefore for any $(I, p_I, \varphi, \varepsilon)$ in $TX \times S^1 \times [0, 1]$ the map

$$\varrho_\varphi \mapsto \frac{1 - K(I, p_I, \varphi, \varepsilon\varrho_\varphi, \varepsilon)}{\omega(I)} \tag{8.9}$$

is Lipschitz continuous with constant $k\varepsilon/\omega_0$.
This in turn implies that for $\varepsilon \in [0, \varepsilon_0]$, the transformation $C^0(TX\times S^1\times[0, \varepsilon_0], \mathbb{R}) \to C^0(TX \times S^1 \times [0, \varepsilon_0], \mathbb{R})$ that maps

$$(I, p_I, \varphi, \varepsilon) \mapsto h(I, p_I, \varphi, \varepsilon)$$

to

$$(I, p_I, \varphi, \varepsilon) \mapsto \frac{K(I, p_I, \varphi, -\varepsilon h(I, p_I, \varphi, \varepsilon), \varepsilon) - 1}{\omega(I)}$$

is Lipschitz continuous with constant $\varepsilon_0 k/\omega_0$. Taking $\varepsilon_0 < \omega_0/k$ this map is a contraction, hence it has a unique fixed point h, and $p_\varphi = -\varepsilon h(I, p_I, \varphi, \varepsilon)$ is the unique solution of $H(I, p_I, \varphi, p_\varphi, \varepsilon) = 0$. □

Finally, from Proposition 8.7, the restriction of the system (8.3) to the submanifold $\{H = 0\}$ may be described by an ordinary differential equation in the variables (I, p_I, φ) where $\dot{p}_I$ is given by

$$\dot{p}_I = -\varepsilon \left(-h(I, p_I, \varphi, \varepsilon)\omega'(I) + \frac{\partial K}{\partial I}(I, p_I, \varphi, -\varepsilon h(I, p_I, \varphi, \varepsilon), \varepsilon) \right) = \mathcal{O}(\varepsilon). \tag{8.10}$$

Hence, in these variables, p_I and I are slow and φ is fast. The solutions of the system (8.3) are then obtained by lifting p_φ as $p_\varphi = \varepsilon h(I, p_I, \varphi, \varepsilon)$.

8.2.2 Averaged dynamic for a single frequency

We present two equivalent averaged systems, the first one is defined by taking the non averaged system parameterized by the time t while the second one is parameterized by the angular variable φ.
For convenience, define the average of K and h by

$$\begin{aligned}
\bar{K}(J,p_J) &:= \frac{1}{2\pi}\int_0^{2\pi} K(J,p_J,\varphi,p_\varphi=0,\varepsilon=0)\,\mathrm{d}\varphi,\\
\bar{h}(J,p_J) &:= \frac{1}{2\pi}\int_0^{2\pi} h(J,p_J,\varphi,\varepsilon=0)\,\mathrm{d}\varphi\\
\bar{h}(J,p_J) &= \frac{\bar{K}(J,p_J)-1}{\omega(J)}
\end{aligned} \tag{8.11}$$

With respect to the time. After the reduction $p_\varphi = -\varepsilon h(I,p_I,\varphi,\varepsilon)$, the non averaged system takes the form

$$\begin{aligned}
\dot{I} &= \varepsilon\frac{\partial K}{\partial p_I}(I,p_I,\varphi,-\varepsilon h(I,p_I,\varphi,\varepsilon),\varepsilon),\\
\dot{p}_I &= -\varepsilon\left(-h(I,p_I,\varphi,\varepsilon)\omega'(I)+\frac{\partial K}{\partial I}(I,p_I,\varphi,-\varepsilon h(I,p_I,\varphi,\varepsilon),\varepsilon)\right),\\
\dot{\varphi} &= \omega(I)+\varepsilon\frac{\partial K}{\partial p_\varphi}(I,p_I,\varphi,-\varepsilon h(I,p_I,\varphi,\varepsilon),\varepsilon).
\end{aligned} \tag{8.12}$$

Applying the averaging method given in Section 7.5, we define an averaged system by the following averaged dynamic

$$\begin{aligned}
\dot{J} &= \varepsilon\frac{1}{2\pi}\int_0^{2\pi}\frac{\partial K}{\partial p_I}(J,p_J,\varphi,p_\varphi=0,\varepsilon=0)\mathrm{d}\varphi\\
&= \varepsilon\frac{\partial \bar{K}}{\partial p_J}(J,p_J)\\
\dot{p}_J &= -\varepsilon\frac{1}{2\pi}\int_0^{2\pi}\left(-h(J,p_J,\varphi,\varepsilon=0)\omega'(J)+\frac{\partial K}{\partial I}(J,p_J,\varphi,p_\varphi=0,\varepsilon=0)\right)\mathrm{d}\varphi\\
&= -\varepsilon\left(-\bar{h}(J,p_J)\omega'(J)+\frac{\partial \bar{K}}{\partial J}(J,p_J)\right)\\
&= -\varepsilon\left(-(\bar{K}(J,p_J)-1)\frac{\omega'(J)}{\omega(J)}+\frac{\partial \bar{K}}{\partial J}(J,p_J)\right)
\end{aligned} \tag{8.13}$$

where we used (8.11) in the last equality.

Proposition 8.8. *The averaged solutions $(J(.),p_J(.))$ satisfy Hamilton's equations with Hamiltonian $\bar{K}$ restricted to the level $\bar{K}=1$.*

$$\frac{\mathrm{d}J}{\mathrm{d}\tau} = \frac{\partial \bar{K}}{\partial p_J}(J,p_J),\quad \frac{\mathrm{d}p_J}{\mathrm{d}\tau} = -\frac{\partial \bar{K}}{\partial J}(J,p_J),\quad \bar{K}(J,p_J)=1 \tag{8.14}$$

where $\tau=\varepsilon t$.

Singular set of the averaged Hamiltonian. According to [15, 112], it is possible to define an averaged system under some regularity assumptions of the vectors fields (typically Lipschitz continuous [112]).

We introduce

$$\widetilde{\Sigma}_\varepsilon = \Sigma_\varepsilon \cap \{(I, p_I, \varphi, p_\varphi) \in T\mathcal{X} \times S^1 \times \mathbb{R} \mid p_\varphi = -\varepsilon h(I, p_I, \varphi, \varepsilon)\} \tag{8.15}$$

where π is the projection (8.6) and Σ_ε is defined in (8.5).

Proposition 8.9. *The Hamiltonians $\bar{K}$ and $\bar{h}$ are smooth on $\Omega := \complement\pi(\widetilde{\Sigma}_0)$ where $\complement(.)$ denotes the complement of a set and $\widetilde{\Sigma}_0$ is given in (8.15).*

In the coplanar case, that is $n = 3$ and $m = 2$, $\widetilde{\Sigma}_0$ is of codimension 2 in $T^*\mathcal{X} \times S^1$. The projection doesn't change the dimension if one of the quantity $p_I \frac{\partial F_i}{\partial \varphi}(I, \varphi, \varepsilon = 0)$, $i = 1, 2, 3$ is not zero. Therefore, $\pi(\widetilde{\Sigma}_0)$ is of codimension 1 in $T^*\mathcal{X}$. Now fixing I and φ, (I, p_I, φ) is on the singular set $\pi(\widetilde{\Sigma}_0)$ if and only if p_I is a straight line in $T^*_I\mathcal{X} \simeq \mathbb{R}^3$. When φ varies, it describes a cone which is impossible to avoid if for instance we have a starting point inside the cone and an end point outside. In that case, the assumption of the non averaged extremals is forbidden. In the full 3-D case, that is $n = 5$ and $m = 3$, when I is fixed, $\widetilde{\Sigma}_\varepsilon$ is a union of planes in $T^*_I\mathcal{X} \simeq \mathbb{R}^5$ and this union have dimension 3. Therefore in this case, given a curve crossing this singular set, a generic perturbation of such a curve would lead to a curve which doesn't cross the singular set.

Remark 8.10. *S. Geffroy defines in her thesis [63] an averaged system by parameterizing the non averaged system by the fast variable φ. Here, we average directly the equations expressed in the time variable t and the fact that this averaged system is Hamiltonian is an important point to see the averaged system as the dynamic coming from an optimal control problem. Moreover in the case of several frequencies, it seems preferable not to parameterize the non averaged system with respect to an angular variable but with respect to the time t.*

With respect to the angle. Differentiating $H(I, p_I, \varphi, -\varepsilon h(I, p_I, \varphi, \varepsilon), \varepsilon) = 0$ with respect to I and p_I yields

$$\begin{aligned}
\dot{I} &= \varepsilon \frac{\partial H}{\partial p_\varphi}(I, p_I, \varphi, -\varepsilon h(I, p_I, \varphi, \varepsilon), \varepsilon) \frac{\partial h}{\partial p_I}(I, p_I, \varphi, \varepsilon), \\
\dot{p}_I &= -\varepsilon \frac{\partial H}{\partial p_\varphi}(I, p_I, \varphi, -\varepsilon h(I, p_I, \varphi, \varepsilon), \varepsilon) \frac{\partial h}{\partial I}(I, p_I, \varphi, \varepsilon) \\
\dot{\varphi} &= \frac{\partial H}{\partial p_\varphi}(I, p_I, \varphi, -\varepsilon h(I, p_I, \varphi, \varepsilon), \varepsilon)
\end{aligned} \tag{8.16}$$

and parameterizing with respect to $s := \varepsilon(\varphi - \varphi(0))$, we get the following proposition.

Proposition 8.11. *The non averaged extremal system is reduced to an non-autonomous Hamiltonian system of the form*

$$\frac{\mathrm{d}I}{\mathrm{d}s} = \frac{\partial h}{\partial p_I}(I, p_I, \frac{s}{\varepsilon} + \varphi(0), \varepsilon), \quad \frac{\mathrm{d}p_I}{\mathrm{d}s} = -\frac{\partial h}{\partial I}(I, p_I, \frac{s}{\varepsilon} + \varphi(0), \varepsilon) \tag{8.17}$$

where $s := \varepsilon(\varphi - \varphi(0))$ *is the normalized time.*

We deduce the following definition

Definition 8.12. *The averaged system is defined by the averaged of the Hamiltonian* h

$$\frac{\mathrm{d}J}{\mathrm{d}s} = \frac{\partial \bar{h}}{\partial p_I}(J, p_J), \quad \frac{\mathrm{d}p_J}{\mathrm{d}s} = -\frac{\partial \bar{h}}{\partial I}(J, p_J) \tag{8.18}$$

with

$$\begin{aligned}\bar{h}(J, p_J) &:= \frac{1}{2\pi}\int_0^{2\pi} h(J, p_J, \varphi, \varepsilon = 0)\mathrm{d}\varphi \\ &= \frac{1}{2\pi}\int_0^{2\pi} \frac{K-1}{\omega}(J, p_J, \varphi, p_\varphi = 0, \varepsilon = 0)\mathrm{d}\varphi\end{aligned}$$

8.2.3 Pulsation depending upon the fast angular variable

The time-derivative of the angle φ in the non-averaged dynamic (8.3) involves a pulsation ω depending upon I only. This was chosen to make the proofs simpler. However, in the Gauss equations given in Subsection 7.3.2, this is the case only if one uses the mean anomaly M (see Section 7.2) as the angle, or $L = \varpi + \Omega + M$. If, instead, either the true anomaly v, the true longitude $l = \varpi + \Omega + v$ or the eccentric anomaly E is used as the angle φ, then the pulsation ω does depend on the angle. In the applications, using M requires to invert the Kepler equation $E - e\sin(E) = M$ (where e is the eccentricity of the orbit) to express the dynamics. We show here that such dependence yields a slightly different expression of the average dynamics but does not change the principles since a mere change of variables transforms the system into one where the pulsation depends on the slow variable only and all the proofs go through.

Let $\varphi = \chi(I, l)$ be the change of variables which transforms the system

$$\begin{aligned}\dot{I} &= \varepsilon\left(\hat{F}_0(I, l, \varepsilon) + \sum_{i=1}^{3} u_k \hat{F}_k(I, l, \varepsilon)\right), \\ \dot{l} &= \Omega(I, l) + \varepsilon\left(\hat{G}_0(I, l, \varepsilon) + \sum_{i=1}^{3} u_k \hat{G}_k(I, l, \varepsilon)\right)\end{aligned} \tag{8.19}$$

into the system

$$\begin{aligned}\dot{I} &= \varepsilon\left(F_0(I, \varphi, \varepsilon) + \sum_{i=1}^{3} u_k F_k(I, \varphi, \varepsilon)\right), \\ \dot{\varphi} &= \omega(I) + \varepsilon\left(G_0(I, \varphi, \varepsilon) + \sum_{i=1}^{3} u_k G_k(I, \varphi, \varepsilon)\right)\end{aligned} \tag{8.20}$$

where

$$\begin{aligned}&F_i(I, \chi(I, l), \varepsilon) = \hat{F}_i(I, l, \varepsilon) \quad i = 0, \ldots 3, \\ &G_i(I, \chi(I, l), \varepsilon) = \frac{\partial \chi}{\partial I}(I, l)\hat{G}_i(I, l, \varepsilon) + \frac{\partial \chi}{\partial l}(I, l)\hat{G}_i(I, l, \varepsilon), \quad i = 0, \ldots 3.\end{aligned}$$

It can be shown that

- $\omega(I) = \int_0^{2\pi} \frac{\mathrm{d}l}{\Omega(I,l)}$,
- $\chi(I,l) = \int_0^l \frac{\omega(I)}{\Omega(I,\lambda)}\mathrm{d}\lambda + R(I)$ where $R(I)$ is an arbitrary function of I that can be used so that $\int_0^{2\pi}(l-\chi(I,l))\frac{\mathrm{d}l}{\Omega(I,l)} = 0$.

In the case of the two body system, χ is the composition of

1. computing $v = l - \varpi - \Omega$,
2. computing E from v (namely via $\cos(E) = (\cos(v)+e)/(1+e\cos(v))$, $\sin(E) = \frac{\sqrt{1-e^2}\sin(v)}{1+e\cos(v)}$)),
3. $M = E - e\sin(E)$
4. $\varphi = \varpi + \Omega + M$

We consider the two time-minimal control problems (TC1) and (TC2) associated respectively with the controlled dynamics (8.19) and (8.20). Following the Sections (8.1)-(8.2), the non averaged extremal system for the problem (TC1) is defined by the Hamiltonian $\hat{H}(I,\hat{p}_I,l,p_l,\varepsilon) = p_l\Omega(I,l) + \varepsilon\hat{K}(I,\hat{p}_I,l,p_l,\varepsilon)$ where

$$\hat{K} := \hat{H}_0 + \sqrt{\hat{H}_1^2 + \hat{H}_2^2 + \hat{H}_3^2}, \quad \hat{H}_i = \hat{p}_I \cdot \hat{F}_i + p_l\hat{G}_i, \quad i = 0\dots 3.$$

Take the canonical transformation $(I,\hat{p}_I,l,p_l) \mapsto (I,p_I,\varphi,p_\varphi)$, we have $\hat{p}_I\mathrm{d}I + p_l\mathrm{d}l = p_I\mathrm{d}I + p_\varphi\mathrm{d}\varphi$. Besides, one has $\mathrm{d}\varphi = \frac{\partial\chi}{\partial I}\mathrm{d}I + \frac{\partial\chi}{\partial l}\mathrm{d}l$ and it leads to

$$\begin{aligned} p_I &= \hat{p}_I - \frac{p_l}{\frac{\partial\chi}{\partial l}(I,l)}\frac{\partial\chi}{\partial I}(I,l), \\ p_\varphi &= \frac{p_l}{\frac{\partial\chi}{\partial l}(I,l)}. \end{aligned} \tag{8.21}$$

(Note that if $p_\varphi = 0$ then $p_I = \hat{p}_I$.)
We have

$$\begin{aligned} H(I,\hat{p}_I,\chi(I,l) - p_l\Big/\frac{\partial\chi}{\partial l}(I,l),p_l\Big/\frac{\partial\chi}{\partial l}(I,l)) &= \hat{H}(I,\hat{p}_I,l,p_l), \\ K(I,\hat{p}_I,\chi(I,l) - p_l\Big/\frac{\partial\chi}{\partial l}(I,l),p_l\Big/\frac{\partial\chi}{\partial l}(I,l)) &= \hat{K}(I,\hat{p}_I,l,p_l) \end{aligned}$$

where H and K are given by (8.1) and (8.1).

Therefore, if $(J(.), \hat{p}_J(.))$ is a solution of the averaged system (8.18), then one has

$$\begin{aligned}
\frac{\mathrm{d}J}{\mathrm{d}t} &= \varepsilon \frac{1}{2\pi} \int_0^{2\pi} \frac{\partial K}{\partial p_I}(J, \hat{p}_J, \chi(J,l), p_\varphi = 0, \varepsilon = 0) \frac{\partial \chi}{\partial l}(J,l)\mathrm{d}l \\
&= \varepsilon \frac{1}{2\pi} \int_0^{2\pi} \frac{\partial \hat{K}}{\partial p_I}(J, l, \hat{p}_J, p_l = 0, \varepsilon = 0) \frac{\omega(J)}{\Omega(J,l)}\mathrm{d}l \\
\frac{\mathrm{d}\hat{p}_J}{\mathrm{d}t} &= -\varepsilon \frac{1}{2\pi} \int_0^{2\pi} \frac{\partial K}{\partial I}(J, \hat{p}_J, \chi(J,l), p_\varphi = 0, \varepsilon = 0) \frac{\partial \chi}{\partial l}(J,l)\mathrm{d}l \\
&= -\varepsilon \frac{1}{2\pi} \int_0^{2\pi} \frac{\partial \hat{K}}{\partial I}(J, l, \hat{p}_J, p_l = 0, \varepsilon = 0) \frac{\omega(J)}{\Omega(J,l)}\mathrm{d}l, \\
\bar{\hat{K}}(J, \hat{p}_J) &= 1.
\end{aligned} \tag{8.22}$$

We have shown the following proposition.

Proposition 8.13. *When the pulsation Ω depends also on the fast angular variable l, the averaged system takes the form*

$$\dot{J} = \varepsilon \frac{\partial \bar{\hat{K}}}{\partial p_I}(J, \hat{p}_J), \quad \dot{\hat{p}}_J = -\varepsilon \frac{\partial \bar{\hat{K}}}{\partial I}(J, \hat{p}_J), \quad \bar{\hat{K}}(J, \hat{p}_J) = 1 \tag{8.23}$$

where

$$\bar{\hat{K}}(J, \hat{p}_J) = \frac{1}{2\pi} \int_0^{2\pi} \hat{K}(J, l, \hat{p}_J, p_l = 0, \varepsilon = 0) \frac{\omega(J)}{\Omega(J,l)}\mathrm{d}l. \tag{8.24}$$

Hence all the proofs made with the angle φ and ω depending on I only may be translated to systems like (8.19) using (8.24) to compute averages.

8.2.4 Case of several frequencies

We define an average system from the extremal system (8.3) where $\varphi = (\varphi_1, \varphi_2) \in \mathbb{T}^2$ (or more generally $\varphi \in \mathbb{T}^k$). The averaged system is derived from the Hamilton equations of the Pontryagin maximum principle. The resonance effect is discarded.

The extremal system, given by the Pontryagin maximum principle, is defined by the Hamiltonian

$$H(I, p_I, \varphi, p_\varphi, p^0, \varepsilon) = p^0 + p_\varphi \cdot \omega(I) + \varepsilon K(I, p_I, \varphi, p_\varphi, \varepsilon),$$

where $p^0 \leq 0$, $\varphi = (\varphi_1, \varphi_2) \in \mathbb{T}^2$, $p_\varphi = (p_{\varphi_1}, p_{\varphi_2}) \in \mathbb{R}^2$, $(I, p_I) \in \mathbb{R}^{2n}$.
The associated dynamic is written as

$$\begin{aligned}
\dot{I} &= \varepsilon \frac{\partial K}{\partial p_I}, \quad \dot{p}_I = -p_\varphi \cdot \omega' - \varepsilon \frac{\partial K}{\partial I}, \\
\dot{\varphi} &= \omega + \varepsilon \frac{\partial K}{\partial p_\varphi}, \quad \dot{p}_\varphi = -\varepsilon \frac{\partial K}{\partial \varphi}.
\end{aligned} \tag{8.25}$$

p_I is, *a priori*, not a slow variable and the system is not in the standard form. We cannot simply apply a reduction on the level $H = 0$ with $p^0 = -\varepsilon$ as we did in

the single frequency case (see Section 8.2.2). An idea is to find a change of variable such that one of the adjoint component of the fast variable disappears from the Hamiltonian and then we apply a reduction on the the level $H = 0$ with $p^0 = -\varepsilon$. We consider the canonical change of variables $(I, p_I, \varphi, p_\varphi) \mapsto (\widetilde{I} := I, \psi := (\alpha, \beta) = \chi(I, \varphi), p_{\widetilde{I}}, p_\psi)$ where

$$\alpha := \varphi \cdot \frac{\omega(I)}{\gamma(I)}, \quad \beta := \varphi \cdot \frac{\omega_\perp(I)}{\gamma(I)}. \tag{8.26}$$

and $\gamma : \mathbb{R}^n \mapsto]0, +\infty[$ is an arbitrary (smooth) function. The resulting adjoint variables $(p_{\widetilde{I}}, p_\psi = (p_\alpha, p_\beta))$ are

$$p_{\widetilde{I}} = p_I - p_\varphi \frac{\partial \chi^{-1}}{\partial \varphi}(I, \varphi) \frac{\partial \chi}{\partial I}(I, \varphi), \quad p_\psi = \frac{\gamma(I)}{|\omega(I)|^2}(p_\varphi \cdot \omega, p_\varphi \cdot \omega_\perp) \tag{8.27}$$

and the Hamiltonian becomes

$$\widetilde{H}(\widetilde{I}, p_{\widetilde{I}}, \psi, p_\psi, p^0, \varepsilon) = p_0 + p_\alpha \frac{|\omega(\widetilde{I})|^2}{\gamma(\widetilde{I})} + \varepsilon \widetilde{K}(\widetilde{I}, p_{\widetilde{I}}, \psi, p_\psi, \varepsilon). \tag{8.28}$$

where

$$\begin{aligned}\widetilde{H}&(\widetilde{I}, p_{\widetilde{I}}, \psi, p_\psi, p^0, \varepsilon) \\ &= H(\widetilde{I}, p_{\widetilde{I}} + \varphi^\intercal (p_\alpha \frac{\partial(\omega/\gamma)}{\partial I} + p_\beta \frac{\partial(\omega_\perp/\gamma)}{\partial I}), \gamma \frac{\alpha\omega + \beta\omega_\perp}{|\omega(\widetilde{I})|^2}, p_\alpha \frac{\omega^\intercal}{\gamma} + p_\beta \frac{\omega_\perp^\intercal}{\gamma}, \varepsilon)\end{aligned}$$

(and the same expression for $\widetilde{K}$).
We have

$$p_\alpha = \varepsilon\gamma \frac{1 - \widetilde{K}}{|\omega|^2} \tag{8.29}$$

on the level $H = 0$ with $p^0 = -\varepsilon$, hence,

$$\dot{p}_{\widetilde{I}} = -p_\alpha \frac{\partial(\omega/\gamma)}{\partial \widetilde{I}} - \varepsilon \frac{\partial \widetilde{K}}{\partial \widetilde{I}} = \mathcal{O}(\varepsilon) \tag{8.30}$$

Since $\partial \widetilde{H}/\partial p_\alpha = \frac{|\omega|^2}{\gamma} + \mathcal{O}(\varepsilon) > 0$ for ε small enough, we use the same arguments than in proposition 8.7 to write $p_\alpha = p_\alpha(\widetilde{I}, p_{\widetilde{I}}, \psi, p_\beta, \varepsilon)$ and divided by ε from 8.29, we have

$$p_\alpha = -\varepsilon \widetilde{h}(\widetilde{I}, p_{\widetilde{I}}, \psi, p_\beta, \varepsilon). \tag{8.31}$$

The extremal system becomes

$$\begin{aligned}\dot{\widetilde{I}} &= \varepsilon \frac{\partial \widetilde{H}}{\partial p_\alpha} \frac{\partial \widetilde{h}}{\partial p_{\widetilde{I}}}, \quad \dot{p}_{\widetilde{I}} = -\varepsilon \frac{\partial \widetilde{H}}{\partial p_\alpha} \frac{\partial \widetilde{h}}{\partial \widetilde{I}}, \\ \dot{\varphi} &= \omega + \varepsilon \frac{\partial K}{\partial p_\phi}, \quad \dot{p}_\beta = -\varepsilon \frac{\partial \widetilde{H}}{\partial p_\alpha} \frac{\partial \widetilde{h}}{\partial \beta}\end{aligned} \tag{8.32}$$

which can be averaged with respect to φ following Section 7.5.
Note that a parameterization with respect to α leads to consider the non-autonomous Hamiltonian $\widetilde{h}(\widetilde{I}, p_{\widetilde{I}}, \alpha, \beta, p_\beta, \varepsilon)$ periodic in $\varphi = \gamma/|\omega|^2 \ (\alpha\omega + \beta\omega_\perp)$.

Definition 8.14. *The double averaged solution* $(J(.), p_J(.), \bar{p}_\beta(.))$ *satisfies*

$$\frac{\mathrm{d}J}{\mathrm{d}\alpha} = \varepsilon \frac{\partial \bar{\bar{h}}}{\partial p_J}(J, p_J, \bar{p}_\beta), \quad \frac{\mathrm{d}p_J}{\mathrm{d}\alpha} = -\varepsilon \frac{\partial \bar{\bar{h}}}{\partial J}(J, p_J, \bar{p}_\beta), \quad \bar{p}_\beta \text{ is constant.} \tag{8.33}$$

where

$$\begin{aligned}
\bar{\bar{h}}(J, p_J, \bar{p}_\beta) &:= \frac{1}{4\pi^2} \int_{\mathbb{T}^2} \widetilde{h}(J, p_J, \alpha, \beta, \bar{p}_\beta, \varepsilon = 0) \mathrm{d}\varphi \\
&= \int_{\mathbb{T}^2} (\widetilde{K}(J, p_J, \alpha, \beta, p_\alpha = 0, \bar{p}_\beta, \varepsilon = 0) - 1) \frac{\gamma(I)}{|\omega(I)|^2} \mathrm{d}\varphi \\
&= \int_{\mathbb{T}^2} (K(J, p_J + \bar{p}_\beta \varphi^\intercal \frac{\partial(\omega_\perp/\gamma)}{\partial I}, \varphi, \bar{p}_\beta \frac{\omega_\perp^\intercal}{\gamma}, \varepsilon = 0) - 1) \frac{\gamma(I)}{|\omega(I)|^2} \mathrm{d}\varphi.
\end{aligned}$$

8.3 Convergence theorems for the boundary value problems

8.3.1 The non averaged and averaged boundary value problem

In the previous section 8.2, we defined an averaged system by using classical averaging. The convergence and errors estimates in Section 7.5 apply to Cauchy problems (given conditions for one time). The situation is more complex when applying the maximum principle: we are faced with a 2 point boundary value problem instead. However, for BC-extremals, we need to deal with a boundary value problem which is different from a dynamical system by a given Cauchy condition.

In the time-minimal control problem, $I(0)$ and $I(t_f)$ are fixed respectively to I_0 and I_f while the fast angular variables φ is free at initial and final time. This leads to the following boundary conditions for non averaged extremals

$$I(0) = I_0, \quad I(t_f) = I_f, \quad p_\varphi(0) = 0, \quad p_\varphi(t_f) = 0, \quad H(I(.), p_I(.), \varphi(.), p_\varphi(.), \varepsilon) = 0.$$

For the reduced non averaged system in the variables $(I, p_I, \varphi))$ given by (8.12) where $p_\varphi = -\varepsilon h(I, p_I, \varepsilon)$, it is written in the slow angle variable $s = \varepsilon(\varphi - \varphi(0))$ as (the ε superscript emphasizes the dependence of the solutions on ε)

$$\frac{\mathrm{d}I^\varepsilon}{\mathrm{d}s} = \frac{\partial h}{\partial p_I}(I^\varepsilon, p_I^\varepsilon, \frac{s}{\varepsilon}, \varepsilon), \quad \frac{\mathrm{d}p_I^\varepsilon}{\mathrm{d}s} = -\frac{\partial h}{\partial I}(I^\varepsilon, p_I^\varepsilon, \frac{s}{\varepsilon}, \varepsilon) \tag{8.34}$$

and the boundary conditions are

$$I^\varepsilon(0) = I_0, \quad I^\varepsilon(s_f) = I_f, \quad h(I_0, p_I^\varepsilon(0), \varphi^\varepsilon(0), \varepsilon) = 0, \quad h(I_f, p_I^\varepsilon(s_f), \varphi^\varepsilon(s_f), \varepsilon) = 0. \tag{8.35}$$

The shooting variables are $(s_f, \varphi(0), p_I(0))$ which provide a well defined boundary value problem.

One frequency averaging. The averaged boundary value problem is defined by

$$\frac{\mathrm{d}J}{\mathrm{d}s} = \frac{\partial \bar{h}}{\partial p_I}(J, p_J), \quad \frac{\mathrm{d}p_J}{\mathrm{d}s} = -\frac{\partial \bar{h}}{\partial I}(J, p_J) \tag{8.36}$$

with the boundary value conditions

$$J(0) = I_0, \quad J(t_f) = I_f, \quad \bar{h}(I_0, p_J(0)) = 0. \tag{8.37}$$

8.3.2 Convergence theorems

Direct convergence. Here we show that all limits as $\varepsilon \to 0$ of non averaged extremals are solutions of the averaged system (8.36) with the same boundary conditions on the slow variable at initial and final time.

We fix V an open subset of the lifted Kepler's elliptical orbits set such that $\pi(\widetilde{\Sigma}_0) \cap V = \varnothing$.

Theorem 8.15. *Let K be a compact subset of V. Let $(I^\varepsilon(.), \varphi^\varepsilon(.), {p_I}^\varepsilon(.), p_\varphi^\varepsilon(.))_{0<\varepsilon\leq\varepsilon_0}$, for some $\varepsilon_0 > 0$, be a family of solutions of (8.3)-(8.4) with $p^0 = -\varepsilon$ such that, for all $\varepsilon \in (0, \varepsilon_0]$ and all $t \in [0, t_f^\varepsilon]$, one has, $(I^\varepsilon(t), p_I^\varepsilon(t)) \in K$.*
Then the family of maps

$$(t \mapsto (I^\varepsilon(\varepsilon t), {p_I}^\varepsilon(\varepsilon t))_{0<\varepsilon\leq\varepsilon_0}$$

is compact in the C^0-topology and for any uniformly convergent subsequence $(t \mapsto (I^{\varepsilon_n}(\varepsilon_n t)), {p_I}^{\varepsilon_n}(\varepsilon_n t))_{n\in\mathbb{N}}$ with $\varepsilon_n \to 0$, the uniform limit, $s \mapsto (\bar{I}(s), \bar{p}_I(s))$ is a solution of (8.36) satisfying the boundary conditions

$$J(0) = I_0 \ \text{ and } \ J(\bar{s}_f) = I_f.$$

Proof. The family $(I^\varepsilon(\varepsilon.), p_I^\varepsilon(\varepsilon.))_{0<\varepsilon\leq\varepsilon_0}$ is equicontinuous because it has a common Lipschitz constant, equal to the maximum size of all second derivatives of the hamiltonian H, hence it is compact by Ascoli's theorem.
Take a sequence $(\varepsilon_n)_{n\in\mathbb{N}}$ such that $\varepsilon_n \to 0$ and the trajectory converges uniformly as $n \to +\infty$. One may then apply the classical averaging theorem to the system (8.12) and the boundary conditions follow by continuity. □

Converse convergence. The second theorem is in a sense the converse of the convergence theorem 8.15. We want to prove that every solution of the average boundary value problem (8.36)-(8.37) where $\bar{z} = (J, p_J)$ is limit of a sequence of solutions of the non-average boundary value problem as $\varepsilon \to 0$.
This is a richer result than theorem 8.15 because we want to take the average system as a reference.

The theorem (8.17) presented below almost proves this. We comment on it after stating it. Let us first introduce a simple definition.

We consider the averaged system (8.18) written as

$$\frac{\mathrm{d}\bar{z}}{\mathrm{d}s}(s) = \overrightarrow{\bar{h}}(\bar{z}(s)), \quad \bar{z}(0) = (I_0, p_{J_0}) \tag{8.38}$$

where $\bar{z}(.) = (J(.), p_J(.))$ and $\overrightarrow{\bar{h}} = (\partial\bar{h}/\partial p_J, -\partial\bar{h}/\partial J)$ is the Hamiltonian vector field associated with $\bar{h}$. Let

$$\bar{S}(s_f, p_{J_0}) := (J(s_f, p_{J_0}) - I_f, \bar{h}(I_0, p_{J_0})) \quad (J(0) \text{ is fixed }) \tag{8.39}$$

the shooting function associated to the averaged dynamic (8.38).
Likewise, we consider the shooting function

$$S_\varepsilon(s_f, p_{I_0}, \varphi_0) := (I(s_f, p_{I_0}, \varepsilon) - I_f, h(I_0, p_{I_0}, \varphi_0)) \tag{8.40}$$

associated with the non averaged dynamic (8.17) written as

$$\frac{\mathrm{d}z}{\mathrm{d}s}(s) = \overrightarrow{h}(z(s), \frac{s}{\varepsilon} + \varphi_0), \quad z(0) = (I_0, p_{I_0}, \varphi_0). \tag{8.41}$$

where $z(.) = (I(.), p_I(.))$ and $\overrightarrow{h} = (\partial h/\partial p_I, -\partial h/\partial I)$ is the Hamiltonian vector field associated with h.

Definition 8.16. *To the average differential equations (8.36), we associate the shooting function (8.39). We say that (s_f, p_{J_0}) is a regular zero of $\bar{S}$ if and only if*

- $\bar{S}(s_f, p_{J_0}) = 0$,
- *the differential of $\bar{S}$ at (s_f, p_{J_0}) is a linear invertible map (an invertible $(n+1) \times (n+1)$ matrix in fixed coordinates.*

For instance, it is well known that this is satisfied if s_f is smaller that the first conjugate time on the trajectory starting from (I_0, p_{J_0}), but the condition is not necessary.

For the rest of this chapter, we will consider the modified shooting function $\tilde{S}_\varepsilon$, associated to the non averaged system (8.41), defined by

$$\tilde{S}_\varepsilon(s_f, p_{I_0}, \varphi_0) := (I(s_f, p_{I_0}, \varepsilon) - I_f, \bar{h}(I_0, p_{I_0})). \tag{8.42}$$

We have the following theorem.

Theorem 8.17. *Consider a solution $\bar{z}(.) = (J(.), p_J(.))$ of the averaged system (8.38) defined on $[0, s_f]$ such that $(s_f, p_J(0))$ is a regular zero of $\bar{S}$ in the above sense. Then there exists ε_0 and for each ε, $0 < \varepsilon \leq \varepsilon_0$, a solution $z^\varepsilon(.) = (I^\varepsilon(.), p_I^\varepsilon(.), \varphi^\varepsilon)$ of the system (8.41) satisfying*

$$I^\varepsilon(0, p_I^\varepsilon(0), \varphi^\varepsilon(0)) = I_0, \quad I^\varepsilon(s_f, p_I^\varepsilon(0), \varphi^\varepsilon(0)) = I_f, \quad \bar{h}(I_0, p_I^\varepsilon(0)) = 0. \tag{8.43}$$

The proof of this theorem is based on the following lemma.

Lemma 8.18. *Let $f : \mathbb{R}^n \to \mathbb{R}^n$ be a continuously differentiable map admitting a regular zero at 0, and let $f_\varepsilon : \mathbb{R}^n \to \mathbb{R}^n$, $\varepsilon > 0$, be a family of continuous functions uniformly convergent to f on a neighborhood of the origin when $\varepsilon \to 0$.*
Then, there exists $\varepsilon_0 > 0$ and $\xi : [0, \varepsilon_0] \to \mathbb{R}^n$ continuous at $\varepsilon = 0$ with $\xi(0) = 0$, and such that

$$f_\varepsilon(\xi(\varepsilon)) = 0, \quad \varepsilon \in (0, \varepsilon_0].$$

Proof of Lemma 8.18. From the invert function theorem, there exists a neighborhood U of the origin such that f induces an homeomorphism from U to $f(U)$. We can assume that f_ε is uniformly convergent to f on U by restricting U. Since $0 \in f(U)$, then $f(U)$ contains a closed ball B centered at the origin. We consider $g_\varepsilon := \mathrm{id} - f_\varepsilon \circ f^{-1}$ on B. The functions g_ε are uniformly convergent to 0, therefore there exists $\varepsilon_0 > 0$ such that $g_\varepsilon(B) \subset B$, $\varepsilon \in (0, \varepsilon_0]$. From the Brouwer fixed point theorem, for each $\varepsilon \in (0, \varepsilon_0]$, there exists a fixed point $y_\varepsilon \in B$ of g_ε, hence satisfying $f_\varepsilon(f^{-1}(y_\varepsilon)) = 0$.
We define $\xi : [0, \varepsilon_0] \to \mathbb{R}^n$ by $\xi(0) = 0$, and $\xi(\varepsilon) = f^{-1}(y_\varepsilon)$ if $\varepsilon > 0$.
Obviously, $f_\varepsilon(\xi(\varepsilon)) = 0$ holds for all $\varepsilon \in (0, \varepsilon_0^-)$. Let us prove continuity of $\xi(.)$ at 0, i.e. $\lim_{\varepsilon \to 0, \varepsilon > 0} \xi(\varepsilon) = 0$. Since $\xi(\varepsilon)$ belongs to the compact B for all ε, we only need to prove that, for any sequence $(\varepsilon_k)_{k \in \mathbb{N}}$ that tends to zero, as $k \to 0$ and is such that $(\xi(\varepsilon_k))_{k \in \mathbb{N}}$ is convergent, the limit is zero. For such a sequence, calling ξ_0 its limit, one has

$$|f_{\varepsilon_k}(\xi(\varepsilon_k)) - f(\xi_0)| \leq |f_{\varepsilon_k}(\xi(\varepsilon_k)) - f(\xi(\varepsilon_k))| + |f(\xi(\varepsilon_k)) - f(\xi_0)|, \quad k \in \mathbb{N}.$$

The first term of the right hand side is controlled by the uniform convergence of f_ε, the second one by the continuity of f at ξ_0, so $f_{\varepsilon_k}(\xi(\varepsilon_k)) \to f(\xi_0)$. However $0 = f_{\varepsilon_k}(\xi(\varepsilon_k))$ for all k, hence $f(\xi_0) = 0$ and, since f is bijective from $f^{-1}(B)$ onto B, we get $\xi_0 = 0$. This concludes the proof. □

Proof of Theorem 8.17. If p_0 and φ_0 are fixed, then $s \mapsto \tilde{S}_\varepsilon(s, \varphi_0, p_0)$ converges uniformly to $s \mapsto \bar{S}(s, p_0)$ on $[0, s_f]$. Besides, by virtue of Proposition 7.9, if p_0 stays in a compact, this convergence is also uniform with respect to p_0. Hence, applying Lemma 8.18 yields the result. □

Remark 8.19. *Let us comment how far this is from the result we "wanted to prove" at the beginning of this paragraph.*

1. *There is a condition on the "average solution" $\bar{z}(t)$: not only it has to be a zero of $\bar{S}$, which is implied by optimality conditions, but it has to be a regular zero. This condition is almost necessary in the sense that there is no hope to prove such a result in general without this non-singularity assumption.*

2. *The conditions (8.43) are not the boundary conditions given by the PMP for the non average problem. It "should" be*

$$I^\varepsilon(0) = I_0, \ I^\varepsilon(s_f) = I_f, \ h(I_0, p_I^\varepsilon(0), \varphi_0) = h(I_f, p_I^\varepsilon(s_f), \varphi_f) = 0.$$

They differ in that we have replaced the vanishing of the (oscillating) function h at initial and final time by the vanishing of the average $\bar{h}$. This is not totally satisfactory.

Converse convergence theorem where the fast angle is free at initial and final time

In the previous Section, we gave a proof of the converse convergence for quasi extremals which is disappointing . Here we give a sketch of a proof of the converse convergence theorem presented in the previous paragraph where we take into account the condition

$$h(\varphi_0, z(0), \varepsilon) = 0 \tag{8.44}$$

and show that the condition

$$h(\varphi_f, z(s_f), \varepsilon) = 0 \tag{8.45}$$

is satisfied if we relax the condition on the slow variables I_f.

More precisely, we consider the shooting function $\bar{S}$ (8.39) of the averaged system (8.38) and the shooting function

$$S_\varepsilon(s_f, p_0) = (I(s_f, p_0, \varepsilon) - I_f, \bar{h}(I_0, p_0)) \tag{8.46}$$

of the non averaged system

$$\frac{\mathrm{d}z}{\mathrm{d}s}(s) = \overrightarrow{h}(s/\varepsilon, z(s), \varepsilon), \quad z(0) = (I_0, p_0). \tag{8.47}$$

The proof results from the following steps

- We apply Lemma 8.18 for the functions S_ε (8.46) and $\bar{S}$ (8.39). This is essentially what we described in Section 8.3.2 but here S_ε doesn't depend on φ_0.
- To take into account the condition (8.44), we make the following assumption on the averaged solution $(\bar{s}_f, \bar{p}_0)$: there exists $\bar{\varphi}_0 \in S^1$ such that

$$h(\bar{\varphi}_0, (I_0, \bar{p}_0), \varepsilon = 0) = 0, \ \frac{\partial h}{\partial \varphi}(\bar{\varphi}_0, \bar{z}_0, \varepsilon = 0) \neq 0.$$

  Under this assumption, there exists an implicit function $\varphi_0(p, \varepsilon)$ defined in a neighborhood of $(\bar{p}_0, \varepsilon = 0)$ and we replace the shooting function (8.46) by

$$S_\varepsilon(s_f, p_0) = (I(s_f, \varphi_0(p_0, \varepsilon), p_0, \varepsilon), \bar{h}(I_0, p_0))$$

  associated with the new non averaged system

$$\frac{\mathrm{d}z}{\mathrm{d}s}(s) = \overrightarrow{h}(s/\varepsilon + \varphi_0, z(s), \varepsilon), \quad z(0) = (I_0, \varphi_0, p_0).$$

  The dependance on φ_0 of the initial condition $z(0)$ doesn't affect the uniform convergence of S_ε to $\bar{S}$ (see [112, Theorem 2.8.9]) and we apply again Lemma 8.18 for S_ε and $\bar{S}$.

- To take into account the condition (8.45), we assume that there exists $\bar{\varphi}_f \in S^1$ such that
$$h(\bar{\varphi}_f, \bar{z}_f, \varepsilon = 0) = 0,\ \frac{\partial h}{\partial \varphi}(\bar{\varphi}_f, \bar{z}_f, \varepsilon = 0) \neq 0.$$
where $\bar{z}_f = \bar{z}(\bar{s}_f, \bar{p}_0)$.
Under this assumption, there exists an implicit function $\varphi_f(p, \varepsilon)$ defined in a neighborhood of $(\bar{z}_f, \varepsilon = 0)$ and we define
$$g_\varepsilon(\varphi) = \varphi_f(z(s_f(\varepsilon) + \varepsilon\varphi, \varphi_0(\varepsilon), p_0(\varepsilon), \varepsilon), \varepsilon)$$
on a closed ball B centered at φ_f. Since g_ε uniformly converges to the constant function $\varphi \mapsto \bar{\varphi}_f$, we have $g_\varepsilon(B) \subset B$ for $\varepsilon > 0$ small enough, hence there is a fix point $\varphi_f(\varepsilon)$ for g_ε (Brouwer).
Since with $\tilde{s}_f(\varepsilon) = s_f(\varepsilon) + \varepsilon\varphi_f(\varepsilon)$ we have that
$$I(\tilde{s}_f(\varepsilon), \varphi_0(\varepsilon), p_0(\varepsilon), \varepsilon) = I_f + O(\varepsilon),$$
the family $(\tilde{s}_f(\varepsilon), \varphi_0(\varepsilon), p_0(\varepsilon))$ is solution for $\varepsilon > 0$ small enough of
$$\begin{aligned} \frac{\mathrm{d}z}{\mathrm{d}s}(s) &= \overrightarrow{h}(s/\varepsilon + \varphi_0, z(s), \varepsilon) \\ I(0) = I_0,\ h(\varphi_0, z(0), \varepsilon) &= 0, \\ I(s_f/\varepsilon + \varphi_0, z(s_f), \varepsilon) = \boldsymbol{I_f + O(\varepsilon)},\ h(s_f/\varepsilon + \varphi_0, z(s_f), \varepsilon) &= 0. \end{aligned}$$

Chapter 9

Numerical results

We present numerical simulations of the time minimal orbital transfer problem with the `HamPath` software using averaging techniques presented in Chapter 8. The convergence results are illustrated and we finish by giving numerical results concerning simple and double averaging.

9.1 Description of the simulated problems

The purpose is to solve numerically the non averaged boundary value problem introduced in section 8.1 of Chapter 8. It is a Hamiltonian system defined by

$$H(I, p_I, \varphi, p_\varphi, \varepsilon) = p_\varphi \cdot \omega(I) + \varepsilon K(I, p_I, \varphi, p_\varphi, \varepsilon) \tag{9.1}$$

and

$$K := H_0 + \sqrt{\sum_{i=1}^{m} H_i^2},$$

$$H_i(I, p_I, \varphi, p_\varphi, \varepsilon) := p_I F_i(I, \varphi, \varepsilon) + p_\varphi G_i(I, \varphi, \varepsilon), \quad i = 0, \dots, m.$$

On top of that, we have the following boundary value conditions

$$I(0) = I_0,\ I(t_f) = I_f,\ p_\varphi(0) = 0,\ p_\varphi(t_f) = 0,\ H = \varepsilon.$$

We used a simple shooting method implemented in `HamPath` and based on a Newton-type algorithm [55] to solve this boundary value problem. However, due to the oscillating nature of the dynamic, the system is not well-conditioned numerically and the algorithm is very sensitive to the initialization.

One frequency averaging In the case of one fast variable, we solve numerically the averaged boundary value problem, introduced in chapter 8

$$\frac{\mathrm{d}J}{\mathrm{d}s} = \frac{\partial \bar{h}}{\partial p_I}(J, p_J), \quad \frac{\mathrm{d}p_J}{\mathrm{d}s} = -\frac{\partial \bar{h}}{\partial I}(J, p_J), \tag{9.2}$$

$$J(0) = I_0, \quad J(s_f) = I_f, \quad \bar{h}(J(0), p_J(0)) = 0. \tag{9.3}$$

where $s = \varepsilon(\varphi - \varphi(0))$ is the normalized angle and

$$\begin{aligned}\bar{h}(J, p_J) &:= \frac{1}{2\pi}\int_0^{2\pi} h(J, p_J, \varphi, \varepsilon = 0)\mathrm{d}\varphi \\ &= \frac{1}{2\pi}\int_0^{2\pi} \frac{K-1}{\omega}(J, p_J, \varphi, p_\varphi = 0, \varepsilon = 0)\mathrm{d}\varphi.\end{aligned}$$

Remark 9.1. *To compute the averaged dynamic by numerical integration, we implement a Newton-Cotes quadrature rules based on a Simpson's rule [117].*

Remark 9.2. *For numerical purpose, to have the same parameterization for the trajectories of the averaged system (9.2) and of the non averaged system (9.1) with respect to the same time t, we add the time variable t and its adjoint p_t to the dynamic of the averaged system. This leads to consider the averaged Hamiltonian*

$$\hbar(J, p_J, t, p_t, \varepsilon) = \bar{h}(J, p_J) + p_t\frac{\mathrm{d}t}{\mathrm{d}s}$$

where $\frac{\mathrm{d}t}{\mathrm{d}s} = \frac{1}{\varepsilon\dot{\varphi}} = 1/\varepsilon/(\omega + \varepsilon G_i(I, \varphi, \varepsilon))$ and p_t is a cyclic variable forced to satisfy $p_t(0) = p_t(s_f) = 0$.

9.1.1 Initialization of the non averaged shooting algorithm

The shooting algorithm for the averaged boundary value problem (9.2) converges very easily and gives a solution $(\bar{s}_f, \bar{p}_{I_0})$. Recall that a solution of the averaged system doesn't depend on ε.
Then, the shooting algorithm of the non averaged boundary value problem is initialized with $(t_f, \varphi(0), p_I(0))$ where

- $t_f = t(\bar{s}_f)$ where $t(.)$ is numerically computed as explained in Remark 9.2,
- $\varphi(0)$ is chosen in $[0, 2\pi)$,
- $p_I(0) = \bar{p}_I(0)$.

9.1.2 Commented numerical results

We use the equinoctial elements (P, e_x, e_y, h_x, h_y) for the slow variable I and the fast variable φ is the true longitude denoted by l. Table 9.1 presents two sets of data used for our simulations. The data set ① was proposed by T. Dargent where he showed that the averaging trajectories obtained by the software T3D [57] may be very far from the trajectories of the non averaged orbital transfer. The second data set ② is a orbital transfer from a low orbit to a geostationary orbit and is taken from the thesis [44]. Note that in both cases, we don't take into account the variation of the mass m_S of the satellite, fixed at $m_S = 3500$ kg for the case ① and $m_s = 1500$ kg for the case ②. Moreover this simulation doesn't take into account the J_2 term in gravitational potential of the Earth (which provides similar results) and the lunar perturbation (which are taken in the double averaging, cf Section 9.2.2).

	Initial orbits I_0		Final orbits I_f	
Equinoctial Elements	Data ①	Data ②	Data ①	Data ②
P (Mm)	34.516	5.0859	42.164	42.164
e_x	0.4	0.75	0	0
e_y	0	0	0	0
h_x	5.24×10^{-3}	6.12×10^{-2}	0	0
h_y	0	0	0	0

Table 9.1: Initial and final values of the orbital elements for the case ① and the case ②.

Figure	Data set	Thrust (ε)
9.1	①	1 N (3.7×10^{-3})
9.2	①	0.5 N (1.85×10^{-3})
9.3	①	0.05 N (1.85×10^{-4})
9.4	②	2 N (1.73×10^{-2})
9.5	②	1 N (8.64×10^{-3})
9.6	②	0.3 N (2.59×10^{-3})

Table 9.2: Values of thrust for each figure.

The parameters involved are the standard gravitational parameter of the Earth fixed at $\mu = 5165.8621\text{Mm}^3/\text{h}^2$ and the maximum thrust F_{max} in kg.Mm/h^2. The parameter ε is defined by $\varepsilon := F_{max}/m_S$. Note that other choices may be considered, namely $\varepsilon = \frac{F_{max}a_f^2}{\mu m_S}$ where a_f is the final semi-major axis of the orbit (see [63]).

In Fig.9.1-Fig.9.3 and Fig.9.4-Fig.9.6, we represent the time evolution of state variables $(P, e_x, e_y, h_x, h_y(, l))$ and of the adjoint variables $(p_P, p_{e_x}, p_{e_y}, p_{h_x}, p_{h_y}(, p_l))$ for both the averaged system, in red, and the non averaged system, in black.
To illustrate the convergence theorems proved in 8.3.2, we take different thrusts of the engine which corresponds to different values of the parameter ε. We observe that, the more ε is small, the more the averaged trajectories is closed to the non averaged ones. We sum up the connection between the data sets and the thrust in Table 9.2.

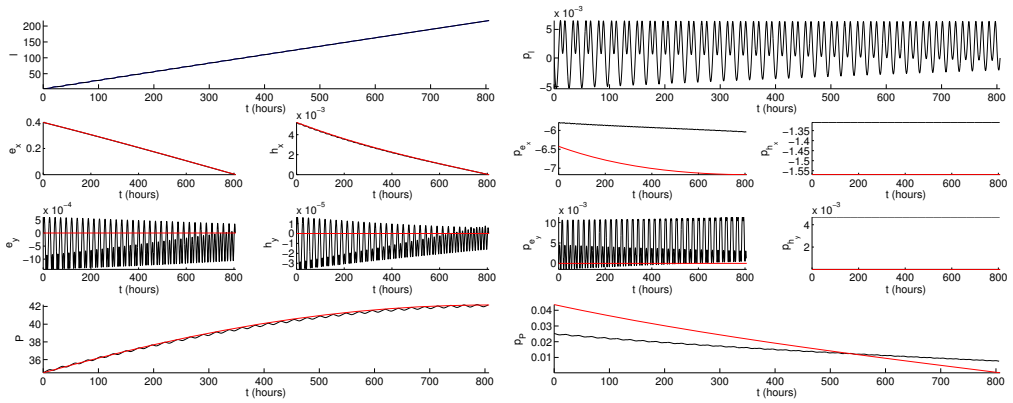

Figure 9.1: Case ①.Time evolution of state and adjoint variables for $\varepsilon = 3.7 \times 10^{-3}$. *(red)* averaged system (9.2), *(black)* non averaged system (9.1).

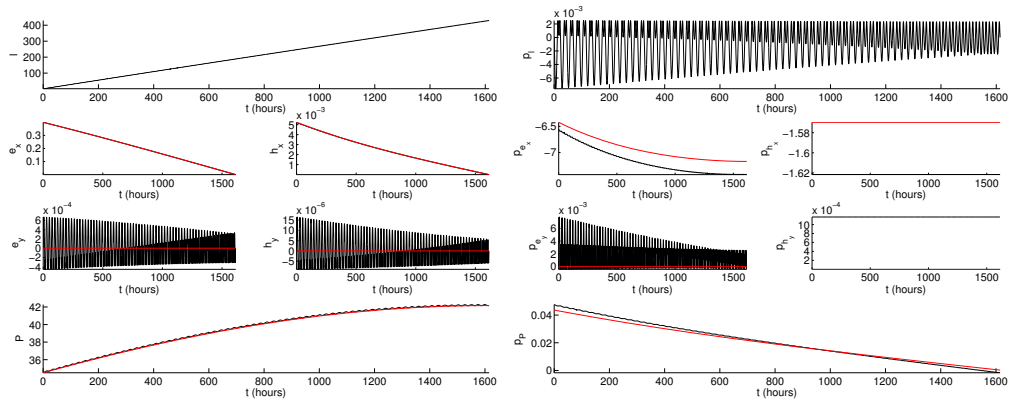

Figure 9.2: Case ①.Time evolution of state and adjoint variables for $\varepsilon = 1.85 \times 10^{-3}$. *(red)* averaged system (9.2), *(black)* non averaged system (9.1).

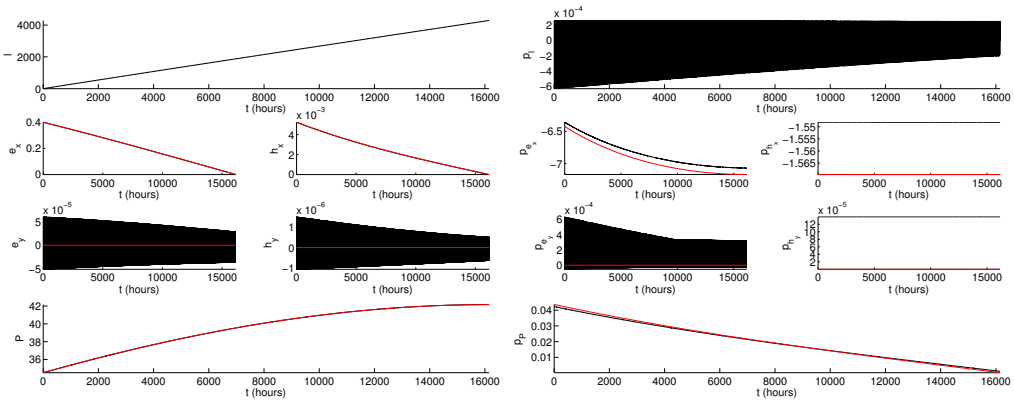

Figure 9.3: Case ①.Time evolution of state and adjoint variables for $\varepsilon = 1.85 \times 10^{-4}$. *(red)* averaged system (9.2), *(black)* non averaged system (9.1).

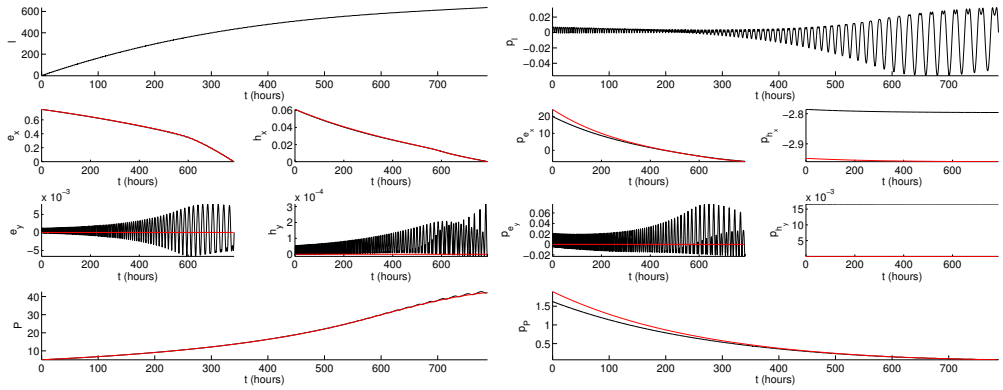

Figure 9.4: Case ②.Time evolution of state and adjoint variables for $\varepsilon = 1.73 \times 10^{-2}$. *(red)* averaged system (9.2), *(black)* non averaged system (9.1).

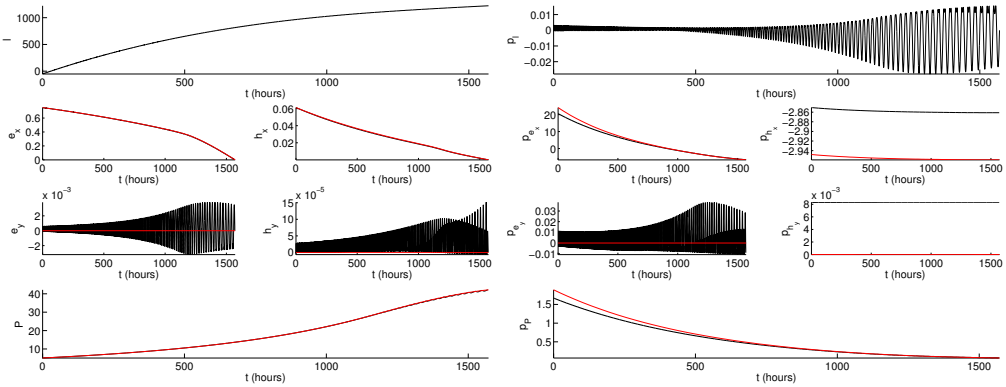

Figure 9.5: Case ②.Time evolution of state and adjoint variables for $\varepsilon = 8.64 \times 10^{-3}$. *(red)* averaged system (9.2), *(black)* non averaged system (9.1).

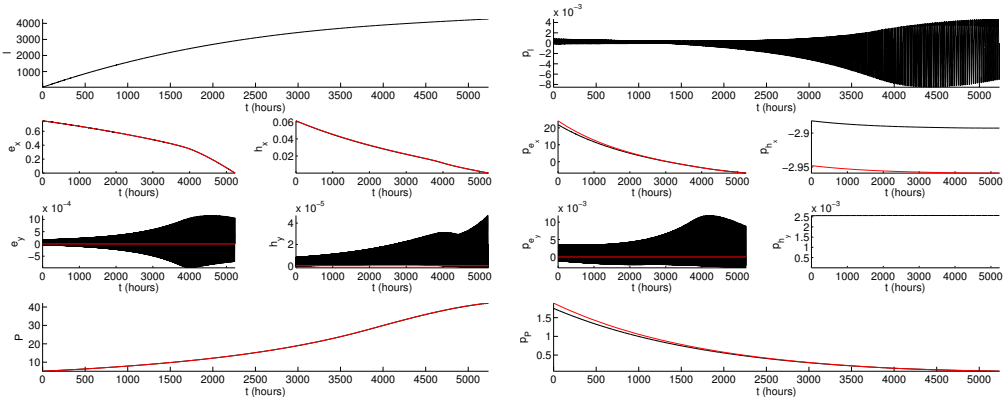

Figure 9.6: Case ②.Time evolution of state and adjoint variables for $\varepsilon = 2.59 \times 10^{-3}$. *(red)* averaged system (9.2), *(black)* non averaged system (9.1).

In Fig.9.7, we superimpose adjoint trajectories with respect to the normalized

angle s for different values of the thrust in both case ① and ②.

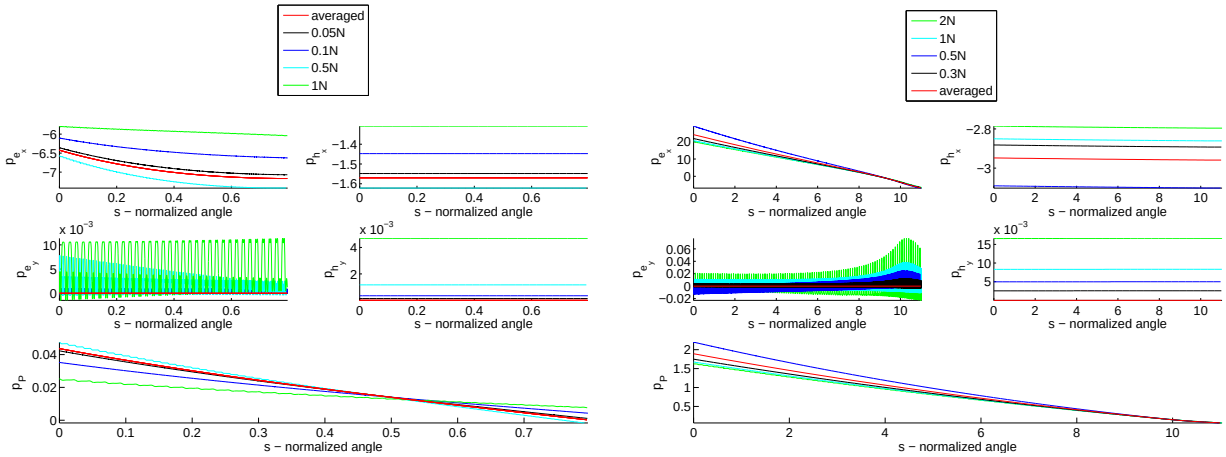

Figure 9.7: Adjoint trajectories parameterized by normalized angle s for different thrusts. *(left)* Case ①, *(right)* Case ②

9.2 Numerical conjecture

9.2.1 Simple averaging

In our theoretical proof of lemma 8.17 of chapter 8, we consider the condition $\bar{h}(I_0, p_0) = 0$ for non averaged extremals instead of the condition $h(s_f/\varepsilon, I_0, p_0) = 0$. This simplification comes from the assumption that we don't know how to prove that the function $\varepsilon \mapsto h(s/\varepsilon, ., .)$ admits a limit as ε tends to 0. Secondly, although the condition $\bar{h}(I_0, p_0) = 0$ is motivated to deduce a structure of the averaged system,it seems, numerically, that $h(s/\varepsilon, ., .)$ has a nonzero limit when $\varepsilon \to 0$.

Instead of considering the averaged boundary conditions given in (9.2), we define the averaged solutions $(J(.), p_J(.))$ as solutions of the boundary value problem

$$\begin{aligned} &\frac{\mathrm{d}J}{\mathrm{d}s} = \frac{\partial \bar{h}}{\partial p_I}(J, p_J), \quad \frac{\mathrm{d}p_J}{\mathrm{d}s} = -\frac{\partial \bar{h}}{\partial I}(J, p_J), \\ &J(0) = I_0, \quad J(s_f) = I_f, \quad \bar{h}(J(0), p_J(0)) = \hbar. \end{aligned} \tag{9.4}$$

where

$$\hbar := 1/t_f \int_0^{t_f} \bar{h}(I(t), p_I(t))\mathrm{d}t$$

and $(I(.), p_I(.))$ is a non averaged solution of (9.1).

We give numerical simulations concerning this new averaged boundary value problem to show that the energy level $\bar{h}$ could interfere with the convergence between the averaged system and the non averaged system.

We consider the same orbital transfers given in Table 9.1. In Fig.9.8-Fig.9.10 and Fig.9.11-Fig.9.13, we represent the time evolution of state variables $(P, e_x, e_y, h_x, h_y(, l))$ and of the adjoint variables $(p_P, p_{e_x}, p_{e_y}, p_{h_x}, p_{h_y}(, p_l))$ for both

Figure	Data set	Thrust (ε)	$\hbar$
9.8	①	1 N (3.7×10^{-3})	-0.598
9.9	①	0.5 N (1.85×10^{-3})	-0.591
9.10	①	0.05 N (1.85×10^{-4})	-0.556
9.11	②	2 N (1.73×10^{-2})	-6.475×10^{-2}
9.12	②	1 N (8.64×10^{-3})	-5.233×10^{-2}
9.13	②	0.3 N (2.59×10^{-3})	-4.471×10^{-2}

Table 9.3: Values of thrusts and values of the level $\hbar$ for each figure.

the averaged system, in red, and the non averaged system, in black. For each case ① and ②, we choose the same values of thrust as summarized in Table 9.3.

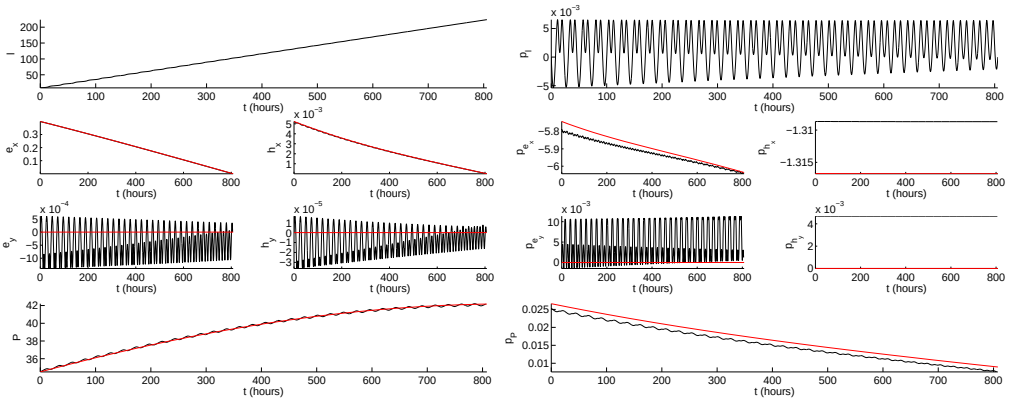

Figure 9.8: Case ①.Time evolution of state and adjoint variables for $\varepsilon = 3.7 \times 10^{-3}$. *(red)* averaged system (9.4), *(black)* non averaged system (9.1).

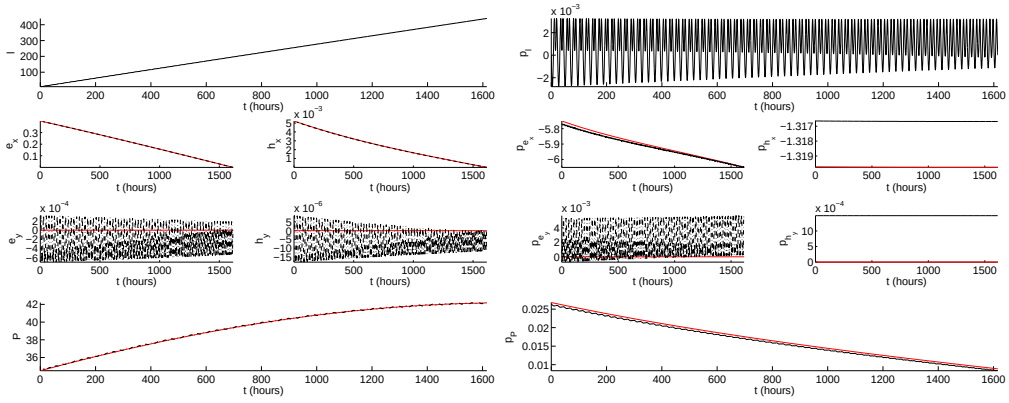

Figure 9.9: Case ①.Time evolution of state and adjoint variables for $\varepsilon = 1.85 \times 10^{-3}$. *(red)* averaged system (9.4), *(black)* non averaged system (9.1).

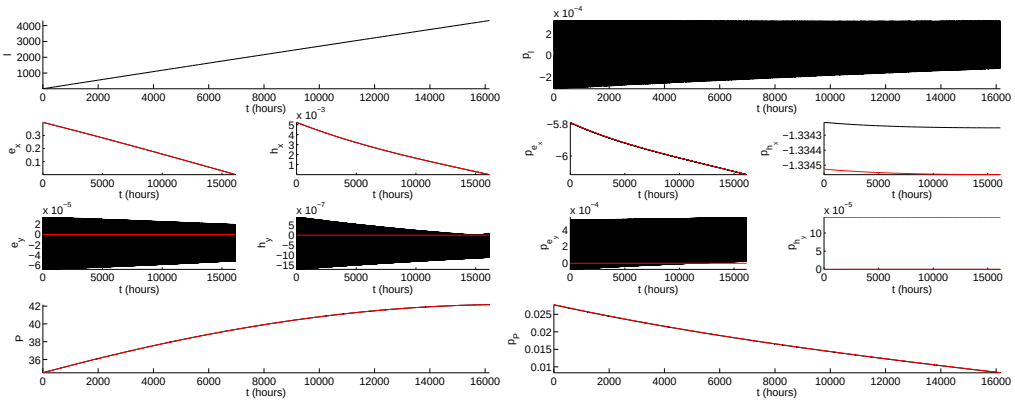

Figure 9.10: Case ①.Time evolution of state and adjoint variables for $\varepsilon = 1.85 \times 10^{-4}$. *(red)* averaged system (9.4), *(black)* non averaged system (9.1).

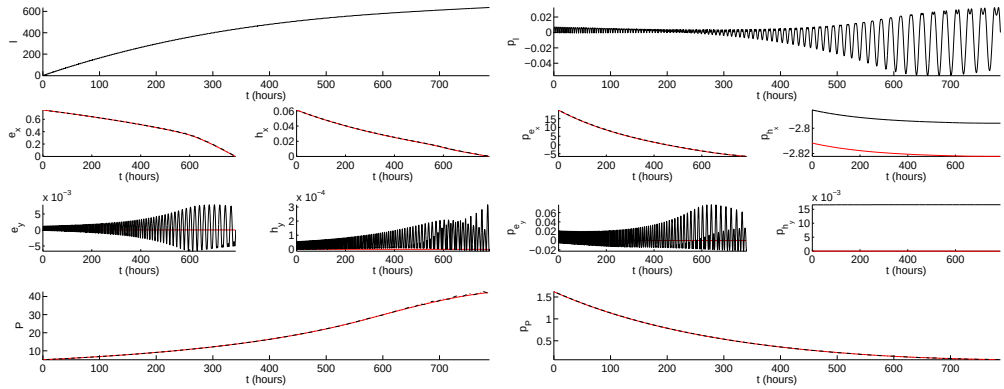

Figure 9.11: Case ②.Time evolution of state and adjoint variables for $\varepsilon = 1.73 \times 10^{-2}$. *(red)* averaged system (9.4), *(black)* non averaged system (9.1).

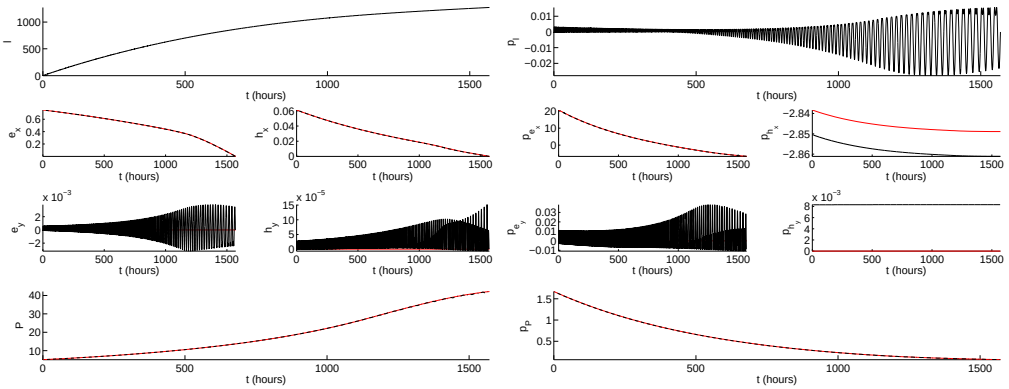

Figure 9.12: Case ②.Time evolution of state and adjoint variables for $\varepsilon = 8.64 \times 10^{-3}$. *(red)* averaged system (9.4), *(black)* non averaged system (9.1).

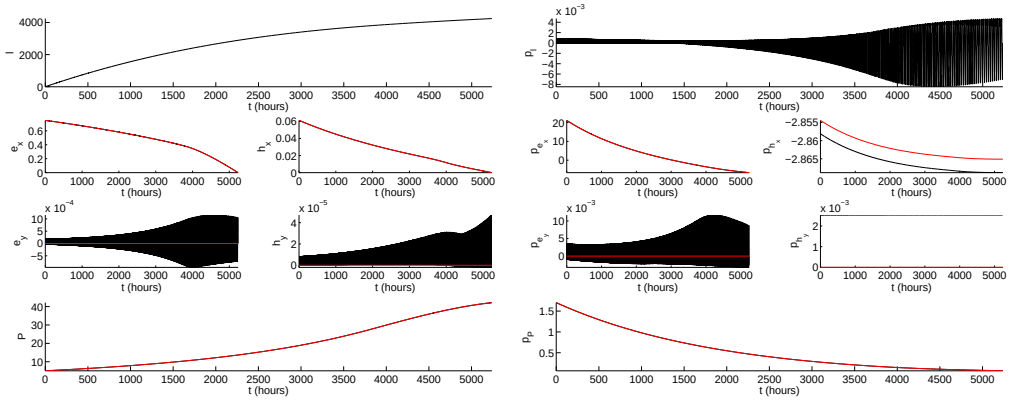

Figure 9.13: Case ②.Time evolution of state and adjoint variables for $\varepsilon = 2.59 \times 10^{-3}$. *(red)* averaged system (9.4), *(black)* non averaged system (9.1).

9.2.2 Double averaging

In this section, we present some results where we take into account the lunar perturbation. Taking $\gamma(I) = |\omega(I)|$ and $\bar{p}_\beta(0) = 0$ in the double averaged system (8.33), we get

$$\frac{\mathrm{d}J}{\mathrm{d}\alpha} = \varepsilon \frac{\partial \bar{\bar{h}}}{\partial p_J}(J, p_J), \quad \frac{\mathrm{d}p_J}{\mathrm{d}\alpha} = -\varepsilon \frac{\partial \bar{\bar{h}}}{\partial J}(J, p_J), \tag{9.5}$$

where

$$\bar{\bar{h}}(J, p_J) = \frac{1}{4\pi^2} \int_{\mathbb{T}^2} \frac{K(J, p_J, \varphi, \bar{p}_\beta = 0, \varepsilon = 0) - 1}{|\omega(I)|} \mathrm{d}\varphi.$$

Averaging of a two frequency system. The initial and final orbits are fixed to initial and final orbits of the non averaged system I_0 and I_f respectively. As for the single frequency case, we may normalize on the level $\bar{\bar{h}} = 0$. Hence, the boundary conditions for the averaged solutions are

$$J(0) = I_0, \quad J(\alpha_f) = I_f, \quad \bar{\bar{h}}(J, p_J, \bar{p}_\beta) = 0, \quad \bar{p}_\beta \text{ constant} . \tag{9.6}$$

However, as in the previous section, we consider slightly different boundary conditions than those presented in (9.6), that are

$$J(0) = I_0, \quad J(\alpha_f) = I_f, \quad p_\varphi = 0, \quad \bar{\bar{h}}(J, p_J) = c. \tag{9.7}$$

where

$$c := 1/t_f \int_0^{t_f} \bar{\bar{h}}(I(t), p_I(t)) \mathrm{d}t$$

and $I(.), p_I(.)$ are extremals of the corresponding non averaged system 9.1.

From the disturbing potential (7.9), we deduce the perturbing force

$$F_p(q, q') = \nabla_q R(q, q') = \mu' \left(\frac{q' - q}{|q' - q|^3} - \frac{q'}{|q'|^3} \right).$$

Figure	Data set	ε	c
9.14	①	1.14×10^{-2} N	-0.651
9.15	①	1.14×10^{-2} N	-0.289
9.16	①	1.14×10^{-2} N	-3.81×10^{-2}
9.17	②	1.73×10^{-2} N	-6.35×10^{-2}
9.18	②	8.64×10^{-3} N	-5.29×10^{-2}
9.19	②	2.59×10^{-3} N	-6.56×10^{-2}

Table 9.4: Values of ε and values of the level c for each figure.

Using (7.2), we express each component of F_p in terms of the equinoctial elements of the satellite $(P, e_x, e_y, h_x, h_y, l)$ and the mean motion M' of the Moon (the others orbital elements of the Moon $(a', e', i', \varpi', \Omega')$ are assumed constants). Then, we write the resulting force in the radial-orthoradial moving frame presented in (7.6). Finally, the perturbed dynamic is obtained from the Gauss equations 7.3.2.

We consider the same orbital transfers given in Table 9.1, but due to the drift on the slow variables, we take $\varepsilon = \max(\varepsilon_S, \varepsilon_M)$ where

- ε_S is the small parameter associated with the engine thrust defined previously by $\varepsilon_S = F_{max}/m_S$,
- ε_M is the small parameter associated with the disturbing potential of the Moon (7.9) and taken as $\varepsilon_M = (a_0/a')^2$ where a_0 is the initial semi-major axis of the satellite's orbit and a' the semi-major axis of the Moon's orbit.

In Fig.9.14-Fig.9.16 and Fig.9.17-Fig.9.19, we represent the time evolution of state variables $(P, e_x, e_y, h_x, h_y(, l))$ and of the adjoint variables $(p_P, p_{e_x}, p_{e_y}, p_{h_x}, p_{h_y}(, p_l))$ for both the double averaged system, in red, and the non averaged system, in black. For each case ① and ②, we choose the values of thrust as summarized in Table 9.4.

According to the problem formulation 7.19, there is no physical sense to take the limit $\varepsilon \to 0$. In these simulations, the parameter ε in front of F_0 is fixed, connected to the value given by the disturbing potential of the Moon. But, it's the maximum thrust of the engine which varies.

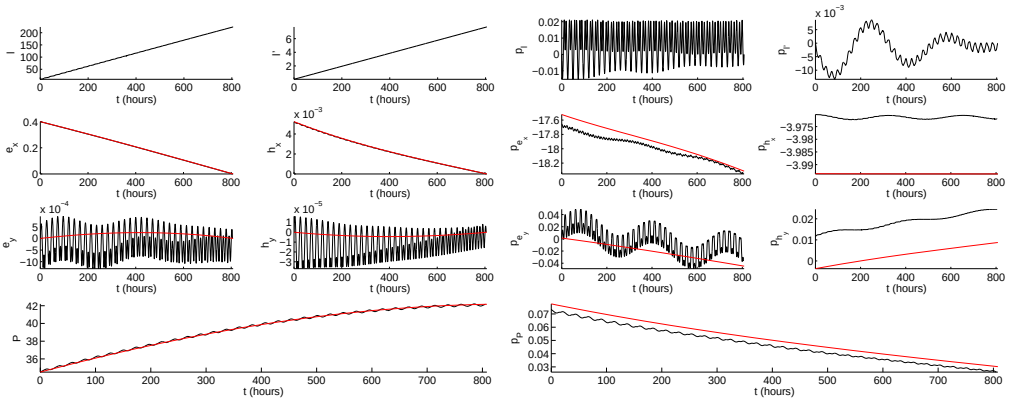

Figure 9.14: Case ①.Time evolution of state and adjoint variables for a thrust of 1N. *(red)* double averaged boundary value problem (9.5) and (9.7), *(black)* non averaged system (9.1).

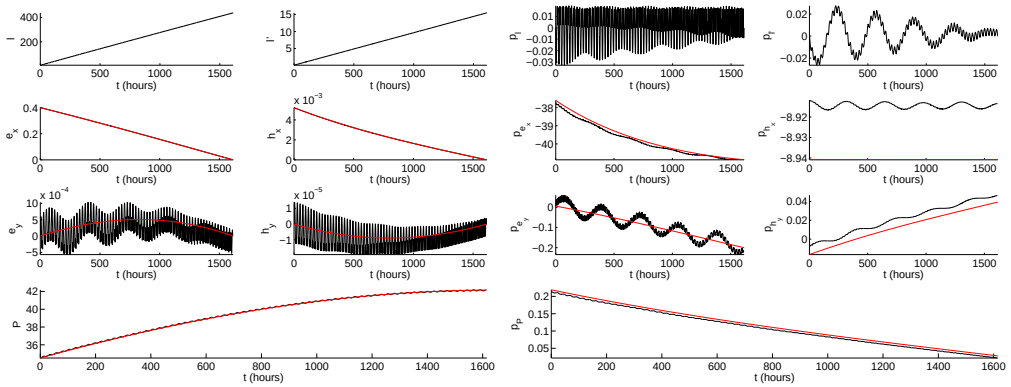

Figure 9.15: Case ①.Time evolution of state and adjoint variables for a thrust of 0.5N. *(red)* double averaged boundary value problem (9.5) and (9.7), *(black)* non averaged system (9.1).

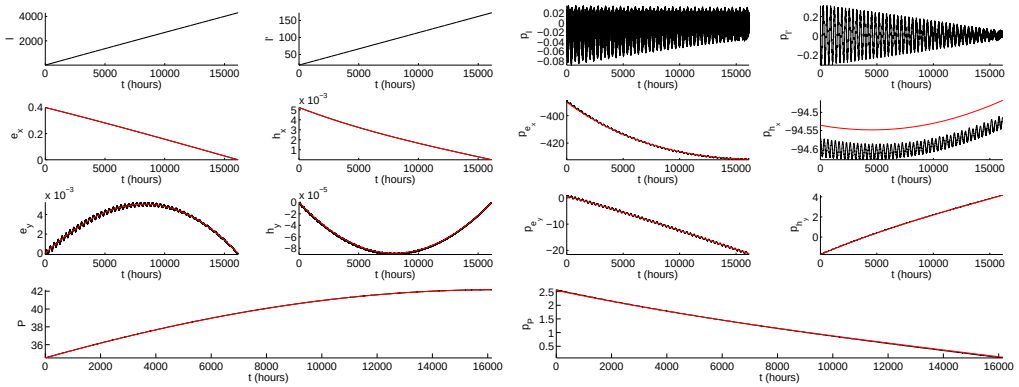

Figure 9.16: Case ①.Time evolution of state and adjoint variables for a thrust of 0.05N. *(red)* double averaged boundary value problem (9.5) and (9.7), *(black)* non averaged system (9.1).

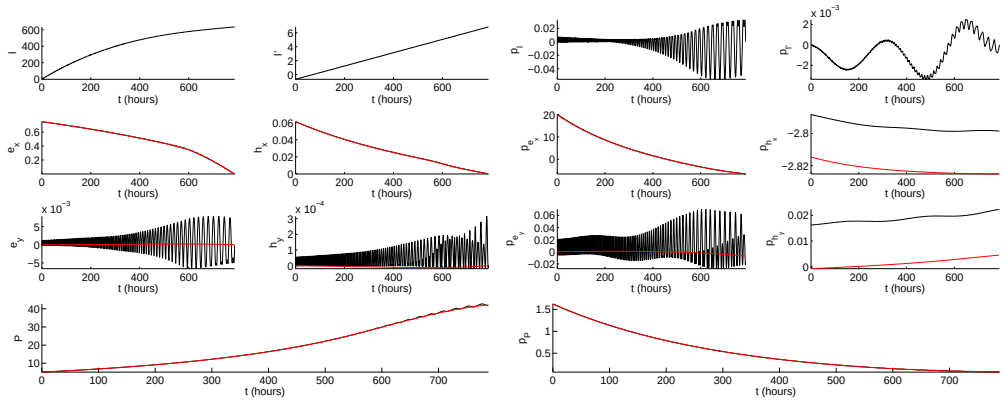

Figure 9.17: Case ②.Time evolution of state and adjoint variables for a thrust of 2N. *(red)* double averaged boundary value problem (9.5) and (9.7), *(black)* non averaged system (9.1).

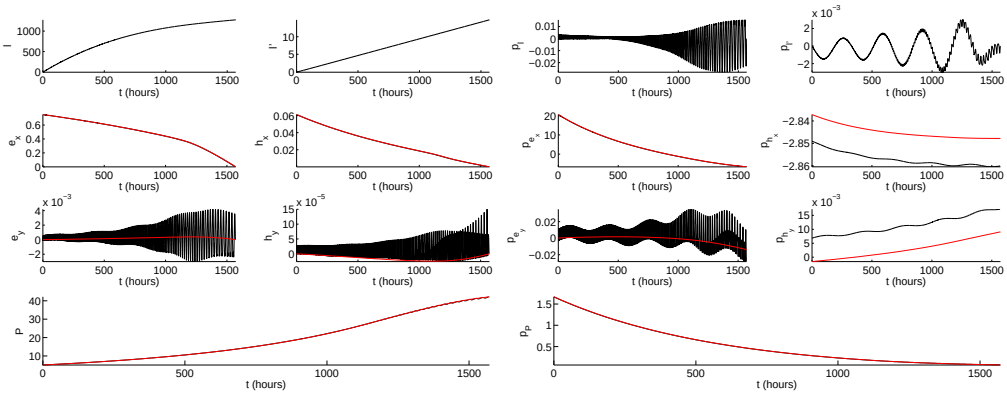

Figure 9.18: Case ②.Time evolution of state and adjoint variables for a thrust of 1N. *(red)* double averaged boundary value problem (9.5) and (9.7), *(black)* non averaged system (9.1).

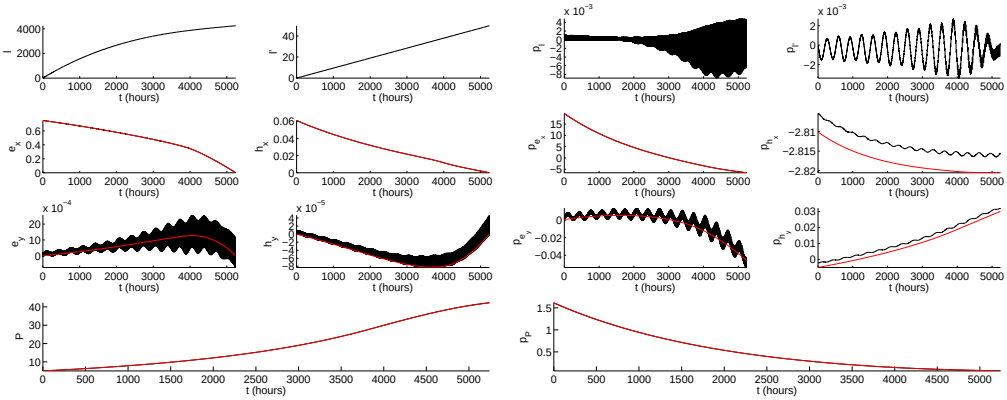

Figure 9.19: Case ②.Time evolution of state and adjoint variables for a thrust of 0.3N. *(red)* double averaged boundary value problem (9.5) and (9.7), *(black)* non averaged system (9.1).

Bibliography

[1] Agrachev, A.; Sarychev, A.: Abnormal sub-Riemannian geodesics: Morse index and rigidity. Ann. Inst. H. Poincaré Anal. Non Linéaire **13**, 6 635-690 (1996)

[2] Agrachev, A.; Sarychev, A.: Strong minimality of abnormal geodesics for 2-distributions. J. Dynam. Control Systems **1** 2 (1995) 139–176 (1995).

[3] Aleexev, V., Tikhomirov, V., Fomine, S.: Commande Optimale. Mir, Moscow (1982)

[4] Allgower, E.; Georg, K.: Introduction to numerical continuation methods. Classics in Applied Mathematics, Soc. for Industrial and Applied Math. **45** Philadelphia, PA, USA, 2003

[5] Alaoui, El-H.C., Gauthier, J.P., Kupka, I.: Small sub-Riemannian balls on R^3. J. Dynam. Control Systems. **2**, 3 359–421 (1996)

[6] Alouges, F.; DeSimone, A.; Giraldi, L.; Zoppello, M.: Self-propulsion of slender micro-swimmers by curvature control: N-link swimmers. Int. J. of Non-Linear Mech. **56** 132–141 (2013)

[7] Alouges, F.; DeSimone, A.; Heltai, L.: Numerical strategies for stroke optimization of axisymmetric microswimmers. Math. Models Methods Appl. Sci. **21**, no.2 (2011)

[8] Alouges, F.; DeSimone, A.; Heltai, L.; Lefebvre-Lepot, A.; Merlet, B.: Optimally swimming Stokesian robots. Disc. Cont. Dyn. Syst. **18**, 1189–1215 (2013)

[9] Alouges, F.; DeSimone, A.; Lefebvre, A.: Biological fluid dynamics: swimming at low Reynolds numbers. Encyclopedia of Complexity and System Science, Springer Verlag, 2009

[10] Alouges, F.; DeSimone, A.; Lefebvre, A.: Optimal strokes for low Reynolds number swimmers: an example. J. Nonlinear Sci. **18**, 277–302 (2008)

[11] Alouges, F.; DeSimone, A.; Lefebvre, A.: Optimal strokes for axisymmetric microswimmers. European Physical Journal E **28**, 279–284 (2009)

[12] Amestoy, P.R.; Duff, I.S.; Koster, J.; L Excellent, J.-Y.: A fully asynchronous multifrontal solver using distributed dynamic scheduling, SIAM Journal of Matrix Analysis and Applications, **23** no. 1, 15–41 (2001)

[13] Arnold, V.I.: Plane curves, their invariants, perestroikas and classifications. Amer. Math. Soc., Providence, RI. **21**, 33–91 (1994)

[14] Arnold, V. I., Guseĭn-Zade, S.M., Varchenko, A.N.: Singularities of differentiable maps. Birkhäuser Boston, Inc., Boston MA. (1985)

[15] Arnold, V.I.; Kozlov, V.V.; Neishtadt, A.I.: Mathematical aspects of classical and celestial mechanics. Springer-Verlag, **3** Berlin, 2006.

[16] Avron, J.E.; Raz, O.: A geometric theory of swimming: Purcell's swimmer and its symmetrized cousin. New Journal of Physics **10**, no.6 063016 (2008)

[17] Bao, D.; Chern, S.-S.; Shen, Z.: An introduction to Riemann-Finsler geometry. Springer-Verlag, **200** New York, 2000.

[18] Batchelor, G.K.: Slender-body theory for particles of arbitrary cross-section in Stokes flow. J. Fluid Mech. **44**, 419–440 (1970)

[19] Becker, L.E., Koehler, S.A., Stone, H.A.: On self-propulsion of micro-machines at low Reynolds number: Purcell's three-link swimmer. J. Fluid Mech. **490**, 15–35 (2003)

[20] Beletski, V.: Essai sur le mouvement des corps cosmiques. MIR (1977)

[21] Bellaïche, A.: The tangent space in sub-Riemannian geometry. J. Math. Sci. (New York) **35**, 461–476 (1997)

[22] Bensoussan, A.; Kokotovic, P.; Blankenship, G.: Singular Perturbations for Deterministic Control Problems. Lect. Notes Contr. Inform. Sci. 9–171 (1986)

[23] Berger, M.: La taxonomie des courbes. Pour la science, 297 56–63 (2002)

[24] Bettiol, P.; Bonnard, B.; Giraldi, L.; Martinon, P.; Rouot, J.: The three links Purcell swimmer and some geometric problems related to periodic optimal controls. Rad. Ser. Comp. App. **18**, Variational Methods, Ed. by M. Bergounioux et al. (2016).

[25] Bombrun, A.; Pomet, J.-B.: The averaged control system of fast oscillating control systems. SIAM J. Control Optim. **51** no. 3, 2280–2305 (2013)

[26] Bonnans, F., Giorgi, D., Maindrault, S., Martinon, P., Grélard, V.: Bocop - A collection of examples, Inria Research Report, Project-Team Commands. **8053** (2014)

[27] Bonnans, F., Giorgi, D., Heymann, B., Martinon, P. and Tissot, O. Bocophjb 1.0. 1-user guide. Technical report (2015).

[28] Bonnard, B.; Caillau, J.-B. : Riemannian metric of the averaged energy minimization problem in orbital transfer with low thrust. Ann. Inst. H. Poincaré Anal. Non Linéaire **24** no. 3, 395–411 (2007)

[29] Bonnard, B.; Caillau, J.-B.: Geodesic flow of the averaged controlled Kepler equation. Forum Math. **21** no. 5, 797–814 (2009)

[30] Bonnard, B.; Caillau, J.-B.; Dujol, R.: Energy minimization of single input orbit transfer by averaging and continuation. Bull. Sci. Math. **130** no. 8, 707–719 (2006)

[31] Bonnard, B.; Caillau, J.-B.; Picot, G.: Geometric and numerical techniques in optimal control of two and three-body problems. Commun. Inf. Syst. **10** no. 4, 239–278 (2010)

[32] Bonnard, B., Caillau, J.-B., Trélat, E.: Geometric optimal control of elliptic Keplerian orbits. Discrete Contin. Dyn. Syst. Ser. B 5, 4 929–956 (2005)

[33] Bonnard, B., Caillau, J.-B., Trélat, E.: Second order optimality conditions in the smooth case and applications in optimal control. ESAIM Control Optim. Calc. Var. **13**, 2 207–236 (2007)

[34] Bonnard, B., Chyba, M.: Singular trajectories and their role in control theory. Springer-Verlag, Berlin (2003)

[35] Bonnard, B., Chyba, M., Rouot, J., Takagi, D.: A Numerical Approach to the Optimal Control and Efficiency of the Copepod Swimmer. *Accepted in IEEE Control Systems Society Conference* (2016)

[36] Bonnard, B., Claeys, M., Cots, O., Martinon, P.: Geometric and numerical methods in the contrast imaging problem in nuclear magnetic resonance. Acta Appl. Math. **135**, 1 5–45 (2015)

[37] Bonnard, B., Cots, O.: Geometric numerical methods and results in the control imaging problem in nuclear magnetic resonance. Math. Models Methods Appl. Sci. **24**, 1 187–212 (2014)

[38] Bonnard, B., Faubourg, L., Trélat, E.: Mécanique céleste et contrôle des véhicules spatiaux. Mathématiques & Applications, Springer-Verlag **51**, Berlin, 2006

[39] Bonnard, B; Trélat, E.: On the role of abnormal minimizers in sub-Riemannian geometry. Ann. Fac. Sci. Toulouse Math. (6) **10**, 3 405–491 (2001)

[40] Bonnard, B., Kupka, I.: Théorie des singularités de l'application entrée/sortie et optimalité des trajectoires singulières dans le problème du temps minimal. Forum Math. **5**, 2 111–159 (1993)

[41] Bliss, G.A.: Lectures on the Calculus of Variations. Univ. of Chicago Press, Chicago (1946)

[42] Agrachev, A., Barilari, D., Boscain, H.: Introduction to geodesics in sub-Riemannian geometry. Geometry, Analysis and Dynamics on Sub-Riemannian Manifolds, Volume II, EMS Series of Lectures in Mathematics (to appear).

[43] Brockett, R.W.: Control theory and singular Riemannian geometry. Springer, New York-Berlin, 11–27 (1982)

[44] Caillau, J.-B.: Contribution à l'étude du contrôle en temps minimal des transferts orbitaux. PhD thesis, ENSEEIHT, Institut National Polytechnique, Toulouse, 2000.

[45] Caillau, J.-B.; Cots, O.; Gergaud, J.: Differential pathfollowing for regular optimal control problems. Optim. Methods Softw. **27** no. 2, 177–196 (2012)

[46] Caillau, J.B., Daoud, .B.: Minimum time control of the circular restricted three-body problem. SIAM J. Control Optim. **50**, 6 3178–3202 (2011)

[47] Caillau, J.-B.; Gergaud, J.; Noailles, J.: Minimum time control of the Kepler equation. Unsolved Problems in Mathematical Systems and Control Theory, 89–92, Princeton University Press (2004)

[48] Capderou, M.: Satellites : de Kepler au GPS. Springer, 2011

[49] Carathéodory, C.: Calculus of Variations and Partial Differential Equations of the First Order. Chelsea, 1965

[50] Carrou, J.-P.: Mécanique spatiale. Cépaduès, 1995.

[51] Cartan, E.: Les systèmes de Pfaff a cinq variables et les équations aux derivées partielles du second ordre. Ann. Sci. École Normale **27**, 109–192 (1910)

[52] Celletti, A.; Chierchia, L.: KAM stability and celestial mechanics. American Mathematical Soc., 2007.

[53] Chambrion, T., Giraldi, L., Munnier, A.: Optimal Strokes for Driftless Swimmers: A General Geometric Approach. *Submitted* (2014)

[54] Chang, Dong Eui; Marsden, Jerrold E.: Geometric derivation of the Delaunay variables and geometric phases. Celestial Mech. Dynam. Astronom. **86** no.2, 185–208 (2003)

[55] Cots, O.: Contrôle optimal géométrique: méthodes homotopiques et applications. PhD thesis, Université de Bourgogne (2012)

[56] Cushman, R. H.; Bates, L. M.: Global aspects of integrable systems. Birkhäuser, 1997.

[57] Dargent, T.: Averaging technique in T 3D: An integrated tool for continuous thrust optimal control in orbit transfers. 24th AAS/AIAA Space Flight Mechanics Meeting, Santa Fé, January 2014.

[58] Domingos, R.C.; de Moraes, R.V.; de Almeida Prado, A.F.: Third-body perturbation in the case of elliptic orbits for the disturbing body. Math. Probl. Eng. 1–15 (2008)

[59] Edelbaum, T.N.: Optimal low-thrust rendez-vous and station keeping. AIAA J. **2** no. 7, 1196–1201 (1964)

[60] Giacaglia, G.; James P.M.; Theodore L.F.: A semi-analytic theory for the motion of a lunar satellite. Celestial Mechanics **3** no.1, 3–66 (1970)

[61] Gamkrelidze, R.V.: Discovery of the maximum principle. J. Dynam. Control Systems **5**, 4 437–451 (1977)

[62] Gavriel, C.; Vinter, R.B.: Second order sufficient conditions for optimal control problems with non-unique minimizers: an abstract framework, Appl. Math. Optim. **70** 411–442 (2014)

[63] Geffroy, S.: Généralisation des techniques de moyennation en contrôle optimal-Application aux problèmes de transfert et rendez-vous orbitaux à poussée faible. PhD thesis, Institut National Polytechnique, Toulouse, CNES, 1997.

[64] Geffroy, S.; Epenoy, R.: Optimal low-thrust transfers with constraints. Generalization of averaging techniques. Acta Astronaut. **41** no. 3, 133–149 (1997)

[65] Gelfand, I.M., Fomin, S.V.: Calculus of Variations. Prentice Hall Inc., Englewood Cliffs, New Jersey (1963)

[66] Giraldi, L.: Méthodes mathématiques pour l'analyse de la natation à l'échelle microscopique. PhD thesis, Centre de Mathématiques Appliquées, École Polytechnique, Palaiseau, 2013.

[67] Giraldi, L.; Martinon, P.; Zoppello, M.: Controllability and Optimal Strokes for N-link Micro-swimmer. Proc. 52th Conf. on Dec. and Contr. (Florence, Italy) (2013).

[68] Giraldi, L.; Martinon, P.; Zoppello, M.: Optimal design of Purcell's three-link swimmer. Physical Review, **91** (2015).

[69] Godbillon, C.: Geométrie différentielle et mécanique analytique. Hermann, Paris (1969)

[70] Gray, J.; Hancock, G. J.: The propulsion of sea-urchin spermatozoa. Journal of Experimental Biology, **32** pp. 802–814 (1955)

[71] Grognard, F.; Akhmetzhanov, A.R.; Bernard, O.: Periodic optimal control for biomass productivity maximization in a photobioreactor using natural light. Inria Research Report, Project-Teams Biocore, **7929** (2012).

[72] Haberkorn, T.; Trélat, E.: Convergence results for smooth regularizations of hybrid nonlinear optimal control problems. SIAM J. Control Optim. **49** no. 4, 1498–1522 (2011)

[73] Hancock, G.J.: The self-propulsion of microscopic organisms through liquids. Proc. R. Soc. Lond. A **217**, 96–121 (1953)

[74] Happel, J., Brenner, H.: Low Reynolds number hydrodynamics with special applications to particulate media. Prentice-Hall, Inc., Englewood Cliffs, N.J. (1965)

[75] Hakavuori, E.; Le Donne, E.: Non-minimality of corners in sub-Riemannian geometry. Preprint (2015).

[76] Henrion, D., Lasserre, J.B., Loefberg, J.: GloptiPoly 3: moments, optimization and semidefinite programming. Optimization Methods and Software, **24**, 4-5 761-779 (2009).

[77] Hermes, H.: Lie algebras of vector fields and local approximation of attainable sets. SIAM J Control Optim. **16**, 5 715-727 (1978)

[78] Jean, F.: Control of Nonholonomic Systems: from Sub-Riemannian Geometry to Motion Planning. Springer International Publishing, SpringerBriefs in Mathematics (2014)

[79] Jurdjevic, V.: Geometric control theory. Cambridge Studies in Advanced Mathematics **52**, Cambridge University Press, Cambridge (1997)

[80] Kanso, E.; Newton, P. K.: Locomotory advantages to flapping out of phase. J. Exp. Mechanics, **50** (2009).

[81] Kaula, W.M.: Theory of satellite geodesy. Dover, 2000

[82] Klingenberg, W.: Riemannian geometry. de Gruyter Studies in Mathematics, Walter de Gruyter and Co., Berlin-New York (1982)

[83] Kupka, I.: Geometric theory of extremals in optimal control problems. i. the fold and Maxwell case. Trans. Amer. Math. Soc. **299**, 1 225–243 (1987)

[84] Kupka, I.: Géométrie sous-riemannienne. Astérisque, Séminaire Bourbaki **1995/96**, 351–380 (1997)

[85] Landau, L., Lipschitz, E.: Physique théorique. Ed. Mir (1975)

[86] Lauga, E., Powers, T.R.: The hydrodynamics of swimming microorganisms. Rep. Progr. Phys. **72**, 9 (2009)

[87] Lawden, D.F.: Elliptic functions and applications. Applied Mathematical Sciences, Springer-Verlag, New York **80** (1989)

[88] Lee, E.B., Markus, L.: Foundations of optimal control theory, Second edition. Robert E. Kreiger Publishing Co., Inc., Melbourne , 1986

[89] Lenz, P.H.; Takagi, D.; Hartline, D.K.: Choreographed swimming of copepod nauplii. Journal of The Royal Society Interface **12**, 112 20150776 (2015)

[90] Liberzon, D.: Calculus of Variations and Optimal Control Theory: A Concise Introduction. Princeton University Press, 2011

[91] Lidov, M.L.; Ziglin, S.L.: Non-restricted double-averaged three body problem in Hill's case. Celestial Mech. **13** no.4, 471–489 (1976)

[92] Lighthill M. J.: Note on the swimming of slender fish, J. Fluid Mech. **9**, 305–317 (1960)

[93] Lohéac, J.: Contrôle en temps optimal et nage à bas nombre de Reynolds. PhD thesis, Université de Lorraine, 2012.

[94] Lohéac, J.; Scheid, J.-F.: Time optimal control for a perturbed Brockett integrator. Application to time optimal axi-symmetric micro-swimmers. Geometric control and related fields (2014)

[95] Lohéac, J.; Scheid, J.-F.; Tucsnak, M.: Controllability and time optimal control for low Reynolds numbers swimmers. Acta Appl. Math. **123**, 175–200 (2015)

[96] Maciejewski, A.J., Respondek, W.: The nilpotent tangent 3-dimensional sub-Riemannian problem is nonintegrable. 2004 43rd IEEE Conference on Decision and Control, (2004)

[97] Meyer, K.R.;Hall, G.R.: Introduction to Hamiltonian dynamical systems and the N-body problem. Springer-Verlag, **40** New York, 1992

[98] Montenbruck, O.; Gill, E.: Satellite orbits. Springer, 2000

[99] Montgomery, R.: A tour of subriemannian geometries, their geodesics and applications. American Mathematical Society, Providence, RI. **91**, 2002.

[100] More, J.J.; Garbow, B.S.; Hillstrom, K.E.: User Guide for MINPACK-1, ANL-80-74, Argonne National Laboratory (1980)

[101] Najafi,A.; Golestanian, R.: Simple swimmer at low Reynolds number: Three linked spheres. Physical Review, **69** (2004).

[102] Or, Y., Zhang, S., Murray, R.M.: Dynamics and stability of low-Reynolds-number swimming near a wall. SIAM J. Appl. Dyn. Syst. **10**, 1013–1041 (2011)

[103] Pascoli, G.: Astronomie fondamentale. Dunod, 2000

[104] Passov, E., Or, Y.: Supplementary document to the paper: Dynamics of Purcell's three-link microswimmer with a passive elastic tail. Supplementary Notes.

[105] Poincaré, H.: Mémoire sur les courbes définies par une équation différentiable. Jour. Math. Pures et Appl. **7** 3 (1881) 375-422; **8** (1882) 251-296; **1** 4 (1885) 167-244; **2** (1886) 151-217.

[106] Poincaré, H.: Œuvres. Tome VII. Éditions Jacques Gabay, Sceaux (1996).

[107] Pontryagin,L.S., Boltyanskii, V.G., Gamkrelidze, R.V.: The Mathematical Theory of Optimal Processes. John Wiley and Sons, New York (1962)

[108] Powell, M.J.D.: A hybrid method for nonlinear equations, In P. Rabinowitz, ed. Numerical Methods for Nonlinear Algebraic Equations, Gordon and Breach (1970)

[109] Purcell, E.M.: Life at low Reynolds number. Am. J. Phys. **45**, 3–11 (1977)

[110] Rifford, L.: Singulière minimisante en géométrie sous-Riemannienne. Séminaire Bourbaki, 68ème année, 1113 (2016), à paraître.

[111] Sachkov, Y.L.: Symmetries of flat rank two distributions and sub-Riemannian structures. Trans. Amer. Math. Soc. **356**, 457–494 (2004)

[112] Sanders, J. A.; Verhulst, F.; Murdock, J.: Averaging methods in nonlinear dynamical systems. Springer, 2007.

[113] San Martín, J.; Takahashi, T.; Tucsnak, M.: A control theoretic approach to the swimming of microscopic organisms. Quart. Appl. Math. **65**, 405–424 (2007)

[114] San Martín, J.; Takahashi, T.; Tucsnak, M.: An optimal control approach to ciliary locomotion. Mathematical Control and Related Fields **6**, no.2 293–334 (2015)

[115] Sontag, E.D.: Mathematical control theory. Deterministic finite-dimensional systems, second edition. Texts in Applied Mathematics **6**, Springer-Verlag, New York (1998)

[116] Speyer, J.L.; Evans, R.T.: A second variational theory for optimal periodic processes. IEEE Trans. Automat. Control **29** , 138–148 (1984)

[117] Stoer, J.; Bulirsch, R.: Introduction to numerical analysis. Springer Science & Business Media, **12** 2013.

[118] Sussmann, H.J., Jurdjevic, V.: Controllability of non-linear systems. J Differential Equations **12**, 95-116 (1972)

[119] Takagi, D.: Swimming with stiff legs at low Reynolds number. Phys. Rev. E 92. (2015)

[120] Tarzi, Z.B.: Optimum low thrust elliptic orbit transfer using numerical averaging. PHD thesis, UCLA, 2012

[121] Taylor,G.I.: Analysis of the swimming of microscopic organisms. Proc. Roy. Soc. London. Ser. A. **209**, 447–461 (1951)

[122] Vinter, R.: Optimal control. Systems & Control: Foundations & Applications, Birkhäuser Boston, Inc., Boston, MA xviii+507, 2000

[123] Vinti, J.P.: Orbital and celestial mechanics. Aiaa **177**, 1998.

[124] Wähter, A.; Biegler, L.T.: On the implementation of a primal-dual interior point filter line search algorithm for large-scale nonlinear programming, Mathematical Programming, **106** no. 1, 25–57 (2006)

[125] Walker, M.J.H.; Owens, J.; Ireland, B.: A set of modified equinoctial orbit elements. Celestial Mechanics. **36**, 409–419 (1985)

[126] Wang, Q. and Speyer, J.L.: Necessary and sufficient conditions for local optimality of a periodic process. SIAM J. Control Optim. 2 **28**, 482–497 (1990)

[127] Zarrouati, O.: Trajectoires spatiales. CNES-Cepadues, 1987

[128] Zhitomirskiĭ, M.: Typical singularities of differential 1-forms and Pfaffian equations. American Mathematical Society, Providence, RI. **113**, 176 (1992)

Conclusion

Some remaining analysis have to be done in our study. First of all, to get a more complete study of the copepod and to justify the numerical computations of the one-parameter family of normal strokes, further analysis is required to generate this family using the appropriate SR-approximation and to compute strokes with small amplitudes. Similarly a same method has to be apply to generate family of limaçons and Bernouilli lemniscates. This in order to get a complete micro-local analysis of the exponential mapping in relation with computing strokes.

Second, the copepod study shows an interesting relation between the existence of non smooth abnormal minimizers and the problem of strokes which has to be clarified.

A more theoretical study is to compute the nilpotent approximation of order 1 for the Copepod model, which is described in [5] (part I) and depend on three parameters (depending on the point where the approximation is computed). For some specific value of the parameter, it may reveal integrable cases to compute families of strokes for the limaçon case and the simple loop case and to find out that the eight stroke could only appear on the side of the abnormal triangle (cf numerical simulations).

Finally, the computed optimal controls have to be experimentally applied on the model confirming the validity of the mathematical model. Note also that the experiments show that additional links can be used modifying the orientation or a 3D-displacement.

Also for the biological point of view, an interesting question is to find the optimal costs related to different kind of observed strokes (inverse optimal control problem).

We may lead further analysis about the orbital transfer problem. For the double averaging, resonance effects have to be analyze in particular one may study if the satellite go through resonances in its evolution. In this purpose, it would be interesting to analyze the effect of the disturbing potential of the Moon where short periodic and non-preponderant terms are discarded.

A study of the structure of the averaged unperturbed orbital transfer problem with low thrust defines a Finsler structure. Adding the J_2-effect, it is an on-going work to get conditions, which ensure that the resulting metric is a Finsler metric.

Last but not least, we obtained weak results about the convergence where some assumptions were made. The numerical results seem promising to get stronger results about the convergence of the non averaged system and the averaged one.

Geometric and numerical methods in optimal control and applications to low thrust orbital transfer and swimming at low Reynolds number

Abstract:

The first part of this work is devoted to the study of the swimming at low Reynolds number. We deal with two models of microswimmers: one is a symmetric 2-link swimmer introduced by D. Takagi to model the movement of an abundant variety of zooplankton called Copepod and the seminal model introduced by E.M. Purcell, called the Purcell Three-link swimmer, which consists of three rigid links and is more intricate.

We propose a geometric and numerical approach with tools of optimal control theory assuming for example that the motion occurs minimizing the energy dissipated by the drag fluid forces in relation with the concept of efficiency of a stroke. The Maximum Principle is used to compute periodic controls considered as minimizing control using proper transversality conditions, in relation with periodicity, minimizing the energy dissipated for a fixed displacement or maximizing the efficiency of a stroke. These problems fall into the framework of sub-Riemannian geometry which provides efficient techniques to tackle these problems, in particular, the nilpotent approximation can be used to compute strokes with small amplitudes and they can be continued numerically to compute more general strokes.

Second order optimality, necessary or sufficient, are presented and numerically used to select weak minimizers, again in the framework of periodic optimal controls. This leads to a complete solution of the optimal problems for the Copepod swimmer, that is to select on each energy level an optimal stroke producing a given displacement and finally using a further selection to compute the most efficient stroke.

In the second part, we focus on the motion of a spacecraft in a central field with perturbations and control. We take into account the perturbation arising from the gravitational interaction of the Moon or the perturbation resulting from the oblateness of the Earth. They are treated as perturbations of the two-body problem composed of the Earth and the spacecraft. Our purpose is to study the time minimal orbital transfer problem with low thrust using both analytical and numerical tools. Due to the small control amplitude, the transfer may take several revolutions around the Earth and our approach is to average the extremal flow provided by Pontryagin maximum principle. Minimizing trajectories are projections of the state space of the flow which lives in an extended space of dimension twice the dimension on the state. The difficulty to apply standard averaging techniques is that there is *a priori* no obvious way to identify orders and weights of variables in this extended space. We define an averaged system and study the related approximations to the non averaged system. We provide proofs of convergence and give numerical results where we use the averaged system to solve the non averaged system using indirect method implemented in the software `HamPath`.